LCH Laboratoire de Constructions Hydrauliques
Laboratory of Hydraulic Constructions

ÉCOLE POLYTECHNIQUE
FÉDÉRALE DE LAUSANNE

Communication 53

Influence of in- and outflow sequences on flow patterns and suspended sediment behavior in reservoirs

M. Müller

Editeur : Prof. Dr A. Schleiss

Lausanne, 2012

Communications du Laboratoire de Constructions Hydrauliques ISSN 1661-1179
Ecole Polytechnique Fédérale de Lausanne
Editeur: Prof. Dr A. Schleiss

N° 27 2006 Symposium érosion et protection des rives lacustres
Bases de dimensionnement des mesures de protection des rives lacustres

N° 28 2007 A. Vela Giró
Bank protection at the outer side of curved channels by an undulated concrete wall

N° 29 2007 F. Jordan
Modèle de prévision et de gestion des crues - Optimisation des opérations des aménagements hydroélectriques à accumulation pour la réduction des débits de crue

N° 30 2007 P. Heller
Méthodologie pour la conception et la gestion des aménagements hydrauliques à buts multiples

N° 31 2007 P. Heller
Analyse qualitative des systèmes complexes à l'aide de la méthode de Gomez & Probst

N° 32 2007 J. García Hernández, F. Jordan, J. Dubois, J.-L. Boillat
Routing System II - Modélisation d'écoulements dans des systèmes hydrauliques

N° 33 2007 Symposium - Flussbauliche Massnahmen im Dienste des Hochwasserschutzes, der Umwelt, Gesellschaft und Wirtschaft / Mesures d'aménagement des cours d'eau pour la protection contre les crues, l'environnement, la société et l'économie

N° 34 2007 B. Rosier
Interaction of side weir overflow with bed-load transport and bed morphology in a channel

N° 35 2007 A. Amini
Contractile floating barriers for confinement and recuperation of oil slicks

N° 36 2008 T. Meile
Influence of macro-roughness of walls on steady and unsteady flow in a channel

N° 37 2008 S. A. Kantoush
Experimental study on the influence of the geometry of shallow reservoirs on flow patterns and sedimentation by suspended sediments

N° 38 2008 F. Jordan, J. García Hernández, J. Dubois, J.-L. Boillat
Minerve - Modélisation des intempéries de nature extrême du Rhône valaisan et de leurs effets

N° 39 2009 A. Duarte
An experimental study on main flow, secondary flow and turbulence in open-channel bends with emphasis on their interaction with the outer-bank geometry

PREFACE

The risks associated with our dependence upon renewable energy sources development, such as solar and wind energy with highly fluctuating/unpredictable production, is somewhat mitigated by pumped-storage power facilities allowing ensuring grid stability and reliable power supply at any moment. In the Alpine countries of Europe, several new pumped-storage plants are planned or already under construction. Very often, artificial lakes of existing storage power plants are used as lower and/or upper reservoir. As with all reservoirs, sedimentation leads to storage loss and endangers the sustainable use of these storage volumes. On the one hand, pumped-storage operation will introduce more turbulence in the reservoirs which can potentially reduce settling of suspended sediment. On the other hand, it will also transfer fine particles from one reservoir to the other bi-directionally according to operation mode (turbine or pumping).

In this research project, Dr. Michael Müller studied for the first time the influence of in- and outflow sequences on flow patterns and suspended sediment behavior in reservoirs. Is sedimentation behavior correlated to pumped-storage sequences? To answer this relevant question, Dr. Michael Müller applied an integrated approach combining prototype measurements with systematic laboratory experiments and numerical simulations.

In order to investigate the influence of pumped-storage operation on flow patterns in a reservoir, in situ flow velocity measurements were performed in Lake Grimsel in Switzerland, which is the lower reservoir of the Grimsel 2 pumped-storage power plant. Furthermore turbidity was measured in the pressurized shaft connecting the two reservoirs. Then the jet behavior and flow patterns were studied in a rectangular basin subject to in- and outflow sequences with numerous experiments. The purpose was to understand the influence of these in- and outflow sequences on the sedimentation behavior of suspended sediment. Numerical simulations completed the knowledge by furnishing additional information on the jet behaviour and flow patterns. The results are helpful in selecting the location and type of inlet and outlet structures of pumped-storage schemes with the objective of maintaining high turbulence in the reservoir in order to minimize sedimentation.

Gratitude is expressed to the members of the PhD committee, Prof. Flavio Anselmetti from EAWAG (now at University of Berne), Dr. Sven Hartmann from University of Stuttgart, Germany, and Prof. Blake Tullis from Utah State University, USA, for their valuable comments and suggestions. The study was part of the research project *HydroNet* focusing on optimized design, manufacturing and operation of pumped-storage plants, funded by the Swiss Competence Center Energy and Mobility (CCEM), swisselectric research and the Swiss Federal Office of Energy. The Kraftwerke Oberhasli AG (KWO) are acknowledged for their support during the prototype measurements at the Grimsel 2 pumped-storage power plant.

Prof. Dr. Anton Schleiss Dr. Giovanni De Cesare

Abstract

Reservoir sedimentation and the resulting storage losses impact reliability, efficiency, safety and thus the sustainability of the hydropower schemes. Beside traditional storage hydropower plants, also pumped-storage facilities are affected. Flexible turbine and pump operations between two reservoirs allow demand-depending electricity production and absorption. Thus, they play a dominant role in peak load energy production as well as grid regulation. The storage volumes are influenced by continuous in- and outflow cycles. Their impact on sediment settling processes has not been addressed in research yet.

Inspired by the cyclic, bidirectional water exchange of pumped-storage plants, a novel method for sediment removal from reservoirs was investigated in the present study. After high sediment yield into the reservoir, fine sediment should remain in suspension in front of the water intake due to the pumped-storage induced turbulence. Thus, the settling process may be delayed and sediment be evacuated by the power or flushing tunnels.

In prototype measurements and laboratory experiments the influence of pumped-storage operations on flow patterns as well as the settling rates and sediment balance in two interconnected reservoirs has been studied. The two approaches were completed by numerical simulations.

In the lower reservoir of a pumped-storage hydropower plant in the Swiss Alps, flow velocities in front of the intake/outlet were measured by Acoustic Doppler Current Profilers (ADCP). The devices with independent energy supply were implemented on the reservoir bottom and sampled 2D flow velocity profiles over several weeks. The measurements showed only local influence of pumping (outflowing water) near the intake, whereas turbine operations (inflowing water) induce large eddy flow fields in the reservoir. Depending on lake topography, patterns with backflow can appear. A frequency analysis of the discharge and flow velocity series indicated a corresponding main period between the flow velocity profiles and the in- and outflow cycles of 1 day. The ANSYS-CFD simulated flow fields corresponded to the in situ flow patterns. The computed turbulent kinetic energy input due to turbine operation was some 25 times higher than the natural input by wind-forcing.

In the upstream part of the power shaft of the same hydropower scheme, a turbidity probe was installed for monitoring reasons. Over a period of eight months, sediment concentration of the operated water was continuously measured. An autonomous remote data acquisition and transfer system may be helpful for real-time monitoring by the hydropower operators. The measurements showed seasonal change of sediment concentration in the power system. In winter, high reservoir levels and ice-cover reduced sediment content, whereas in spring, snowmelt and low reservoir levels increased sediment yield. Short-term variations of sediment concentration up to 16% correlated with the in- and outflow cycles, especially for low reservoir filling. During the sampling period, about 45’000 t of fine sediment were moved between the two lakes. However, the sediment balance due to pumped-storage operation remained equilibrated. Fine sediment was kept in suspension in front of the intake/outlet structure by the operation induced flow patterns. Pumped-storage facilities would only increase sedimentation in case of unequal sediment concentrations in the two reservoirs.

The impact of magnitude and frequency of the in- and outflow cycles on flow field and fine sediment settling behavior was studied in laboratory experiments. Between two interconnected rectangular basins, sediment-laden water was pumped back and forth

according to regular in- and outflow cycles. In both volumes, turbidity was continuously measured. In the main basin, Ultrasonic Velocity Profilers (UVP) allowed 2D flow velocity measurements and the analysis of the developing inflowing jet. In a numerical model, time for achieving steady state conditions in the reservoir was defined. This discharge dependent duration indicated the frequency of the initial in- and outflow cycles. A reference test in stagnant water conditions defined the sediment settling curve without operation, corresponding to a basis of comparison for the investigated test configurations.

During five in- and outflow cycles of various magnitude and frequency, the evolution of suspended sediment ratio *SSR* was measured and compared to the reference case. Sediment influx and release (influx sediment rate *ISR* and evacuated sediment rate *ESR*) and thus the sediment balance *SB* of the system could be defined. In a first stage, 60% of the initially suspended sediment settled independently from magnitude of the in- and outflow cycles. High cycle frequency applied during this phase led to considerably higher *SSR* by the end of the test sequence. Low discharges increased particle suspension by 10 to 40% compared to conditions without operation, whereas high discharges increased concentration by 50 to 80%, depending on cycle frequency. With an intake/outlet structure close to the bottom or to the reservoir surface, 20% higher sediment concentrations could be achieved than in case of intermediate position. Sediment balance is only marginally impacted by in- and outflow cycles.

In situ as well as laboratory investigations highlight the fact that pumped-storage operations influence the flow patterns in reservoirs, especially in the near intake area. The induced turbulence keeps fine sediment in suspension, leading to an extensive sediment exchange between the storage volumes. The sediment balance remains unaffected, as long as the sediment concentrations in the reservoirs are similar.

Keywords: Reservoir sedimentation, suspended sediment, settling behavior, flow patterns, in- and outflow cycles, prototype investigations, Acoustic Doppler Current Profilers, turbidity monitoring, laboratory experiments, cycle magnitude, cycle frequency, kinetic energy

Résumé

Influence des séquences de pompage-turbinage sur les conditions d'écoulement et le comportement des sédiments fins dans les retenues

La sédimentation des réservoirs et les pertes de capacités qui en résultent affectent la fiabilité, l'efficience, la durée de vie et la sécurité des aménagements hydroélectriques. Comme tous les aménagements traditionnels d'accumulation, les aménagements de pompage-turbinage sont concernés. Par un turbinage et pompage flexible entre deux réservoirs, ces derniers permettent de produire de l'énergie ou de l'absorber, selon les besoins. Ainsi, ils jouent un rôle clé dans la régulation des réseaux et dans l'approvisionnement en énergie de pointe. Les réservoirs de ces aménagements sont soumis à des séquences de pompage-turbinage dynamiques, dont l'influence sur les processus de sédimentation est relativement peu connue.

L'objectif de la présente recherche est d'étudier une nouvelle méthode contribuant à l'évacuation des sédiments fins des réservoirs des aménagements de pompage-turbinage, basée sur les allers-retours d'eau provoqués par les cycles d'exploitation. L'idée est de garder en suspension les particules fines par des séquences de pompage-turbinage quand elles arrivent dans le réservoir et plus précisément devant la prise d'eau. Ainsi, leur dépôt pourrait être retardé et permettrait leur évacuation par les turbines ou éventuellement par des systèmes de vidange ou de purge.

L'effet des cycles de pompage-turbinage sur les conditions d'écoulement et le comportement des sédiments fins a donc été étudié par des mesures sur prototype et des essais en laboratoire. Les deux méthodologies ont été complétées par des simulations numériques.

Le réservoir inférieur d'un aménagement de pompage-turbinage des Alpes Suisses a été équipé de plusieurs Acoustic Doppler Current Profilers (ADCP) afin de mesurer les vitesses d'écoulement devant la prise d'eau. Ces instruments à alimentation énergétique autonome ont enregistrés des profils de vitesses 2D pendant plusieurs semaines. Les données montrent que les séquences de pompage, donc de soutirage d'eau, n'affectent que le champ très proche de la prise. En revanche, pendant les opérations de turbinage, des recirculations à grande échelle sont provoquées par le débit entrant dans le lac. Sous l'influence de la topographie, des écoulements de retour se créent en direction de la prise. Une analyse fréquentielle des séries temporelles de débit et de vitesse révèle que la période prédominante des vitesses enregistrées correspond à celle des cycles pompage-turbinage. Les champs d'écoulements calculés numériquement avec ANSYS-CFD confirment les tendances observées sur les mesures in-situ. La contribution calculée en énergie cinétique turbulente due à l'exploitation hydroélectrique est environ 25 fois plus importante que celle introduite par le vent.

La partie supérieure du puits blindé du même aménagement a été équipé d'un système de monitoring de turbidité. Pendant huit mois, les concentrations sédimentaires des eaux pompées et turbinées ont été mesurées en continu. Le système d'acquisition permettait un transfert de données à distance ainsi que l'observation en temps réel et pouvait être connecté au système de contrôle existant de la centrale. Les mesures montrent l'évolution de la concentration au cours des saisons. Pendant l'hiver, quand le niveau des lacs est haut et que les réservoirs sont couverts de glace, les concentrations sont plus faibles qu'au printemps, après la fonte des neiges et des niveaux des lacs abaissés pour des raisons d'exploitation. Des

variations de concentrations jusqu'à 16% corrélées avec l'évolution temporelle des séquences de pompage-turbinage ont été observées principalement pendant des périodes de lac bas. Au cours des huit mois de mesure, plus de 45'000 t de sédiment fin ont été transportées entre les deux réservoirs. Cependant, le bilan sédimentaire dû à l'exploitation pompage-turbinage est équilibré. Ceci indique que les particules fines sont gardées en suspension par les écoulements induits par l'aménagement. Les séquences de pompage-turbinage ne sont susceptibles de contribuer activement à la sédimentation seulement quand un des deux réservoirs présente une concentration sédimentaire considérablement plus élevée que l'autre.

Lors des essais en laboratoire, l'influence du débit et de la fréquence des cycles de pompage-turbinage sur les conditions d'écoulement et la sédimentation des particules fines a été étudiée. De l'eau chargée en sédiments a été pompée entre deux bassins rectangulaires. Des mesures continues de turbidité ont permis de suivre l'évolution des concentrations dans les deux bassins. De plus, le bassin principal a été équipé de sondes à Ultrason (UVP) afin d'enregistrer les champs d'écoulement 2D et d'analyser la trajectoire du jet entrant. Avant de réaliser les essais avec sédiments, un modèle numérique a permis de déterminer le temps nécessaire pour développer des conditions d'écoulement stationnaires dans le bassin. Ce temps dépend du débit et a permis de fixer la fréquence de base des cycles de pompage-turbinage. La courbe de sédimentation des particules utilisées a été établie lors d'un essai de référence en eau calme et a servi par la suite de référence pour la comparaison des différentes configurations testées.

Pendant cinq cycles de pompage-turbinage à débits et fréquences variés de manière systématique, l'évolution temporelle du taux de sédiments en suspension (Suspended Sediment Ratio *SSR*) a été mesurée et comparée à l'essai de référence. La quantité en sédiments entrant et sortant (Influx Sediment Rate *ISR* et Evacuated Sediment Rate *ESR*) et donc le bilan sédimentaire (*SB*) du système a pu être calculé. Pendant une première phase de sédimentation, environ 60% des sédiments sont décantés indépendamment de la magnitude et de la fréquence des cycles pompage-turbinage. Néanmoins, une exploitation à haute fréquence de pompage-turbinage dans cette phase permet de créer des conditions initiales favorables pour un taux de sédiments en suspension élevé. Des débits faibles conduisent à des taux entre 10 et 40% plus élevés que dans une situation sans exploitation. Avec des débits élevés, des taux entre 50 et 80% sont atteints, en fonction de la fréquence des cycles. Une prise d'eau plus proche du fond du bassin ou de la surface libre permet d'augmenter le taux de sédiments en suspension de 20% par rapport à la configuration d'une prise au centre du bassin. Le bilan sédimentaire du système n'est que marginalement influencé par les séquences de pompage-turbinage.

Les mesures sur prototype et en laboratoire ont montré que les séquences de pompage-turbinage affectent les conditions d'écoulement dans un réservoir, particulièrement pendant les périodes d'eau entrante. La turbulence provoquée permet de garder en suspension les sédiments fins, ce qui conduit à des masses considérables transportés dans le système. Globalement, le bilan sédimentaire reste équilibré tant que les deux réservoirs présentent des concentrations similaires.

Mots clés: Sédimentation des reservoirs, sédiments fins, champs d'écoulement, séquences de pompage-turbinage, mesures sur prototype, Acoustic Doppler Current Profilers, monitoring de turbidité, essais en laboratoire, magnitude, frequence, énergie cinétique

Zusammenfassung

Einfluss von Pumpspeichersequenzen auf die Strömungsverhältnisse und das Absetzverhalten von Feinsedimenten in Stauseen

Die Stauraumverlandung und die daraus resultierenden Kapazitätsverluste beeinträchtigen Zuverlässigkeit, Effizienz, Lebensdauer und Sicherheit von Wasserkraftanlagen. Nebst traditionellen Speicherkraftwerken sind auch Pumpspeicherwerke betroffen. Diese erlauben durch flexibles Turbinieren und Pumpen zwischen zwei Stauhaltungen je nach Bedarf Strom zu produzieren oder zu absorbieren. Sie spielen deshalb eine wichtige Rolle bei der Stromnetzregulierung und der Bereitstellung von Spitzenenergie. Die Speicher dieser Kraftwerke sind dynamischen Pump- und Turbiniersequenzen ausgesetzt, deren Auswirkungen auf die Verlandungsprozesse verhältnismässig unbekannt sind.

Inspiriert durch das zyklische Hin-und-her-Bewegen der Wassermassen der Pumpspeicherwerke hat die vorliegende Studie zum Ziel, eine alternative Methode zum Austrag von Feinsedimenten aus betroffenen Stauseen zu untersuchen. Dabei sollen die Feinsedimente nach deren Eintrag in den Stausee im Bereich der Wasserfassung durch die von Pumpspeichersequenzen erzeugte Turbulenz möglichst lange in Suspension gehalten werden. So könnte das Absetzen verzögert und die Feinsedimente durch den Triebwasserstollen abturbiniert oder allenfalls durch einen Spülstollen abgeführt werden.

Mit Prototypmessungen und Laborversuchen wurden die Auswirkungen des Pumpspeicherbetriebs auf die Strömungsverhältnisse in Staubecken sowie auf die Absetzraten und die Massenbilanz zweier verbundener Speicher studiert. Die beiden Lösungsansätze wurden durch numerische Simulationen ergänzt.

Im Unterbecken eines Pumpspeicherkraftwerks in den Schweizer Alpen wurden Strömungsgeschwindigkeiten im Bereich der Wasserfassung gemessen. Acoustic Doppler Current Profilers (ADCP) mit autonomer Energieversorgung wurden auf dem Seegrund positioniert um über mehrere Wochen 2D-Geschwindigkeitsprofile aufzuzeichnen. Die Messungen zeigen, dass Pumpsequenzen, d.h. aus dem See ausfliessendes Wasser, nur das Strömungsfeld unmittelbar vor der Fassung beeinflussen. Das zu Turbinierzeiten in den See einströmende Wasser verursacht grossräumige Zirkulationströmungen im Becken. Unter dem Einfluss der Seetopografie kommt es zum Teil zu Rückströmungen in Richtung Fassung. Eine Frequenzanalyse der Abfluss- und Geschwindikeitsdaten zeigt, dass die Hauptperiode der aufgezeichneten Geschwindigkeitsprofile mit derjenigen der Pumpspeicherzyklen übereinstimmen. Die mit ANSYS-CFD simulierten Geschwindigkeitsfelder entsprechen den im Stausee beobachteten Strömungsverhältnissen. Der errechnete Eintrag an turbulenter kinetischer Energie durch den Kraftwerksbetrieb ist ca. 25 mal höher als jener, der auf natürliche Weise durch Wind induziert wird.

Am oberen Ende des Druckschachts derselben Anlage wurde zu Monitoringzwecken eine Trübungsmessstelle eingerichtet. Über einen Zeitraum von acht Monaten wurde die Sedimentkonzentration des gepumpten oder turbinierten Wassers kontinuierlich aufgezeichnet. Ein Akquisitionssystem erlaubte den Datentransfer und eine Echtzeitüberwachung der Messresultate und könnte bei Bedarf des Kraftwerksbetreibers an das bestehende Kontrollsystem der Anlage angeschlossen werden. Die Messungen zeigen die

jahreszeitbedingte Veränderung der Sedimentkonzentration im Kraftwerkssystem. In den Wintermonaten bei hohem Seestand und eisbedecktem See, wurden tiefere Werte gemessen als im Frühling nach einsetzender Schneeschmelze und betriebsbedingtem tiefen Seespiegel. Konzentrationsschwankungen von bis zu 16%, die mit dem zeitlichen Verlauf der Pumpspeichersequenzen korrelieren, wurden vor allem bei tiefem Seestand gemessen. Über die acht Monate Messzeit wurden rund 45‘000 t Feinsediment zwischen den Seen hin- und hertransportiert. Die auf den Pumpspeicherbetrieb zurückzuführende Sedimentbilanz ist jedoch neutral. Dies zeigt, dass die Feinsedimente durch die kraftwerksbedingten Strömungen vor der Fassung in Suspension gehalten werden. Der Pumpspeicherbetrieb würde allenfalls erst dann aktiv zur Verlandung beitragen, wenn eines der beiden Staubecken wesentlich höhere Sedimentkonzentrationen aufweist.

Im Versuchsstand wurde der Einfluss von Abfluss und Frequenz der Pumpspeicherzyklen auf die Strömungsverhältnisse und das Absetzverhalten von Feinsedimenten untersucht. Zwischen zwei prismatischen Becken, wurde sedimenthaltiges Wasser hin- und hergepumpt. In beiden Becken wurden kontinuierlich Trübungsmessungen durchgeführt. Im Hauptbecken wurden mit Ultrasonic Velocity Profilers (UVP) zusätzlich 2D-Geschwindigkeitsfelder sowie die Entwicklung des einströmenden Wasserstrahls dokumentiert. Im Vorfeld der Sedimentversuche wurde in einem numerischen Modell die Zeitdauer ermittelt, die nötig ist, um im Becken stationäre Strömungsbedingungen aufzubauen. Sie ist vom Abfluss abhängig und definierte die Grundfrequenz der zu testenden Pumpspeicherzyklen. Ein Referenzversuch in stillem Wasser definierte die Absetzkurve der Feinsedimente und diente als Vergleichsgrundlage zwischen den getesteten Zyklen.

Während fünf Pumpspeicherzyklen verschiedener Abflüsse und Frequenzen wurde die zeitliche Entwicklung des in Suspension gehaltenen Sedimentanteils (Suspended Sediment Ratio *SSR*) gemessen und mit dem Referenzversuch verglichen. Sedimenteintrag und -austrag (Influx Sediment Rate *ISR* und Evacuated Sediment Rate *ESR*) und damit die Sedimentbilanz (*SB*) des Systems konnten so errechnet werden. In einer ersten Phase setzen sich rund 60% der Feinsedimente unabhängig von der Magnitude der Pumpspeicherzyklen ab. In dieser Phase können durch erhöhte Pumpspeicherfrequenz Voraussetzungen geschaffen werden, um die Suspensionsrate über längere Zeit hoch zu halten. Geringe Abflüsse halten zwischen 10 und 40% mehr Partikel in Suspension als bei Nichtbetrieb, während mit hohem Abfluss Suspensionsraten 50 bis 80% erreicht werden, in Abhängigkeit der Zyklenfrequenz. Liegt die Wasserfassung näher beim Beckenboden oder dem Freiwasserspiegel, wird die Suspensionsrate im Vergleich zu einer Lage in Beckenmitte um rund 20% erhöht. Die Sedimentbilanz wird durch den Pumpspeicherbetrieb nicht wesentlich beeinflusst.

Prototypmessungen sowie Laborversuche zeigen, dass Pumpspeichersequenzen die Strömungsbedingungen in Staubecken und insbesondere im Nahbereich der Wasserfassung beeinflussen. Die verursachte Turbulenz hält Feinsedimente in Suspension, so dass beträchtliche Sedimentmassen im System hin- und hertransportiert werden. Die Sedimentbilanz bleibt jedoch neutral, solange beide Stauhaltungen ungefähr gleiche Partikelkonzentrationen aufweisen.

Stichwörter: Stauraumverlandung, Feinsedimente, Absetzverhalten, Strömungsverhältnisse, Pumpspeicherzyklen, Prototypmessungen, Acoustic Doppler Current Profilers, Trübungsmonitoring, Laborversuche, Zyklendauer, Zyklenfrequenz, kinetische Energie

Contents

Chapter 1

Introduction

Many reservoirs with the purpose to store water for hydropower production, flood protection, drinking water supply or irrigation are subject to sedimentation processes. When the construction of a dam interrupts the continuity of sediment transport of a river, the deposition and settling processes by the particles supplied from the upstream catchment area start filling up the reservoir. Both sustainability and safety are endangered. In case of hydropower, the accumulating sediments reduce storage capacity and lead to reduced operation efficiency. Deposits in front of intake/outlet structures or clogging of bottom outlets can lead to severe exploitation perturbations and safety problems.

Sedimentation issues in traditional storage hydropower plants have been studied quite abundantly. Sediment transport theory and various measures against reservoir sedimentation are developed and described. However, pumped-storage hydropower plants are faced with new challenges regarding reservoir sedimentation.

On the one hand, pumped-storage operations alter the sediment balance of reservoirs. Suspended sediment are no longer just deposited in the reservoir or transported downstream, but are continuously influenced by the pumping and turbine operations between the reservoirs of the system. Furthermore, even a reservoir without a natural river basin and thus without sediment inflow can be affected by sedimentation due to pump operations from a river or lake with sediment supply.

On the other hand, flow conditions in reservoirs with pumped-storage facilities and especially in the area close to the water intake/outlet can alternate from one state to another within relatively short laps of time. The energy input from the power plant leads to mixing processes in the water body and thus alters the stratification and the particle dynamics of reservoirs.

Whether and how flow patterns and suspended sediment behavior are affected by such in- and outflow sequences and if settling processes can be actively reduced was studied in the framework of this research project.

1.1 Context

The work is associated to the multidisciplinary research project *HydroNet*, set up and supported by the *Competence Center of Energy and Mobility* (CCEM) and *swisselectric research*. *HydroNet* (Figure 1.1) brings together seven research institutes of the hydropower sector, provides monitoring and experimental knowhow, model test facilities and computation resources and maintains strong collaboration with industrial partners in the fields of hydrodynamics, monitoring systems, electrical, mechanical, ecological and civil engineering. The consortium aims to *converge toward a consistent standardized methodology for design, manufacturing, operation, monitoring and control of pumped-storage power plants in order to give new impulsions to the hydropower technology*.

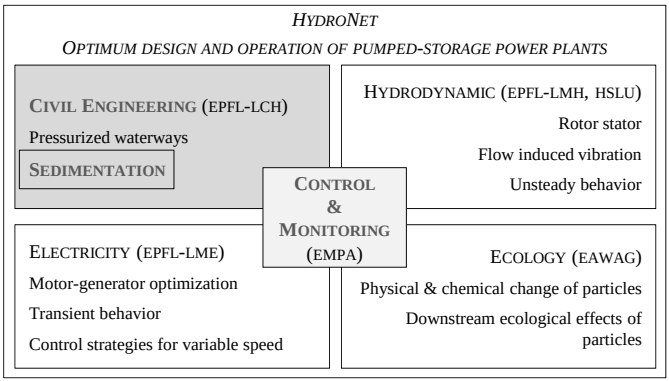

Figure 1.1 Partners and tasks of the *HydroNet* project consortium

Within *HydroNet*, two civil engineering aspects of pumped-storage plants were analyzed at the Laboratory of Hydraulic Constructions (LCH) of Ecole Polytechnique Fédérale de Lausanne (EPFL). Hachem (2011) analyzed pressurized shafts and tunnels. The present study concerns reservoir sedimentation. Previous studies at LCH focused on turbidity currents, their influence on hydraulic structures, such as water intakes, and possible mitigation measures against the phenomenon (De Cesare, 1998; Oehy, 2003). Jenzer Althaus (2011) investigated sediment evacuation from reservoirs through intakes by jet induced flows. The present thesis studies the idea of using turbulence, induced by in- and outflow sequences of high frequency, to keep fine sediment in suspension and to evacuate them through the power system downstream.

1.2 Objectives

The main goal of this research project is to investigate whether sediment behavior and flow patterns in reservoirs can be correlated to pumped-storage sequences, focusing on fine sediment near the intake/outlet structure. If particles were kept in suspension by pumped-storage induced turbulence, settling processes could be slowed down for further downstream transfer through water intakes or bottom outlets.

Three approaches – prototype measurements, laboratory experiments and numerical modeling – were followed, as presented in Figure 1.2.

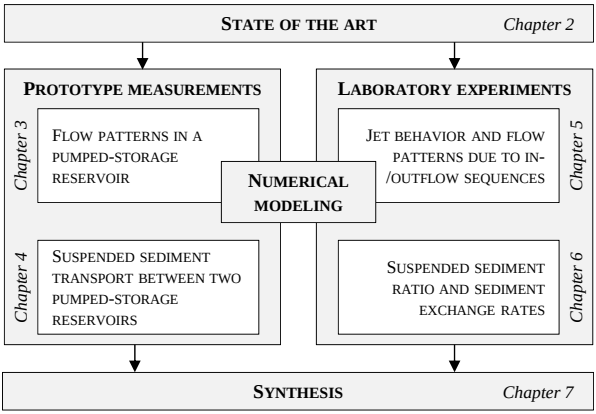

Figure 1.2 Methodology and structure of the research project

In order to evaluate prototype monitoring concepts, the Grimsel 2 pumped-storage plant in Switzerland was equipped with measurement devices for flow velocity sampling near the intake/outlet structure as well as turbidity measurements of the water exchanged between the two reservoirs (pressurized shaft).

The laboratory experiments were carried out on a test facility to evaluate different alternating in- and outflow sequences and to measure flow velocities and suspended sediment concentration in a rectangular prismatic basin. The objective consisted in a parameter study of the frequency and magnitude of in- and outflow sequences, of the initial sediment concentration as well as of the intake position to evaluate the flow patterns, kinetic energy, suspended sediment ratio and sediment exchange rates.

The two approaches were completed with numerical simulations which allowed comparison to in situ measurements and laboratory experiments on the one hand, and carrying out sensitivity analyses on the other.

Thus, the following key objectives could be addressed:

- Keeping fine sediment in suspension by means of in- and outflow sequences
- Monitoring flow patterns in reservoirs and sediment transport between two storage volumes of a pumped-storage scheme
- Long-term prediction of sedimentation processes by the help of the developed monitoring system
- Parameter study in laboratory experiments on a rectangular prismatic reservoir, investigating the effect of frequency and magnitude of in- and outflow sequences, relative sequence duration, initial sediment concentration and intake/outlet position on flow patterns, suspended sediment ratio and sediment exchange rates
- Recommendations for active long-term sediment management of pumped-storage schemes.

1.3 Structure

The report is divided in seven chapters. Chapters 1 and 2 introduce the scope of the study as well as the relevant literature for reservoir sedimentation issues and the driving physical phenomenon. Chapters 3 and 4 present the results of the prototype measurements on an existing pumped-storage plant. Chapters 5 and 6 present and discuss the experimental study and focus on the influence of magnitude and frequency of in- and outflow sequences on suspended sediment behavior in a rectangular reservoir. Chapter 7 summarizes the prototype and experimental results and suggests recommendations for real case and future research possibilities.

The main body is written as papers to be published in scientific journals. An outline of each of these chapters is described hereafter:

Chapter 3, *In situ measurement and numerical modeling of flow fields in a reservoir subject to pumped-storage operation*, presents the in situ measurements of flow patterns in Lake Grimsel, the lower reservoir of the Grimsel 2 pumped-storage scheme. Flow velocities were recorded over three periods of four to eight days by three Acoustic Doppler Current Profilers (ADCP) aligned in front of the intake/outlet structure. One and two-dimensional velocity profiles are analyzed and correlated to the pumped-storage operations of the plant. 2D profiles are compared to flow patterns calculated by a numerical model. Finally, turbulent kinetic energy input due to turbine operation is compared to naturally wind-induced energy input.

Chapter 4, *Continuous long-term observation of suspended sediment transport between two pumped-storage reservoirs* focus on monitoring of suspended sediment transport through the pressurized system of the Grimsel 2 scheme. Turbidity data were recorded over a period of eight months by a turbidity probe installed on the pressurized shaft. Results show seasonal variation of suspended sediment concentration from winter to summer months as well as correlation between short-term variations in sediment load and pumping and turbine operations. The sediment balance due to pumped-storage operations is calculated and discussed.

Chapter 5, *Experiments on jet behavior and flow patterns in a rectangular basin subject to in- and outflow sequences*, presents the numerical and experimental description of flow conditions near the intake/outlet, carried out for mainly clear water conditions. 2D flow patterns as well as axial and transversal jet velocities were measured by Ultrasonic Velocity Profilers (UVP). The velocity measurements allow description of the evolution of kinetic energy in the basin, available for mixing the water body and slowing down fine sediment settling. Finally, the influence of the intake/outlet position is discussed.

Chapter 6, *Experiments on the effect of in- and outflow sequences on suspended sediment exchange rates*, provides the results of experimental investigations with suspended sediment. The experimental set-up and measuring techniques as well as the different test configurations are presented. Results are analyzed, for reference cases without in and outflow sequences as

well as for test series with systematically varying parameters. The suspended sediment ratio and the sediment balance under the effect of in- and outflow sequences are discussed.

Since written as publications, the four chapters are self-contained and therefore some redundancy may be present in the description of the case study and the experimental set-up. The appendices provide complementary information to the in situ records (Appendices A and B), as well as supplementary experimental test results (Appendix C).

Chapter 2

Literature review

This chapter outlines relevant scientific background on reservoir sedimentation, possible concerns due to pumped-storage operation and monitoring methods and provides the basic jet and turbulence notions necessary for the understanding of the present research. More references related to the study are mentioned in chapters 3 to 6.

The theory of sediment settling processes and reservoir sedimentation is well developed and documented (Morris *et al.*, 2008). An extensive summary on the origin of sediment as well as on the problems and possible measures related to reservoir sedimentation was presented by Jenzer Althaus (2011). Therefore, only the most important notions are given in this literature review, completed with the more recent aspect of pumped-storage operation.

The concept of mixing particles by jets is not novel and has been the subject of many studies, especially in the field of chemical engineering, where mixing is a common process; jet mixing has become an alternative to conventional impeller mixing (Wasewar, 2006). However, most jet mixing studies have focused mainly on improvements of the mixing process by studying the jet angle, jet location, jet length, tank geometry, and the jet characteristics like velocity, diameter, momentum flux, Reynolds number and Froude number. The effect of cyclic in- and outflow sequences on the mixing effect on suspended sediment has not been addressed yet.

Monitoring in hydropower plants is of major importance for the power producers to control the good functioning of their scheme, detect eventual damages in the system and optimize exploitation efficiency. Meticulous surveillance is often attached to mechanical or electrical equipment of the plants or the important civil engineering works such as dams and pressurized shafts and tunnels. With the growing problem of reservoir sedimentation, the owners of hydropower plants are more and more interested in possible monitoring systems addressing sedimentation issues.

2.1 Reservoir sedimentation

Filling up of reservoirs due to sedimentation processes is a long-term problem with increasing significance and impact in the decades to come. The capacity of any artificial reservoir with the purpose to store water for hydropower production, flood protection, drinking water supply or irrigation can be decreased over time by sediment deposits.

When the construction of a dam interrupts the continuity of sediment in- and output of a river, the initial fluvial transport processes are altered due to very low flow velocities in the reservoir. Thus, deposition and settling processes of particles transported into the storage start filling up parts of the storage volume. This phenomenon ends up in a problem of sustainability and safety (Schleiss *et al.*, 2010). At long-term, the accumulating sediment reduce reservoir storage volume and decrease or eventually even eliminate capacity for flow regulation and benefits of water or energy supply and flood protection (Graf, 1982; ICOLD, 1989; LCH, 2005). As soon as deposits reach the level of intake and outlet structures, operation efficiency and safety of hydropower schemes are severely endangered (De Cesare, 1998; Schleiss *et al.*, 2010). Adequate sedimentation management is required to guarantee the sustainable use of storage power plants (Fan and Morris, 1992; Morris and Fan, 1998; Wang and Hu, 2009).

Several measures against sedimentation problems in reservoirs have been developed in the past and are used today to slow down the filling up process of artificial storages. Nevertheless, the application of these methods cannot guarantee a use over the whole life cycle of a reservoir, which should be the objective for sustainable reservoir management (Laffitte and De Cesare, 2005).

Pumped-storage plants are affected by reservoir sedimentation as any other traditional storage hydropower plant. However, new processes might appear, as water is moved back and forth between two storage volumes which inevitably leads to an alteration of initial flow conditions and sediment balance of the reservoirs. So far, the link between pumped-storage operation and reservoir sedimentation is barely treated and therefore has been addressed in this research project.

2.1.1 Storage loss due to sedimentation

On a worldwide scale, sedimentation rate of reservoirs, and consequently storage loss due to reservoir filling up, is estimated to be 1 to 2% annually (Jacobsen, 1999). Oehy (2003) stated the evolution of storage capacity and of volume losses due to sedimentation over the last century and estimated the future development of these two parameters (Figure 2.1). Considering that the annual increase of storage volume due to the construction of new reservoirs is close to 1%, the problem of sustainability becomes apparent. Without effective, sustainable measures against reservoir sedimentation, the major part of the worldwide useful volume will be lost until the end of the 21st century.

Figure 2.1 shows that Swiss Alpine reservoirs present a mean annual sedimentation rate of approximately 0.2%, which is much lower than the worldwide average (Beyer Portner and Schleiss, 2000).

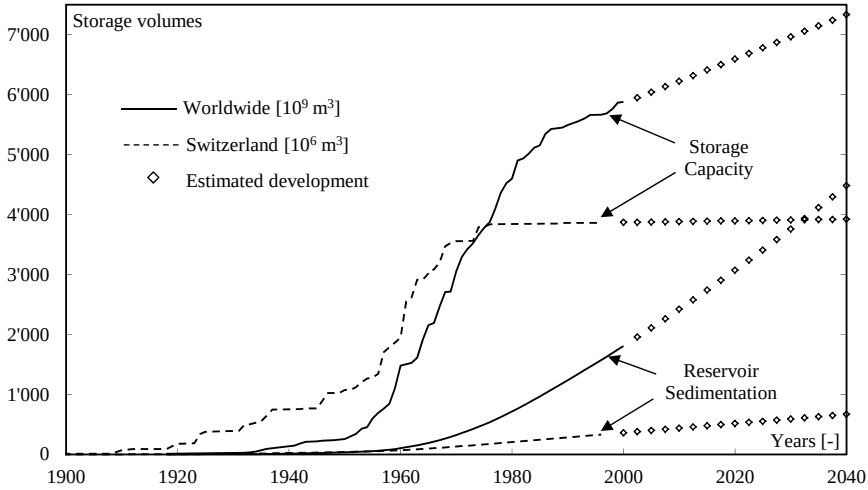

Figure 2.1 Increase of reservoir capacity by the construction of new dams and storage volume loss by sedimentation worldwide and in Switzerland (Oehy, 2003)

In fact, sedimentation rate of a particular reservoir is highly variable and depends on geomorphology, climate and the conception of the entire hydropower scheme. Batuca and Jordaan (2000) as well as Basson (2009) provide a detailed collection of sedimentation rates in regions all over the world. Highest erosion rates are present in the Alps, the Himalaya, the Andes and the mountains at the Pacific coast of America (Knoblauch *et al.*, 2005). According to Oehy (2003), the lower sedimentation rate in the Swiss high altitude reservoirs is due to the geologic characteristics of the catchment areas. Even if Swiss Alpine storages are more sustainable considering capacity losses, their safe operation can be threated after decades of operation due the sedimentation by turbidity currents (De Cesare *et al.*, 2001).

2.1.2 Sediment origin

Soil erosion and landslides in a catchment, as well as riverside and riverbed erosion define the sediment load of a river. From the higher catchment regions in the mountains toward the highlands and plains, exogenous processes such as wind, rainfall, temperature, glaciers and vegetation act on the earth crust and lead to weathering, loosening, diminishing and transporting of the soil materials (Bechteler, 2008). This process ends in lakes or the sea where particles settling occurs due to decreasing flow velocity.

There are multiple factors influencing the erosion rate, amongst others the grain size distribution, content of organic matter and soil permeability. Some of them are quasi negligible, others are of major importance. Based on the analysis of sedimentation data of 19 Swiss reservoirs Beyer Portner and Schleiss (2000) described the annual erosion volume per surface by an empirical equation. For the studied reservoirs, this erosion volume could be connected to a formula including the mean rainfall during summer months, surface cover and average annual relative change of glacier length.

Rivers usually carry sediment particles within a wide range of sizes, with the coarser components transported near the river bed (bed load) and suspended sediment generated by superficial erosion as well as by smashing and abrasion of the bigger grains. Sediment discharge is particularly high during flood events due to larger erosive forces and transport capacity with increasing discharge. In many river systems, 80 to 90% of the transported sediment during such periods corresponds to size fractions smaller than sand (Alam, 1999; Sinniger *et al.*, 1999).

When the sediment-laden river enters a reservoir it plunges and follows, according to density difference, the thalweg to the deepest area, which is normally close to the dam and the power intakes. This phenomenon, known as turbidity current is the main sedimentation process affecting large Alpine storage reservoirs. It has been the subject of many studies reported in literature (De Cesare, 1998; De Cesare and Schleiss, 1999; Bühler *et al.*, 2005; Sequeiros *et al.*, 2009). Sediment concentration within such currents covers a range of 0.2 to70 g/l. When arriving at the dam, the current is slowed down and starts depositing fine sediment, forming a so-called muddy lake.

2.1.3 Measures against reservoir sedimentation

Schleiss and Oehy (2002) as well as Hartmann (2007) provide an inventory of possible measures for sediment management, which include measures in the catchment area, in the reservoir or at the dam (Figure 2.2). Not all of them are sustainable, efficient and affordable. Dam heightening, or the raise of outlet structures for example, do not result in sustainable solutions (Boillat and Delley, 1992). However, the most efficient method would consist in restoring the sediment balance of reservoirs by transferring sediment downstream. Such, the sediment budget across the storage volumes could be assured. Furthermore, sediment management is not limited to the reservoir itself, it extends also to the downstream river, which should be included in a sustainable sediment strategy (Morris and Fan, 1998).

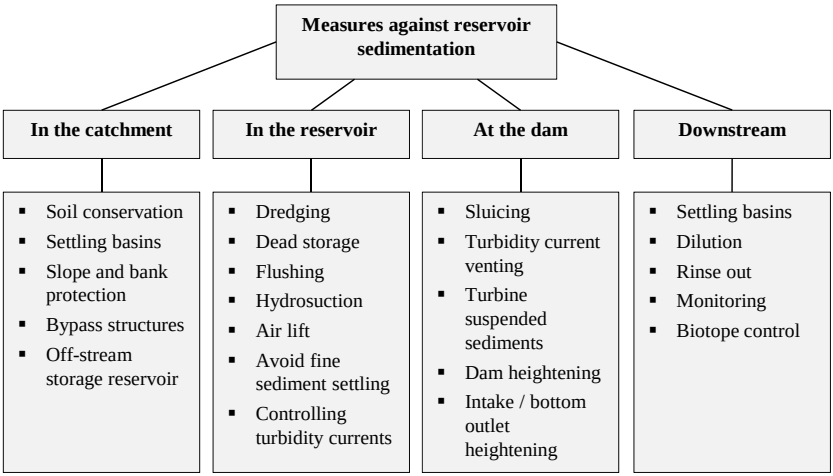

Figure 2.2 Inventory of preventive or retroactive measures for sediment management (Schleiss and Oehy, 2002)

Regarding turbidity current driven sedimentation, several measures have been studied. On the one hand, the incoming sediment-laden flow can be routed under water and through bottom outlets at the dam. This procedure is commonly known as venting. The efficiency of venting operations depends mainly on the timing of opening and closing the gate, as a maximum of the density current should be evacuated with minimum water losses (Chen and Zhao, 1992). In some case, even turbine operation may contribute to partial venting of turbidity currents (Schneider *et al.*, 2007).

On the other hand, methods such as obstacles stopping the current propagation or maintaining particles in suspension in front of intakes to be evacuated by the turbines have been studied by Oehy and Schleiss (2007) and Oehy *et al.* (2010). Latter concept is a promising solution regarding sediment transfer through reservoirs. Jenzer Althaus (2011) investigated the effect of rotating jet induced flow close to intake structures on sediment mixing, also with the objective to proceed to a sediment transfer through the headrace tunnel. However, these measures require construction works for their implementation, whereas the present study focuses on benefiting from turbulent mixing induced only by the operation of the plant.

2.1.4 Effect of pumped-storage operation

Like any other traditional storage hydropower plant, pumped-storage schemes are affected by reservoir sedimentation. The hydraulic structures in reservoirs of such schemes are not only functioning as intake structure for water withdrawal, but also as outlet structure when water is released during turbine or pump operation. Very often, intake and outlet correspond to one and the same structure.

However, new processes might appear, as water is moved back and forth between two storage volumes. Flow conditions and sediment balance of the reservoirs can be changed. When an existing traditional storage hydropower scheme is enhanced to a pumped-storage system, origin and upstream input of sediment remains basically unchanged. However, due to the connection of two storage volumes, fine sediment can be moved from one reservoir to the other and provoke changes in the settling and sedimentation behavior.

When natural storage volumes are connected to artificial reservoirs, the latter can suffer from sedimentation problems. For example, the pumped-storage plant Säckingen in Germany operates water between the Rhine River and the artificial Eggberg Basin, providing a volume of 2.1×10^6 m^3 for mainly daily pumped-storage operation. Over the years, the reservoir was partially filled up with fine sediment originating from the natural “lower reservoir” of the scheme (Figure 2.3). Basin drawdown and mechanical sediment removal were required to regain convenient plant operation. A second pumped-storage scheme of the plant operator Schluchseewerk AG links the artificial Hornberg Basin to the natural Wehra Basin and suffers from similar problems (Klebsattel and Rost, 2010).

With increasing pumped-storage activity, the reservoirs and especially the areas close to intake and outlet structures are submitted to fast and frequent changes between turbulent flow conditions with an inflowing jet and relatively slow potential flow conditions. Therefore, physical and chemical properties of the involved water bodies can be significantly altered (Potter *et al.*, 1982). The mixing processes due to pumped-storage operation were shown to weaken thermal stratification and to affect nutrients and ecosystems in reservoirs and downstream rivers (Girgidov *et al.*, 1990; US Bureau of Reclamation, 1993; Finger *et al.*,

2007). Imboden (1980) developed a mathematical model of vertical temperature structure and predicted a shift of seasonal thermal stratification of Lake Lucerne (Switzerland) due to a hypothetical pumped-storage plant. Bonalumi *et al.* (2011) were of the first to describe effects of pumped-storage operations on particle dynamics.

Figure 2.3 Drawdown of Eggberg Basin for sediment removal in 1992 (photo courtesy of G. Klebsattel)

The degree of disturbance depends on the initial hydrological, sedimentological and ecological conditions of the water body before pumped-storage operation in addition to the layout and exploitation mode of the plant. As such, the water column properties of a relatively small and shallow lake was found not to be altered by pumped-storage operations (Anderson, 2010) while other, bigger reservoirs were highly affected (Imboden, 1980; US Bureau of Reclamation, 1993). However, in most cases an important impact of hydropower operation on stratification could be shown. In some cases, the turbulent kinetic energy (TKE) input from power plants is high enough to keep in suspension small particles or even resuspend fine bottom sediment (US Bureau of Reclamation, 1993). Wolanski *et al.* (1992) present an application in maritime turbulence-induced mixing.

This energy could be used to slow down settling processes in the reservoirs and to eventually evacuate suspended sediment through the power intakes or bottom outlets. However, mixing conditions depend on the pumping and turbine operation, the reservoir shape and the layout of hydraulic inlet and outlet structures. Thus, a potential of positively affecting the sedimentation process by in- and outflow sequences exists.

2.1.5 Sediment settling process

Until now, mainly practical and applied aspects of reservoir sedimentation have been provided. This subchapter states the most important notions and of the main physical processes related to settling processes, from a more theoretical point of view.

Fall velocity of a particle in a fluid is a behavioral property (van Rijn, 1984). The stationary settling velocity w_S (reached after having accelerated) of non-cohesive spherical particles in calm water can be simply described by the fall velocity when flow resistance F_D

(fluid drag force) on the particle is in equilibrium with the gravity force *G* reduced by the buoyancy:

$$F_D = c_D \cdot \rho_s / 2 \cdot w_s^2 \cdot d_s^2 \cdot \frac{\pi}{4} = G = (\rho_s - \rho_w) \cdot g \cdot d_s^3 \cdot \frac{\pi}{6} \quad \text{(Eq. 2.1)}$$

$$w_S = \sqrt{\frac{4}{3} \cdot \frac{(\rho_S - \rho_w) \cdot g \cdot d_S}{\rho_w \cdot c_D}} \quad \text{(Eq. 2.2)}$$

where ρ_s: the density of the particle [kg/m^3],
ρ_w: the density of the fluid [kg/m^3],
d_s: the diameter of the particle [m], and
c_D: the drag coefficient [-].

The drag coefficient c_D depends strongly on the Reynolds number Re_s of the settling process and varies according to different authors:

$$\mathrm{Re}_S = \frac{w_S \cdot d_S}{\nu} \quad \text{(Eq. 2.3)}$$

$$c_D = \frac{24}{\mathrm{Re}_s} \quad \text{(Region of Stokes law, } \mathrm{Re}_s < 0.1\text{)} \quad \text{(Eq. 2.4)}$$

$$c_D = \frac{24}{\mathrm{Re}_S} \cdot \left(1 + \frac{3}{16}\mathrm{Re}_S\right) \quad 0.1 < \mathrm{Re}_s < 1.0 \text{ (Oseen, 1972)} \quad \text{(Eq. 2.5)}$$

$$c_D = \frac{24}{\mathrm{Re}_s} + \frac{4}{\sqrt{\mathrm{Re}_s}} + 0.4 \quad 1.0 < \mathrm{Re}_s < 2 \text{ x } 10^5 \text{ (Kaskas, 1970)} \quad \text{(Eq. 2.6)}$$

Brown and Lawler (2003) provide an expression for c_D valuable for all viscosities $\nu \leq 2 \text{ x } 10^{-5}$ m^2/s:

$$c_D = \frac{24}{\mathrm{Re}_s} \cdot \left(1 + 0.150 \cdot \mathrm{Re}_s^{0.681}\right) + \frac{0.407}{1 + \frac{8.71}{\mathrm{Re}_s}} \quad \text{(Eq. 2.7)}$$

For laminar flows the particle friction forces are dominant while for turbulent flows, the inertial forces define the flow resistance. Outside the Stokes region, c_D decreases rapidly and becomes nearly constant for $10^3 < \mathrm{Re}_s < 10^5$, yielding w_s proportional to $d_S^{0.5}$. For larger Reynolds numbers the literature gives numerous empirical relationships between c_D and Re_s (Zanke, 1982). Bouvard (1984) collected and compared several analyses of the settling velocity of different authors.

Two more parameters influence the settling velocity: the shape of the particles *SF* as well as sediment concentration. For non-spherical particles *SF* should be considered:

$$SF = \frac{c_S}{\sqrt{a_S \cdot b_S}} \quad \text{(Eq. 2.8)}$$

where a_s, b_s: the diameters of the particle [m], and
c_s: the diameter for the shortest axis [m].

The shape effect is largest for relatively large particles ($d_S > 300$ µm) which deviate more from a sphere than small particles. Experiments show differences in settling velocity of around 30% for $0.5 \leq SF \leq 1.0$. The influence of particle size is given as follows (van Rijn, 1984):

$$w_s = \frac{(\rho_s/\rho_w - 1)\cdot g \cdot d_s^{\,2}}{18\cdot \upsilon} \qquad \text{for } 1 < d_s \leq 100\ \mu\text{m} \qquad \text{(Eq. 2.9)}$$

$$w_s = \frac{10\upsilon}{d}\cdot\left(1+\frac{0.01\cdot(\rho_s/\rho_w - 1)\cdot g \cdot d_s^{\,3}}{\upsilon^2}\right) \qquad \text{for } 100 < d_s \leq 1000\ \mu\text{m} \qquad \text{(Eq. 2.10)}$$

$$w_S = 1.1\cdot\sqrt{(\rho_S/\rho_w - 1)\cdot g \cdot d_S} \qquad \text{for } d_s > 1000\ \mu\text{m} \qquad \text{(Eq. 2.11)}$$

The settling velocity of a single particle is higher than of a cloud of particles. This effect is commonly known as hindered settling and caused by the fluid return flow induced by the settling velocities. In this state of fluidization, the upward drag forces on the particles become equal to the downward gravity forces, resulting in no net vertical movement of the particles. According to Oliver (1961) the fall velocity in a fluid-sediment suspension is:

$$w_{S,m} = (1 - 2.15\cdot c)\cdot(1 - 0.75\cdot c^{0.33})\cdot w_S \qquad \text{(Eq. 2.12)}$$

where $w_{s,m}$: the particle settling velocity in fluid with suspended material [m/s],
w_s: the particle settling velocity in a clear fluid [m/s], and
c: volumetric sediment concentration [-]

2.2 Main jet mixing notions

The objective of maintaining fine sediment suspended by in- and outflow sequences similar to pumped-storage operation is linked to jet mixing phenomena. In fact, when water is injected through the intake/outlet structure into a reservoir, a jet is formed. In the laboratory experiments, a so-called submerged turbulent jet develops during inflow sequences. Thus, the basic notions of such phenomena are given hereafter. Further literature on jet induced mixing is resumed in the work of Jenzer Althaus (2011).

2.2.1 Submerged turbulent jet

A jet is a source of momentum and energy in a fluid reservoir. According to Revill (1992) a jet is fully turbulent when its Reynolds number $\text{Re}_j \geq 1'000$ to $2'000$ and laminar for $\text{Re}_j < 100$. Blevins (1984) gives a limit between laminar and turbulent jet of $\text{Re}_j = 3'000$.

A submerged turbulent jet consists in an initial core, a transition zone and a fully developed jet region (Figure 2.4, Blevins (1984)). The core flow is nearly free of shear and its velocity is equal to the nozzle exit velocity v_0 under uniform inflow conditions. The core flow is surrounded by a turbulent shear or mixing layer, forming a boundary between the core flow and the reservoir fluid. The imprint of the nozzle shape disappears when the turbulent eddies in the shear layer destroy the nozzle core flow and penetrate to the jet axis. The resulting eddy-dominated flow is called fully developed and starts at a distance between 4.3 and 10 D_j from the nozzle. After about 400 D_j, the mixing effect of a turbulent jet is generally considered as insignificant (Revill, 1992).

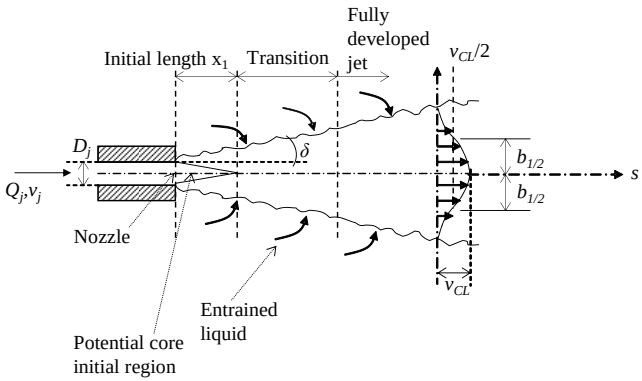

Figure 2.4 Jet flow behavior according to Blevins (1984)

The main characteristics of a jet are its momentum flux M_j, discharge Q_j. and Reynolds number Re_j:

$$M_j = v_0^2 \cdot A_j \qquad \text{(Eq. 2.13)}$$

$$Q_j = v_0 \cdot A_j \qquad \text{(Eq. 2.14)}$$

$$\mathrm{Re}_j = \frac{v_0 \cdot D_j}{\upsilon} \qquad \text{(Eq. 2.15)}$$

where v_0: the efflux velocity [m/s],
A_j: the outlet section [m^2],
D_j: the pipe diameter [m], and
v: the fluid viscosity [m^2/s].

The densimetric jet Froude number is:

$$Fr_j = \frac{v_j}{\sqrt{g' \cdot D_j}} \qquad \text{(Eq. 2.16)}$$

where $g' = g \cdot \left(\frac{\rho_S - \rho_w}{\rho_w} \right)$ the reduced gravitational acceleration.

For axisymmetric flow at constant pressure, the momentum equation becomes (in polar coordinates):

$$u\frac{\partial u}{\partial s} + v\frac{\partial u}{\partial r} = -\frac{1}{r}\frac{\partial}{\partial r}\left(\nu r \frac{\partial u}{\partial r} - r\,\overline{u'v'} \right) \qquad \text{(Eq. 2.17)}$$

where $\overline{u'v'}$: the turbulent shear stress.

The continuity equation is written as (in polar coordinates):

$$\frac{\partial u}{\partial s} + \frac{1}{r}\frac{\partial rv}{\partial r} = 0 \qquad \text{(Eq. 2.18)}$$

2.2.2 Centerline jet velocity

In the fully developed jet region, the centerline velocity v_{CL} continuously decreases with the distance s in jet direction. Many authors defined the centerline velocity as

$$v_{CL}(s) = C_1 \cdot \frac{v_0 \cdot D_j}{s} \qquad \text{(Eq. 2.19)}$$

where C_1: a constant [-], and
s: the distance from the nozzle.

Abramovich (1963) gives a value of $C_1 = 7.32$, while Revill (1992) and Blevins (1984) found $C_1 = 6$. Rajaratnam (1976) presents results from several studies, in which C_1 ranges from 5.75 to 7.32. Jirka (2004) provides a slightly different formulation of the centerline velocity, resulting in $C_1 = 6.43$.

2.2.3 Velocity at transverse distance

When the jet enters the basin, it expands at an expansion angle δ. In the literature δ between 15° and 25° are found for jet Reynolds numbers $\mathrm{Re}_j > 100$ (Wasewar, 2006). At the transverse distance $r = b_{1/2}$ from the jet axis, axial velocity $v(r)$ falls to half of the centerline velocity v_{CL}. Assuming a Gaussian distribution over the jet width, the velocity at transverse distance r in s direction can be written as:

$$v\left(r = b_{1/2}\right) = C_2 \cdot \frac{v_{CL}}{2};\; v(r) = v_{CL} \cdot e^{-C_3\left(r^2/s^2\right)} \qquad \text{(Eq. 2.20)}$$

where C_2, C_3: constants [-].

Values of $C_2 = 0.082$ to 0.1 and $C_3 = 70$ to 104.1 are found in literature (Abramovich, 1963; Rajaratnam, 1976; Blevins, 1984). Jirka (2004) assumed a Gaussian distribution with a slightly different correlation between jet width and centerline velocity, resulting in $C_3 = 82.6$.

2.2.4 Volume flux due to entrainment

The total volume flux $Q(s)$ increases with distance s from the nozzle due to lateral entrainment. The volumetric flow rate of the bulk liquid entrained by the jet Q_e is difficult to measure and the available experimental data are widely scattered. Jirka (2004) describes the volume flux as a function of the square root of the momentum at the nozzle, and Blevins (1984) writes a simple expression with the discharge at the nozzle and the nozzle diameter. Developing the expression of Jirka (2004), it agrees with Blevins (1984). Donald and Singer (1959) give the total volumetric flow rate in the jets as a function of the same parameters and additionally consider kinematic viscosity:

$$Q(s) = \sqrt{2\pi} \cdot 2 \cdot \alpha_{jet} \cdot \sqrt{M_j} \cdot s = 4 \cdot \sqrt{2} \cdot \alpha_{jet} \cdot \frac{s}{D_j} \cdot Q_j \qquad \text{Jirka (2004)} \qquad \text{(Eq. 2.21)}$$

$$Q(s) = 0.32 \cdot \frac{s}{D_j} \cdot Q_j \qquad \text{Blevins (1984)} \qquad \text{(Eq. 2.22)}$$

$$Q(s) = Q_j \cdot \left(\frac{0.576 \cdot \nu^{0.133} \cdot s}{D_j} \right) \qquad \text{Donald and Singer (1959)} \qquad \text{(Eq. 2.23)}$$

The liquid entrained per unit time at the distance s from the nozzle, Q_e is described as follows (Wasewar, 2006):

$$Q_e = \left(0.234 \cdot \frac{s}{D_j} - 1 \right) \cdot Q_j \qquad \text{(Eq. 2.24)}$$

2.2.5 Jet mixing

In jet mixers, a fast moving jet stream of liquid is injected into a slow moving or stationary bulk liquid. The relative velocity between the jet and the bulk liquid creates a turbulent mixing layer at the jet boundary. This mixing layer grows in the direction of the jet flow, entraining and mixing the jet liquid with the bulk liquid. As a result, the jet grows in diameter but its centreline velocity and the turbulence of jet reduce in magnitude because the jet flow momentum is spread over a steadily increasing flow area. In addition to entrainment, strong shear stresses exist at the boundary between the jet and the surrounding liquid. These stresses tear off eddies at the boundary and generate considerable turbulence, which also contributes to the mixing action.

Wasewar (2006) gives a critical analysis of the available literature data and some general conclusions concerning the various parameters. The influence of the tank dimensions in cylindrical tanks, jet characteristics like the jet velocity, jet diameter and their product, jet Reynolds number, and jet Froude number, the jet location, jet angle and jet length, and multiple jets on mixing time has been reported. Some authors studied the influence of the residence time and circulation time on mixing time; others investigated the flow patterns in respect to mixing time (Stefan and Gu, 1992; Chhabra *et al.*, 2005; Liang and Maxworthy, 2008; Hsiao *et al.*, 2010).

Numerous experimental works on sedimentation and deposition from particle laden turbulent jets and plumes have been carried out (Ernst *et al.*, 1996; Cardoso and Zarrebini, 2001a, 2001b; Lane-Serff and Moran, 2005; Cuthbertson and Davies, 2008). However, the effect of repetitive in- and outflow sequences and the influence of their amplitude and frequency on fine sediment behavior have not been investigated so far.

2.3 Monitoring methods

Hydropower plants are usually equipped with a control and management system operated by the plant owner. Very often, detailed monitoring is applied on mechanical or electrical equipment of the plants or the important civil engineering works such as dams and pressurized shafts and tunnels. Real-time measurement of flow patterns in a reservoir or turbidity in the pressurized system are rather rare, but could provide important information to the plant operator, i.e. about the response of the water body to specific operation scenarios or the sediment concentration in front of intake/outlet structures.

2.3.1 Flow patterns in reservoirs

Monitoring of flow conditions by Acoustic Doppler Velocity Profilers (ADCP) is commonly used for sampling in rivers, lakes and estuaries and provide a non-intrusive measurement technique, i.e. without disturbing the recorded flow field (Gordon *et al.*, 1999; Cook *et al.*, 2007). Several authors report the use of ADCP for discharge measurements or concentrations

of suspended solids (Gartner, 2004; Kostaschuk *et al.*, 2005). Early long-term measurements were carried out by Schott and Johns (1987) who installed an upward-looking instrument in the Somali Current and recorded data for more than six months. In situ measurements are often used to calibrate numerical or mathematical models or to compare prototype results to physical modeling (Kostaschuk *et al.*, 2005; Laval *et al.*, 2005; Elci *et al.*, 2007).

Velocity measurements in front of intake structures are applied either to design the civil engineering works or to observe and confirm their adequate functioning and their influence on the flow conditions. Goto and Tsuchiyama (1998), Vermeyen (2003) and Dorfmann and Knoblauch (2008) used vessel mounted ADCP to study flow fields in a reservoir, to define withdrawal for stratified and destratified reservoir conditions and to develop flushing concepts for a run-of-river power plant. Cook *et al.* (2007) as well as Vermeyen (2002) fixed downward-looking instruments close to power intakes to study velocities at a Kaplan turbine draft tube and provide information about flow velocities previous to conducting diving operations.

Furthermore, ADCP permit to record eventual longitudinal or transversal movement of the reservoir (internal seiches, Munnich *et al.* (1992); Stevens and Lawrence (1997); Lemmin *et al.* (2005); Bouffard (2008)).

Thus, this sampling method is well adapted for prototype monitoring purpose and was applied in the present research in a Swiss Alpine reservoir.

2.3.2 Turbidity monitoring

Turbidity measurements to determine suspended sediment concentration in water volumes are not novel. However, most applications are aiming river sampling, while monitoring in power plants is not commonly applied. Gray and Gartner (2009) summarize different monitoring techniques for suspended sediment, focusing on river applications. Minella *et al.* (2008) discusses calibration issues when suspended sediment concentration is derived from turbidity measurements. Orwin and Smart (2005) propose a turbidity measuring device for proglacial streams. Most applications in hydropower plants are aiming to detect the arrival of turbidity currents in front of hydraulic outlet structures in order to proceed to venting operations (Müller and De Cesare, 2009).

Chapter 3

In situ measurement and numerical modeling of flow fields in a reservoir subject to pumped-storage operation

To describe flow patterns in a reservoir subject to pumped-storage operation, in situ measurements were carried out in Lake Grimsel, the lower reservoir of the Grimsel 2 pumped-storage plant in the Swiss Alps. Three upward-looking frame-mounted Acoustic Doppler Current Profilers (ADCP) placed on the reservoir bottom measured water column flow velocities at seven locations near the intake/outlet structure of the plant.

One- and two-dimensional velocity profiles in front of the water intake were measured, analyzed and compared to the hydropower operation series. Water withdrawal by pumping (outflow) only marginally affects the flow patterns in front of the intake, whereas water injected during turbine mode lead to important backflow above the reservoir bottom, a preferred inflow sector and the generation of a large scale recirculation cell confined by the topography of the lake bottom. Periods without any pumped-storage activity are marked by non-structured movement in the water body. Frequency analysis of the recorded velocities shows that sampled flow patterns are correlated to pumped-storage cycles.

Simulations in a numerical model could reproduce in situ conditions. The main characteristics of flow patterns in front of the intake/outlet are represented adequately. Temporal evolution of flow patterns could be analyzed and a sensitivity study on temperature difference between effluent and resident water was carried out.

Turbulent kinetic energy input due to turbine operation is estimated and compared to energy input by wind-forcing. Lake Grimsel is subject to high energy inputs during turbine mode, leading to destratification of the water column, as well as slowing down the settling of fine particles.

3.1 Introduction

Over the last decades, pumped-storage hydropower plants have gained in importance since they allow short-term regulation of the power grid, storing energy during low demand and generating peak electricity. Such facilities normally consist of two reservoirs at different elevations, between which water is moved up and down. Like in traditional storage hydropower plants, these reservoirs are often subject to sedimentation which reduces reservoir capacity, impacting operational and structural safety (Graf, 1982; ICOLD, 1989; Schleiss *et al.*, 2010). Sediment originate from the rivers which lose transport capacity due to the impoundment by an artificial dam and the consequent drop of flow velocities. In pumped-storage reservoirs, sediment inflow can also result from the connection of two initially separated systems, i.e. particles can be transferred from one reservoir to the other. In the framework of the consortium *HydroNet – Modern Methodologies for Design, Manufacturing and Operation of pumped-storage power plants*, sedimentation issues in reservoirs of such schemes are studied focusing on prototype monitoring methods for flow conditions and fine sediment transport.

With increasing pumped-storage activity, the reservoirs and especially the areas close to intake and outlet structures are subjected to fast and frequent changes between turbulent flow conditions with an inflowing jet and relatively slow potential flow conditions. Therefore, physical and chemical properties of the involved water bodies can be significantly altered (Potter *et al.*, 1982). The mixing processes due to pumped-storage operation were shown to weaken thermal stratification and to affect nutrients and ecosystems in reservoirs and downstream rivers (Girgidov *et al.*, 1990; US Bureau of Reclamation, 1993; Finger *et al.*, 2007). Imboden (1980) developed a mathematical model of vertical temperature structure and predicted a shift of seasonal thermal stratification of Lake Lucerne (Switzerland) due to a hypothetical pumped-storage plant. The degree of disturbance depends on the initial hydrological, sedimentological and ecological conditions of the water body before pumped-storage operation in addition to the layout and exploitation mode of the plant. As such, the water column properties of a relatively small and shallow lake was found not to be altered by pumped-storage operations (Anderson, 2010) while other, bigger reservoirs were highly affected (Imboden, 1980; US Bureau of Reclamation, 1993). However, in most cases an important impact of hydropower operation could be shown.

In some cases, the turbulent kinetic energy (TKE) input from power plants is high enough to keep in suspension small particles or even resuspend fine bottom sediment (US Bureau of Reclamation, 1993). Wolanski *et al.* (1992) present an application in maritime turbulence-induced mixing. This energy could be used to disrupt settling processes in the reservoirs and to eventually evacuate suspended sediment through the power intakes or bottom outlets. However, mixing conditions depend on the pumping and turbine operation, the reservoir shape and the layout of hydraulic inlet and outlet structures. Thus, a potential of positively affecting the sedimentation process by in- and outflow sequences exists.

Knowledge of flow conditions in front of intake/outlet structures during in- and outflow sequences is required to estimate the potential of keeping fine sediment in suspension. Therefore, the objective of this study was to implement a possible long-term monitoring method, for flow patterns in an Alpine reservoir, namely Acoustic Doppler Current Profilers (ADCP). Velocity profiles were recorded near the intake/outlet structure to define the impact of the hydropower operation on flow fields.

The chapter introduces the study site and presents the ADCP measuring equipment. Then, the recorded one- and two-dimensional velocity profiles in front of the intake/outlet are presented and compared to the turbine and pumping sequences of the power plant as well as to simulated flow patterns. Finally, the turbulence induced by the pumped-storage operations and its application to (re)suspend fine sediment are discussed.

3.2 Investigation Site

The Oberhasli region is located in Berne canton, in the central Alps of Switzerland. In the beginning of the 20th century, the area was recognized as being particularity appropriate for hydropower exploitation. The favorable hydrological, geological and topographical conditions led to the construction of a complex system of dams, water intakes, waterways and power plants since the 1930s. Today, Kraftwerke Oberhasli AG (KWO) operates nine power plants fed by eight main reservoirs, the largest being Lake Grimsel, Oberaar and Räterichsboden.

3.2.1 Reservoir characteristics

Since 1982, the Grimsel 2 pumped-storage power plant has operated water from Lake Oberaar and Grimsel located at 2303 and 1909 m a.s.l. respectively. Lake Oberaar (Oa), impounded by the Oberaar gravity dam, provides an exploitable storage volume of 57 x 10^6 m^3 and has a maximum depth of 90 m. Lake Grimsel (Gr), impounded by the Spittellamm arch dam and the Seeuferegg gravity dam, has a gross storage volume of 95 x 10^6 m^3 and a maximum depth of 100 m. The two lakes are connected by a 5 km long pressurized waterway, guiding the water from the two intake/outlet structures to the power house Grimsel 2. Figure 3.1 gives an overview of the location and the layout of the pumped-storage scheme.

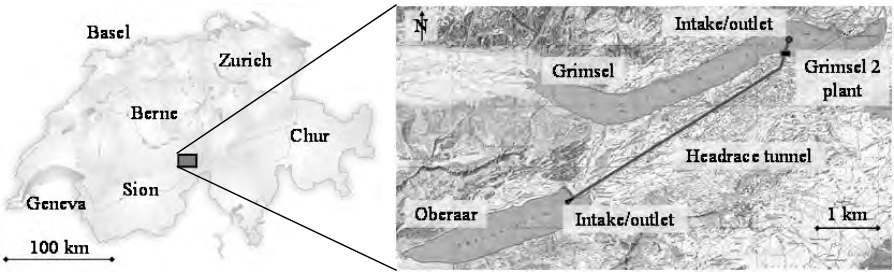

Figure 3.1 Location map and layout of the Grimsel 2 pumped-storage scheme

A volume of about 600 to 700 x 10^6 m^3 of water is pumped annually from Lake Grimsel into Lake Oberaar and moved back during turbine mode. Thus, the volumes of the lower and upper reservoir are exchanged several times throughout one year of hydropower operation.

The catchment areas of the two reservoirs are partly glaciated. Denudation rate is 1 to 2 mm/year (Anselmetti *et al.*, 2007), leading to high sediment supply, generally above 50 mg/l (Finger *et al.*, 2006). The sediment characteristics of this “glacier milk” in both lakes were recently investigated by Bühler and Siegenthaler (2003) and Bonalumi *et al.* (2011). Anselmetti *et al.* (2007) showed that since hydropower exploitation, approximately 85% of

the annual sediment supply of 272 kt/year settles in the reservoirs, while only 40 kt/year are released downstream. To slow down sedimentation, small particles could be maintained in suspension by pumped-storage operation. Downstream transfer or evacuation of fine sediment would be possible through the power intakes and the bottom outlets at Spittellamm dam.

In situ measurements by Bonalumi *et al.* (2011) showed that the two reservoirs are ice-covered and inversely stratified in winter. In Lake Oberaar, a water temperature of T_w = 2.5 °C was measured along the entire water column except for the first two meters below the ice, where T_w = 0 °C. In Lake Grimsel, below the slightly thicker transition layer, temperature remains stable at T_w = 2.5 °C. In summer, both reservoirs are ice-free and thermally stratified, with surface temperatures reaching T_w = 14 to 15 °C in the upper and 10 °C in the lower reservoir. In Lake Oberaar, the thermocline is located at 15 m depth and bottom temperature is about T_w = 4 °C, while Lake Grimsel has no well-defined thermocline and a bottom temperature of some T_w = 5 °C.

3.2.2 Intake/outlet specifications

At the foot of a 750 m long inclined steel-lined shaft, four independent pump-turbine units are located in the Grimsel 2 underground power house and provide a capacity of 350 MW. The power house is linked by a pressure tunnel of diameter D = 7.50 m to the intake/outlet structure in Lake Grimsel, where discharges up to Q_{Turb} = 93 m^3/s are injected during turbine mode. During pumping mode, a maximum discharge of Q_{Pump} = 80 m^3/s is withdrawn.

The Lake Grimsel intake/outlet is a submerged circular structure (Figure 3.2) embedded in a recess of the lake topography, with its foundation platform located at 1842 m a.s.l. The lateral open cylinder has an effective height H_i = 6.25 m and a diameter D_i = 21.70 m. Ten guiding walls are supposed to equally distribute the out-flowing discharge on the ten sectors of the tulip. Considering the diameter and the height of the structure, the circumferential outflow section is A_i = 65.35 m^2. However, the effective in-/outflow section is reduced to $A_{i,eff}$ = 15.63 m^2 by a dense trash rack which was found to be the most effective measure to guarantee uniform flow distribution at the circumferential section (VAW, 1982).

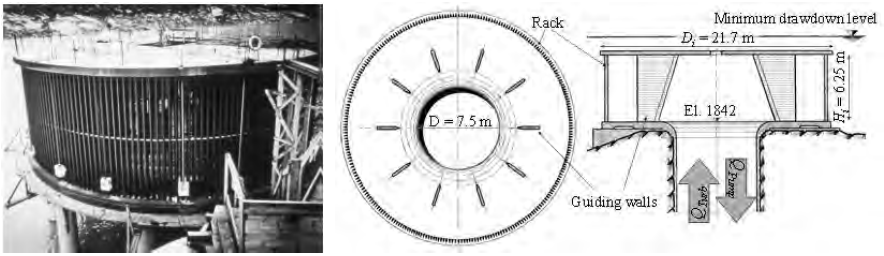

a) b) c)

Figure 3.2 Grimsel 2 intake/outlet structure in Lake Grimsel; photo during construction period (a, source: IUB Engineering AG), schematic plan view (b) and cross section (c, source: KWO archives)

Considering operational discharges and assuming uniform flow distribution in the cross sections, water is injected at a speed of up to v = 2.1 m/s at the shaft end. At the trash rack,

flow velocities of almost v = 1.0 m/s should be observed. Minimum drawdown level of Lake Grimsel is 1850 m a.s.l., resulting in an intake submergence of 2 m.

Close to Spittellamm Dam, a second intake structure is located at 1833 m a.s.l. to feed the Grimsel 1 power plant between Lake Grimsel and Räterichsboden and deviate water into Lake Gelmer, feeding the Handeck 1 plant. As the potential velocity field in front of intakes decreases with the square of distance from the structure, withdrawal by the Gelmer/Grimsel 1 intake is not expected to directly influence the flow patterns in front of the Grimsel 2 intake/outlet.

However, other studies carried out on pumped-storage reservoirs have shown that a sediment-laden inflowing jet from an intake/outlet structure can be guided toward another intake or a bottom outlet. As a consequence, the potential of transferring turbid water through the reservoir depends on the intake/outlet geometry, the layout of the hydraulic works and the lake bathymetry. Lake Grimsel is unlikely to provide adequate conditions for this concept, as the inflowing jet is injected circumferentially from the outlet into the reservoir and thus not clearly oriented. Nevertheless, it was briefly analyzed in the numerical model, to see if water injected from Grimsel 2 can reach the Grimsel 1 intake for downstream sediment transfer to Lake Räterichsboden.

3.3 Methods

Acoustic Doppler Velocity Profilers (ADCP) are commonly used for flow velocity sampling in rivers, lakes and estuaries and provide a non-intrusive measurement technique, i.e. without disturbing the recorded flow field (Gordon *et al.*, 1999; Cook *et al.*, 2007). Several authors report the use of ADCP for discharge measurements or concentrations of suspended solids (Gartner, 2004; Kostaschuk *et al.*, 2005). Early long-term measurements were carried out by Schott and Johns (1987) who installed an upward-looking instrument in the Somali Current and recorded data for more than six months. In situ measurements are often used to calibrate numerical or mathematical models or to compare prototype results to physical modeling (Kostaschuk *et al.*, 2005; Laval *et al.*, 2005; Elci *et al.*, 2007).

Velocity measurements in front of intake structures are applied either to design the civil engineering works or to observe and confirm their adequate functioning and their influence on the flow conditions. Goto and Tsuchiyama (1998), Vermeyen (2003) and Dorfmann and Knoblauch (2008) used vessel mounted ADCP to study flow fields in a reservoir, to define withdrawal for stratified and destratified reservoir conditions and to develop flushing concepts for a run-of-river power plant. Cook *et al.* (2007) as well as Vermeyen (2002) fixed downward-looking instruments close to power intakes to study velocities at a Kaplan turbine draft tube and provide information about flow velocities previous to conducting diving operations.

3.3.1 ADCP settings

In the current study, flow velocity data were recorded by three 300 kHz ADCP (Teledyne RDI, USA). Together with a 12 V lead-acid battery (Yuasa, UK), each unit was mounted on an aluminum and PVC frame, positioned on the bottom of the Grimsel reservoir and fixed to a mooring buoy. Dual axis gimbals guaranteed a permanent upward-orientation of the instrument.

The low frequency four beam ADCP sampled the entire water column and were operated with a bin length of 1.0 m and a fixed number of 85 bins. In this configuration, measurement error on horizontal velocity components is +/- 12 mm/s. The mooring height of the device of 0.8 m and the profiler blanking distance of 2.96 m placed the first recording bin at 3.7 m above the reservoir bottom. Consequently, current profiles were registered from 3.7 m up to 75.0 m above the reservoir bottom, according to the lake level during measurement periods. The cells located above the reservoir surface were omitted.

3.3.2 Profiler position

The alignments of the three ADCP measurement lines were chosen according to the intake/outlet geometry and surrounding topography. Assuming an equally distributed discharge over the ten sectors (Figure 3.2), the measuring devices were aligned along the supposed main directions of the inflowing jets. The bathymetry of Lake Grimsel restricted the implementation possibilities for the devices as relatively steep rock slopes surround the intake/outlet structure in the West. Eastward, in the direction of Spittellamm dam, the reservoir bottom is flat according to topographical records carried out in 2006 (FLOTRON AG, 2006) and situated almost 10 m below the intake level. This invert area provides most suitable conditions for velocity sampling since it guarantees a stable position of the ADCP and provides maximum data sampling on the water column.

Additionally, adequate locations of the profilers avoid interference between the emitted ultrasonic beam and the concrete civil engineering works or the beam of the neighboring unit. Considering the maximum sampling height of 75 m and the 20° beam angle of the profiler, the ADCP were placed at 50, 150 and 250 m from the intake in the flat Eastern part of the reservoir, and at 30 and 90 m from the intake/outlet in the steeper Northern and Southern part (Figure 3.3). The closest device to the intake/outlet is named P1, the farthest P3.

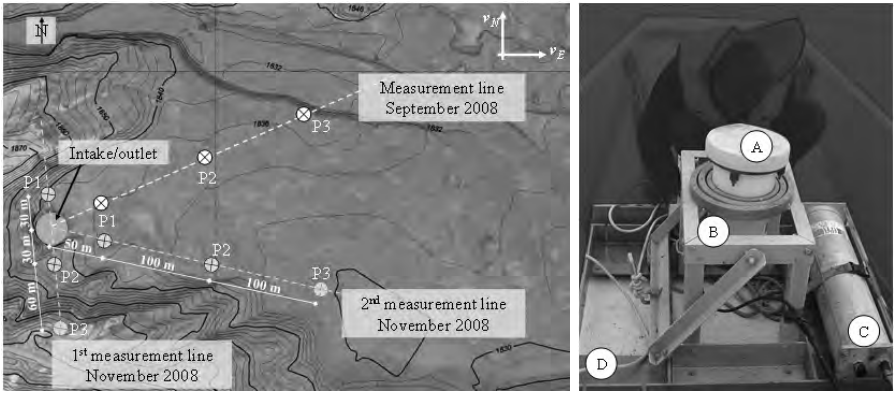

a) b)

Figure 3.3 Lake Grimsel bathymetry and positions of the ADCP for the three measurement periods (a) and photo of the frame-mounted ADCP device (b); A is the upward-looking ADCP instrument (with protection cap); B, the dual axis gimbals; C, the power supply and D, the aluminum/PVC frame

During the first campaign in September 2008, the ADCP were placed on the flat part of the reservoir bottom in line with the outlet sector orientated in the main geographical orientation of Lake Grimsel (E-NE). From a vessel, the ADCP were placed at the corresponding profiler positions controlled by GPS (Geko, Garmin, USA). A manual echo sounder allowed measuring the water depth to confirm the foreseen recording depth of the instrument. Positioning accuracy was +/- 5 m in both East and North direction.

According to results of this first sampling period, the two other measurement lines were defined for the second campaign in November 2008. The first was orientated almost exactly N-S, the second again in the flat part, in E-SE. Beside the influence of in- and outflow on the flow patterns in front of the intake/outlet, this profiler position allows evaluation of reservoir bathymetry effects and eventual longitudinal or transversal movement of the entire lake (internal seiches). The latters are large scale dynamics and have been investigated by Stevens and Lawrence (1997) for several Canadian lakes and reservoirs, as well as by Bouffard (2008) and Lemmin *et al.* (2005) for lake Geneva in Switzerland. Munnich *et al.* (1992) investigated vertical seiche modes and calculated horizontal velocities of 2 to 4 cm/s on the bottom of the 33 m deep Lake Alpnach in Switzerland.

3.3.3 Velocity and water temperature data from ADCP

During the first in situ campaign, the ADCP data were recorded for 5 days from September 15th to 20th. In November 2008, sampling went on for two more weeks from November 6th to 20th. Due to technical problems of P3, only two ADCP were operational in November. Pitch and roll movement were recorded by the ADCP, defining the moment of stabilized samplings for reliable recording periods. KWO provided Grimsel 2 operation discharges and Lake Grimsel level (Gr, Figure 3.4) for the measurement periods.

For September 2008, reliable data were recorded from Monday to Friday September 16th 00:00 to 19th 12:00 (called *Sept*). As shown in Figure 3.4a, turbine sequences were predominant during this term, while pumping activity was moderate during nighttime. Three times, the plant was operated at maximum discharge over 1 to 3 h. In November, data were available from Friday November 7th 00:00 to Tuesday 11th 12:00 for the first (*Nov1*) and from Wednesday November 12th 00:00 to Thursday 19th 12:00 for the second measurement line (*Nov2*). That sampling period included main pumping sequences during the night and especially during the weekends, whereas the turbines were run at reduced capacity during most of the sequences (Figure 3.4b & c). Consequently, flow velocities were registered for a large spectrum of in- and outflow sequences, including relatively long periods of turbine mode during weekdays and pumping mode during weekends, but also short-term alternating pumped-storage cycles.

Over the reliable sampling periods, the ADCP recorded East- and North-velocity components on the water column at a time increment of 5 minutes.

Pressures recorded by the ADCP allow determining exact altitude of the devices on the reservoir bottom. Data reveal that the instruments are placed slightly higher than predicted due to evolution of reservoir bottom since 2006 and positioning error. Table 3.1 gives the altitude of the ADCP and the corresponding first bin of velocity recording. Except for the Nov1 campaign where ADCP were placed in the steeper surroundings of the intake/outlet, the first sampling bin is always located below the intake/outlet platform and permits to cover the entire in- and outflow section.

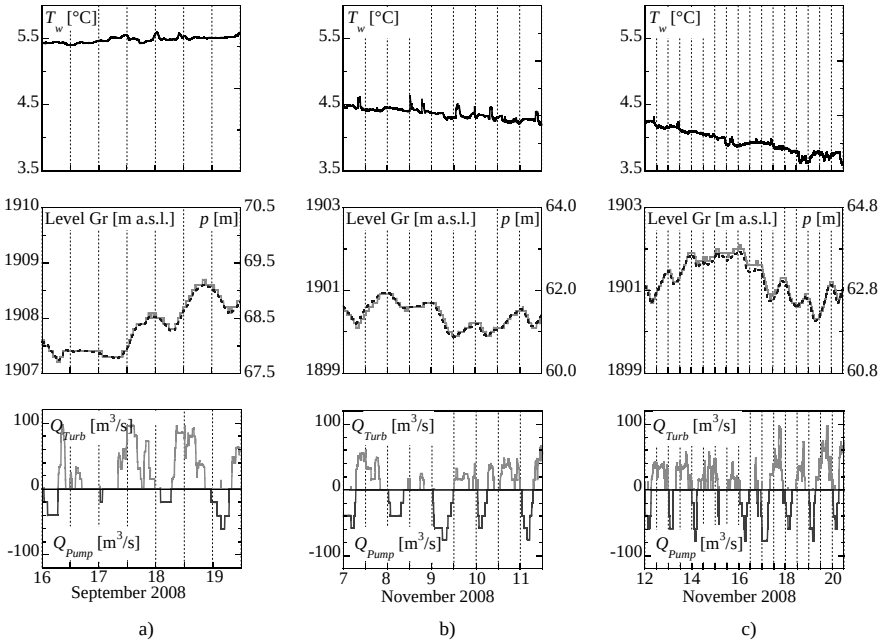

Figure 3.4 Temperature T_w on the reservoir bottom recorded by P1 (top), Lake Grimsel level (Gr, dashed line) and pressure p recorded by P1 (middle) and pumped-storage discharge $Q_{Turb,\ Pump}$ of Grimsel 2 plant (bottom) during ADCP sampling periods Sept (a), Nov1 (b) and Nov2 (c)

Table 3.1 Altitude [m a.s.l.] of ADCP instruments and of the first sampling point as well as Lake Grimsel level

		P1	P2	P3	Lake Grimsel level
Sept	Device	1839.0	1840.0	1835.0	1907.2 – 1908.6 (1910*)
	1st bin	1842.0	1843.0	1838.0	
Nov1	Device	1839.0	1845.0	1863.0	1899.9 – 1900.9 (1900*)
	1st bin	1842.0	1848.0	1866.0	
Nov2	Device	1838.0	1835.0	1835.0	1900.3 – 1901.9 (1900*)
	1st bin	1841.0	1838.0	1838.0	

*constant value assumed for numerical simulations

The first 20 to 30 m from the instrument include reliable velocity records before excessive values start indicating a lack of sound scatterers. These high velocities arise from insufficient suspended particles in the measuring cell to get a representative velocity average over the sampled water volume, so that standard deviation of the velocity for these cells is much larger. Thus, no reliable data were recorded over an intermediate zone of about 30 m until the free surface, which is marked again by unreliable excessive values due to more intense signal returns from the water-air interface.

Temperature measured on the lake bottom remained almost constant at T_w = 5.5 °C in September (Figure 3.4a), with variations of +/-0.15°C. During November campaigns, a continuous decrease from T_w = 4.5 to 3.5 °C indicates the process toward inversely stratified reservoir conditions (Figure 3.4b & c). Mid-term evolution of deep water temperature seems not to be affected by the pumped-storage activity. However, most peaks recorded by the ADCP closest to the intake/outlet correspond to turbine operations and are probably related to the heat dissipation by the hydraulic machines.

3.3.4 Meteorological data

Wind direction and wind speed data for seiche estimations and turbulent kinetic energy (TKE) input were taken from the weather station "Grimsel Hospitz" located next to Spittellamm Dam, provided by the *Swiss Federal Office of Meteorology and Climatology* (MeteoSwiss) and the *Swiss Federal Office of Energy* (SFOE). As the weather station was out of order in September 2008, no data are available for the first measuring campaign. For the three weeks measuring period in November 2008, data at a time interval of 10 minutes was considered. Main wind direction was transversal to Lake Grimsel, direction S and S-SE, with maximum wind speed up to U_a = 12 m/s (Figure 3.5a). Air temperature varied from T_a = -5 to 5 °C and precipitation was limited to less than P = 1 mm over relatively short periods. No important rainfall or flood event is thus expected to affect flow conditions in the lake.

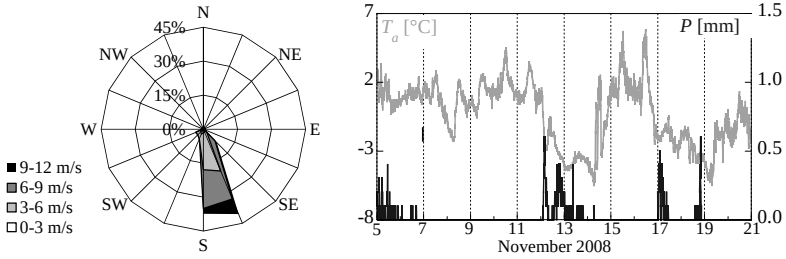

Figure 3.5 Wind direction and magnitude (a) and evolution of air temperature T_a and precipitation P (b) for the period from November 5th to 21st 2008

3.4 Numerical model

The flow conditions in Lake Grimsel corresponding to the three measurement periods were simulated numerically in an ANSYS-CFD model to study eventual influence of bathymetrical conditions on the jet direction and backflow zones in the reservoir. Three basic scenarios were studied, corresponding to the three in situ measurement periods (Table 3.1). Additional simulations were carried out on the first turbine sequence of the September scenario to study the sensitivity to temperature differences between the injected and the resident water.

3.4.1 Geometry and meshing

Based on topographical data records during a reservoir drawdown in 2006 (*FLOTRON AG*, 2006) the lake geometry of equidistant contour lines of 10 m between 1830 and 1910 m a.s.l. was defined. The model represented 60% of the total Lake Grimsel volume. The upstream part of the study area was defined as irrelevant for appropriate approach conditions.

The elements of the unstructured mesh are mainly tetrahedral and their size in the surroundings of the intake/outlet structure and the entire area from 1830 to 1860 m a.s.l. was fixed to 5 m with a growth rate of 1.2 toward the lake surface. Boundaries were meshed with an element size of 1 m except the shaft section and the intake body on which 0.5 m was imposed. The zones with minor influence on the flow conditions were meshed with element sizes inferior to 20 m. These settings lead to a mesh composed by 1.4 million cells.

3.4.2 Boundary conditions and simulation controls

The main assumption regarding boundary conditions concerns a constant reservoir level at 1910 and 1900 m a.s.l. respectively for the simulation of Sept and Nov1 & 2 scenarios. Measured level variations during the three periods were limited to only +/-2.0 m. As the model works at constant water level, variations due to withdrawn or injected water through the intake/outlet structures of Gelmer/Grimsel 1 and Grimsel 2 are compensated at the up- and downstream end of the model. Upstream, water is provided through a 10 m thick layer at the surface and over the entire reservoir width. Downstream, a virtual 10 m high spillway opening over the total width of Seeuferegg dam allows evacuating water during turbine mode. The reservoir bottom and the two dams are simulated as no-slip boundaries while at the lake surface free slip conditions were applied. The model of Lake Grimsel and the corresponding boundary conditions are illustrated in Figure 3.6.

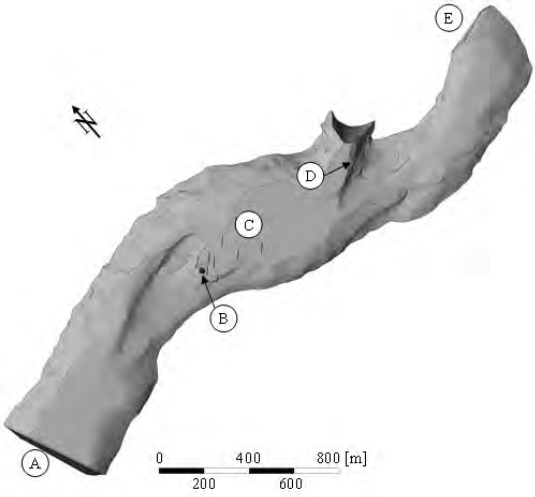

Figure 3.6 Numerical model of Lake Grimsel (ANSYS-CFD); A is the upstream boundary condition (inlet); B, the Grimsel 2 intake structure (inlet/outlet); C, the ADCP; D, the Gelmer/Grimsel 1 intake (outlet) and E, the downstream boundary condition (outlet, Seeuferegg Dam with implemented spillway crest)

Similar to the lake bottom, flow velocities are also imposed to be zero at concrete works such as walls and the top cover of the intake/outlet structure. The vertical connection between intake/outlet and shaft is reproduced with a length of 5 m and the in- or outlet boundary condition is set at the end of the vertical conduit.

Simulation control comprises clear water and isotherm conditions, respecting water characteristics at a temperature of $T_w = 5.5$ °C. However, differences in sediment concentration or temperature between the two lakes might affect flow patterns in front of the intake/outlet, especially during generating mode, when density differences between resident and inflowing water lead to jet stratification. Two additional scenarios simulate flow fields when warmer or colder water from the upper reservoir is injected into Lake Grimsel. Temperature differences of $\Delta T_w = +/-0.5$ °C were admitted in these cases, based on the ADCP observations.

Simulation time steps varied between $t = 1$ to 10 s according to convergence criteria. Transient results were registered every five minutes, respecting the sampling frequency of the in situ measuring devices.

3.5 Results and discussion

The ADCP recorded velocity components in East v_E and North direction v_N, indicated in Figure 3.3a. Three types of analyses were carried out on the flow velocity data extracted from the measuring devices. First, one- and two-dimensional profiles were plotted to visualize the recorded flow patterns. Second, signal processing methods were applied on velocity and discharge series to correlate recorded velocities and pumped-storage activities of the power plant. Finally, measured flow patterns were compared to the results of numerical modeling.

3.5.1 Flow patterns in front of the intake/ outlet: in situ measurements

As described before, ADCP records comprised two interference zones with excessively high velocities, the first originating from the loss of signal at a distance of some 20 to 30 m from the instrument and the second corresponding to the free surface of the reservoir. In order to get a better image of the velocity profile in the relevant area, East or North-components higher than $v = 10$ cm/s were not considered for the illustration of flow fields. This unavoidably led to gaps in the velocity time series, also in the interesting zone of measurements. Consequently average velocity resultants were calculated over five time steps, slightly smoothing the profile but allowed keeping information on the dynamics in front of the intake/outlet.

First, velocities were analyzed in the planes built by the ADCP, i.e. resultants were projected on the measurement lines. Figure 3.7 present typical axial flow velocity profiles for pumping and turbine sequences during campaigns Sept and Nov1 and reveals the above mentioned non-valid sampling zones near the surface and in the mid-water body.

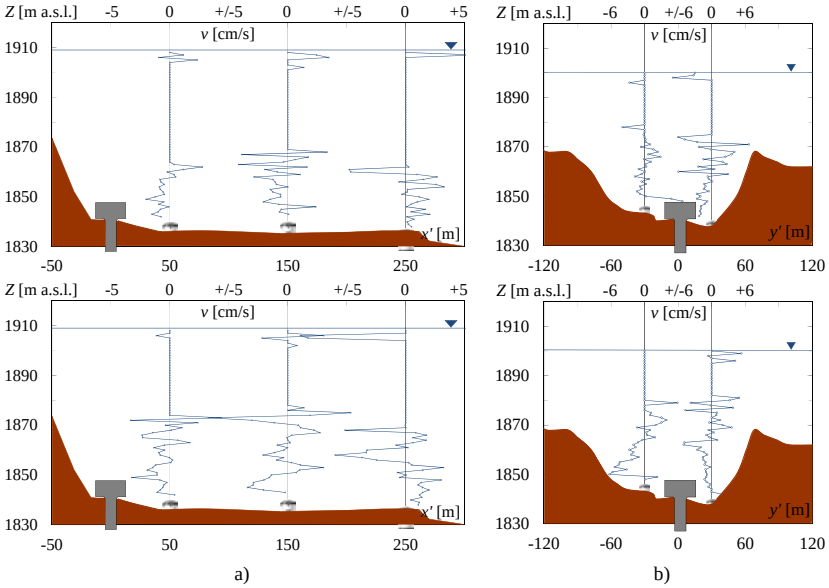

Figure 3.7 Flow velocities *v* recorded by the three ADCP, projected on the measurement lines for periods of pumping (outflow, above) and turbine mode (inflow, below); scenarios Sept (a) and Nov1 (b)

When water is pumped out of the reservoir, only the profiles close to the intake are affected. P2 and P3 on the Sept line do not clearly show the influence of the pumping operations and present non-structured fluctuations. In N-S direction, maximum axial velocity of v = 6 cm/s is reached at y' = 30 m from the intake, with an alteration of the water column corresponding to the intake height, approximately. In the flat part of the reservoir (W-E), only small axial velocities are measured. At x' = 50 m to the East, some v = 2 cm/s were recorded. Velocities can be low in this area or not oriented in the representation plane.

During turbine sequences (inflow), globally higher axial velocities are measured than during pumping mode. Some 5 m above the reservoir bottom the Sept line flow directions at P1 and P2 start pointing toward the intake/outlet most of the time, revealing a backflow phenomenon in front of the intake structure of axial velocities up to v = 5 cm/s. Only P3 in the flat reservoir part indicates velocity vectors pointing away from the intake/outlet with v = 3 to 5 cm/s. For the Nov2 line, similar behavior was observed, with backflow zones about 5 m above the bottom. However, flow directions toward the dam are more frequent.

The Nov1 line reveals that flow to the North of the intake (profile on the right of the intake/outlet in Figure 3.7b) is not primarily orientated in the intake-ADCP direction. Apparently, flow is deviated quickly after expulsion in the zone close to the steep rock slope. To the South, where the slope is less steep, velocity profiles show a clear tendency away from the intake/outlet with relatively high velocities around v = 7 to 8 cm/s.

To get a better idea of the flow patterns, and the main orientation of velocity vectors, three-dimensional plots were established and presented Figure 3.8. As discussed for axial velocities, inflowing water is mainly directed toward E-SE (corresponding to the Nov2 measurement

line, Figure 3.8e). It is probable that a large scale circulation cell is developing due to the confining topography. Highest absolute velocities up to v = 12 cm/s are observed close to the intake/outlet, as well as at both profilers in the main direction (Nov2). The few still very high velocity vectors located at the limit toward the blind zone and the water-air interface are not taken into account. In the backflow zones, mean velocity is estimated at v_m = 3 to 4 cm/s.

During pumping mode, main influence and absolute velocities of around v = 6 cm/s are observed at the profile to the North of the intake, probably amplified by the recirculation cell in the reservoir, which is starts rotating counterclockwise during turbine mode and continues turning even after stopping the power generation.

The deep zone of the water body is agitated continuously and moves not only when pumps or turbines are working, but also during periods with no in- or outflow from the power plant. However, the ADCP measurements did not allow a clear evaluation of the temporal evolution of the flow pattern, i.e. the response and delays of velocity profiles with respect to changes in the exploitation direction. This aspect is discussed based on numerical results.

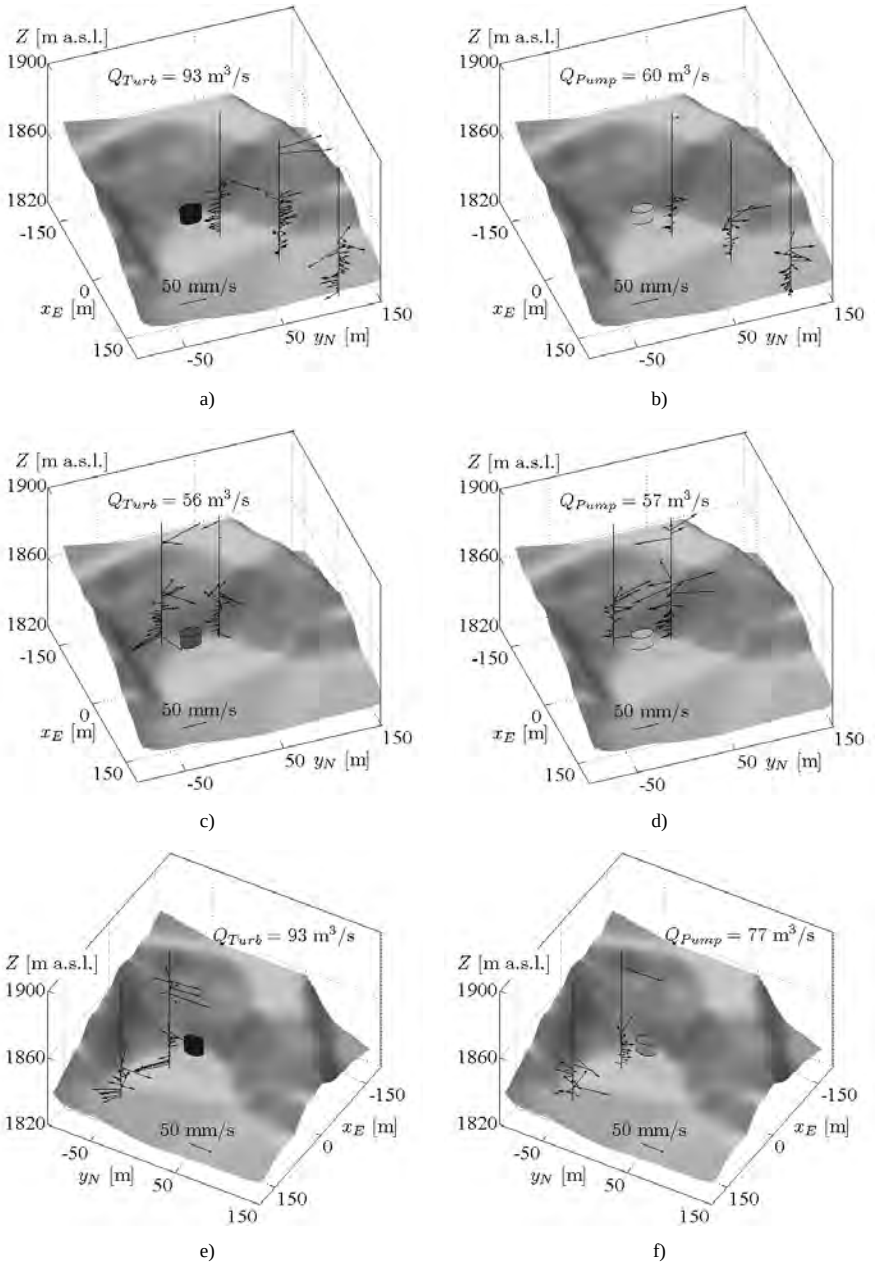

Figure 3.8 2D-velocity profiles near the Grimsel 2 intake/outlet structure during turbine (inflow, left) and pumping modes (outflow, right); September 17th 13:20 h (a), September 19th 05:00 h (b), November 07th 10:30 h (c) and 05:50 h (d), November 17th 18:20 h (e) and 02:10 h (f)

3.5.2 ADCP signal processing

Power spectra of ADCP data series were compared to those of discharge data to correlate velocities and pumped-storage operations. Based on the Fast Fourier Transform (FFT) this approach is often used in signal processing and allows relating the power of a signal to its corresponding frequency (Lyons, 2004). A rectangular windowing function was applied for calculation and raw ADCP data were used in order to separately study the E- and N-velocity components. However, only the first 20 cells above the reservoir bottom are considered hereafter, as with increasing distance from the measuring device, the spectra of the velocity signal becomes strongly affected by noise.

Discharge signal is characterized by three main peaks, at frequencies of $f = 0.3 \times 10^{-5}$, 1×10^{-5}, and 2.2×10^{-5} Hz corresponding to periods $1/f$ of approximately 4, 1 and 0.5 days (Figure 3.9). These frequencies are present for all three measurement terms, whereas Sept scenario has a slightly higher magnitude.

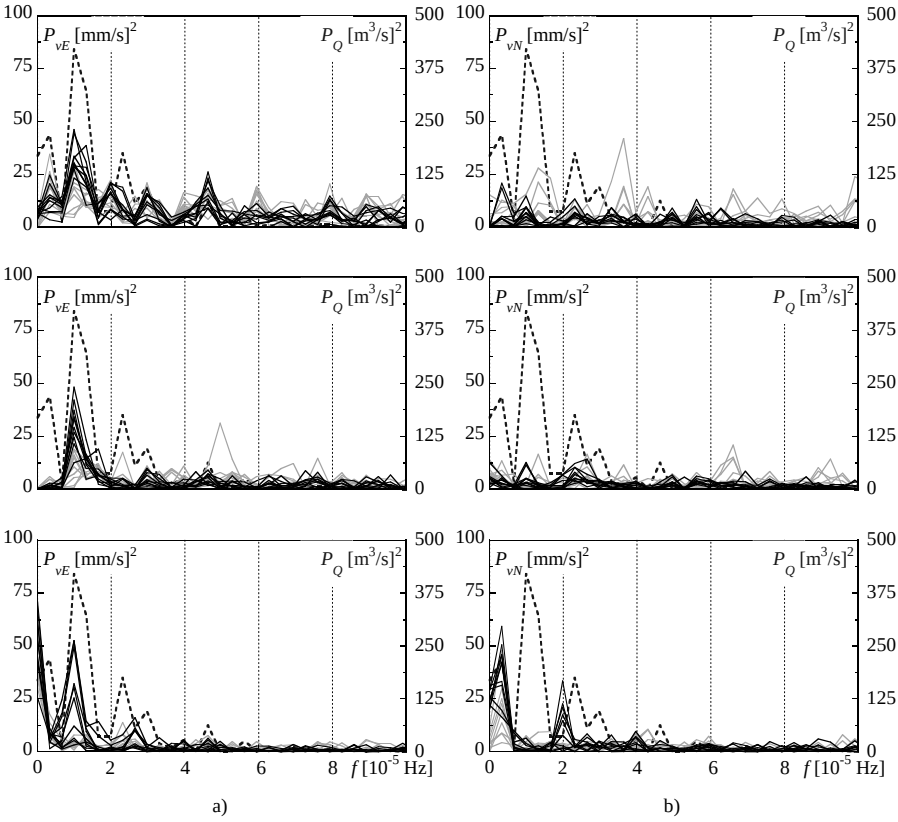

Figure 3.9 Power spectra for discharge Q and velocity components $v_{E,N}$ at P1 (top), P2 (middle) and P3 (bottom) for the Sept measurement line; E-velocity components (a) and N-velocity components (b). Dark lines correspond to bins 1 to 10 from the bottom, grey lines to bins 10 to 20. Discharge spectrum is represented by the dashed line.

Generally, velocity spectra flatten out into noise spectra at frequencies around $f = 4 \times 10^{-5}$Hz. Data sets recorded farther away from the device present more fluctuations and do not show distinct peaks (gray lines in Figure 3.9 and Figure 3.10). The signals of the first recording cells show the interaction between the temporal evolution of velocity profiles and pumped-storage operation.

For P1 and P2 of the Sept measurement line, the E-component shows a clear response to the three main peaks of discharge with a main frequency of $f = 1 \times 10^{-5}$ Hz. The signal of N-components is more scattered and distinct peaks are absent. At P3, E-velocities present similar behavior, but a response of N-components close to the bottom is observed at a frequency of $f = 0.3 \times 10^{-5}$ Hz.

The velocity spectra of data recorded in Nov1 line presents different characteristics. P1 and P2 both reveal a correlation between pumped-storage cycles and N-velocity component (Figure 3.10b, above). Additionally, an important peak amplitude of E-velocity component is observed at P2 at a frequency of $f = 1 \times 10^{-5}$ Hz for the bins 2 to 6, confirming the redirection of the flow toward the East of the intake/outlet.

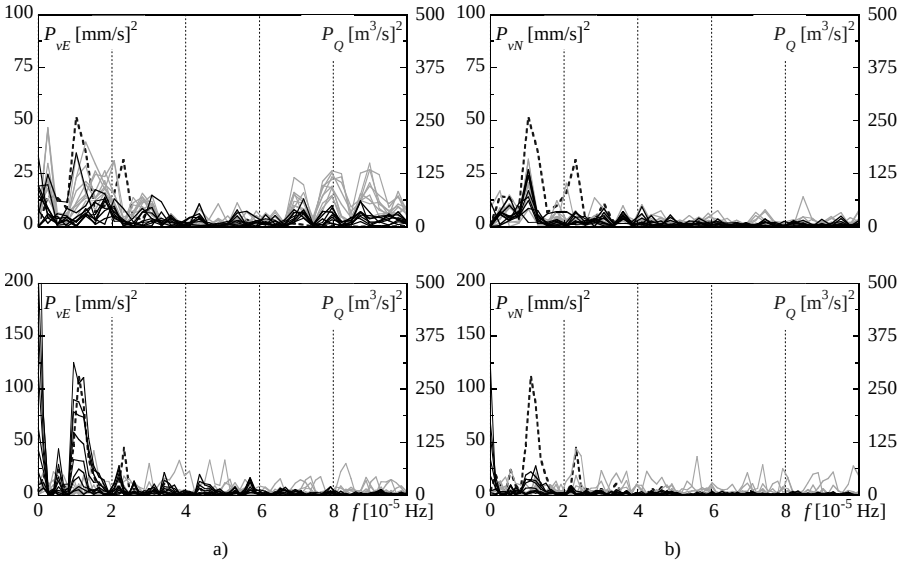

Figure 3.10 Power spectra for discharge Q and velocity components $v_{E,N}$ for Nov1 (above) and Nov2 measurement lines (below); E-velocity components (a) and N-velocity components (b) at P1. Dark lines correspond to bins 1 to 10 from the bottom, grey lines to bins 10 to 20. Discharge spectrum is represented by the dashed line.

Nov2 line in the invert is again presenting a strong correlation between discharge and E-velocity components, with higher amplitudes than observed at the same distance from the intake in September (Figure 3.10, below). Again, both velocity components have a main frequency of $f = 1 \times 10^{-5}$ Hz, the predominant frequency for all measured profiles.

Seiche periods in longitudinal and transversal directions of Lake Grimsel were computed considering a lake length of 6 km and a width of 500 m, as well as depth ranges from 37 m to 100 m. Thus, longitudinal seiches would result in frequencies from f_L = 1.6 to 2.6 x 10^{-3} Hz and transversal ones from f_T = 1.9 to 3.1 x 10^{-2} Hz. As peaks in this frequency range are not observed for the recorded velocity signals, it is assumed that no significant internal oscillation was altering the flow field measurements.

3.5.3 Comparison to numerical results

In numerical simulations, all nine ADCP positions were analyzed for the three different in situ measurement periods. The model identified the main influences of topography on the flow fields and recirculation cells and provided order of magnitude data regarding flow velocities and temporal response of flow patterns. Simulated velocity profiles cover the entire water column, from the very bottom to the free surface. Some of the information retrieved from the numerical model was thus complementary to the in situ measurements, especially the behavior of flow patterns in the near-bottom zone and in intermediate depths which lacked accurate in situ sampling.

Results show very low effect of pumping operation (withdrawal) at Grimsel 2 intake on the surrounding water body. Only at the closest profilers, some low velocities are observed. Otherwise the developed flow field around the structure is not generating measurable velocity vectors in the numerical model.

Turbine mode creates characteristic flow patterns with a circumferential inflow from the intake/outlet section on the lowest 5 to 7 m of the water column. Above this jet area, a strong backflow zone develops toward the outlet (Figure 3.11). These main characteristics correspond to results of in situ flow patterns. However, the model presents a higher consistency of flow profiles in time, with less temporal fluctuation of velocity vectors.

The velocity vectors on the reservoir bottom are slightly oscillating but keeping their main direction. In contrast to the 2D ADCP flow fields, the Nov2 line is less influenced by the inflowing jet, especially P2 seems to be placed in a sheltered zone of almost no velocities. In fact, during the entire simulation time the vertical velocity profile at this location remains unaffected by the inflowing water.

The measured profiles at P1 and P2 in the Nov1 line are very well reproduced by the numerical model, emphasizing the complexity and instability of the flow fields in front of the Grimsel 2 intake/outlet.

Evaluation of the temporal evolution of flow patterns, especially during turbine mode, could not be clearly stated based on the ADCP measurements. The numerical model allows systematic estimation of flow development. As such, average flow velocities could be calculated for the reaches between the profiler locations. When turbines are started after pumping or no operation, the flow injected into Lake Grimsel reaches the two N-S profilers (Nov1) located 30 m from the intake/outlet after t = 5 to 10 min. The first profilers in the invert at 50 m (Sept and Nov2) is reached after t = 10 to 20 min, depending on discharge. This corresponds to mean jet velocities of v = 4 to 10 cm/s. The response time between profilers is t = 30 to 65 min from P1 to P2 and t = 45 to 75 min from P2 to P3 with corresponding flow velocities of v = 2 to 5 cm/s. The temporal development of the velocity profiles around the Grimsel 2 intake/outlet is illustrated in Figure 3.11 for the Sept scenario.

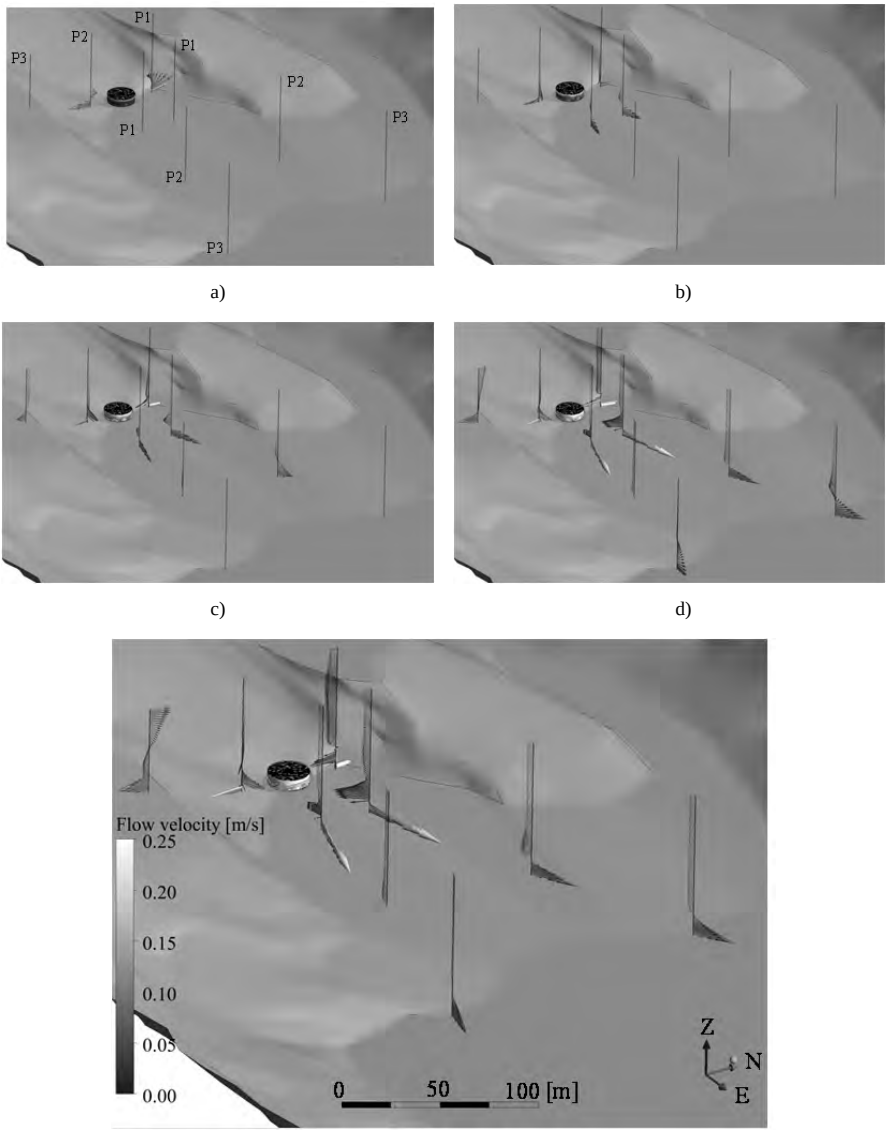

Figure 3.11 Development of computed flow patterns around Grimsel 2 intake/outlet during turbine mode (inflow); t = 10 (a), 20 (b), 70 (c), 110 (d) and 140 minutes (e) after the beginning of the turbine sequence on September 16th 2008 07:00 h

The mentioned velocities are valuable for jet propagation in nearly calm water conditions in the lake, i.e. when the water body flow is not moving any more after pumping sequences or no operation periods. However, the developed jet, which is continuously fed by water from the intake/outlet, can reach higher velocities. At P1, up to v = 20 cm/s are computed in the model and at P2 and P3, computed flow velocities reach v = 8 to 10 cm/s.

The flow connection between the Grimsel 2 and Gelmer/Grimsel 1 intakes is established only after more than nine hours of continuous turbine operation at Grimsel 2. The circumferentially inflow is not creating a well oriented jet and velocities decrease quickly with increasing distance from the intake/outlet. Thus, using the two plants for suspended sediment transfer from Lake Oberaar through Lake Grimsel into Lake Räterichsboden is not a feasible measure.

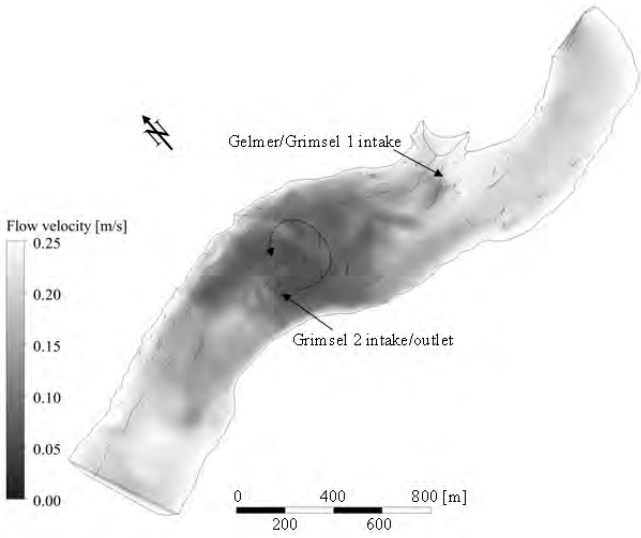

Figure 3.12 Volumetric distribution of flow velocity after t = 9 h of turbine mode on September 18th. The large scale recirculation cell is indicated by the dashed arrow.

According to results of the two additional scenarios, based on the first 3 h of turbine mode on September 16th, a temperature difference of ΔT_w = +/-0.5 °C between inflowing and resident water does not fundamentally change the flow patterns in Lake Grimsel. Due to relatively low density differences for the simulations, buoyancy effects remain small and do not change the distribution of the inflowing jet. However, if fluid properties diverged more, for example in the case of sediment-laden water injected into less turbid water, buoyancy effects would probably affect the jet trajectory considerably and change the flow fields near the intake/outlet structure.

3.5.4 Turbulent kinetic energy input due to pumped-storage operation

Settling of the small particles in the water body near the intake/outlet occurs if flow velocities are tending to very low values, i.e. when energy available for mixing is insufficient. To estimate turbulent kinetic energy (TKE) input induced by power generation, Imboden (1980) gives the following formula (adapted):

$$\eta_{Turb} = \frac{Q_{Turb} \cdot U_{Turb}^{\ 2} \cdot \rho_{IN}}{2 \cdot A_0} \qquad \text{(Eq. 3.1)}$$

where Q_{Turb}: the turbine discharge [m^3/s],
U_{Turb}: the efflux velocity at the intake [m/s],
ρ_{IN}: the density of injected water [kg/m^3], and
A_0: the lake surface area [m^2].

For maximum discharge of Q_{Turb} = 93 m^3/s and the Lake Grimsel area of 2.63 km^2 an energy input of η_{Turb} = 7.4 x 10^{-3} W/m^2 is caluclated. TKE input of natural convective mixing or pumping activity is not included due to its low influence on mixing of the water column (Anderson, 2010). Taking into account an average turbine operation of 6.5 h/d, the daily mean TKE input is of η_{Turb} = 2 x 10^{-3} W/m^2.This TKE input can be compared to the natural TKE input per unit area and time due to average wind-forcing (Anderson, 2010):

$$\eta_a = C_k^* \cdot \rho_w \cdot \left(\frac{c_D \cdot \rho_a}{\rho_w} \right)^{3/2} \cdot U_a^{\ 3} \qquad \text{(Eq. 3.2)}$$

where C_k^*: an efficiency factor for converting wind energy to TKE [-],
ρ_w: the density of water [kg/m^3],
ρ_a: the density of air [kg/m^3],
c_D: the drag coefficient [-], and
U_a: the wind speed [m/s].

The annual average wind speed at Grimsel Hospitz is of U_a = 5.6 m/s and fluid densities of ρ_w = 995 kg/m^3 (water at 5.5 °C) and ρ_a = 1.2 kg/m^3 are assumed. According to Anderson (2010), C_k^* = 0.23 and c_D = 0.0013 can be considered. Thus, a TKE input from wind of η_a = 7.9 x 10^{-5} W/m^2 can be defined.

Consequently, Lake Grimsel is submitted to a TKE input due to pumped-storage operations which is about 25 times higher than energy naturally generated by wind. Such high energy input has been found to effectively weaken stratification and increase mixing frequency in pumped-storage reservoirs (Imboden, 1980; Potter *et al.*, 1982). Thus, Lake Grimsel, especially near the intake and outlet structure, is affected by important mixing processes of high TKE, which explain the weakened stratification observed by Bonalumi *et al.* (2011), and are most likely to slow down fine sediment settling.

3.6 Conclusions

Flow velocities in front of the intake/outlet structure in Lake Grimsel were continuously sampled with three ADCPs over four and nine day periods for analysis of flow patterns influenced by pumped-storage activities.

From a monitoring point of view, the instruments are well adapted to be applied as a continuous observation method, due to an autonomous power supply for up to several months. Real-time data could be transmitted to shore by a cable link or an acoustic modem. However, fixation of the devices includes buoys and cables which should not interfere with eventual leisure or maintenance activities on the reservoir. Lake Grimsel is a high Alpine reservoir, which complicates ADCP monitoring during the winter months due to ice-cover and considerable water level variation. Recording in Lake Grimsel showed that velocity sampling can be incomplete due to the lack of sound scatterers in the water column. In fact, optimum ADCP sampling frequency and bin length for the given in situ conditions could be revealed by additional in situ tests.

The one- and two-dimensional velocity fields established based on the collected in situ data showed that pumping mode (withdrawal from the reservoir) affects the water body close to the intake and leads to flow velocities of about v = 6 cm/s at 30 m from the structure. The velocity profiles at 150 and 250 m from the intake are not influenced by the flow field. Periods without pumped-storage activity are marked by non-structured velocity fluctuations in the water body.

Turbine mode (inflow) systematically generates flow patterns with important backflow in the zones between 5 and 20 m above the reservoir bottom. A main inflow sector was observed in ESE-direction. Close to the outlet, flow velocities up to v = 12 cm/s were recorded by the ADCP. To the North and South, the steep rock slopes deflect flow eastward into the flat reservoir part. The natural confinement seems to generate a large-scale circulation cell, rotating counterclockwise in the basin in front of the Grimsel 2 intake/outlet.

Frequency analysis of the recorded velocity signal correlate the sampled flow patterns to pumped-storage cycles. Main frequencies of discharge and ADCP signals match well, especially for the E-velocity component, indicating and confirming the main flow direction in the studied area. The predominant period is of $1/f$ = 1 day, corresponding to the daily pumped-storage cycles of the plant. Seiche frequencies are not discovered in the velocity spectra.

The numerical model results confirm the in situ observations and adequately represent the main characteristics of the flow patterns in front of the intake/outlet. However, the model computes slightly higher flow velocities, due to a higher consistency of flow patterns in time with less temporal fluctuation of velocity vectors. Analysis of the temporal evolution of the flow fields indicates stable conditions after approximately 150 minutes of continuous turbine operation. Nine hours are needed until water injected by the Grimsel 2 intake/outlet reaches the Gelmer/Grimsel 1 intake. Thus, the idea of transferring sediment-laden water from Lake Oberaar downstream into Lake Räterichsboden has to be discarded. The scenarios comprising two fluids of different temperature showed that ΔT_w = +/- 0.5 °C does not significantly change flow patterns in Lake Grimsel.

Finally, turbulent kinetic energy (TKE) input due to turbine operations is 25 times higher than the natural TKE input by wind-forcing. Lake Grimsel is subject to very high energy input during turbine mode, weakening the thermal stratification of the water column and increasing

mixing frequency. From a reservoir sedimentation point of view, the high energy input is favorable as it keeps fine sediment in suspension and consequently slows down fine particles' settling.

Pumped-storage activities have a measurable impact on reservoir dynamics. Outflowing water only influences flow patterns close to the outlet structure, whereas inflowing water induces large eddy flow fields in the reservoir, depending on lake topography and operated discharge. Compared to natural wind induced kinetic energy input, hydropower operation can become the driver parameter governing flow dynamics in a storage volume. As flow patterns, turbulence, sediment settling, lake stratification are related, flow monitoring in combination with numerical modeling is a crucial step toward a sustainable reservoir management.

Chapter 4

Continuous long-term observation of suspended sediment transport between two pumped-storage reservoirs

Transport of suspended sediment between the two reservoirs of a pumped-storage plant in Switzerland was monitored over an eight months period. A turbidity probe was installed on the upstream end of the pressurized shaft. Real time monitoring was undertaken by automatic data acquisition and remote control.

Suspended sediment concentrations varied considerably over the year. From December to April, when reservoirs were ice- and the catchment area entirely snow-covered, particle load was low. By the end of April, when snowmelt started, suspended sediment concentration increased and remained high in May and June.

Pumped-storage sequences correlated with the short-term evolution of suspended sediment concentration, especially when reservoir levels were low. Higher concentrations during pumping mode were observed for low levels in the lower reservoir, while low levels in the upper reservoir generated higher concentration in turbine mode. Concentration ratio between pumping and turbine mode between 0.93 and 1.16 were observed. Periods with higher particle load were observed more frequently during pumping mode. Nevertheless, the suspended sediment balance due to pumped-storage operations was equilibrated, pointing out the high correlation between the transported sediment volume and hydropower operation.

The applied monitoring system is easy to implement and could be connected to the existing power plant control and management system. The plant operator could detect an increase in suspended sediment load and, if desired, adapt the operation mode to actively manage reservoir sedimentation. Furthermore, the system continuously measures suspended sediment transport between the two reservoirs to estimate and predict long-term sediment balance.

4.1 Introduction

Nowadays, about 56% of Swiss electricity production comes from hydropower and the federal government is further promoting the use of this renewable energy source to a greater extent due to the increasing energy demand.

Especially the development of new pumped-storage facilities for grid regulation and peak energy supply has become a crucial task for sustainable power production. Maximum plant efficiency, production reliability and structural safety are required. Reservoir sedimentation is one of the problems to be looked at, causing storage losses and clogging intakes and outlet works (Fan and Morris, 1992; Knoblauch *et al.*, 2005; LCH, 2005; Hartmann, 2007). Therefore, sedimentation issues in pumped-storage reservoirs are studied, with a focus on monitoring suspended sediment transport. The case study is located in the Swiss Alps.

The main sedimentation process affecting large Alpine storage reservoirs are turbidity currents. When a sediment-laden river enters a reservoir it plunges and follows, according to density difference, the thalweg to the deepest area, which is normally close to the dam and/or the power intakes. This phenomenon takes place sporadically during yearly floods and occurs mainly during peak precipitation. It has been investigated by De Cesare (1998) and De Cesare *et al.* (2001).

For storage hydropower plants, several measures against turbidity current driven sedimentation have been studied by Oehy and Schleiss (2007) and Oehy *et al.* (2010), i.e. obstacles stopping the current propagation or maintaining particles in suspension in front of intakes to be evacuated by the turbines. Jenzer Althaus (2011) investigated the effect of rotating jet induced flow close to intake structures on sediment mixing.

Pumped-storage operation mode may keep fine sediment suspended in the water column, as it has been shown that pumped-storage activity alters thermal stratification, entrains organisms and could even resuspend fine bottom sediment (Imboden, 1980; Potter *et al.*, 1982; US Bureau of Reclamation, 1993; Anderson, 2010). Bonalumi *et al.* (2011) investigated how particle dynamics in high Alpine reservoir are modified by pumped-storage operation. However, the magnitude of the mixing process depends on the pump and turbine operation, on reservoir shape and as well as the design of hydraulic works.

The present study evaluates the influence of pumped-storage activity on suspended sediment concentration in pumped-storage schemes, illustrated by a case study in Switzerland, situated at high altitude in a glacierized catchment area. In addition, long-term observations, as sediment balance, are addressed to provide a monitoring system for analysis of fine sediment behavior. Real time sediment monitoring is not novel. Most applications are aiming to detect the arrival of turbidity currents in front of hydraulic outlet structures in order to proceed to venting operations (Müller and De Cesare, 2009). Gray and Gartner (2009) summarize different monitoring techniques for suspended sediment, focusing on river applications. Continuous turbidity monitoring to correlate suspended particle concentrations to pumping or turbine operations has not been addressed so far.

The chapter provides a description of the case study, the turbidity sampling equipment and the acquisition system for monitoring. Temporal evolution of suspended sediment concentration is measured and analyzed, revealing both long-term variations due to seasonal changes in particle inflow and short-term changes due to hydropower operation. Finally, the sediment balance of the scheme is discussed.

4.2 Site description

The Oberhasli region, drained by the upper Aare River is located in the Central Alps of Switzerland and hosts several interconnected reservoirs and powerhouses which are operated by *Kraftwerke Oberhasli AG* (KWO). The nine power plants fed by eight reservoirs provide 8.1% of the total installed storage hydropower capacity in Switzerland and produce 10.1% of the corresponding electrical energy (SFOE, annual report 2011).

KWO is currently investigating a large upgrading program including technical, economic and ecological improvements of the scheme, such as an increase of the installed capacity of the machines and the storage capacity of the reservoirs. The enhancement project includes a new 600 MW pumped-storage plant. A further pumped-storage project's feasibility is evaluated, emphasizing the importance of pumped-storage for future energy supply.

Several studies on the impact of hydropower on the lakes and the river system in the Oberhasli area have been carried out. Wüest *et al.* (2007) showed that the increased winter runoff heavily impacted the downstream river. Other investigations concerning Lake Brienz, at the outlet of the Oberhasli watershed, revealed hydropower related changes for light regime of the lake water (Jaun *et al.*, 2007) and primary production (Finger *et al.*, 2007). Many of these concerns are directly or indirectly linked to sediment issues, like concentration and particle characteristics of released water during frequent turbine or infrequent flushing operations.

4.2.1 Grimsel 2 pumped-storage scheme

The Grimsel 2 pumped-storage plant (Figure 4.1) is operating water between Lake Oberaar (Oa) and Grimsel (Gr) since 1982. The upper reservoir at 2303 m a.s.l. has a storage volume of $V_{Oa} = 57 \times 10^6$ m^3, while the lower basin at 1909 m a.s.l. impounds $V_{Gr} = 95 \times 10^6$ m^3. Minimum drawdown levels of the two reservoirs are 2250 and 1850 m a.s.l., leaving water depths of 14 and 5 m over the center of the intake/outlet section, respectively. Maximum discharge in turbine mode is $Q_{Turb} = 93$ m^3/s (Oa – Gr), while pumping discharges reach $Q_{Pump} = 80$ m^3/s.

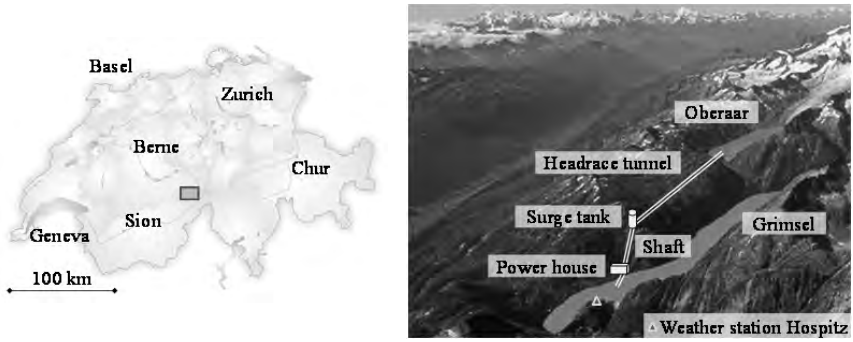

a) b)

Figure 4.1 Location map (a) and layout (b) of the Grimsel 2 pumped-storage scheme

The power plant consists in an underground powerhouse, equipped with four independent pump-turbine units of 350 MW total installed capacity. From Lake Oberaar, a 4 km long headrace tunnel with an internal diameter $D = 6.8$ m connects the intake/outlet structure to a vertical surge tank of 123.0 m height and diameter $D = 13.0$ m. From there, a 750 m long steel-lined shaft ($D = 3.8$ m) guides the water toward the power house. Downstream of the surge tank, a security butterfly valve allows disconnecting the shaft from the upstream headrace tunnel.

The catchment areas of the two reservoirs are partly glacieted. Anselmetti *et al.* (2007) state denudation rates of 1 to 2 mm/year leading to high sediment supply. The construction of the dams led to high retention rates of suspended sediment. Only some 40 kt/year are released downstream of the three main KWO reservoirs (Lake Oberaar, Grimsel and Räterichsboden), while about 230 kt/year are retained. Hence, from a reservoir sedimentation point of view, a sediment transfer toward downstream would be desirable. If the layout of hydraulic structures permits this downstream transfer, the turbulence generated by pumped-storage sequences could contribute by keeping fine sediment in suspension and thus increase transfer efficiency.

The suspended sediment characteristics of Oberaar and Grimsel waters have been analyzed in detail by Blaser and Bühler (2001), studying the hydro-mechanical effect of pumps and turbines on the water turbidity, by Bühler and Siegenthaler (2003), aiming a description of particle sizes and suspended sediment transport as well as by Bonalumi *et al.* (2011), investigating the particle dynamics in the reservoirs due to pumped-storage operation. Grain sizes of diameter $d_S = 0.2$ to 40 µm were measured, with a mean diameter $d_m = 3$ to 4 µm. In addition, suspended sediment concentration along the year varies between $C = 50$ and 200 mg/l in the deep water of two reservoirs. Surface waters of Lake Oberaar rarely presents particle loads higher than $C = 50$ mg/l, while Lake Grimsel surface waters can reach $C = 150$ mg/l in summer (Bonalumi *et al.*, 2011) due to turbidity currents or glacier melt.

Bühler *et al.* (2005) showed that turbidity currents arriving at the Spittellamm dam impounding Lake Grimsel can be detected by a significant increase of turbidity in the pressurized system of the Grimsel 1 storage plant, located downstream of Lake Grimsel. For the sampled water at the pressure tunnel of the Grimsel 1 intake $C = 700$ mg/l was measured during a turbidity current event in 2001.

Bonalumi *et al.* (2011) carried out periodical conductivity, temperature, depth (CTD) sampling over two years, described the particle concentration structure of Lake Oberaar and Grimsel and modeled the particle balance of the reservoirs with and without pumped-storage activity.

4.2.2 Monitoring location

The existing KWO monitoring system at Grimsel 2 provides information about water levels in the two reservoirs and pump and turbine discharge of each unit. All acquired data series are directly transmitted to the KWO control and command center. However, sediment concentration is not recorded by KWO, neither for the inflowing rivers, nor in the pressurized system of the plant.

Three possible accesses to the steel-lined shaft were evaluated. The security butterfly valve downstream of the surge tank is located in a cavern which provides an access to the

pressurized system of Grimsel 2 for inspection and maintenance reasons. Other accessible steel-liner reaches are located on the high pressure side just upstream of the flow diverter toward the four units inside the power house as well as on the low pressure side at the exit of the tailrace tunnel of the power house.

The turbidity measuring equipment requires low pressure at its inflow section. Therefore, monitoring locations are limited to the valve chamber near the surge tank and the tailrace channel. Low temperatures and low humidity in the valve chamber provide optimal conditions for electronic data acquisition devices. Therefore, the monitoring system was installed on the accessible reach of the steel-liner just downstream of the surge tank, where a drainage by-pass provides a direct water sampling possibility (Figure 4.2).

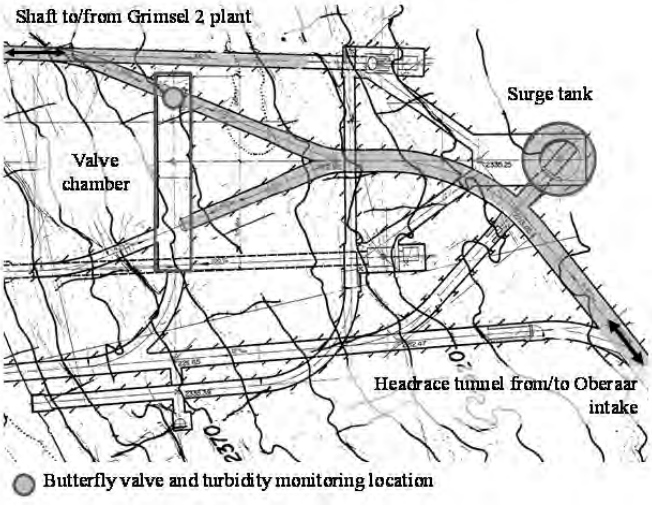

Figure 4.2 Schematic plan view of the vicinity of the Grimsel 2 surge tank, with indicated headrace tunnel, pressurized shaft and turbidity monitoring location in the valve chamber (source: KWO archives)

4.3 Sampling and data acquisition

The monitoring system for suspended sediment concentration consisted of a turbidity probe and a data acquisition system installed next to the sampling location. The main components of this system are presented hereafter.

4.3.1 Turbidity sensor

From the sampling location at the shaft, water passes through the pressure regulating valve and the de-aerator to the measuring cylinder (Figure 4.3). In there, turbidity is measured by a *Cosmos®25-E* probe (Züllig AG, Switzerland). Inflow is limited to $Q = 1$ to 2 l/s, guaranteeing a residence time of analyzed water superior to the sampling time of the probe. From the measuring cylinder, the water flows toward a sewer in the drain below the steel-liner. The system was periodically purged by the mean of a small valve in order to evacuate eventual sediment deposits on the cylinder bottom.

The turbidity measurement is based on a two channel multi-beam pulsed infrared light system combined with a six channel multi-angle-measuring, making the system very robust and insensitive to most kind of disturbances.

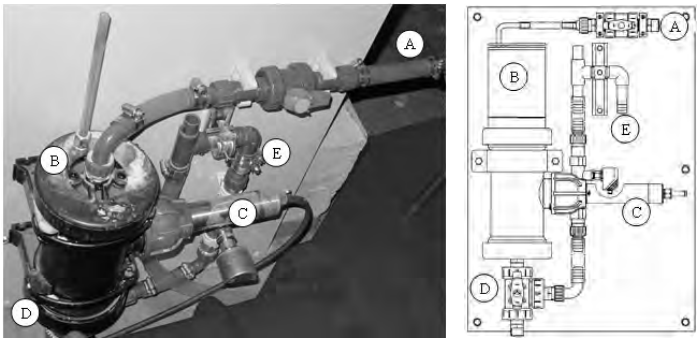

a) b)

Figure 4.3 Photo (a) and drawing (b, source: Zuellig AG) of the turbidity measuring equipment at Grimsel 2. A is the inlet; B, the measuring cylinder; C, the *Cosmos®25-E* probe; D, the purge valve and E, the outlet toward the sewer

4.3.2 Calibration

The *Cosmos®25-E* probe needs only one calibration point in the application range of the expected turbidity values at Grimsel 2. After an initial 60 minutes measuring period, the turbidity sensor was put into calibration mode and water samples were taken at the outlet of the measuring board. These samples were then analyzed by the *Swiss Federal Institute of Aquatic Science & Technology* (Eawag), permitting to define the correlation between the measured turbidity *TU* [FNU] and the suspended sediment concentration *C* [mg/l]. Over the total monitoring period two validation samples were taken.

4.3.3 Acquisition system

The turbidity sensor is connected to a *b-line II* amplifier (Züllig AG, Switzerland, Figure 4.4a) generating an output signal between 4 and 20 mA correlated with a user defined turbidity range. From the amplifier, the signal is transmitted by cable to the new in situ data acquisition system (Figure 4.4b) composed by a signal conditioner, an acquisition card *NI-USB-6259 M series* (NI Instruments, USA) and an industrial computer (kontron, USA).

At the signal conditioner, current is transformed into a voltage signal within a range of 2 to 10 V. The upper limit sediment concentration of initially $C = 1000$ mg/l was set to 300 mg/l after the first two months of measurement, as in winter and spring sediment load is smaller than in summer. By the end of June, the maximum concentration value was fixed at $C = 700$ mg/l in order to record eventual increases in sediment concentration due to annual flood and turbidity current events in summer, as observed by Bühler *et al.* (2005).

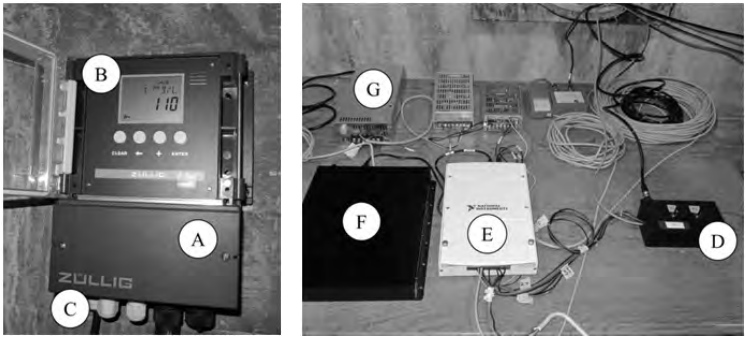

a) b)

Figure 4.4 Turbidity *b-line II* amplifier (a) and acquisition system (b) at Grimsel 2. A is the *b-line II*; B, the real time suspended sediment concentration display; C, the power input and signal output toward the acquisition system; D, the signal conditioner; E, the acquisition card; F, the computer and G, the power supply

The LabVIEW based data acquisition tool sampled with a frequency of $f = 0.2$ Hz and stored data series every 30 minutes. The program started the storage loop opening a *.tdms* file with date and time assigned according to the PC clock, synchronized with the KWO server. A Virtual Private Networking internet connection (VPN) allowed online controlling and data download.

4.4 Monitoring data and results

Suspended sediment concentration data, measured by the turbidity probe and acquired by the monitoring system, are available for almost the entire sampling period. Some sampling interruptions occurred: by the end of December, maintenance work at the monitoring location led to a shut-down of the entire system until February 2011. Three times, measurements were briefly stopped to adjust the acquisition system and interface, leading to lack of data for one- to three-day periods. On April 30th the sampling valve on the pressurized shaft started to clog with sediment and lost its functionality completely for ten days until a cleaning intervention. On July 4th, a technical problem stopped the monitoring period. As such, reliable data are available for 174 days, between October 26th 2010 and June 30th 2011 (Table 4.1).

The turbidity signal was smoothed by a moving average over 60 time steps, corresponding to five minutes of sampling. The phenomenon of oscillating disturbances is linked to the very small particles in the sampled water (glacier milk) and was already reported by the manufacturer from former in situ applications. However, calibration and validation samples showed that the turbidity probe worked properly in the case study conditions.

4.4.1 Pumped-storage exploitation

Annually, $V = 600$ to 700×10^6 m^3 water are pumped from Lake Grimsel to Lake Oberaar and moved back during turbine mode. Thus, the volumes of the lower and upper reservoir are exchanged six to ten times throughout one year. During the monitoring period, $V_{Turb} = 419.6 \times 10^6$ m^3 and $V_{Pump} = 420.8 \times 10^6$ m^3 were moved by pumping and turbine

operations respectively. Weekly water volumes transferred ranged between $V_{Pump,\,Turb}$ = 5 and 23 x 10^6 m^3 (Figure 4.5).

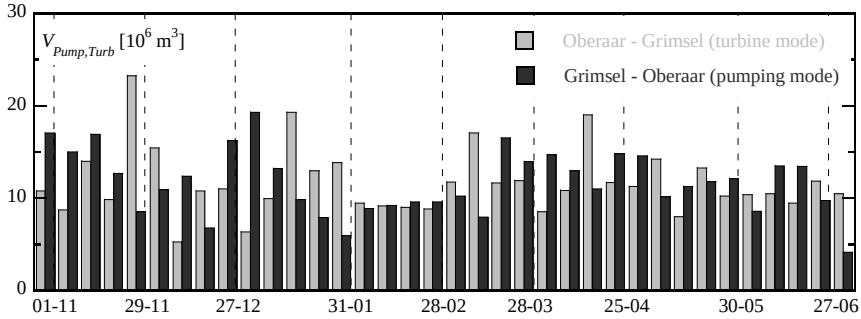

Figure 4.5 Weekly volumes $V_{Pump,\,Turb}$ operated by the Grimsel 2 pumped-storage plant during the entire monitoring period from October 26th 2010 to June 30th 2011

Lake Oberaar level was highest during mid-November 2010, when it reached 2302 m a.s.l., while the Grimsel reservoir was fullest by the end of November, at 1906 m a.s.l. Low levels around 2260 (Oa) and 1862 m a.s.l. (Gr) were measured several times in April and May 2011. From October to March, the weekly level variations were of 2 to 12 m in Lake Oberaar and of 2 to 6 m in Lake Grimsel. During periods of low reservoir level, weekly variations up to 18 (Oa) and 12 m (Gr) were recorded.

4.4.2 Meteorological data

In the Oberhasli region, rainfall and particularly snowmelt are the main origins of increased particle inflow into the reservoirs. Bonalumi *et al.* (2011) define four characteristic particle inflow periods: no inflow when both reservoirs are ice-covered (November to May +/- two weeks), high inflow during snowmelt (May to August), low particle inflow during fall (September, October) and peak particle inflow during main rain events in summer.

Knowledge on meteorological conditions is thus relevant to forecast periods of high suspended sediment concentration. Such, air temperature T_a, precipitation P as well as snow height data were taken from the "Grimsel Hospitz" weather station next to Spittellamm Dam (Figure 4.1b, *Swiss Federal Office of Meteorology and Climatology*, MeteoSwiss). In addition, daily inflow from the catchment areas (KWO) were considered. Figure 4.6 presents meteorological data for a selected period from March 28th to June 20th, corresponding to the period of the main changes in observed suspended sediment concentration.

Due to warm weather in early spring, main snowmelt in 2011 occurred already in March and April. Three significant peaks in natural inflow were observed during the weeks from May 9th to 16th, May 23rd to 30th and June 13th to 20th.

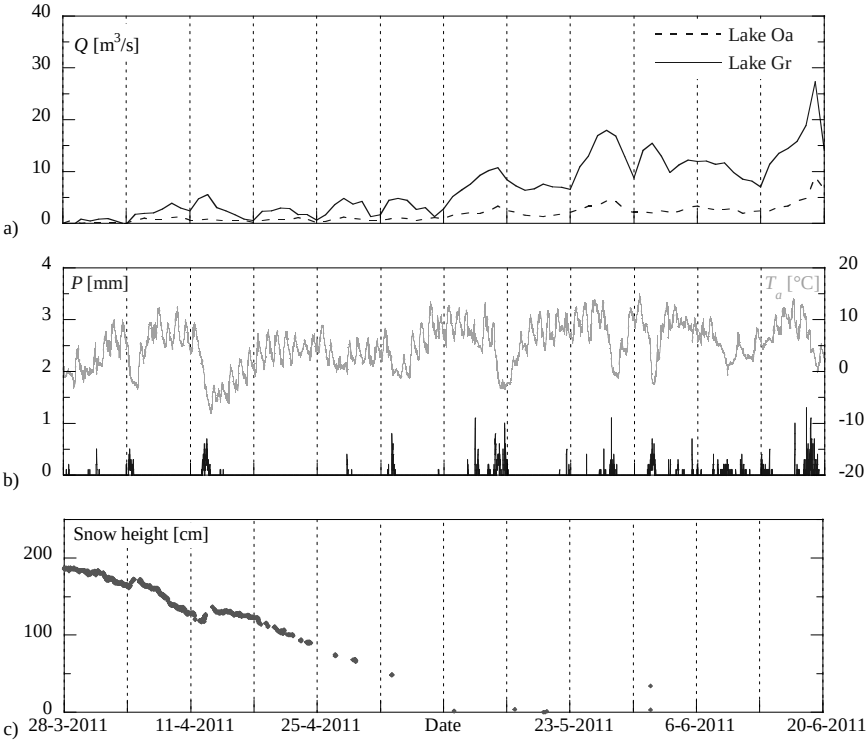

Figure 4.6 Data series of natural inflow Q to Lakes Grimsel and Oberaar (a, source: KWO), air temperature T_a and precipitation P (b) and snow height (c) at weather station Grimsel Hospitz (source: MeteoSwiss) for the monitoring period from March 28th to June 20th 2011

4.4.3 Suspended sediment concentration

Suspended sediment concentration C varied over the measurement period with monthly means around $C_m = 80$ mg/l in November/December, decreasing to $C_m = 55$ to 60 mg/l between February and April and increasing again to $C_m = 80$ mg/l in May and June (Table 4.1). In addition, short-term variations during pumping and turbine sequences were observed. To describe these variations, the mean concentration measured during a pumping sequence $C_{m,Pump}$ was compared to the mean concentration sampled during the previous and following turbine sequence $C_{m,Turb}$. Thus, five to ten values for the ratio $C_{m,Pump}/C_{m,Turb}$ were obtained per week, according to the number of pumping sequences. The range of calculated ratio between suspended sediment concentration in pumping and turbine mode is represented in Table 4.1.

Table 4.1 Measurement periods with indication of reliable turbidity sampling days, monthly mean of suspended sediment concentration C_m and range of suspended sediment concentration ratio between pumping and turbine sequences $C_{m,Pump}/C_{m,Turb}$

	Measurement period	Monthly mean C_m [mg/l]	Range of $C_{m,Pump}/C_{m,Turb}$ [-]
2010	Oct (6 days of data)	91.90	0.95 to 1.02
	Nov (30 d)	81.47	0.96 to 1.02
	Dec (19 d)	79.55	0.96 to 1.04
2011	Jan (no records)	-	-
	Feb (14 d)	61.15	0.97 to 1.05
	Mar (29 d)	55.47	0.94 to 1.04
	Apr (30 d)	60.11	0.93 to 1.11
	May (16 d)	83.98	0.93 to 1.16
	Jun (30 d)	75.96	0.93 to 1.09

Figure 4.7 and Figure 4.8 present four monitoring charts which illustrate the main observations during the measurement period. From October to December, the reservoir levels were high, the level variation relatively small and particle load fluctuated around C_m = 80 mg/l, independent from the pumping and turbine sequences (Figure 4.7a). Then, concentration started decreasing till the two lakes were ice-covered and inversely stratified as well as natural sediment inflow was lowest. By the end of March, Lake Grimsel level was down to 1866 m a.s.l., leaving just 18 m above minimum drawdown. During the first two weeks of April, the pumped-storage cycles started to be reflected by the suspended sediment concentration (Figure 4.7b). More turbid water was pumped up into Lake Oberaar, with concentrations up to 11% higher than during turbine operation.

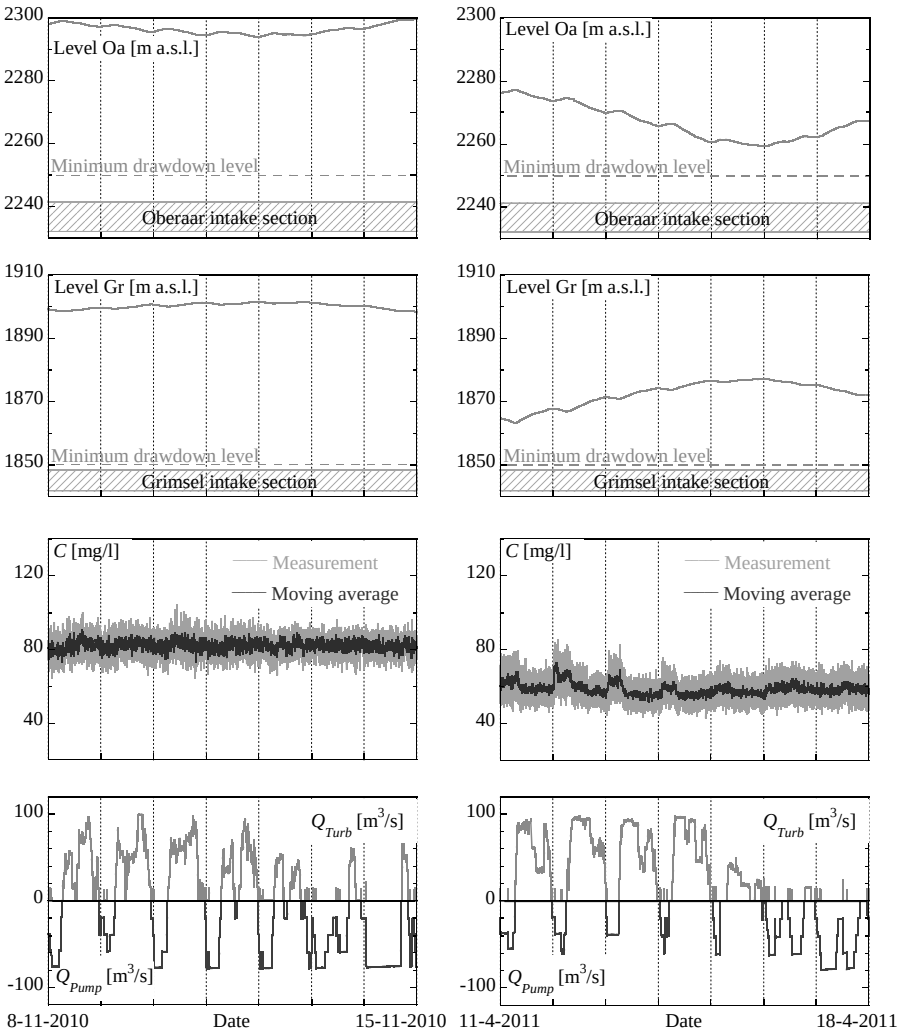

Figure 4.7 Reservoir levels of Lake Oberaar (Oa) and Grimsel (Gr), measured suspended sediment concentration C and discharge data $Q_{Pump,\ Turb}$. Weekly evolution during measurement periods from November 8th to 15th 2010 (a) and from April 11th to 18th 2011 (b)

By the end of April and with ongoing snowmelt, the mean suspended sediment concentration increased to reach again some C_m = 80 mg/l. During the first three pumping sequences in the week from May 16th to 23rd, the suspended sediment concentration was up to 16% higher than in the previous and following turbine cycle (Figure 4.8a), with C_{max} = 100 mg/l. Again, Lake Grimsel level at 1864 m a.s.l. was very low at that moment. With increasing level, the difference in particle load between pumping and turbine mode decreased.

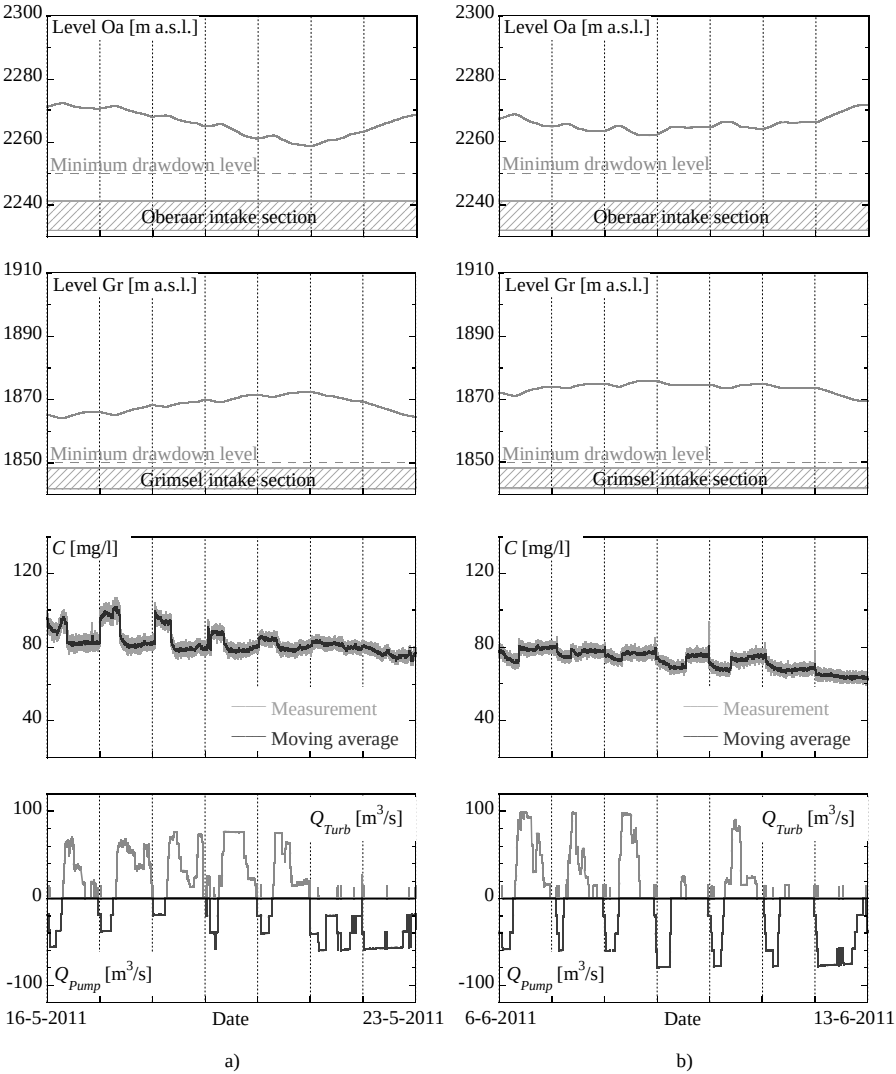

Figure 4.8 Reservoir levels of Lake Oberaar (Oa) and Grimsel (Gr), measured suspended sediment concentration *C* and discharge data $Q_{Pump,\ Turb}$. Weekly evolution during measurement periods from May 16th to 23rd 2011 (a) and from June 6th to 13th 2011 (b)

On the one hand, these two observation examples of increased particle load during pumping mode occurred during snowmelt in April and two days after an important increase of natural inflow in Lake Grimsel in May, which are events expected to increase particle load in the water body. Thus, the higher concentrations in pumped water are at least affected by meteorological conditions. However, suspended sediment concentrations recorded along other weeks do not show similar sensitivity to meteorological conditions.

On the other hand, reservoir level plays a predominant role, as in both cases the concentration ratio between suspended sediment concentration in pumping and turbine mode $C_{m,Pump}/C_{m,Turb}$ was high during low Lake Grimsel level. With increasing water surface, the effect decreased again. When Lake Oberaar level dropped to the lowest values recorded during the monitoring period, the response of suspended sediment concentration reversed and presented systematically higher particle load in turbine mode (Figure 4.8b).

4.5 Discussion

The sampling of suspended sediment concentration in an Alpine pumped-storage scheme allowed the detection of seasonal increases and decreases of particle load in the pump or turbine operated water. Thus, also the arrival of turbidity currents near the intake/outlet area could be defined, increasing concentrations drastically within a short time. As no such important event was recorded during the monitoring period, this aspect is not discussed further on. Hereafter, sediment balance of the studied Grimsel 2 scheme and the correlation between suspended sediment concentration and pumped-storage sequences is discussed.

4.5.1 Sediment balance of the Grimsel 2 scheme

Turbidity records allow direct estimation of the transported suspended sediment volumes from one reservoir to the other. Weekly moved volumes V_S and the evolution of volume difference ΔV_S over the entire sampling period are presented in Figure 4.9.

Volumes were calculated assuming a density of $\rho_s = 1500$ kg/m^3 (Bühler *et al.*, 2004). Weeks containing restricted turbidity sampling but at least 126 h of reliable records were completed by values calculated based on real pumping or turbine discharge and average turbidity values of the previous or following day. Twice, concentration data were only available for a short duration of 54 and 58 h during weekends, for the weeks from February 7th to 14th and from May 9th to 16th (marked "WE" in Figure 4.9). Neither the period from December 27th to February 7th, nor from May 5th to 14th were taken into account for sediment balance estimation because the turbidity sensor was out of order.

Even though there are big differences in the weekly sediment transfer, the transport between the two lakes is balanced over the monitoring period of eight months, with a total of $M_{S,\,Oa\,-\,Gr} = 22.2$ kt transferred from the upper into the lower reservoir and $M_{S,\,Gr\,-\,Oa} = 23.0$ kt pumped up from Lake Grimsel into Lake Oberaar. This corresponds to a total volume of $V_{S,\,Oa\,-\,Gr} = 14'820$ and $V_{S,\,Gr\,-\,Oa} = 15'306$ m^3. Consequently, the difference in transferred volumes for the two operation directions is $\Delta V_S \approx 0$.

Anselmetti *et al.* (2007) gave total sedimentation rates for Lake Oberaar and Grimsel of 22'200 and 74'650 m^3 respectively. Bonalumi *et al.* (2011) calculated a natural annual inflow of suspended sediment of 6.6 for Oberaar and 51.2 kt/year for Grimsel based on periodical in situ CTD measurements over two years. A comparison to these values emphasizes how much suspended sediment is constantly moved up and down by the Grimsel 2 plant. A mass corresponding to almost seven times the suspended sediment inflow to Lake Oberaar calculated by Bonalumi *et al.* (2011) was transported between the two reservoirs during the monitoring period. Suspended sediment volumes moved between the two lakes reach 130% and 40% of the annual deposited volumes in the upper and lower reservoir respectively. If the volume kept in suspension by the pumped-storage operations would contribute to the filling

up of Lake Oberaar or Grimsel, a volume corresponding to 0.26 or 0.15% of the reservoir volumes would be lost. These values are in the order of magnitude given by Beyer Portner and Schleiss (2000) for natural filling processes in Swiss reservoirs.

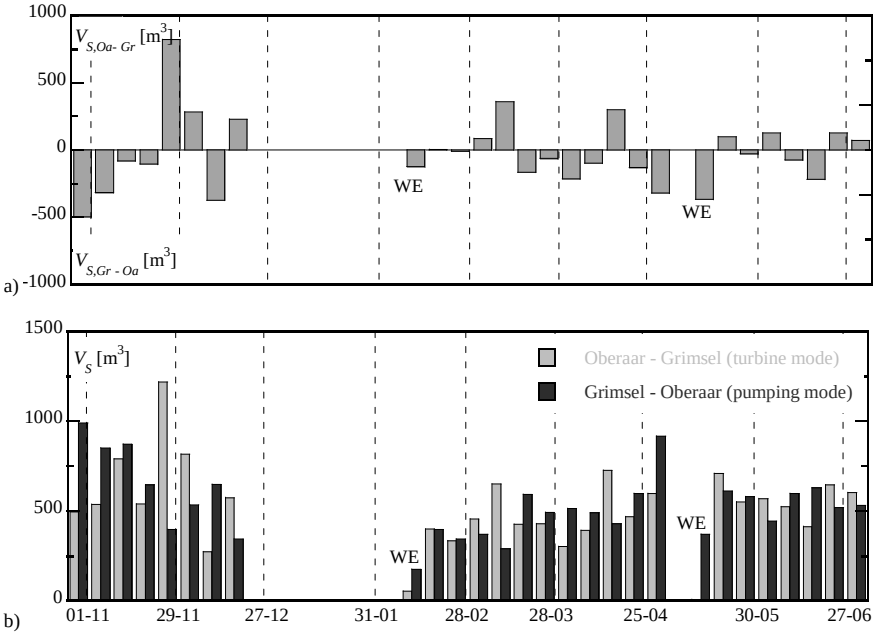

Figure 4.9 Sediment volumes V_S transferred during pumping (Gr - Oa) and turbine mode (Oa – Gr) (a) and sediment balance (b) over the sampling period from October 26th to June 20th

On an annual scale, sediment exchange will increase because the eight month balance will be completed with sediment contributions during summer months, contributing usually to about 70% of the sediment inflow into the reservoirs. Consequently, sediment volumes transported between the two lakes would be higher than mentioned in this study.

However, measurements show that an important amount of the sediment from pumping is moved back to the lower reservoir during turbine mode. Thus, pumped-storage activity does not induce an amplification of the actual sedimentation rate of the reservoirs. The pumped-storage generated turbulence is sufficient to keep the main part of the fine sediment in suspension. Periods of no operation, when neither pumps nor turbines are working, could lead to settling of sediment and thus influence the sediment balance.

4.5.2 Response of suspended sediment concentration to pumped-storage operation

The suspended sediment load in the pump and turbine water depends on the particle concentration in the two reservoirs. It is therefore linked to meteorological conditions, mainly snowmelt and rainfall events, governing the net particle inflow to the lakes. If one reservoir has a considerably higher concentration in front of the intake/outlet structure, suspended

sediment load will be initially different between the two operation modes and perceptible in the monitoring plots. This difference will remain as long as particle concentrations in the reservoirs have not been equilibrated.

However, for similar initial concentrations C_0, the ratio between suspended sediment concentration in pumping and turbine mode ($C_{m,Pump}/C_{m,Turb}$, Table 4.1) is driven by other parameters than C_0. The monitoring plots revealed high $C_{m,Pump}/C_{m,Turb}$ ratio for periods of low particle load around C_m = 60 mg/l as well as for C_m = 80 mg/l.

According to measurements of this study, reservoir level is the main parameter for differences between pumping and turbine mode. During late autumn and winter, when reservoir levels are high, no direct correlation between pumped-storage sequences and suspended sediment concentration in the transported water can be observed. When reservoir levels are low in spring, suspended sediment concentration is dependent on the pumping and turbine operations. Maximum and minimum ratios were $C_{m,Pump}/C_{m,Turb}$ = 1.16 and 0.93 respectively. High ratios, indicating higher concentrations in the pump water, are measured when the Grimsel reservoir level is below ~1870 m a.s.l., corresponding to an intake submersion of less than 22 m. Low ratios are observed when Lake Oberaar level drops below ~2268 m a.s.l., leaving an intake submersion of less than 36 m. Apparently, suspended sediment concentration in front of the intake/outlet zone is highest for low water level conditions due to increased turbulent mixing.

When the average particle load is the same during pumping and turbine mode, sediment transfer between the two reservoirs is mainly storage management dependent. However, even weeks with a high or low concentration ratio $C_{m,Pump}/C_{m,Turb}$ have rather equilibrated sediment balances. Figure 4.10 illustrates this observation and compares the volume ratio of suspended sediment $V_{S,Turb}/V_{S,Pump}$ to the water-sediment-mixture V_{Turb}/V_{Pump} exchanged by the Grimsel 2 plant. Values $V_{Turb}/V_{Pump} < 1.0$ indicate that more water is pumped upward into Lake Oberaar than turbined in the other direction.

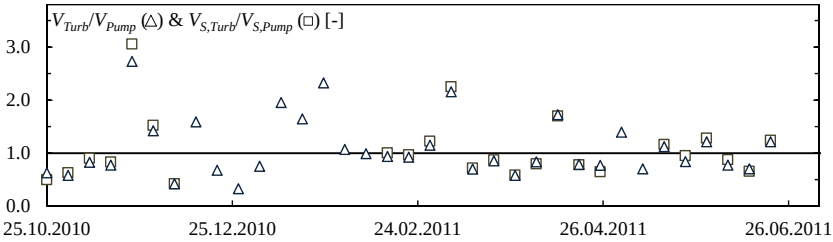

Figure 4.10 Volume ratios of water-sediment-mixture V_{Turb}/V_{Pump} (calculated based on discharge data provided by KWO) and suspended sediment $V_{S,Turb}/V_{S,Pump}$ (computed based on turbidity measurements) for the sampling period from October 26th 2010 to June 30th 2011

During 16 of 24 monitored weeks, more water and sediment were pumped from Lake Grimsel into Lake Oberaar. Nevertheless, sediment balance is equilibrated over the total monitoring period. Thus, sediment balance depends on the frequency and magnitude of the pumped-storage cycles.

4.6 Conclusions

Suspended sediment concentration in the water passing through the Grimsel 2 pumped-storage plant was continuously measured over a period of eight months by a turbidity probe installed on the upstream part of the pressurized shaft. An acquisition system provides data storage, remote access as well as real-time data display.

Sampled data reveal major changes in mean suspended sediment concentration C_m between late autumn, winter and spring months. In November/December a monthly average around C_m = 80 mg/l was measured. From February to April when reservoirs are ice and the catchment area is snow-covered, particle load is low with values between C_m = 55 and 60 mg/l. Suspended sediment concentration during snowmelt increased to C_m = 75 to 85 mg/l by May and June.

The sediment volumes moved by pumped-storage operations between Lake Oberaar and Grimsel correspond to 130% of the volume which is deposited annually in Lake Oberaar and to 40% of the annual sediment rate of Lake Grimsel. If comparing to the natural particle inflow of Lake Oberaar calculated by Bonalumi *et al.* (2011), the sediment mass transported up and down between the reservoirs is more than three times higher.

However, most of the suspended sediment volume entering the upper reservoir is transported back during turbine mode. The suspended sediment balance due to pumped-storage is equilibrated for the eight months monitoring period. The concentrations measured in the shaft show that an important part of the sediment is moved back to the lower reservoir during turbine mode. Therefore, pumped-storage activity in the observed conditions does not induce an amplification of the actual sedimentation rate of the reservoirs. Mixing processes allow keeping in suspension the main part of the fine sediment in front of the intake/outlet structures. By slowing down the settling of fine sediment continuous pumped-storage operation could contribute to an increased downstream transfer of suspended sediment, if the latter can be assured by a sluice opening or a bottom outlet close to the intake/outlet structure.

Pumped-storage sequences are reflected in the short-term evolution of sediment concentration especially when reservoir levels are low. Under such conditions, suspended sediment concentrations are highest in the intake/outlet zone. Periods with higher particle load during pumping mode are observed more frequently, with concentration ratios between pumping and turbine mode of $C_{m,Pump}/C_{m,Turb}$= 1.16. Lowest ratio is $C_{m,Pump}/C_{m,Turb}$= 0.93. Nevertheless, the global sediment balance of the two reservoirs due to pumped-storage operations is equilibrated, indicating the correlation between sedimentation load and frequency and magnitude of pumped-storage sequences.

Finally, the sediment monitoring system may be connected to the existing one of the power plant's control and management system. Thus, the plant operator could detect increasing sediment load in the pressurized shaft, indicating high sediment load in front of the intake/outlet structure and eventually adapt its operation concept to actively manage reservoir sedimentation. For example, after the arrival of a turbidity current in front of the intake/outlet structure, the plant operator could choose not to run the hydraulic machines but to proceed to a downstream transfer of the sediment laden flow, if hydraulic structures such as bottom outlets are located close to the intake/outlet zone. Else, he could adopt increased pumped-storage operation to guarantee increased mixing of the water column. Evidently, electricity marked will always constrain such operative measures. In addition to providing short-term

information, the turbidity monitoring system allows establishing a continuous sediment balance for long-term monitoring issues.

Sediment load in a power system depends on the reservoir level as well as the sediment yield from the catchment area. Snowmelt, heavy rainfalls and low reservoir levels increase suspended sediment in the operated water. In case of pumped-storage plants, concentration correlates with the in- and outflow cycles. High turbidity in front of the water intakes leads to significant moved sediment quantities. The sediment balance remains only in equilibrium as long as the turbine and pump operations have similar durations and sediment concentrations in the storage volumes are equal. Pumping of suspended sediment from a river or watershed with high erosion may lead to considerable sediment supply to the upstream lake and thus to reservoir sedimentation. Hence, turbidity monitoring in the power shafts allows estimation of long-term sediment balance and thus intervention planning.

Chapter 5

Experiments on jet behavior and flow patterns in a rectangular basin subject to in- and outflow sequences

The effect of in- and outflow sequences on flow patterns in a rectangular cuboidal basin was investigated by laboratory experiments combined with numerical simulations.

The experimental set-up consists of two interconnected basins with a bidirectional flow diverting system. 2D flow velocities were sampled by Ultrasonic Velocity Profilers (UVP) and turbidity was recorded continuously. Magnitude and frequency of the in- and outflow cycles were analyzed in a parameter study. In a preliminary test, centerline velocity and transversal velocity profiles of the jet were analyzed and discussed.

In a second phase, numerical simulations defined the time required to reach steady state conditions and thus constant kinetic energy in the test volume. Inflowing jets need more time to become established than flow fields during outflow sequences. The so-called “time to peak” t_P is defined for different discharges. For outflow sequences, computed flow patterns showed very low velocities toward the intake and low kinetic energy. During inflow conditions a quite stable jet with several recirculation cells was computed.

The UVP sampled flow fields confirmed the low velocity patterns during outflow sequences with flow orientation close to the intake and revealed rather fluctuating velocities in the rest of the basin. For inflow sequences, the measurements showed jet oscillation with recirculation cells. Outflow patterns were often influenced by the preceding inflow sequence. Horizontal flow mapping indicated backflow zones close to the bottom, developing mainly at high discharges.

The kinetic energy level in the basin depends on the cycle magnitude (discharge) and is much higher for inflow sequences. Cycle frequency has less influence. Intake positions close to the bottom or close to the free water surface lead to higher energy levels due to the development of vertical circulation cells, resulting in increased mixing..

5.1 Introduction

Knowledge of particle movement and flow patterns in a closed volumes by in- or outflow is important for many engineering applications, such as describing the disinfection process in drinking water storage tanks (Clark *et al.*, 1996), reservoir selective withdrawal, ventilation of confined spaces or smoke propagation in tunnels (Shammaa and Zhu, 2010). In chemical industries, where mixing is a common process, jet mixing has become an alternative to conventional impeller mixing (Wasewar, 2006). Inflow conditions are often described as turbulent jets, which have been studied extensively due to their practical relevance (Abramovich, 1963; Rajaratnam, 1976; Fischer *et al.*, 1979; Jirka, 2004).

In hydraulic engineering, the understanding of flow behavior in reservoirs subject to in- and outflow cycles allows specific design of intake/outlet structures as well as sluice gates and helps describing entrainment and settling processes of suspended particles. (Shammaa *et al.*, 2005, 2009) carried out experimental studies on flow fields upstream of orifices and sluice gates as well as in a shallow basin with a line inlet and a circular outlet. Kantoush *et al.* (2008) focused on flow patterns and sedimentation behavior in shallow reservoirs. De Cesare *et al.* (2006) described circulation in stratified lakes due to turbidity currents. Berezinskii *et al.* (1985) and Mikhailov *et al.* (1992) conducted experiments on the flow at the intake/outlet structures of pumped-storage plants.

However, most of the studies concern the evolution of flow patterns due to either in- or outflow, while the effect of in- and outflow sequences with different magnitude and frequency has not been analyzed yet. Inspired by the operating mode of pumped-storage plants, the objective of the present study was to analyze the flow patterns and the suspended sediment settling processes in a basin impacted by in- and outflow sequences.

Prior to experimental tests with sediment, jet development in clear water conditions was studied. Based on these results, a numerical model could be calibrated and applied to define the time to reach peak kinetic energy in the test volume for different discharges. This so-called “time to peak” t_P is one of the parameters that was varied during the experiments.

In this chapter, the experimental set-up and the measurement facilities are introduced. Jet characteristics in the given test conditions are defined and discussed. The numerical model and the simulation results are presented. The experiments with sediment focused on the description of the flow patterns and the development of kinetic energy induced by the in- and outflow sequences. The results of the experimental tests and numerical simulations are compared and discussed.

5.2 Experimental set-up and parameters

The laboratory test facility consists of two basins interconnected by a reversible flow diverting system with a pump for generating in- and outflow sequences. Pump discharge, flow velocities and turbidity in the main reservoir are measured. The experimental set-up, measuring techniques and test procedures are described hereafter.

5.2.1 Basins and flow diverter

Measurements were carried out in the rectangular main basin (subscript *MB*) with an inner length of $L_{MB} = 4.0$ m, an inner width of $B_{MB} = 2.0$ m and a height of $H_{MB} = 1.5$ m. The

smaller secondary reservoir or mixing tank (subscript *MT*) has a volume of V_{MT} = 1.0 x 2.0 x 1.2 m^3. The two reservoirs are interconnected through a pipe system equipped with a pump and a flow diverter allowing two flow directions:

- *IN*-sequence jet entering the main basin (inflow)
- *OUT*-sequence water flowing out of the main basin (withdrawal)

Figure 5.1 illustrates the experimental facility. The elliptical bell mouth shaped intake/outlet is located at the front wall of the main basin and can be implemented at z_i = 0.25, 0.5 and 0.75 m above the reservoir bottom. The bell mouth design reduces head losses and turbulence disturbing the flow in the vicinity of the structure (Jenzer Althaus, 2011). The intake is followed by a cylindrical throat with an inner diameter of D_i = 4.8 cm, connected to a rigid PVC pipe of the same diameter and a length of L = 1.5 m (~30 D_i). Thus, secondary effects such as pipe irregularities or bends in the approach section are minimized.

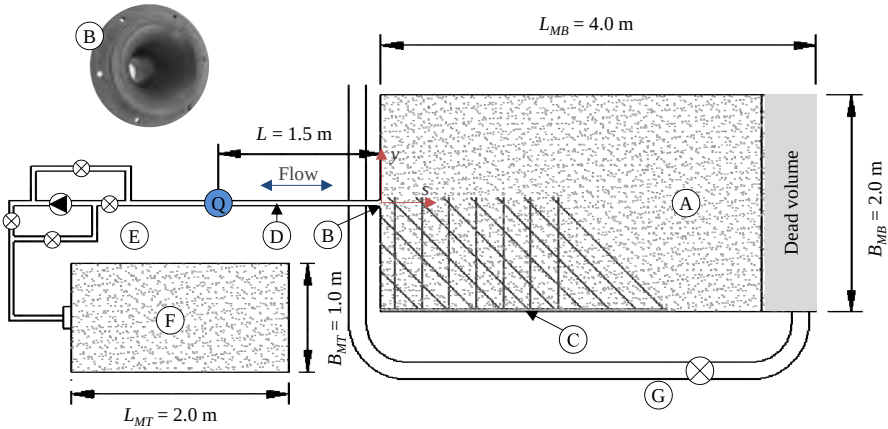

Figure 5.1 Laboratory set-up: A is the main basin; B, the intake/outlet; C, the UVP-frame with velocity measurement grid; D, the rigid pipe between the flow meter (Q) and the intake/outlet; E, the flow diverter; F, the mixing tank and G, the feeding conduit for initial filling of the system

Distances are generally normalized by B_{MB}. Velocities and time are commonly normalized by the approach flow velocity in the pipe $v_0 = Q_{IN,OUT}/A$ and the mean residence time $t_m = V_{MB}/Q_{IN,OUT}$ respectively (Stefan and Gu, 1992). For the description of jet behavior, length is normalized by the jet diameter D_j.

5.2.2 Ultrasonic velocity profiler

To describe jet characteristics for inflow sequences as well as flow fields in front of the intake for outflow sequences, the main basin has been equipped with *Ultrasonic Velocity Profilers* (UVP, MetFlow, Switzerland (SA, 2000)). The UVP technique was developed by Takeda (1995) and allows the measurement of instantaneous flow velocity profiles by the Doppler shift of echoes reflected by small particles in the liquid. In former studies, turbidity currents and 2D flows in shallow reservoirs have been successfully measured by this flow mapping system (De Cesare and Schleiss, 1999; Kantoush *et al.*, 2008). Suspended sediment provides

the optimal flow tracer to obtain good sampling echo. For clear water conditions, hydrogen bubbles were generated in the system (Meile *et al.*, 2008).

Horizontal 2D velocity fields were measured at several levels in the main basin. Seventeen 2 MHz UVP transducers were aligned along the side wall of the test volume on an aluminum frame, guaranteeing non-intrusive measurement. Operating azimuth angles of 90° and 45° were applied, allowing flow velocity sampling at 28 grid points in one quadrant of the test volume (Figure 5.1) corresponding to an area of 1.0 x 2.0 m^2. The frame was moved vertically to perform measurements at z = 0.25, 0.50 and 0.75 m from the bottom.

For measuring the centerline and transversal velocities of the jet, two MetFlow prototype transducers with sampling frequencies of f = 0.5 and 1.0 MHz were applied for the first time in laboratory conditions. These devices are especially well suited for long distance measurements in the jet axis. The sensors were fixed on a steel bar and placed in the jet axis between s = 0.5 to 1.7 m from the intake/outlet in the main basin. As both probes gave satisfying and consistent results, the presented results are based on both 0.5 and 1.0 MHz UVP data.

5.2.3 Turbidity probe

For tests with suspended sediment, two *SOLITAX sc* turbidity sensors (HACH LANGE, Germany) were used. Connected to the acquisition and display system *SC100 Controller* of the same manufacturer, the probe determines the turbidity in the sampled water based on an infrared absorption scattered light technique. The linear relationship between the turbidity *TU* [FNU] and the suspended sediment concentration C [g/l] was preliminarily defined for known sediment concentrations between C = 0.3 and 1.5 g/l.

In the main basin, the turbidity probe continuously recorded at intake height in the opposite quadrant of the UVP measurements. During the test, the probe was moved vertically to evaluate the distribution of the suspended sediment over the height. In the mixing tank, the measurements were performed in the center of the volume at the entering height of the inflow/outflow pipe.

5.2.4 Experimental parameters

Settling process is affected by the viscosity v and density ρ_w of the surrounding fluid as well as the diameter d_S, material density ρ_S, shape SF and concentration C_0 of the particles (van Rijn, 1984). During the experiments, water temperature varied between T_w = 14 and 17 °C. Viscosity effects on settling velocity are therefore small and can be neglected.

The suspended sediment was reproduced by walnut shell powder, a homogeneous material appropriate for reservoir sedimentation modeling (Kantoush *et al.*, 2008; Jenzer Althaus, 2011). Its specific density is ρ_s = 1480 kg/m^3 and the mean particle diameter is d_m = 121 µm. As such, they allow the reproduction of the prototype ratios between flow velocities and settling velocities in the reservoir. The particles are slightly angular shaped, like real sediment. The resulting ratios between flow velocities in the reservoir and settling velocities are similar to prototype conditions.

To investigate the influence of in- and outflow sequences on the flow patterns and the fine sediment behavior, the following five parameters were varied:

- Discharge Q: flow patterns, turbulence and kinetic energy in the reservoir were measured for five different discharges between $Q = 0.3$ and 1.1 l/s, as presented in Figure 5.2a, b and c. These values were given by the volume of the main basin as well as real case pumped-storage cycles.
- Frequency of in- and outflow cycles Kt_P: the basic configuration considered in- and outflow sequences of the duration t_P ("time to peak") to achieve steady conditions in the main basin. Further, this duration was multiplied by the parameter Kt_P, resulting in four different cycle frequencies (Figure 5.2b, d, e and f). Due to the equal duration of in- and outflow sequences, the discharge curves correspond to a square wave function.
- Relative duration between in- and outflow $t_{P,IN}/t_{P,OUT}$: Two additional configurations were tested, where the inflow sequence was twice as long as an outflow sequence and vice-versa.
- The influence of initial sediment concentration was addressed by varying the initial concentration C_0 in the two basins.
- Position of the intake/outlet structure above the reservoir bottom z_i: flow patterns were assumed to change with the intake/outlet position. Therefore, three different positions were investigated.

t_P depends on the discharge. As illustrated in Figure 5.2, five in- and outflow cycles were fixed for the experiments, resulting in test duration of 1 h 20 min to 13 h 36 min. Between in- and outflow sequences no dissipation period without operation was assumed.

The experiments were performed according to the Froude similarity criterion, respecting the same ratio between inertia and gravity forces in prototype (subscript *prot*) and model conditions (subscript *mod*). Such, geometric (L) and cinematic parameters (v, t, Q) follow the relations

$$\lambda_L = \frac{L_{prot}}{L_{mod}}; \qquad \lambda_{v,t} = \lambda_L^{1/2}; \qquad \lambda_Q = \lambda_L^{5/2} \qquad \text{(Eq. 5.1)}$$

The Reynolds number at the intake/outlet is $7'560 \leq \mathrm{Re}_i \leq 29'180$ and thus turbulent for every tested discharge.

5.2.5 Test procedure

After filling the main basin to $H_{0,MB} = 1.15$ m and the mixing tank to its full level $H_{0,MT} = 1.06$ m, the two reservoirs were disconnected from the laboratory circuit. According to needed initial concentration, walnut shell powder was mixed with water by a pressurized air supply on the reservoir bottom. The whirling flow conditions maintained the sediment in suspension until the start of the in- and outflow sequences at $t = 0$ s. As the total water volume remained constant over the test duration, the water level in the basins changed according to the operation mode. Maximum level variation in the main basin reached $\Delta H_{MB} = 0.18$ m.

UVP measures were carried out one to three times per sequence, depending on the cycle duration.

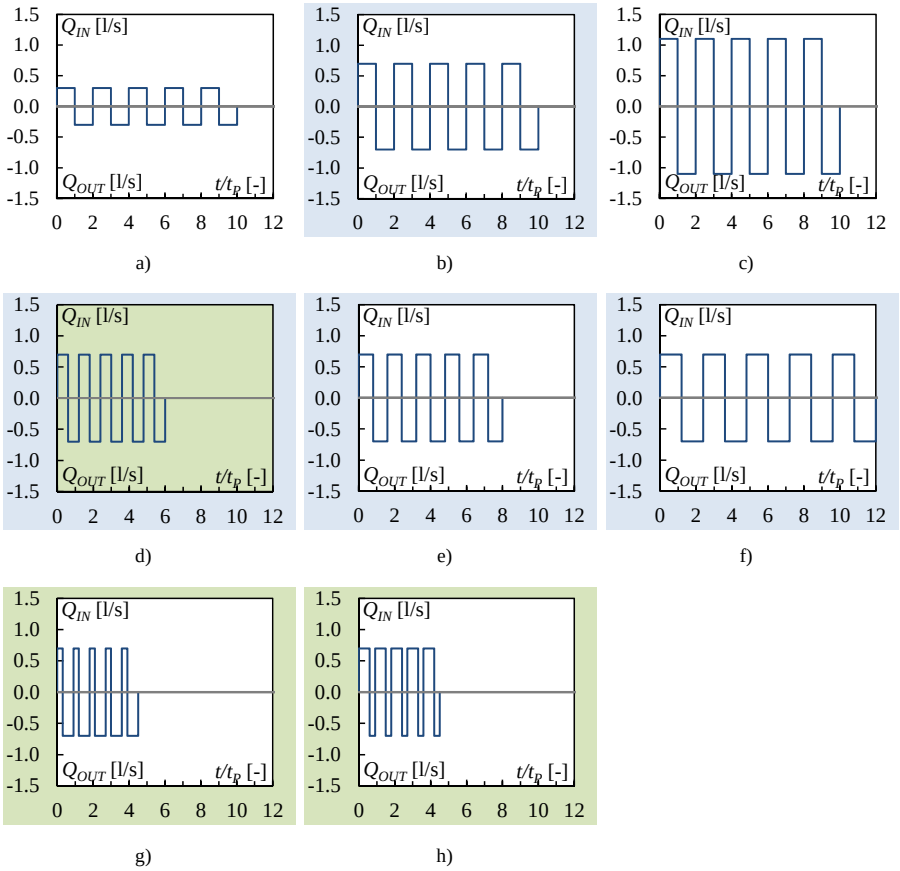

Figure 5.2 In- and outflow cycles for six test configurations. Variation of discharge Q = 0.3 (a), 0.7 (b) and 1.1 l/s (c) for Kt_P = 1.0. Variation of cycle frequency Kt_P = 0.6 (d), 0.8 (e) and 1.2 (f) for Q = 0.7 l/s. Variation of relative cycle duration $t_{P,IN}/t_{P,OUT}$ = 0.5 (g) and 2.0 (h) for Q = 0.7 l/s and Kt_P = 0.6

5.3 Preliminary experiments

Water injected into the basin during inflow sequences is a source of momentum and energy for the water body. A so-called turbulent jet is formed when its Reynolds number is Re_j > 2000 to 3000 (Blevins, 1984; Revill, 1992; Jirka, 2004). In this study, the inflowing fluid was the same as in the reservoir, leading to a submerged axisymmetric turbulent round jet. Centerline velocity and the transversal velocity profile, measured by the UVP, are presented and compared to common jet theory.

5.3.1 Submerged turbulent jet notions

A submerged turbulent jet consists of an initial core, a transition zone and a fully developed jet region (Figure 5.3). The core flow is nearly free of shear and its velocity is equal to the

nozzle exit velocity v_0 under uniform inflow conditions. The core flow is surrounded by a turbulent shear or mixing layer, forming a boundary between the core flow and the reservoir fluid. The imprint of the nozzle shape disappears when the turbulent eddies in the shear layer destroy the nozzle core flow and penetrate to the jet axis. The resulting eddy-dominated flow is called fully developed and starts at a distance between 4.3 and 10 D_j from the nozzle. After about 400 D_j, the mixing effect of a turbulent jet is generally considered as insignificant (Revill, 1992).

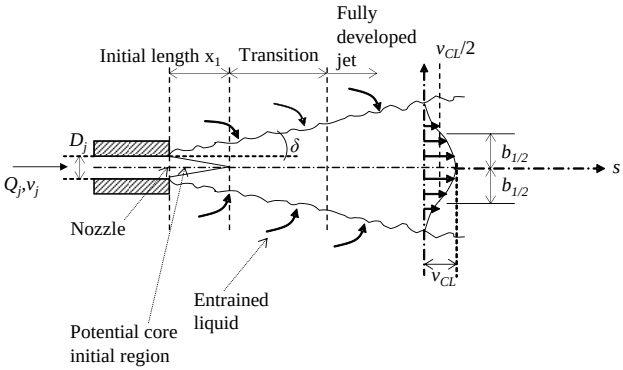

Figure 5.3 Jet flow behavior according to Blevins (1984)

Jet momentum flux M_j, discharge Q_j and Reynolds number Re_j are defined as follows:

$$M_j = v_0^2 \cdot A_j \qquad \text{(Eq. 5.2)}$$

$$Q_j = v_0 \cdot A_j \qquad \text{(Eq. 5.3)}$$

$$\mathrm{Re}_j = \frac{v_0 \cdot D_j}{\upsilon} \qquad \text{(Eq. 5.4)}$$

where v_0: the efflux velocity [m/s],
A_j: the outlet section [m^2],
D_j: the pipe diameter [m], and
v: the fluid viscosity [m^2/s].

5.3.2 Centerline jet velocity

In the fully developed jet region, the centerline velocity v_{CL} continuously decreases with the distance s in jet direction. Many authors defined the centerline velocity as

$$v_{CL}(s) = C_1 \cdot \frac{v_0 \cdot D_j}{s} \qquad \text{(Eq. 5.5)}$$

where C_1: a constant [-], and
s: the distance from the nozzle.

Abramovich (1963) gives a value of $C_1 = 7.32$, while Revill (1992) and Blevins (1984) found $C_1 = 6$. Rajaratnam (1976) presents results from several studies, in which C_1 ranges

from 5.75 to 7.32. Jirka (2004) provides a slightly different formulation of the centerline velocity, resulting in C_1 = 6.43.

5.3.3 Velocity at transverse distance

When the jet enters the basin, it expands at an expansion angle δ. In the literature δ between 15° and 25° are found for jet Reynolds numbers $Re_j > 100$ (Wasewar, 2006). At the transverse distance $r = b_{1/2}$ from the jet axis, axial velocity $v(r)$ falls to half of the centerline velocity v_{CL}. Assuming a Gaussian distribution over the jet width, the velocity at transverse distance r in s direction can be written as:

$$v\left(r = b_{1/2}\right) = C_2 \cdot \frac{v_{CL}}{2};\ v(r) = v_{CL} \cdot e^{-C_3\left(r^2/s^2\right)} \qquad \text{(Eq. 5.6)}$$

where C_2, C_3: constants [-].

Values of C_2 = 0.082 to 0.1 and C_3 = 70 to 104.1 are found in literature (Abramovich, 1963; Rajaratnam, 1976; Blevins, 1984). Jirka (2004) assumed a Gaussian distribution with a slightly different correlation between jet width and centerline velocity, resulting in C_3 = 82.6.

5.3.4 Experimental results

Preliminary experiments studied jet behavior in the main basin during inflow sequences. The measured velocities were compared to literature. Furthermore, the experimental results were used to define the adequate turbulence model for the numerical simulations.

According to the measuring distance, the UVP probes are able to record velocity magnitudes in a certain range. For a given sampling frequency, short distance measurements allow recording higher velocities than long distance measurements. Thus, a sensor placed far away from the jet nozzle will record reliable data until the point when the emitted ultrasonic beam exceeds the jet. From there, the probe starts to take into account ambient slow flow, underestimating the jet velocity. Thus, the centerline velocity $v_{CL}(s)$ over a distance up to s/D_j = 30 is established by several measurements, as illustrated in Figure 5.4a and b. For the core velocity measurement, up to s/D_j < 6 to 10, the 1 MHz probe resulted more appropriate and was therefore used for completing the centerline velocity development (Figure 5.4b to d).

Due to the intake/outlet geometry, the jet characteristics are slightly different than the one from other authors. The jet core is short and the centerline velocity is higher than the estimated inflow velocity v_0 in the pipe approach section. The distance up to $5D_j$ is marked by a drop to approximately v_{CL}/v_0 = 0.8. Then, the decrease of centerline velocity follows the theoretical curves with C_1 = 6 approximately. For higher discharges the jet approaches the curve given by Revill (1992), as shown in Figure 5.4. However, the short and fast decrease of v_{CL} over a length of approximately s/D_j = 5 to 6 is common for all tested discharges.

Velocity in axis direction, but at transverse distance r from the centerline was measured at eight locations between s = 0.1 and 1.1 m. The measurements show a deceleration and an expansion of the jet with increasing distance from the outlet. Comparison with values from literature confirms fast jet expansion and the rapid decrease of velocities (Figure 5.5). The difference at $r/r_j = s/D_j = 0$ might come from the velocity averaging by the probe, taking into account still ambient water.

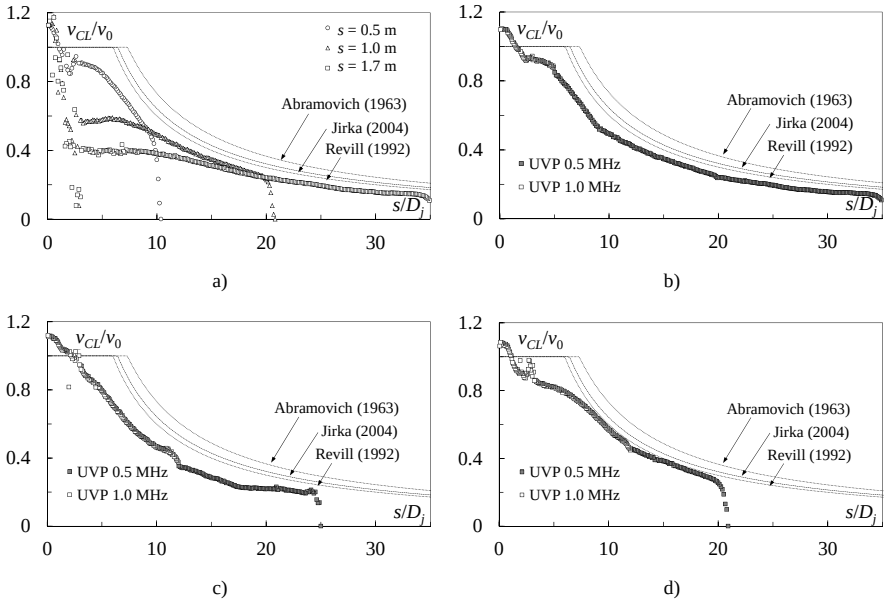

Figure 5.4 Dimensionless jet centerline velocity v_{CL}/v_0 as a function of dimensionless distance from the outlet nozzle s/D_j. Comparison between experimental results and values from literature. Velocities recorded by the 0.5 MHz UVP placed at different distances s from the nozzle for discharge Q_{IN} = 0.7 (a) and envelope curves completed with 1.0 MHz UVP measurements for discharges Q_{IN} = 0.7 (b), 0.3 (c) and 1.1 l/s (d)

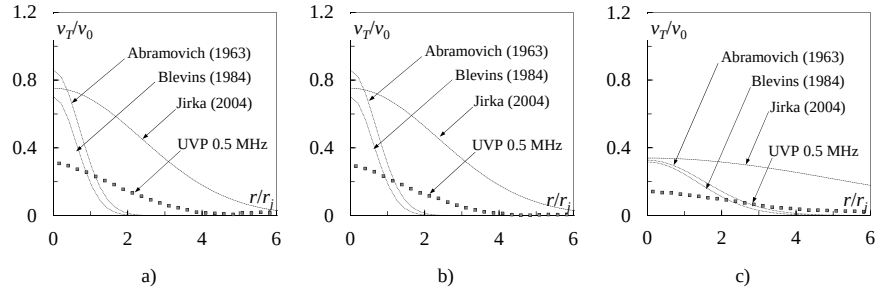

Figure 5.5 Dimensionless jet velocity in s-direction v_T/v_0 as a function of dimensionless transverse distance from the jet axis r/r_j. Values from literature as well as experimental results. UVP measurements for Q_{IN} = 0.7 l/s at s = 0.6 m (a) and for Q_{IN} = 1.1 l/s at s = 0.6 (b) and 1.1 m (c)

5.4 Numerical modeling

Numerical simulations were carried out with ANSYS-CFD to investigate the development of flow patterns and kinetic energy in the main basin as well as to provide the parameter t_P for the laboratory experiments. The k-ε turbulence model is commonly used (Cai *et al.*, 2009;

Khosronejad and Rennie, 2010). In the framework of this project, an evaluation of the most suitable turbulence model was carried out, based on the analysis of the centerline velocity and transversal velocity profiles of the jet. Simulation time step was optimized according to the kinetic and the turbulent kinetic energy evolution in the test volume. Then, inflow, outflow and so-called dissipation-sequences (no operation after an in- or outflow sequence) were simulated for the same five discharges as investigated in experiments.

5.4.1 Geometry, meshing and boundary conditions

The model reproduces the entire main basin and L = 0.5 m of the rigid pipe for water supply or withdrawal (Figure 5.6). As the model is operated at constant water level, mass balance is assured by a slightly asymmetrical overflow condition on the rear wall of the basin, designed as an opening with relative pressure p_{rel} = 0 bar. The elements of the structured mesh are mainly hexahedral. The maximum cell size was set to 2 cm in the pipe and the area of jet and 10 cm in the remaining volume. The overflow section and the reservoir bottom were meshed with 5 cm elements. Transition between the blocks is assured by a tetrahedral meshing.

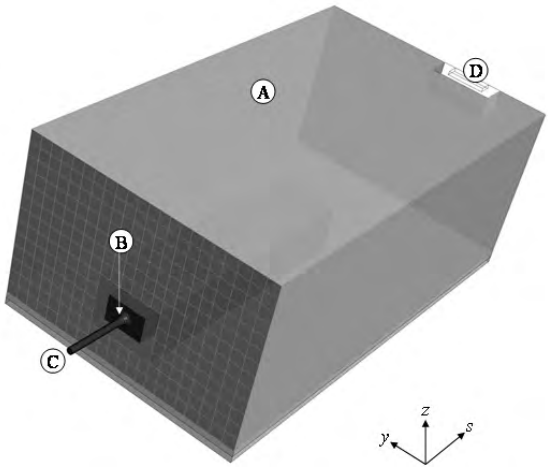

Figure 5.6 Numerical model of the experimental facility with indicated mesh for ANSYS-CFD modeling. A is the main basin; B, the intake/outlet; C, the pipe from/toward the intake/outlet (inlet or outlet boundary) and D, the spillway section (opening boundary, p_{rel} = 0)

Depending on in- or outflow sequence, the end of the pipe was defined as inlet or outlet boundary condition with a fixed discharge. All vertical walls, the bottom and the pipe walls were considered as so-called no slip boundaries on which flow velocity is v = 0 cm/s. Free water surface is a so-called free slip wall with no shear stress and a normal velocity component of 0.

5.4.2 Turbulence model

Two different families of turbulence models were analyzed, eddy viscosity turbulence models on the one hand (*k-ε* and eddy viscosity transport) and the explicit algebraic Reynolds stress model (EARSM) on the other hand.

All tested turbulence models well represented the non-uniform velocity distribution at the outlet, marked by an initial core velocity higher than the mean velocity in the approaching pipe section. The short core is well reproduced as well. The numerical model overestimates the centerline velocity compared to the experimental results.

The explicit algebraic Reynolds stress model (EARSM) largely overestimates velocities in the fully developed jet region. The *k-ε* and eddy viscosity transport turbulence models reproduce the fast decreasing core velocities and fit relatively well to values from literature. Especially the eddy viscosity transport model shows good agreement with values from literature for the fully developed jet.

To check the model stability the three turbulence models were tested at several discharges. As for the experiments, centerline velocity and relative core length are quite insensitive to discharge variations. The EARSM was abandoned as it leads to less satisfactory results than the two eddy viscosity turbulence models (Figure 5.7).

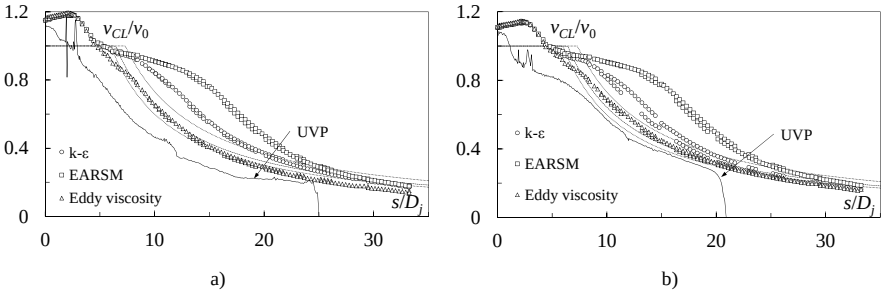

Figure 5.7 Dimensionless jet centerline velocity v_{CL}/v_0 as a function of dimensionless distance from the outlet nozzle s/D_j. Comparison between numerical computation, experimental results and values from literature for discharges Q = 0.3 l/s (a) and 1.1 l/s (b)

The comparison between computed transversal velocity profiles and the values given by Abramovich (1963), Blevins (1984) and Jirka (2004) reveals that both *k-ε* and eddy viscosity transport models correctly reproduce the Gaussian distribution. Velocity distributions are closer to literature than the experimental results. For low discharges the eddy viscosity transport model overestimates velocities for $r/r_j > 2$, while the *k-ε* model is more adopted and consequently used for further numerical simulations (Figure 5.8).

With the *k-ε* model, the calculation time step Δt was optimized to provide good results within reasonable simulation time. On the one hand, the temporal evolution of kinetic energy indicates flow stability in the test volume. On the other hand, turbulent kinetic energy allows the evaluation of adequate simulation of turbulent phenomena. Kinetic energy converged to a stable value for Δt = 10 s with high fluctuations of turbulent kinetic energy (Figure 5.9). Thus,

Δt = 5 s has been adopted, giving satisfying results for both kinetic and turbulent kinetic energy evolution.

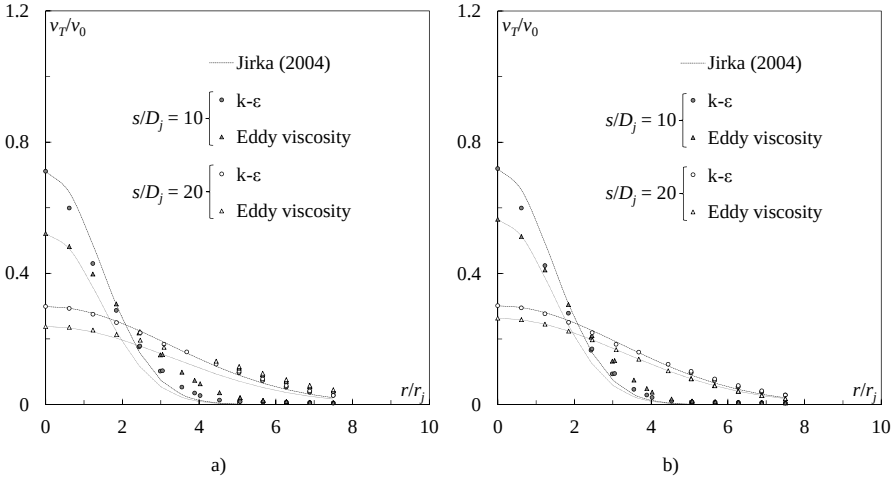

Figure 5.8 Dimensionless velocity in s-direction v_T/v_0 as a function of dimensionless distance to the jet axis r/r_j. Comparison between computation results of the ANSYS-CFD model and values from literature for discharges for different turbulence models and Q = 0.3 l/s (a) and 1.1 l/s (b)

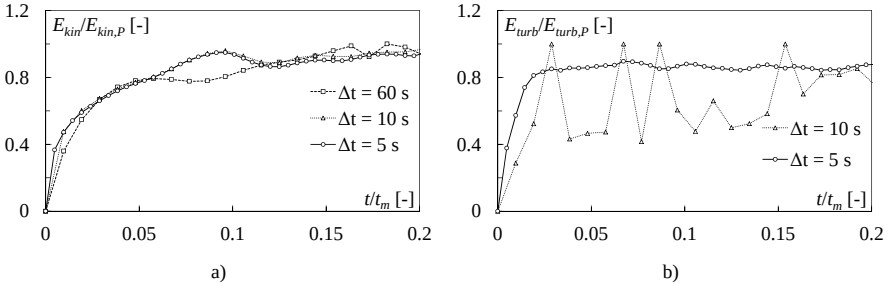

Figure 5.9 Evolution of dimensionless kinetic energy $E_{kin}/E_{kin,P}$ (a) and dimensionless turbulent kinetic energy $E_{turb}/E_{turb,P}$ (b) as a function of dimensionless time t/t_m. Inflow sequence for discharge Q = 1.1 l/s and time steps Δt = 5, 10 and 60 s

5.4.3 Evolution of kinetic energy

The time to achieve steady state conditions in the main basin depends on discharge. The so-called “time to peak” t_P defines the duration to reach maximum kinetic energy in the test volume, indicated by fluctuations on the peak value smaller than 5% over the following 24 simulation time steps. In the numerical model, the total kinetic energy was calculated based on the flow velocities computed in each grid cell. t_P was determined for three different conditions (inflow, dissipation and outflow) and for five discharges. Values of

$10 \leq t_P \leq 68$ minutes were found according to discharge and operation mode. t_P is higher for the inflow sequences. The jet formation requires more time than the flow field for flow withdrawal. Table 5.1 gives the mean residence time t_m and the time to reach maximum kinetic energy for in and outflow conditions $t_{P,IN}$ and $t_{P,OUT}$ for the five discharges.

Table 5.1 Mean residence time t_m, time to peak $t_{P,OUT}$ & $t_{P,IN}$ as well as the ratio $t_{P,IN}/t_m$ for different discharges Q

Q [l/s]	t_m [s]	$t_{P,OUT}$ [s]	$t_{P,IN}$ [s]	$t_{P,IN}/t_m$ [-]
0.3	30’056	3840	4080	0.136
0.5	18’034	1680	2280	0.126
0.7	12’881	1200	1500	0.116
0.9	10’019	930	1080	0.108
1.1	8’197	750	810	0.099

Figure 5.10 shows the evolution of kinetic energy in the test volume during consecutive inflow-dissipation-outflow conditions. It reveals that an outflow sequence generates only 60% of the kinetic energy due to a preceding inflow sequence. Steady state conditions are reached faster for outflow and dissipation sequences with no operation. At the beginning of the inflow sequence, the jet entering the basin generates a fast increase of kinetic energy, with similar growth rates up to $E_{kin}/E_{kin,P} = 0.6$ for all discharges. After reaching a high energy level, fluctuations appear until values achieve peak energy and stabilize. While high discharges require less absolute time to develop steady state conditions, smaller ones generate rates present less fluctuation around the peak energy value.

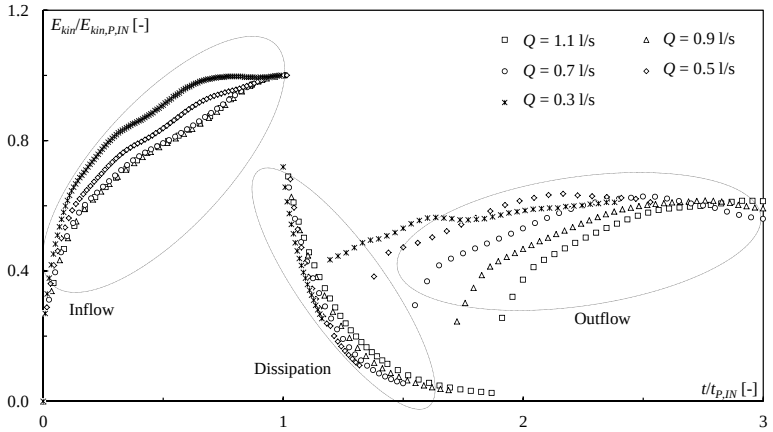

Figure 5.10 Evolution of dimensionless kinetic energy $E_{kin}/E_{kin,P,IN}$ as a function of dimensionless time $t/t_{P,IN}$. Inflow-dissipation-outflow-cycles for discharges Q = 0.3 to 1.1 l/s

Dissipation requires more time after inflow sequences for high discharges. As such, a dissipation period after an inflow sequence at Q = 1.1 l/s lasts about 0.8 $t_{P,IN}$, whereas only 0.2 $t_{P,IN}$ is required to regain still water conditions after an inflow sequence for Q = 0.3 l/s.

Finally, when water is withdrawn from the basin, kinetic energy develops slower than during an inflow sequence. Velocities start increasing slowly in front of the intake and develop a stable flow field in the volume. Specific duration $t_{P,OUT}$ is less than $t_{P,IN}$ because the relevant phenomena are less turbulent and the evolution of kinetic energy is less affected by fluctuations around the peak value.

Thus, the configuration of an inflowing jet is the critical case regarding the development of steady state conditions in the main basin. The time to peak for an inflow sequence $t_{P,IN}$ will serve as reference time for the cycle duration of the experiments.

5.4.4 Flow patterns in clear water conditions

Numerical modeling was carried out in clear water conditions for an intake position z_i/B_{MB}= 0.25 and five discharges. Later, the intake position was changed to z_i/B_{MB}= 0.125 and 0.375 to analyze the influence on the flow patterns. Flow fields in the main basin were sampled in three vertical (at y/B_{MB}= -0.25, 0 and 0.25) and three horizontal sections (at z/B_{MB}= 0.125, 0.25 and 0.375) of the reservoir.

Computations show flow patterns with velocities smaller than v/v_0 = 0.08 at s/D_j = 1 for outflow sequences at maximum discharge. Figure 5.11 gives the flow field at z/B_{MB}= 0.25. At the end of the outflow sequence, two recirculation cells are observed in the rear part of the basin. The behavior is independent of the discharge, affecting only the magnitude of the flow velocities in the test volume.

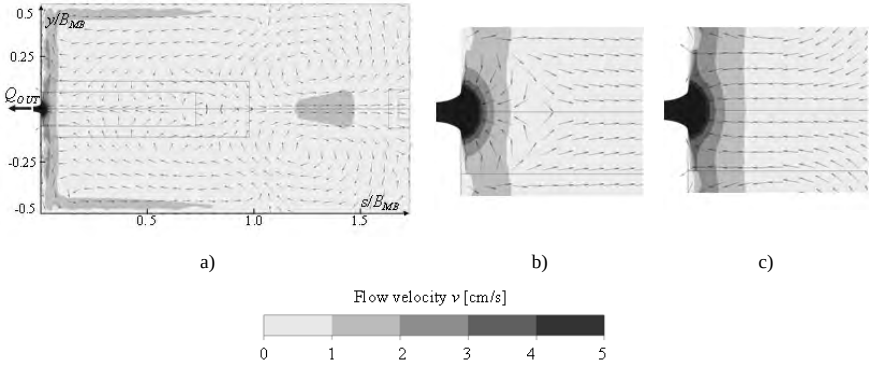

Figure 5.11 Horizontal flow patterns computed by ANSYS-CFD at z/B_{MB} = 0.25 (intake axis), velocity v for Q = 1.1 l/s at t = 240 s before the end of an outflow sequence (a). Zoom to flow field close to the intake at t = 120 s after the start (b) and t = 240 s before the end (c) of an outflow sequence

During an inflow sequence and after the jet development, two recirculation cells appear at z/B_{MB}= 0.25 (Figure 5.12a). However, flow conditions in the volume are not stable yet. Once the jet is properly developed, the secondary currents in the basin become stable in space and time with two almost symmetrical recirculation cells in the fully developed jet zone (Figure 5.12b).

Toward the end of the inflow sequence, the circulation cells tend to split in two, but no clear separation into four entirely developed cells occurs. In the vertical section through the

intake/outlet, one main rotating cell forms at the rear of the basin, stabilizing immediately after the beginning of the sequence, remaining rather stable (Figure 5.12).

The jet is slightly expanding toward the basin bottom. Flow patterns at z/B_{MB}= 0.125 and 0.375 have the same main characteristics as in the jet axis (Figure 5.13) with lower velocities.

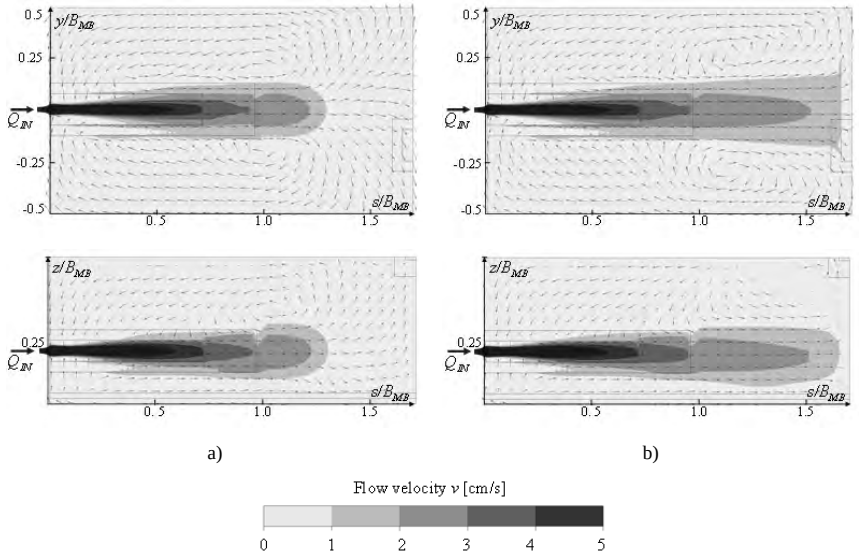

Figure 5.12 Horizontal flow patterns at z/B_{MB} = 0.25 (above, at intake axis) and vertical flow patterns at y/B_{MB} = 0 (below, at intake axis) computed by ANSYS-CFD. Velocity v for Q = 1.1 l/s at t = 120 s after the start (a) and t = 240 s before the end (b) of an inflow sequence

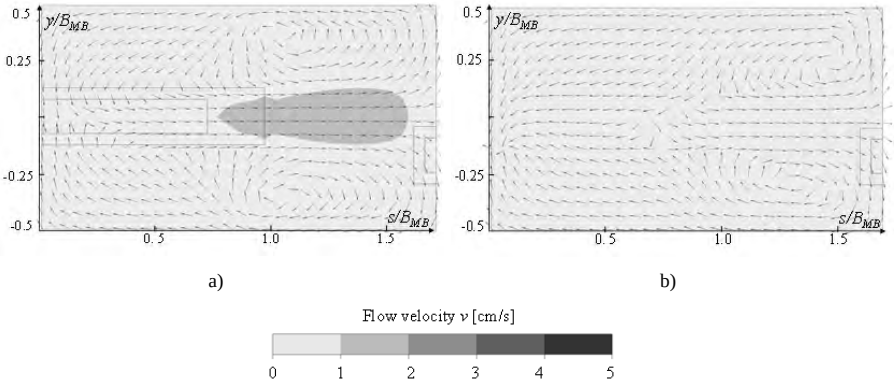

Figure 5.13 Horizontal flow patterns computed by ANSYS-CFD at z/B_{MB} = 0.125 (a) and 0.375 (b), velocity v for Q = 1.1 l/s at t = 240 s before the end of an inflow sequence

5.5 Experimental results and discussion

Results from laboratory investigations are presented for varying discharge Q and cycle duration t_P. The measured flow fields are represented for one quadrant of the main basin (Figure 5.1). Based on the 28 UVP measuring points, linear interpolation allowed a finer grid to illustrate the 2D flow patterns. Kinetic energy evolution is calculated according to the velocity measurements and compared to numerical results.

5.5.1 Horizontal flow patterns for variable discharge

Preliminary numerical simulations revealed that inflow sequences generates a jet including some three-dimensional movement in the basin with two horizontal and one vertical recirculation cell. The 2D UVP measurements define horizontal flow patterns at z/B_{MB} = 0.125, 0.25 and 0.375. Hence, some 3D behavior in the main basin can be characterized.

Figure 5.14 presents the development of horizontal 2D flow patterns during an inflow sequence, for the five investigated discharges at t = 120 s after the beginning and t = 240 s before the end of an inflow sequence. Velocities are normalized with the jet outflow velocity $v_0 = Q_j/A_j$. The jet develops immediately after the start of the inflow sequence and oscillates slightly along its axis. Small circulation cells are formed at the boundary between the jet and the surrounding water. This initial behavior is similar for all discharges. By the end of the sequence, a quite important recirculation cell is established which occupies the entire sampling section for the discharges Q = 0.9 and 1.1 l/s (Figure 5.14d and e, ii). For lower discharges, the boundary of the recirculation cell establishes at s/B_{MB} = 0.4. The corner area of the basin remains almost unaffected.

Characteristic normalized horizontal flow patterns for an outflow sequence are presented in Figure 5.15 for the five discharges at t = 120 s after the beginning and t = 240 s before the end of an outflow sequence. In most test runs, the measurement shortly after the change in operation mode reveals that the big recirculation cell forming for high discharges persists in time before dissipating its energy and disappearing. Generally, velocities are decreasing very fast. Especially for low discharges the flow patterns recorded t = 120 s after the start of the outflow sequence are already characterized by very low flow velocities. By the end of the sequence, the velocities near the intake/outlet are mainly orientated toward the latter, while the rear of the sampled section is quasi stagnant without any preferential flow orientation.

The sampling on horizontal sections above and below the intake/outlet axis may allow a detection of some three-dimensional movements. The 2D flow patterns at z/B_{MB} = 0.125 and 0.375 are very similar for outflow sequences with fluctuating flow orientation, influenced by the precedent inflow sequence. The flow field near the intake has only a restricted effect on the flow field.

Horizontal flow patterns at z/B_{MB} = 0.125 and 0.375 during inflow sequences show the expansion of the jet as well as some unsteady behavior with an oscillating and sometimes deflected jet due to secondary flow phenomena. Mostly, jet expansion becomes visible at s/B_{MB} = 0.6 either in the section above or below the intake/outlet axis. These sections then also include the recirculation cells around the jet (Figure 5.16a and b).

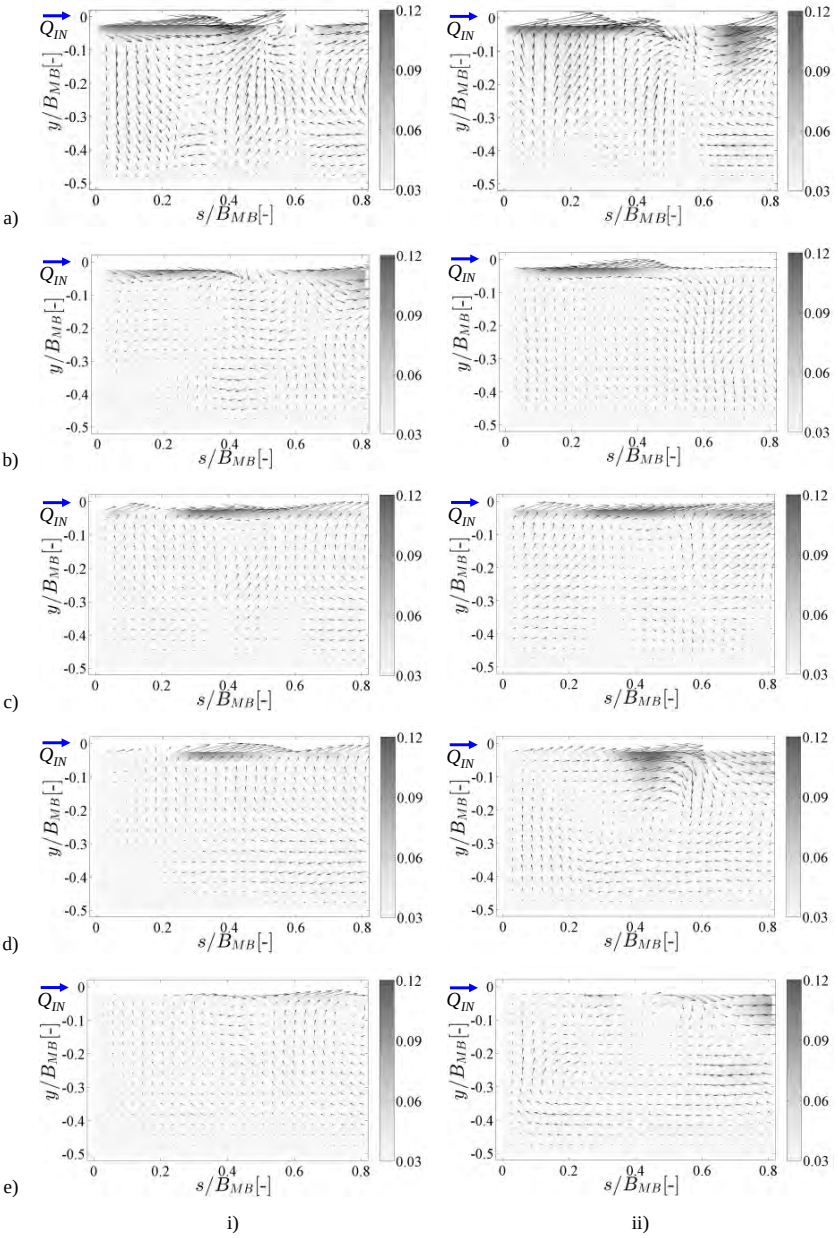

Figure 5.14 UVP sampled horizontal flow patterns at z/B_{MB} = 0.25 (intake axis), dimensionless velocity v/v_0 for Q = 0.3 (a), 0.5 (b), 0.7 (c), 0.9 (d) and 1.1 l/s (e) and t = 120 s after the start (i) and t = 240 s before the end (ii) of an inflow sequence

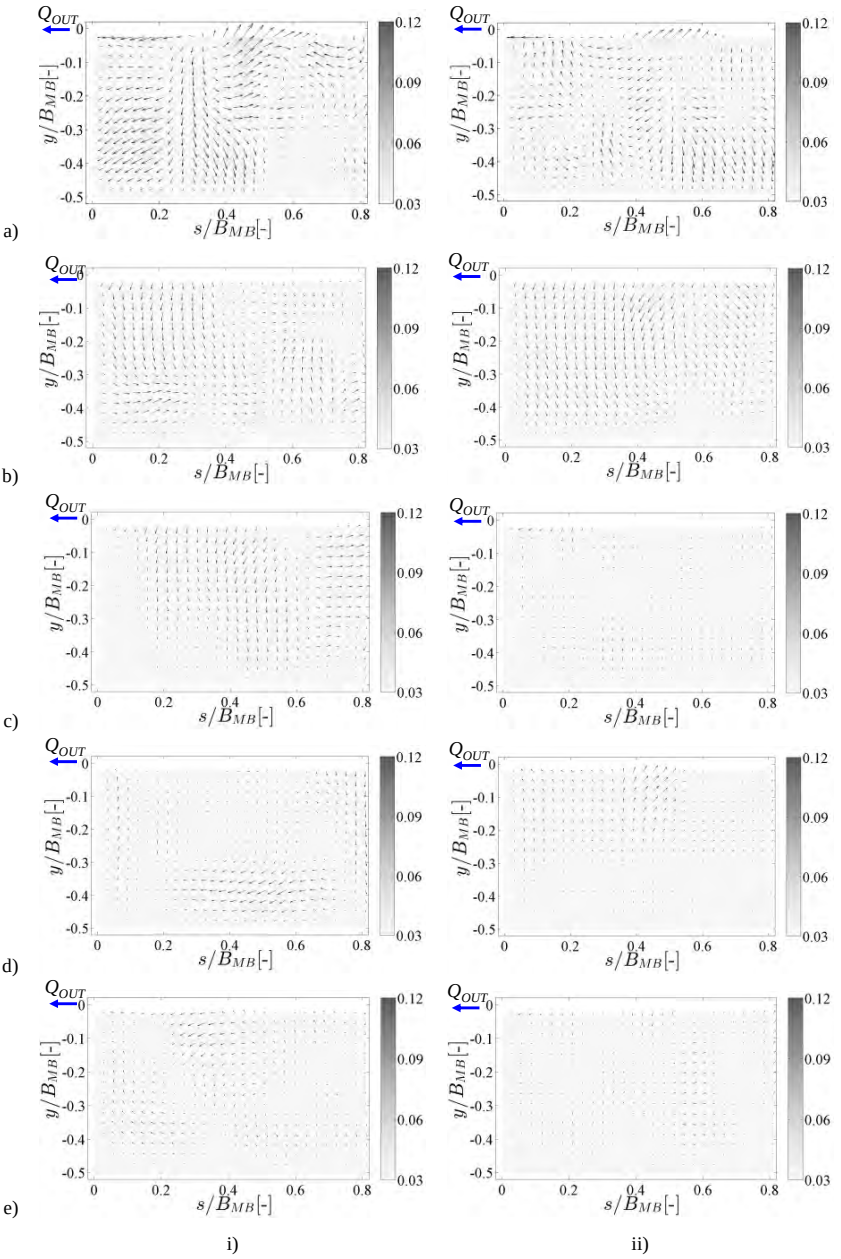

Figure 5.15 UVP sampled horizontal flow patterns at z/B_{MB} = 0.25 (intake axis), dimensionless velocity v/v_0 for Q = 0.3 (a), 0.5 (b), 0.7 (c), 0.9 (d) and 1.1 l/s (e) and t = 120 s after the start (i) and t = 240 s before the end (ii) of an outflow sequence

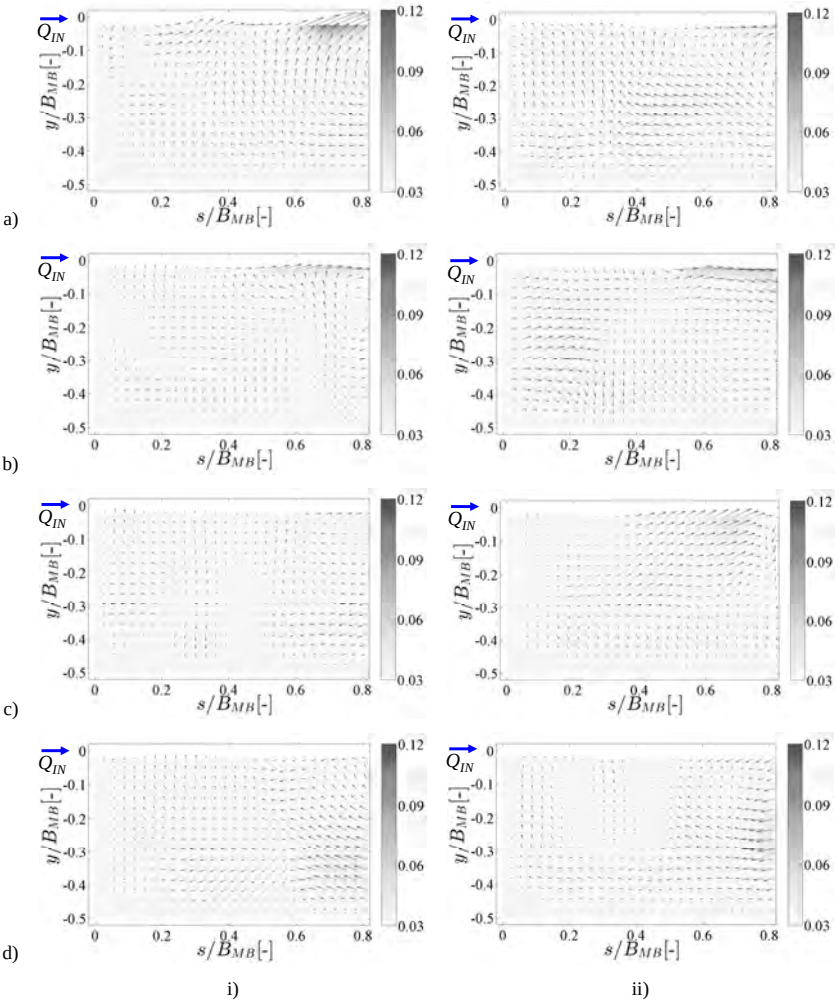

Figure 5.16 UVP sampled horizontal flow patterns at z/B_{MB} = 0.375 (a, b, above intake axis) and 0.125 (c, d, below intake axis), dimensionless velocity v/v_0 for Q = 0.7 (a, c) and 1.1 l/s (b, d) and t = 120 s after the start (i) and t = 240 s before the end (ii) of an inflow sequence

For discharges above Q = 0.7 l/s, backflow zones toward the intake/outlet are observed at z/B_{MB} = 0.125 (Figure 5.16d). For lower discharge, these conditions only develop when the jet is slightly deflected toward the basin bottom. This movement on the bottom layer of the basin may be interesting regarding suspension of fine sediment.

5.5.2 Horizontal flow patterns for variable cycle frequency

Cycle frequency influences the time for flow patterns development. For Kt_P = 0.6 and 0.8, flow sequence may be reversed before flow in the main basin reached steady state conditions. For Kt_P = 1.2, the flow patterns are supposed to be steady as observed for Kt_P = 1.0. Figure 5.17 and Figure 5.18 illustrate the measured flow patterns for the different cycle frequencies for discharge Q = 0.7 l/s for inflow and outflow sequences respectively.

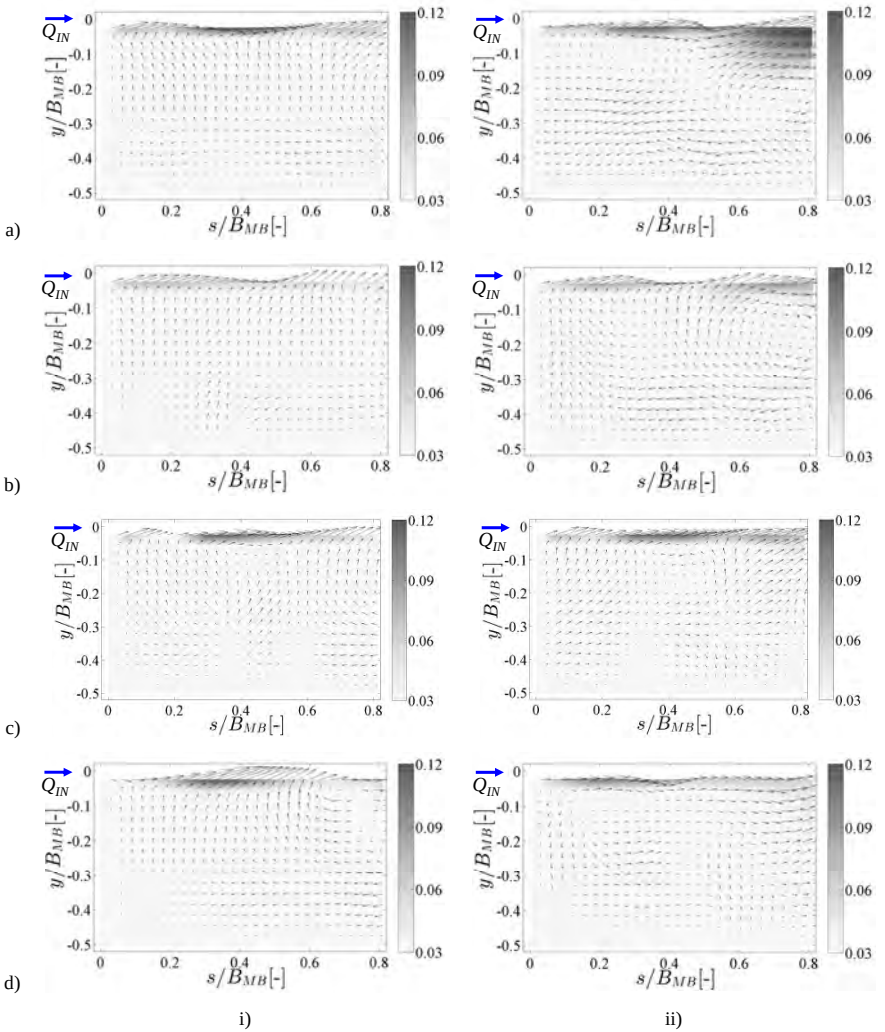

Figure 5.17 UVP sampled horizontal flow patterns at z/B_{MB} = 0.25 (intake axis), dimensionless velocity v/v_0 for Q = 0.7 l/s, Kt_P = 0.6 (a), 0.8 (b), 1.0 (c) and 1.2 (d) 1.1 l/s (e) and t = 120 s after the start (i) and t = 240 s before the end (ii) of an inflow sequence

Higher frequency in in- and outflow cycles leads to an amplification of movement in the main basin. The shorter outflow sequences do not allow entire dissipation of the recirculation cells. This leads to a slightly faster net formation during the following inflow sequence.

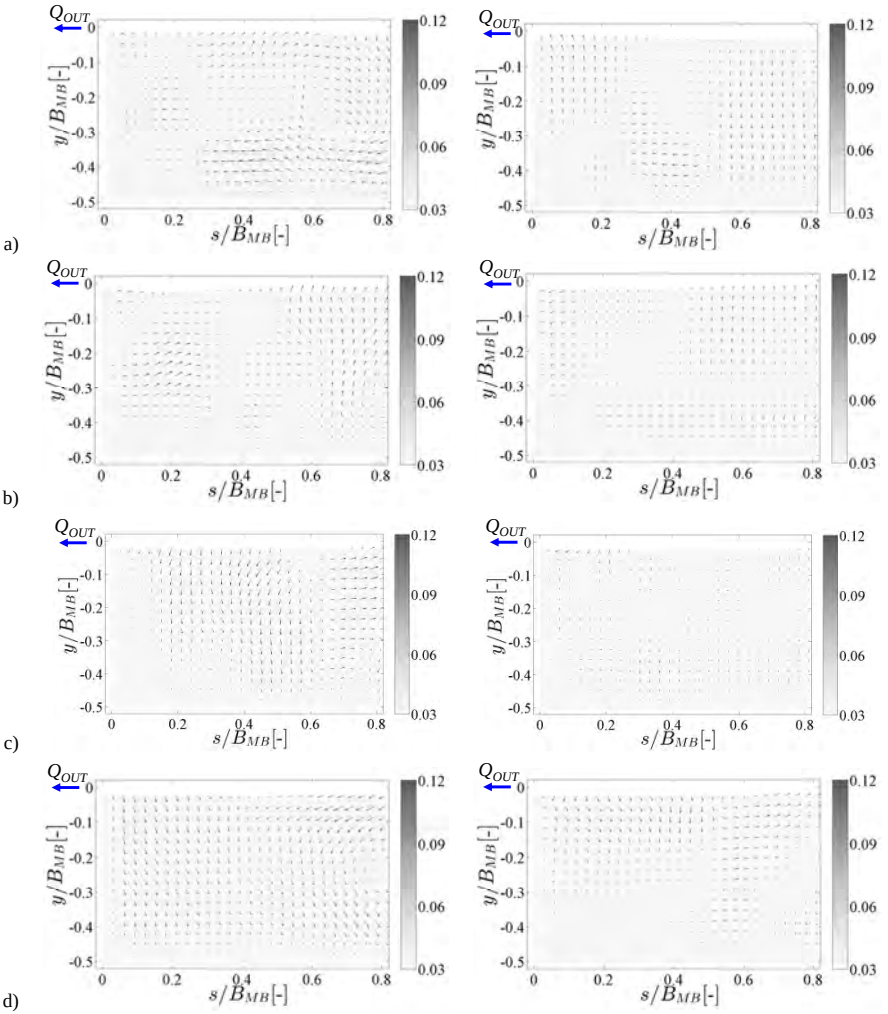

Figure 5.18 UVP sampled horizontal flow patterns at z/B_{MB} = 0.25 (intake axis), dimensionless velocity v/v_0 for Q = 0.7 l/s, Kt_P = 0.6 (a), 0.8 (b), 1.0 (c) and 1.2 (d) 1.1 l/s (e) and t = 120 s after the start (i) and t = 240 s before the end (ii) of an outflow sequence

5.5.3 Evolution of kinetic energy

Based on UVP velocity measurements, the kinetic energy in the sampled volume was calculated, assuming that the total kinetic energy of the entire volume is equal to the sum of the energy of each cell in the UVP measurement grid, taking into account all three sampled horizontal sections:

$$E_{kin} = \frac{1}{2} m \sum_{n} v_n^{\,2} \qquad \text{(Eq. 5.7)}$$

where n: the number of UVP sampling points [-].

The calculated values of the velocity contribution $\frac{1}{2} v^2$ are given as a function of the cycle duration t_P. Evolution of kinetic energy correlates with the applied in- and outflow sequences. The cycle magnitude directly affects the magnitude of kinetic energy in the test volume, as illustrated in Figure 5.19a. The cycle frequency has less influence. Shorter sequences lead to higher energy input due to the remaining inflow recirculation cells in the test volume during outflow sequences (Figure 5.19b to d).

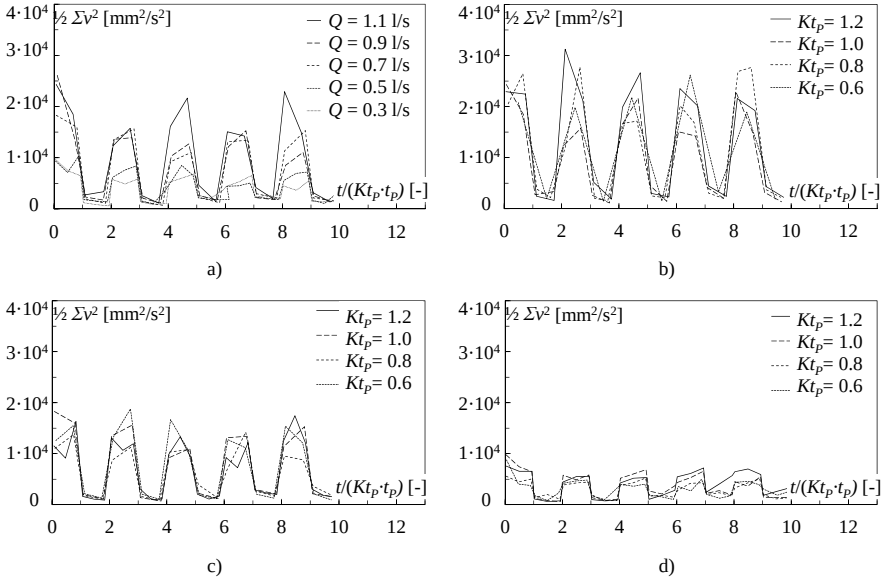

Figure 5.19 Evolution of the velocity component $\frac{1}{2}\Sigma v^2$ as a function of dimensionless time $t/(Kt_P \cdot t_P)$ for different discharges Q and Kt_P = 1.0 (a) and for different cycle frequencies Kt_P and Q = 1.1 (b), 0.7 (c) and 0.3 l/s (d)

During outflow sequences, the energy drops to 5 to 10% of the peak value during inflow. However, mean outflow energy levels correspond to 12.8 to 29% of the inflow energy level, phenomena increasing with increasing discharge. The inflow energy level with the lowest discharge of Q = 0.3 l/s is 33% of the one with Q = 1.1 l/s (Figure 5.21a).

Figure 5.20 illustrates the development of kinetic energy for two additional tests, which were carried out for different relative in- and outflow durations $t_{P,IN}/t_{P,OUT}$ and for varying

intake position z_i/B_{MB}. The first reveals the low influence on the kinetic energy, despite of the fact that almost the same energy level is reached within shorter time.

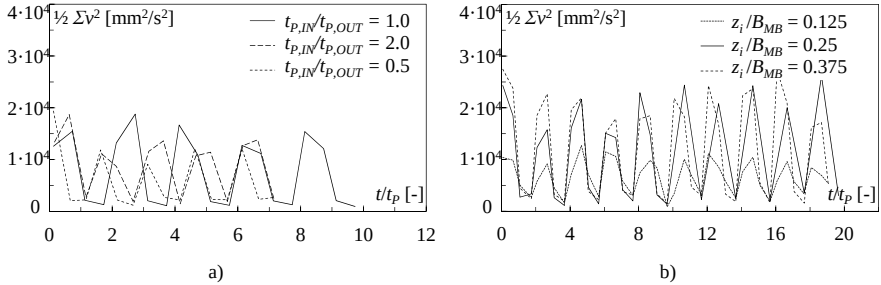

Figure 5.20 Evolution of the velocity component $½\Sigma v^2$ as a function of dimensionless time t/t_P for Q = 0.7 l/s, Kt_P = 1.0 and different relative sequence durations $t_{P,IN}/t_{P,OUT}$ (a) and for Q = 1.1 l/s, Kt_P = 1.0 and different intake positions z_i/B_{MB} (b)

The second shows similar energy levels for an intake position at z_i/B_{MB} = 0.25 and 0.375, whereas for an intake position close to the basin bottom quite low kinetic energy was calculated.

5.5.4 Comparison to numerical results

The comparison between numerical simulations and experimental results show that the ANSYS-CFD model predicted even lower kinetic energy for low discharges, at some 10% of the level at maximum discharge. The difference may come from the limited sampling volume taken into account for the kinetic energy analyses of the laboratory experiments.

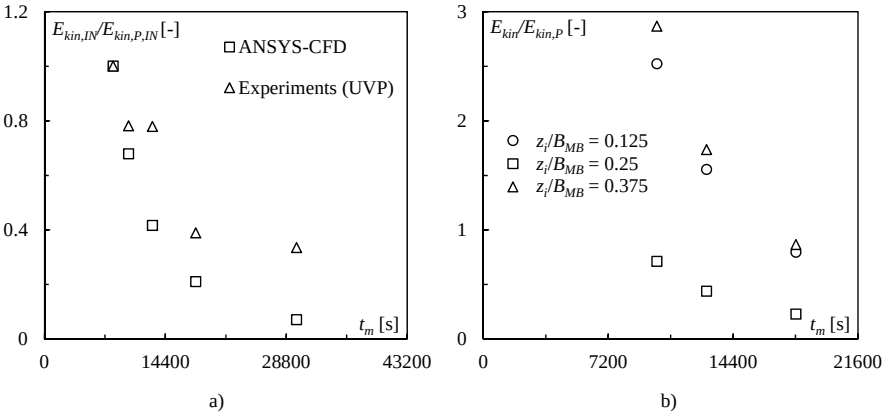

Figure 5.21 Mean dimensionless kinetic energy $E_{kin,IN}/E_{kin,IN,max}$ for inflow sequences as a function of the mean residence time t_m. Comparison between numerical and experimental results (a). Energy computed numerically for different intake levels z_i/B_{MB} (b)

The variation of the intake/outlet position was expected to significantly alter kinetic energy in the basin relative to the initial configuration. The numerical model predicted energy levels up to three times higher for an intake/outlet located closer to the bottom or to the free water surface (Figure 5.21b). The experimental flow patterns and the corresponding kinetic energy calculations show a slightly higher kinetic energy during inflow sequences at an intake level at $z_i/B_{MB} = 0.375$, but rather low energy levels for the intake at $z_i/B_{MB} = 0.125$.

The analysis of UVP measurements revealed that the jet was deflected either toward the bottom or the opposite quadrant of the basin and was only partly sampled by the velocity measurements. Such jet deflection was computed during preliminary simulations by the ANSYS-CFD model, as illustrated in Figure 5.22. In numerical models, such behavior usually occurs in the presence of a certain asymmetry which in this case was provided by the overflow section. However, for an intake position at $z_i/B_{MB} = 0.25$ the jet was not deflected neither in the computation, nor the laboratory experiments.

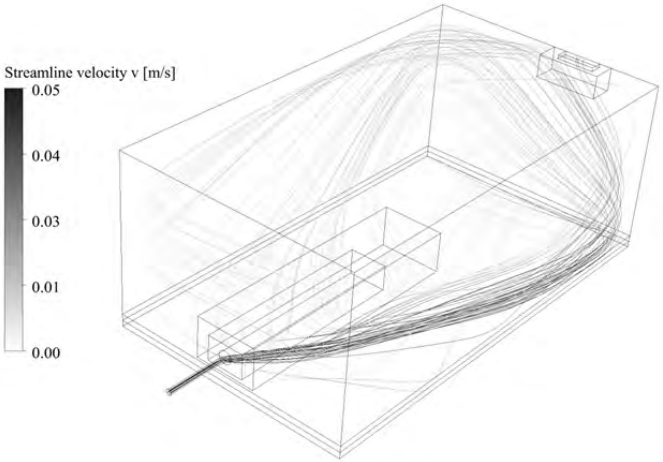

Figure 5.22 Jet deflection during an inflow sequence, streamlines computed by the numerical model for $z_i/B_{MB} = 0.125$ and $Q = 0.9$ l/s

5.6 Conclusions

In- and outflow cycles in a rectangular basin were investigated by laboratory experiments to describe flow patterns and the development of kinetic energy in the test volume for different magnitudes and frequencies of the in-/outflow cycles. Ultrasonic Velocity Profilers (UVP) sensors provided non-intrusive sampling for measuring centerline velocities as well as transversal velocity profiles of the jet during inflow sequences. Horizontal 2D flow patterns could be defined for one quadrant of the test volume.

In preliminary tests, the jet behavior during inflow sequences was measured by UVP, revealing the influence of the intake/outlet shape on the jet behavior. For the applied geometry, the evolution of the centerline velocity reveals a jet with a very short core and a

fast drop of centerline velocities in the transition zone. Hence, centerline velocity decreases by increasing distance to the nozzle, following quite well the curves from literature.

Numerical simulations allowed the determination of the time to reach steady state conditions and thus constant kinetic energy in the test volume. This “time to peak” between t_P/t_m = 0.099 and 0.136 defined the experimental test duration for different discharges. Numerically simulated flow patterns reveal rather low flow velocities during outflow with flow velocities orientated toward the intake. For inflow sequences, steady flow patterns with a jet and two horizontal recirculation cells are defined.

Flow patterns sampled during the experiments show jet oscillations and recirculation cells for inflow sequences and rather fluctuating low velocity patterns, partially influenced by the preceding inflow sequence. Measures above and below the jet axis indicate backflow zones toward the intake/outlet close to the bottom during inflow sequences and mainly for high discharges. Otherwise, the upper and lower horizontal sections present the same recirculation cells as in the jet axis, with lower velocity magnitudes.

Cycle magnitude considerably affects the kinetic energy in the basin. According to the experimental results, a high discharge generates up to three times more energy than a low one. Numerical results even predict a ratio of ten between maximum and minimum discharge. Cycle frequency has less influence, while an intake position closer to the bottom or the free water surface leads to considerably higher energy levels.

Chapter 6

Experiments on the effect of in- and outflow sequences on suspended sediment exchange rates

In laboratory experiments, the influence of in- and outflow sequences on the behavior of fine sediment was investigated. The experimental set-up consists of two interconnected rectangular basins, between which water is moved back and forth. Suspended sediment concentration in the main basin is derived from turbidity measurements and Ultrasonic Velocity Profilers (UVP) allow the measurement of 2D flow patterns at several levels in the test volume.

The suspended sediment ratio *SSR* and sediment exchange rates (influx sediment rate *ISR* and evacuated sediment rate *ESR*) were measured. In twenty test runs, a parametric study on the magnitude and frequency of in- and outflow cycles, the relative duration between in- and outflow sequences, the initial sediment concentration as well as the intake position was carried out. An initial test with stagnating water described the settling behavior of fine sediment and served as reference scenario.

Test results show that settling of fine particles near the intake/outlet structure can be considerably reduced by the in- and outflow sequences. High cycle magnitude and frequency lead to maximum suspended sediment ratio in the system. For low discharges, the evolution of suspended sediment concentration cannot be directly correlated to the in- and outflow cycles. However, compared to “no operation” conditions, suspended sediment ratio could be increased by 10 to 40% locally. For high discharge, the evolution of concentration correlated with discharge cycles and suspended sediment ratios between 50 and 80% higher than in stagnant water could be achieved. Similar ratios could be obtained when the intake is located closer to the bottom or to the free water surface.

Meanwhile, the overall sediment balance remained equilibrated over the test period, indicating that the influx and evacuated sediment rates are not significantly influenced by the in- and outflow cycles.

6.1 Introduction

Reservoir sedimentation is affecting most of the artificial storage volumes for drinking water supply, flood retention or hydropower production. When the construction of a dam interrupts the continuity of sediment transport of a river, the deposition and settling processes of the particles supplied from the upstream catchment area start filling up the reservoir. Both sustainability and safety are endangered (Schleiss *et al.*, 2010). In case of hydropower, the accumulating sediment reduce storage capacity as well as operational efficiency. Deposits in front of intake/outlet structures or clogging of bottom outlets can lead to exploitation perturbations and safety concerns (Boillat and Pougatsch, 2000).

In Alpine storage reservoirs the main sedimentation process are turbidity currents, taking place generally during annual flood events and occurring mainly during peak inflow (De Cesare *et al.*, 2001b). According to the density difference, the sediment-laden flow follows the thalweg to the deepest area of the reservoir, which is normally close to the dam and/or the power intakes, and forms a so-called muddy lake. For storage hydropower plants, several measures against turbidity current driven sedimentation have been studied (Oehy and Schleiss, 2007; Oehy *et al.*, 2010), i.e. obstacles stopping the current propagation or maintaining particles in suspension in front of intakes to be evacuated by the turbines. Jenzer Althaus (2011) investigated the effect of a rotating jet induced flow close to intake structures on sediment mixing.

Further experimental research on suspended sediment behavior in reservoirs was carried out by Yu *et al.* (2000), describing the deposition behavior in the muddy lake area, by Meilan *et al.* (2000), analyzing sediment re-suspension by a turbulent jet in an intake pond, by Kantoush *et al.* (2008), focusing on shallow flows as well as by Toniolo and Schultz (2005), studying trap efficiency of a reservoir depending on the outlet location.

Sediment can be kept in suspension by jet induced flow. In industrial applications, jet mixing has become an alternative to conventional impeller mixing (Wasewar, 2006). Numerous experimental works on sedimentation and deposition from particle laden turbulent jets and plumes have been carried out (Ernst *et al.*, 1996; Cardoso and Zarrebini, 2001a, 2001b; Lane-Serff and Moran, 2005; Cuthbertson and Davies, 2008). However, the effect of repetitive in- and outflow sequences and the influence of their amplitude and frequency on fine sediment behavior have not been investigated so far.

Pumped-storage activity alters reservoir stratification and particle dynamics (Imboden, 1980; US Bureau of Reclamation, 1993; Anderson, 2010; Bonalumi *et al.*, 2011). Inspired by the operating mode of pumped-storage plants, a new approach of keeping fine particles in suspension is presented in this chapter. The objective is to experimentally investigate how repetitive in- and outflow sequences affect the settling processes of suspended sediment and the sediment balance of the system.

This chapter describes the experimental set-up and the measuring equipment. Parameter variations, measurement uncertainties and the different test configurations are presented. The influence of magnitude and frequency of in- and outflow cycles, relative sequence duration, initial sediment concentration as well as intake position on suspended sediment ratios and sediment exchange rates are discussed.

6.2 Test facility and instrumentation

The laboratory experimental facility consisted of two basins interconnected by a reversible water circuit for generating in- and outflow sequences. Discharge was regulated and controlled during the experiment, flow velocities were recorded by Ultrasonic Velocity Profiler (UVP) and turbidity in both basins was continuously measured. The set-up and the measuring techniques are described hereafter.

6.2.1 Main basin with intake/outlet

Most of the relevant measurements were carried out in the rectangular main basin (subscript *MB*, Figure 6.1). It has an inner length of L_{MB} = 4.0 m, an inner width of B_{MB} = 2.0 m and a height of H_{MB} = 1.5 m. One lateral wall and the front wall are made of glass for flow visualization, whereas the other walls and the horizontal bottom are made of steel.

A perforated steel plate is inserted vertically at 0.5 m from the back wall to disconnect the test volume from the zone influenced by the feeding conduit, the security spillways, the purge outlet and the pressurized air supply of the main basin.

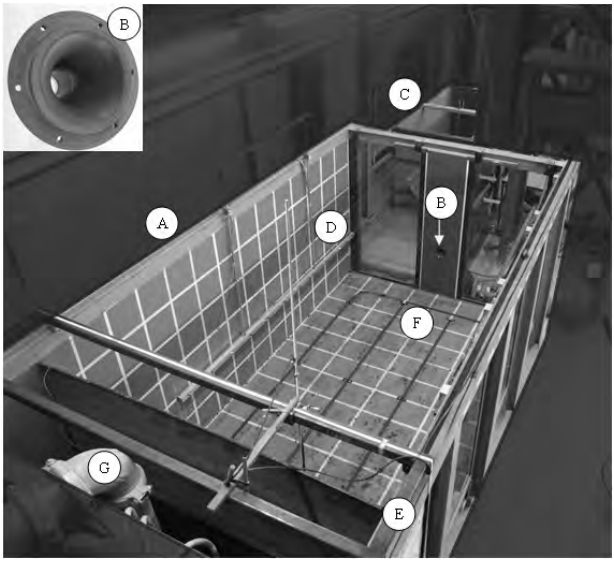

Figure 6.1 Photo of the laboratory set-up; A is the main basin; B, the intake/outlet; C, the mixing tank; D, the frame with UVP sensors; E, the movable frame with the turbidity probe; F, the pressurized air supply and G, the feeding conduit for initial filling of the system

The water intake/outlet is located at the front wall and can be placed at z_i = 0.25, 0.50 or 0.75 m above the reservoir bottom. The water intake has been designed to reduce head losses and turbulence disturbing the flow in the vicinity of the structure (Jenzer Althaus, 2011). It consists of an elliptical bell mouth shaped intake followed by a cylindrical throat with an inner diameter D_i = 48 mm (detail B in Figure 6.1).

6.2.2 Mixing tank

The mixing tank (subscript *MT*, C in Figure 6.1) consists of a rectangular prismatic tank with vertical PVC walls reinforced by steel frames. With its inner dimensions of L_{MT} = 1.98 m, B_{MT} = 0.98 m and H_{MT} = 1.06 m, it provides a volume of approximately V_{MT} = 2 m^3. Similar to the main basin it is equipped with pressurized air supply for mixing purposes at the beginning of the experiments.

This basin provides mixing possibility and storage volume to move water from or to the main basin. Thus, its intake/outlet is not specially designed and just consists of a conduit entering the tank at z = 0.25 above the bottom.

6.2.3 Flow diverter

A flow diverting system of soft plastic and rigid aluminum pipes allowed a flow operation in the two directions defined as follows:

- *IN*-sequence water entering the main basin (inflowing jet)
- *OUT*-sequence water withdrawn from the main basin (outflow)

A rigid conduit of diameter D = 4.8 cm and length L = 1.5 m between the flow diverting system and the intake/outlet of the main basin assures uniform approach flow (straight jet) especially during the inflow sequences. Discharge is measured by an electromagnetic flow meter and regulated by a pump. The semi-rigid diverting conduits are connected by four small manual valves which allow changing flow direction during the experiment.

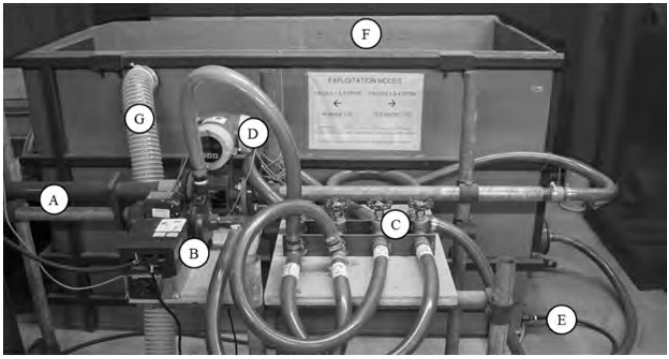

Figure 6.2 Mixing tank and flow diverting system; A is the rigid PVC conduit to the main basin; B, the pump and its velocity regulator; C, the flow diverting valves; D, the flow meter; E, the pressurized air supply; F, the mixing tank and G, the security spillway connected to a sewer

6.2.4 Turbidity probe

Turbidity in the two basins was measured by two *SOLITAX sc* sensors (HACH LANGE, Germany, Figure 6.3a) connected to the acquisition and display system *SC100 Controller* of the same manufacturer. Based on an infrared absorption scattered light technique, the probe determines the turbidity in the sampled water. In the present study, turbidity values were acquired at a frequency of f = 0.2 Hz. The linear relationship between the turbidity *TU* [FNU] and the suspended sediment concentration C [g/l] was determined in the laboratory for known

sediment concentrations from C = 0.3 to 1.5 g/l. In addition, the initial sediment concentration C_0 at the beginning of each test run were considered as validation points. The following calibration relationship was derived (Figure 6.3b):

$$C_{MB} = 0.0038 \cdot TU_{MB} - 0.0099$$
$$C_{MT} = 0.0041 \cdot TU_{MT} - 0.0138 \quad \text{(Eq. 6.1)}$$

where C_{MB}: the suspended sediment concentration in the main basin [g/l], and
C_{MT}: the suspended sediment concentration in the mixing tank [g/l].

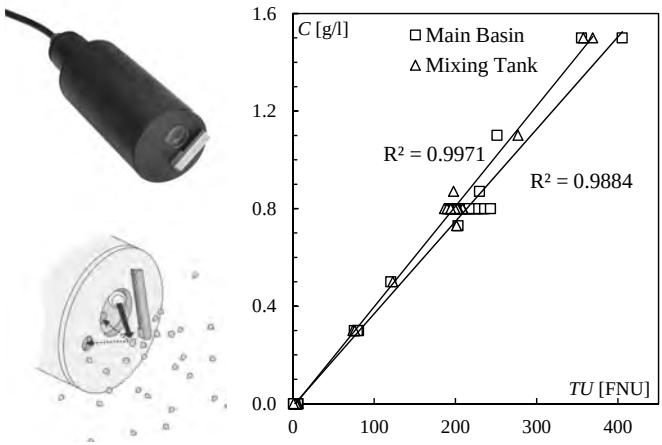

Figure 6.3 Photo (above) and measuring system (below, source: HACH LANGE manual) of the *SOLITAX sc* turbidity sensor (a) and turbidity calibration curve for the two probes (b)

In the main basin, the turbidity sensor was installed in the opposite quadrant to the UVP measurements. During experiments, the concentration was continuously recorded at intake height z_i. After every third flow inversion, the probe was temporally moved vertically to evaluate vertical distribution of suspended sediment. In the mixing tank, the measuring point is located in the center of the volume at the entering height of the inflow/outflow conduit.

It is assumed that the point measurement of suspended sediment concentration is representative for the whole test volume, accepting an uncertainty due to possible spatial variations of the suspended sediment concentration. The root mean square error of the concentration measurements was determined using the sampled *TU*-*C* pairs. The average error ERR_C is:

$$ERR_C = \sqrt{\sum \frac{(C_{calc} - C_0)^2}{n-1}} \quad \text{(Eq. 6.2)}$$

where C_{calc}: the concentration [g/l] estimated using the calibration equation,
C_0: the known initial concentration [g/l] applying $C = M/V$, and
n: the number of samples taken into account for error estimation [-].

The average error introduced due to calibration is $ERR_{C,MB}$ = +/-0.048 g/l for the probe in the main basin and $ERR_{C,MT}$ = +/-0.024 g/l in the mixing tank.

6.2.5 Ultrasonic velocity profilers

Flow patterns in the main basin were measured with *Ultrasonic Velocity Profilers* (UVP, MetFlow, Switzerland (SA, 2000)). This technique, developed by Takeda (1995), allows instantaneous velocity profile measurement by using the Doppler shift of echoes reflected by small particles in the fluid. In former studies, turbidity currents and 2D flows in shallow reservoirs were successfully monitored by this flow mapping technique (De Cesare and Schleiss, 1999; Kantoush *et al.*, 2008). Suspended sediment provides an excellent flow tracer and assures high reliability of velocity measurements.

Seventeen 2 MHz UVP transducers were aligned on an movable aluminum frame along the side wall of the test volume to measure horizontal 2D velocity fields at several levels in the main basin. The configuration with operating UVP azimuth angles of 90° and 45° minimizes the influences of the measuring equipment on the flow conditions. Flow velocity was sampled at 28 points in one quadrant of the test volume, resulting in 2D flow patterns of 1.0 x 2.0 m^2.

6.3 Experimental parameters

6.3.1 Similarity rule and normalizing parameters

The experiments are carried out respecting the criterion of Froude similarity. The same relationships for inertia and gravity forces apply in prototype (subscript prot) and model (subscript mod). Such, geometric (L) and cinematic (v, t, Q) parameters follow the relations

$$\lambda_L = \frac{L_{prot}}{L_{mod}}; \qquad \lambda_{v,t} = \lambda_L^{1/2}; \qquad \lambda_Q = \lambda_L^{5/2} \qquad \text{(Eq. 6.3)}$$

The Reynolds number at the intake/outlet is $7'560 \leq \mathrm{Re}_i \leq 29'180$ and thus turbulent for every tested discharge.

The main basin width B_{MB} was chosen for normalizing lengths. Velocities and time are normalized by the approach flow velocity in the pipe $v_0 = Q_{IN,OUT}/A$ and the mean residence time $t_m = V_{MB}/Q_{IN,OUT}$ respectively. Latter was proposed by Stefan and Gu (1992) to be used for normalization of time in jet mixing problems. However, in the presentation of results there may be some exceptions when real time presentation is necessary for better understanding.

6.3.2 Sediment material

Settling processes are affected by properties of the surrounding fluid (viscosity v and density ρ_w) and particle characteristics (diameter d_S, material density ρ_S, shape SF and concentration C_0, van Rijn (1984)). The water temperature during the experiments varied between T_w = 14 and 17 °C. Viscosity effects on settling velocity are small in this range and can thus be neglected.

The experiments were carried out using walnut shell powder to reproduce the suspended sediment. Former research showed that this homogeneous material presents ideal behavior to model reservoir sedimentation processes (Kantoush *et al.*, 2008; Jenzer Althaus, 2011).

Specific density is $\rho_s = 1480$ kg/m^3, the mean particle diameter is $d_m = 121$ µm and the particles are slightly angular shaped. Such, they allow the reproduction of the prototype ratios between flow velocities and settling velocities in the reservoir. As organic material is subject to swelling, long-term tests on the behavior of the nutshell powder were carried out. Swelling is negligible over the investigated test duration and does allow correct turbidity measurement.

Sediment concentration influences the settling velocity in a fluid. Therefore, the initial concentration C_0 was varied in the two basins. Generally, tests were carried out for $C_0 = 0.8$ g/l in both basins. Two experiments were done with lower and higher concentrations of $C_0 = 0.3$ and 1.5 g/l respectively.

6.3.3 Magnitude and frequency of in- and outflow cycles

The experiments were carried out for five different discharges from $Q = 0.3$ to 1.1 l/s. These magnitudes of the in- and outflow cycles were given by the volumes of the main basin and the mixing tank and the design of the water intake/outlet (Jenzer Althaus, 2011) as well as real case pumped-storage cycles.

The initial frequency of in- and outflow cycles was determined in numerical simulations and under clear water conditions. For inflow, outflow and "no operation" sequences, time necessary to reach steady state conditions in the main basin, i.e. maximum and stable kinetic energy, was defined. This duration t_P ("time to peak") depends on the discharge. It was determined by preliminary numerical simulation and served as reference time for the cycle duration of the experiments.

Table 5.1 lists the mean residence time t_m, the time to peak t_P and corresponding dimensionless time t_P/t_m for the five tested discharges.

Table 6.1 Mean residence time t_m and time to peak t_P for different discharges Q

Q [l/s]	t_m [s]	t_P [s]	t_P/t_m [-]
0.3	30'056	4080	0.136
0.5	18'034	2280	0.126
0.7	12'881	1500	0.116
0.9	10'019	1080	0.108
1.1	8'197	810	0.099

The base configuration for each discharge consists in five cycles resulting in experiment durations $10t_P$ between 2 h 15 min and 11 h 20 min (Figure 6.5a to e). The shape of the experimental hydrograph is similar to a square wave. Dissipation or "no operation" sequences were not reproduced and in- and outflow cycles have a cycle frequency $Kt_P = 1.0$.

Four different cycle frequencies Kt_P were studied (Figure 6.5f to h). Higher frequencies $Kt_P = 0.6$ and 0.8 implicate faster changes in operation mode and reduce the time to reach steady state conditions in the test volume. $Kt_P = 1.2$ is assumed to prolongate the steady conditions in the basin before the inversion of flow direction. The variation of cycle frequency was tested for three of the five discharges (Figure 6.4).

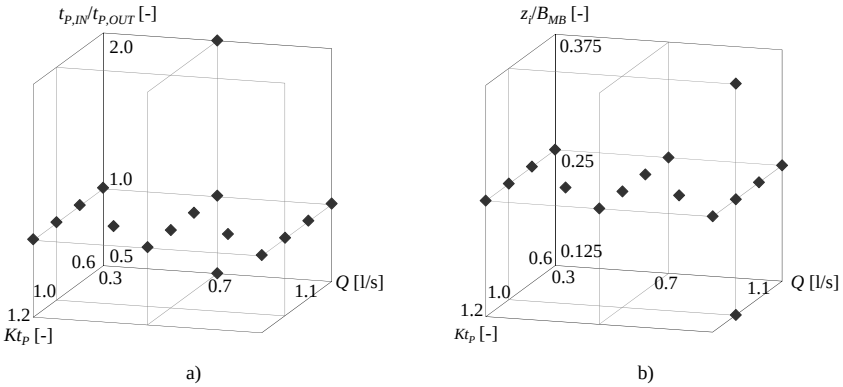

Figure 6.4 Three-dimensional illustration of experimental test configurations: variation of cycle magnitude Q and frequency Kt_P (horizontal section). Base configuration is Q = 0.7 l/s and Kt_P = 1.0. Test configurations relative to changing sequence duration $t_{P,IN}/t_{P,OUT}$ (a) and intake position z_i/B_{MB} (b)

The presented variation of magnitudes and frequencies of in- and outflow cycles cover quite a wide range of short and long sequences with high and low discharges. However, in engineering applications such as pumped-storage plants, perfect cyclic behavior of in- and outflow sequences is rare. In real cases, rather random operational hydrographs with sometimes varying discharges within the proper cycles are observed. Nevertheless, most of the pumped-storage operations present a cyclic behavior, according to daily, weekly or seasonal production/absorption purpose.

Two additional experiments with a different relative sequence duration $t_{P,IN}/t_{P,OUT}$ were tested. An inflow sequence occupied double the time of an outflow sequence and vice-versa (Figure 6.5i and j). Figure 6.4a presents the entire matrix of tested magnitudes and frequencies of in- and outflow cycles for $t_{P,IN}/t_{P,OUT}$ = 1.0 as well as the two configurations with different relative sequence duration.

6.3.4 Intake/outlet position

Flow patterns in the test volume are changing when the intake/outlet is located closer to the reservoir bottom or the free surface. With changing flow conditions, the behavior of suspended sediment is expected to be altered as well. Therefore, the position of the intake/outlet structure above the basin bottom z_i/B_{MB} was changed for two experiments, from the initial location at z_i/B_{MB} = 0.25 m to z_i/B_{MB} = 0.125 and 0.375 m for a discharge of Q = 1.1 l/s (Figure 6.4b).

6.3.5 Experimental procedure

After filling the main basin to $H_{0,MB}$ = 1.15 m and the mixing tank to its full level $H_{0,MT}$ = 1.06 m, the two reservoirs are disconnected from the laboratory circuit and exploited in short circuit. For the experiments with sediment, the desired mass of walnut shell powder was mixed with water and poured into the basins. Pressurized air supply on the bottom generated whirling flow conditions to mix and maintain the sediment in suspension. Air

bubbles were interrupted and in- and outflow cycles were started at t = 0 s. As the total water volume remained constant over the experimental duration, the water level in both basins varied in time. Maximum level variation in the main basin was of ΔH_{MB} = +/-0.18 m for one cycle.

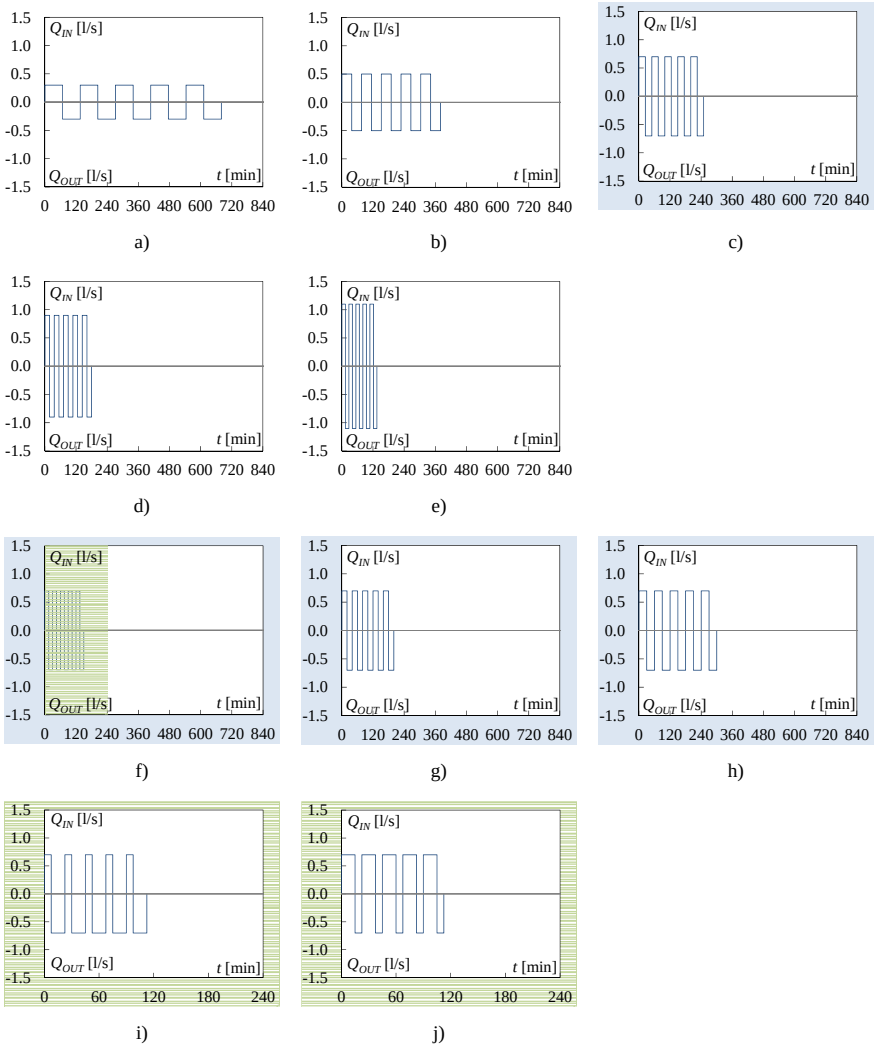

Figure 6.5 Selection of ten investigated in- and outflow cycles. Variation of discharge Q = 0.3 (a), 0.5 (b), 0.7 (c), 0.9 (d) and 1.1 l/s (e) for cycle frequency Kt_P = 1.0. Variation of cycle frequency Kt_P = 0.6 (f), 0.8 (g), and 1.2 (h) for discharge Q = 0.7 l/s. Variation of relative sequence duration $t_{P,IN}/t_{P,OUT}$ = 0.5 (i) and 2.0 (j) for discharge Q = 0.7 l/s and cycle frequency Kt_P = 0.6

Suspended sediment concentrations C in the main basin and the mixing tank were continuously measured. UVP measures were carried out one to three times per sequence, according to the cycle duration. At the end of a test run, the final sediment content in the mixing tank was measured after resuspending all sediment in the latter.

6.4 Experimental results and analysis

After having measured the reference settling curve of the sediment under "no operation" conditions, the suspended sediment ratio *SSR* could be defined for each experiment:

$$SSR(t) = \frac{\sum M_{susp}(t)}{M_0} = \frac{M_{susp,MB}(t) + M_{susp,MT}(t)}{M_{0,MB} + M_{0,MT}} \qquad \text{(Eq. 6.4)}$$

where M_{susp}: the suspended sediment mass in the system [g], and
M_0: the initial sediment mass in the system [g].

The efficiency of in- and outflow sequences on keeping the fine sediment in suspension is defined by the normalized increase INC_{SSR} of suspended sediment ratio with and without in- and outflow cycles:

$$INC_{SSR}(t) = \frac{SSR(t) - SSR_{Ref}(t)}{SSR_{Ref}(t)} \qquad \text{(Eq. 6.5)}$$

High values of INC_{SSR} represent high impact of the tested sequences, values close to 0 indicate that the settling behavior of the suspended sediment is only marginally influenced by the in- and outflow sequences.

6.4.1 Reference tests

To evaluate the influence of in- and outflow sequences on suspended sediment ratio, preliminary experiments were carried out in stagnant water during almost 14 h. Suspended sediment concentration was measured in both tanks continuously at $z/B = 0.25$ above the bottom. Figure 6.6 shows the suspended sediment ratio *SSR* as a function of time *t*. The settling behavior follows a power law.

Periodical samples in the main basin taken at $z/B_{MB} = 0.125$, 0.375 and 0.5 show that the bottom layers of the water body are slightly more turbid (peaks in Figure 6.6a). As settling behavior in calm water depends on the particle concentration in the test volume, reference tests were carried out for the two other initial concentrations as well. Figure 6.6b reveals that the temporal evolution of *SSR* is very similar for all three cases.

During the first four hours, the suspended sediment ratio drops to a value of approximately $SSR = 0.06$. Then, it decreases slowly to about $SSR = 0.03$. The base test configuration for $Q = 0.7$ l/s and $Kt_P = 1.0$ and with a duration of $t = 15'000$ s covers these four hours during which most of the suspended sediment is settling.

The experimental results presented in paragraph 6.4 focus on varying cycle magnitude and frequency for $C_0 = 0.8$ g/l. The influence of initial sediment concentration C_0 is discussed in paragraph 6.5.

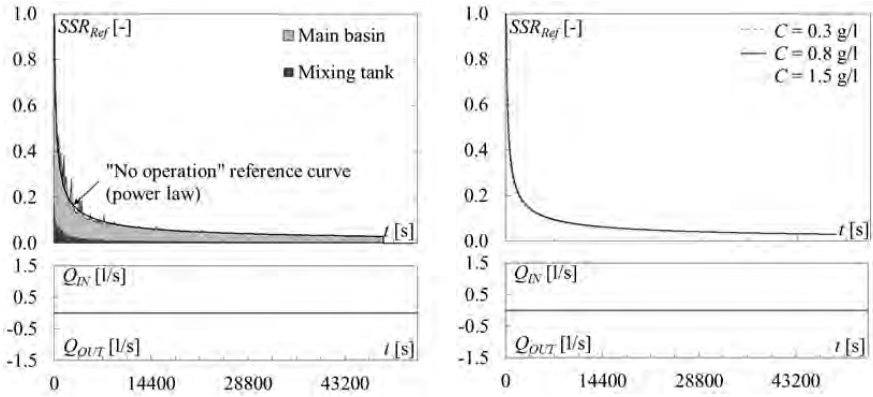

Figure 6.6 Suspended sediment ratio *SSR* as a function of time *t* in calm water conditions for initial sediment concentration C_0 = 0.8 g/l (a) and power law curves for the three different initial concentrations (b)

6.4.2 Suspended sediment ratio *SSR*

Continuous turbidity measurements over the test period determined the suspended sediment concentration at a time step of Δt = 5 s during the whole experiment. Knowing the varying volume in the two basins the suspended sediment mass was calculated and *SSR* defined (Equation 6.4). The relative increase INC_{SSR} was calculated.

Figure 6.7 and Figure 6.8 present *SSR* and INC_{SSR} as a function of dimensionless time t/t_m, for cycle frequency Kt_P = 1.0 and five different discharges. For discharges Q = 0.3 and 0.5 l/s, the evolution of the suspended sediment ratio does not clearly correlate with the discharge curve. However, the increased fluctuation of the *SSR* compared to the reference test and the relative increase reveal a final suspended sediment ratio which is approximately 20 to 30% higher than in stagnant water.

With increasing discharge, the evolution of *SSR* starts to correlate with the discharge cycles. The suspended sediment ratio fluctuates according to in- and outflow sequences with relative increases between INC_{SSR} = 50 and 60% during inflow Q = 0.9 and 1.1 l/s.

During the first in-out-cycle or until t/t_m = 0.2 approximately, the settling process is predominant. Nevertheless, the magnitude of the cycles plays an important role in slowing down this process (Figure 6.8). Whether the cycles start with an in- or an outflow sequence only influences marginally the overall *SSR* in the two basins (Figure 6.7c and d).

Higher cycle magnitudes lead to increased *SSR* at the end of five in- and outflow cycles and allow up to 60% more particles in suspension than without in- and outflow cycles. However, also for Q = 0.9 and 1.1 l/s, the overall trend of the *SSR* curve is still decreasing by the end of the experiment.

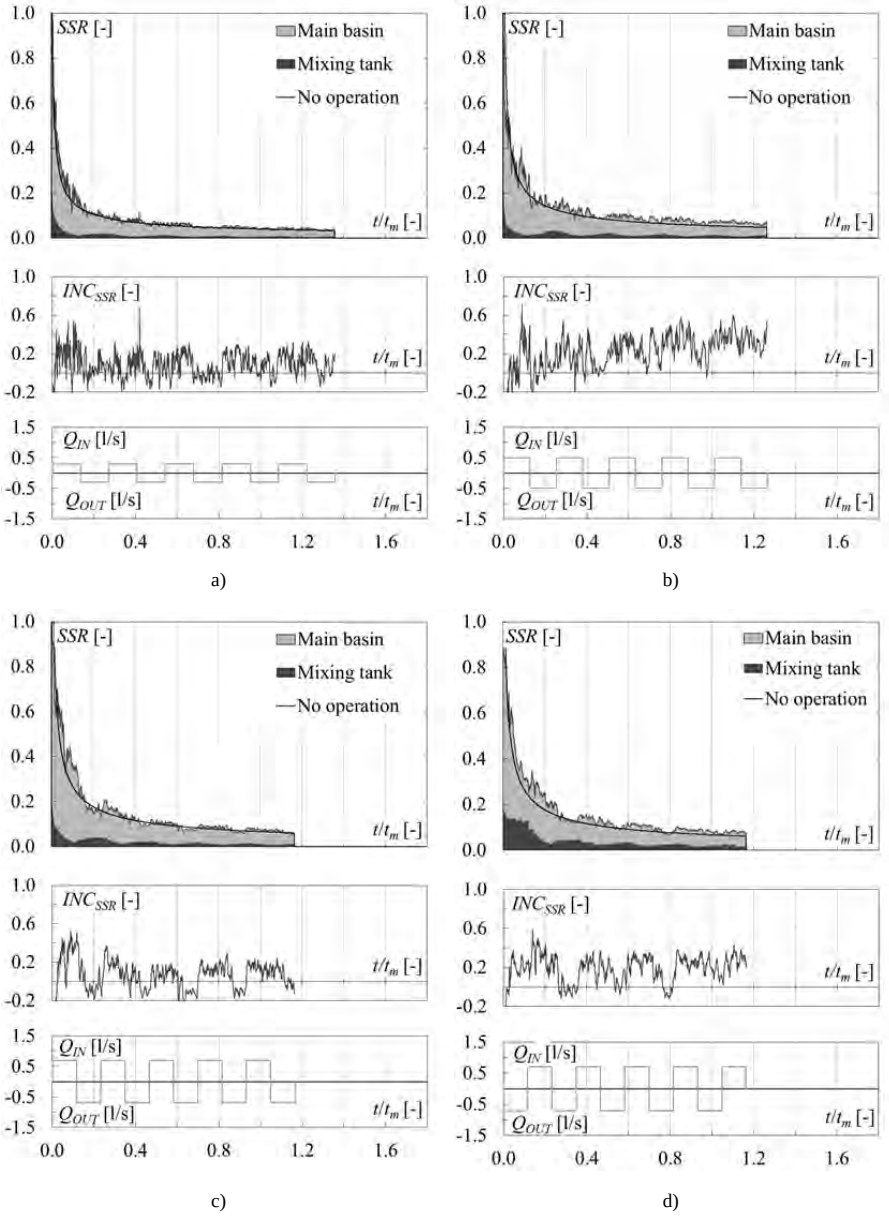

Figure 6.7 Suspended sediment ratio *SSR*, dimensionless increase INC_{SSR} and discharge Q as a function of dimensionless time t/t_m for C_0 = 0.8 g/l, Kt_P =1.0 and Q = 0.3 (a), 0.5 (b), and 0.7 l/s (c). Reversed in-out-cycle for C_0 = 0.8 g/l, Kt_P =1.0 and Q = 0.7 l/s (d)

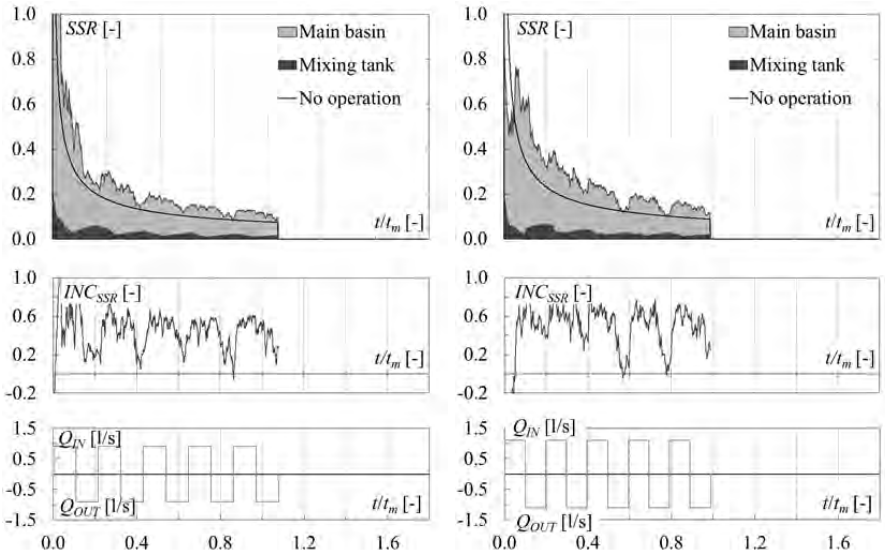

Figure 6.8 Suspended sediment ratio *SSR*, dimensionless increase INC_{SSR} and discharge Q as a function of dimensionless time t/t_m for C_0 = 0.8 g/l, Kt_P =1.0 and Q = 0.9 (a) and 1.1 l/s (b)

To evaluate if *SSR* can be maintained at a higher level due to the in- and outflow sequences, the experiments for Q = 0.9 and 1.1 l/s were prolongated to the absolute duration of the basic configuration (Q = 0.7 l/s and Kt_P =1.0). Two and five more cycles respectively were added to cover the entire main settling phase of approximately four hours defined during reference tests. The comparison is illustrated in Figure 6.9 for Q = 0.3, 0.7, 0.9 and 1.1 l/s.

In Figure 6.9, *SSR*, INC_{SSR} and Q are plotted as a function of real experimental time to match with results presented for the reference case (Figure 6.6). As for low discharges, the correlation between suspended sediment ratio and discharge cycles disappears at mid-term; the fluctuations on the *SSR* curve become smaller. However, *SSR* remains considerably high, with values of INC_{SSR} = 50 and 60% for the two highest discharges and thus in the same range as after less cycles.

The influence of cycle frequency on suspended sediment ratio is shown in Figure 6.10 for Q = 1.1 l/s. At increased cycle frequency Kt_P = 0.6 or 0.8, the main basin is assumed not to reach steady state conditions. This is confirmed by the suspended sediment ratio, as it remains high due to the increased cycle frequency, reflecting discharge cycles less clearly than for Kt_P = 1.0 and 1.2. The illustrated behavior of the suspended sediment ratio is also found for the other discharges Q = 0.3 and 0.7 l/s.

For Kt_P = 0.8, relative increase is $INC_{SSR} \sim 80\%$ during inflow sequences, while for Kt_P = 0.6, 1.0 and 1.2 it is around 60%. For the other two tested discharges Q = 0.3 and 0.7 l/s, lower relative increase of INC_{SSR} = 20 to 40% is found, according to the results for the cycle magnitude variation.

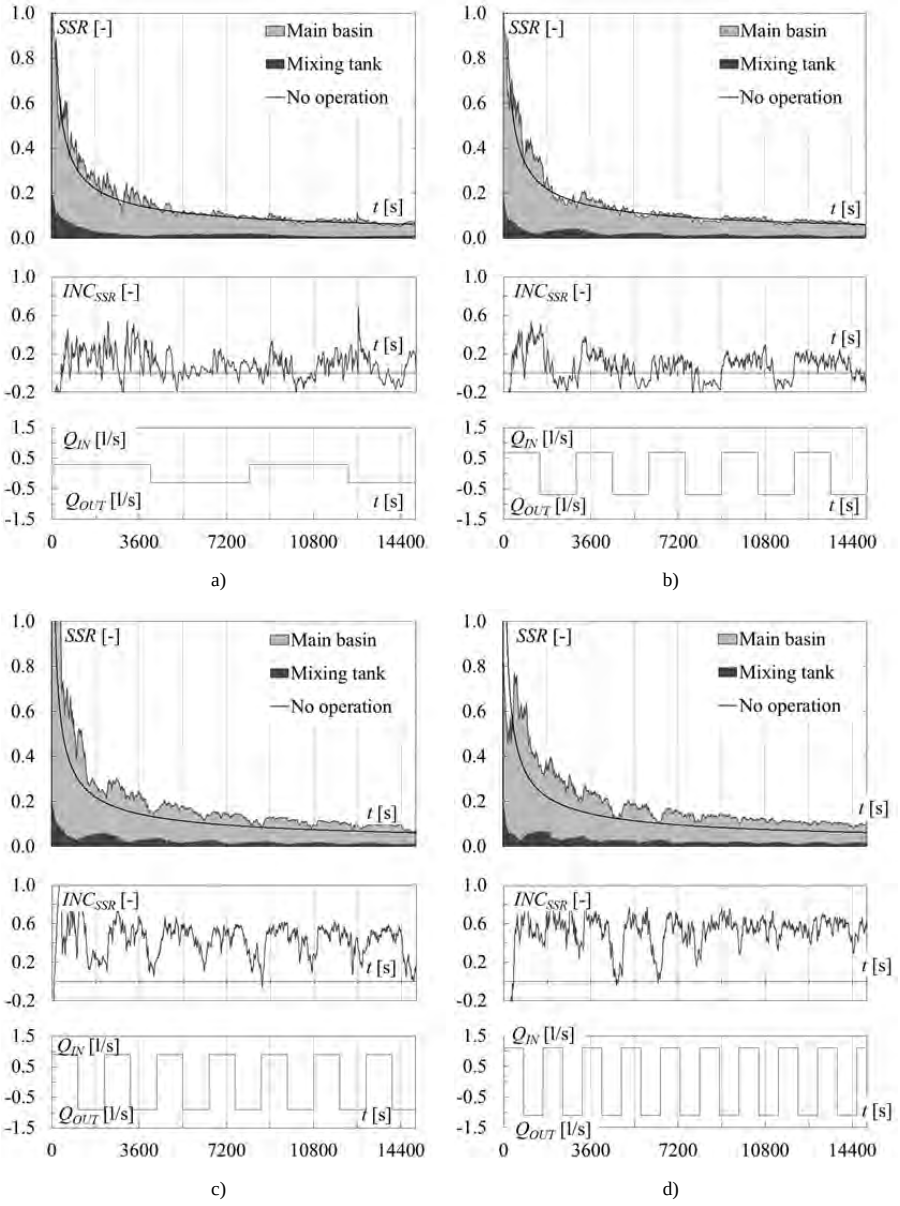

Figure 6.9 Suspended sediment ratio *SSR*, dimensionless increase INC_{SSR} and discharge Q as a function of time t for C_0 = 0.8 g/l, Kt_P =1.0 and Q = 0.3 (a), 0.7 (b), 0.9 (c) and 1.1 l/s (d)

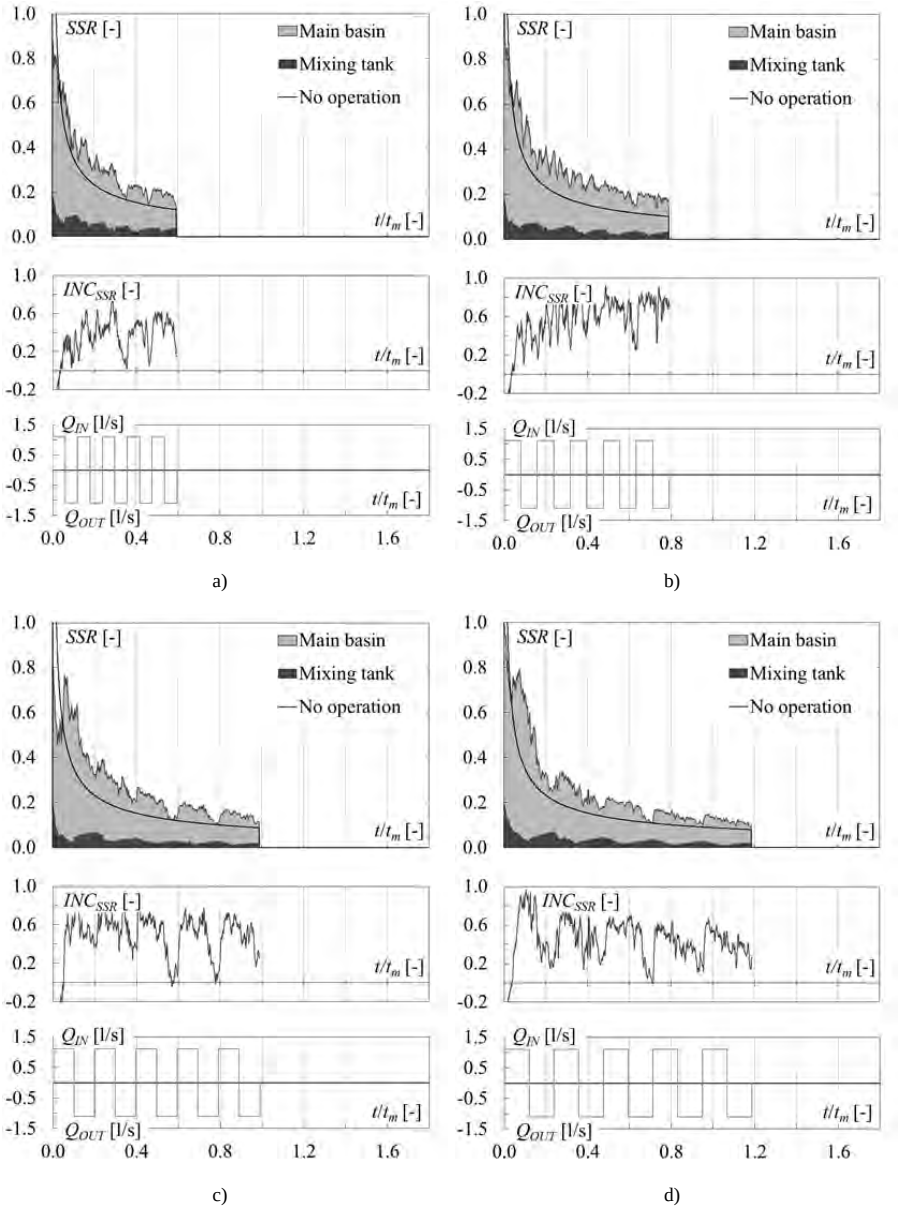

Figure 6.10 Suspended sediment ratio *SSR*, dimensionless increase INC_{SSR} and discharge *Q* as a function of dimensionless time t/t_m for C_0 = 0.8 g/l, *Q* = 1.1 l/s and Kt_P = 0.6 (a), 0.8 (b), 1.0 (c) and 1.2 (d)

6.4.3 Sediment exchange rates

Assuming a uniform distribution of suspended sediment in the two test volumes, the influx sediment rate *ISR* and the evacuated sediment rate *ESR* of the main basin can be calculated for each cycle:

$$ISR(t) = \frac{M_{S,IN}(t)}{M_0} = \frac{\sum Q_{IN} \cdot C_{MT}(t) \cdot \Delta t}{M_{0,MB} + M_{0,MT}} \quad \text{(Eq. 6.6)}$$

$$ESR(t) = \frac{M_{S,OUT}(t)}{M_0} = \frac{\sum Q_{OUT} \cdot C_{MB}(t) \cdot \Delta t}{M_{0,MB} + M_{0,MT}} \quad \text{(Eq. 6.7)}$$

The evolution of the cumulated influx and evacuated sediment rate are presented in Figure 6.11 as a function of t/t_m. The two sediment rates are developing practically symmetrically in time, indicating that the sediment balance *SB* of the system is almost equilibrated.

As high cycle magnitude keeps suspended sediment ratio at a higher level in the system, influx and evacuated sediment rates increase with increasing discharge. The growth rates of the two curves are developing proportionally to the suspended sediment ratio, i.e. slope is steeper during the first cycles and then the curves flatten toward the end of the experiment. After five in- and outflow cycles, *ISR* and *ESR* are both around 9% for Q = 1.1 l/s. For the lowest discharge Q = 0.3 l/s, values around 5% were computed (Figure 6.11a).

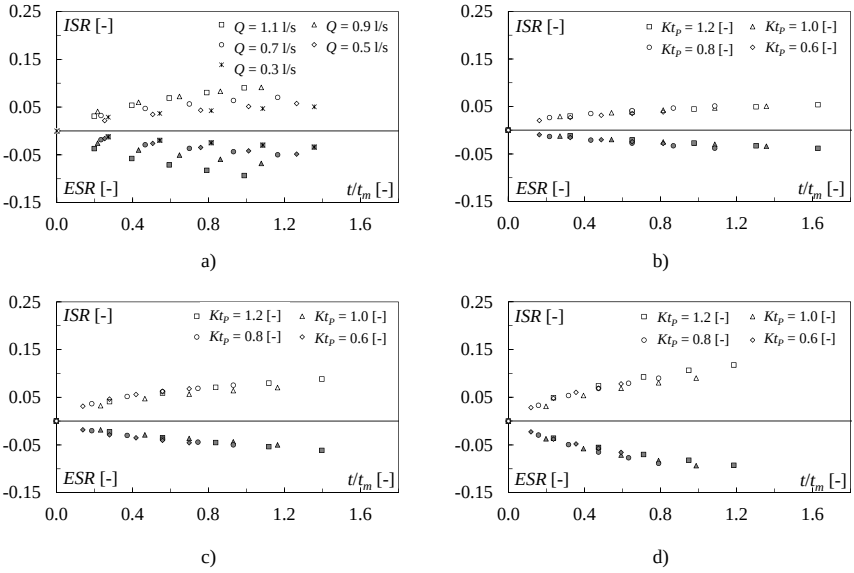

Figure 6.11 Influx sediment rate *ISR* and evacuated sediment rate *ESR* as a function of dimensionless time t/t_m for C_0 = 0.8 g/l, Kt_P =1.0 and different cycle magnitudes Q (a), and for C_0 = 0.8 g/l, different cycle frequencies Kt_P and discharges Q = 0.3 (b), 0.7 (c) and 1.1 l/s (d)

Cycle frequency affects the final influx and evacuated sediment rate. Longer test duration increase the amount of sediment entering and leaving the main basin. However, Figure 6.11b to d reveals that high frequency cycles of Kt_P = 0.6 and 0.8 reach approximately the same influx and evacuated sediment rates as the lower frequency cycles.

6.5 Discussion

To discuss the influence of cycle magnitude Q and frequency Kt_P as well as other parameters relative to sequence duration $t_{P,IN}/t_{P,OUT}$, initial sediment concentration C_0 and intake position z_i, the mean values of suspended sediment ratio SSR_m and relative increase INC_{SSR} over each inflow and outflow sequence are considered. Flow velocity measurements by the Ultrasonic Velocity Profilers (UVP) allowed the computation of kinetic energy in the basin in order to explain the influenced settling behavior of the sediment.

For all analyzed cycles, the first in- and outflow cycle is dominated by the settling process of the sediment. Up to t/t_m = 0.2, a decrease to approximately SSR = 0.4 is observed. About 60% of the fine sediment settled over this period, almost independently from the in- and outflow cycles' magnitude or frequency. Therefore, the evolution of suspended sediment ratios SSR < 0.4 (Figure 6.12b) is of major interest for the induced cycle analysis.

6.5.1 Cycle magnitude

Figure 6.12 gives the mean suspended sediment ratio SSR_m as well as the mean relative increase $INC_{m,SSR}$ as a function of t/t_m. For low discharges Q = 0.3 to 0.7 l/s, SSR can be increased by 10 to 40% compared to a scenario without operation. Higher cycle magnitudes Q = 0.9 and 1.1 l/s increase the ratio by 50 to 60% (Figure 6.12b). SSR and the resulting $INC_{m,SSR,final}$ after five cycles are presented in Table 6.2.

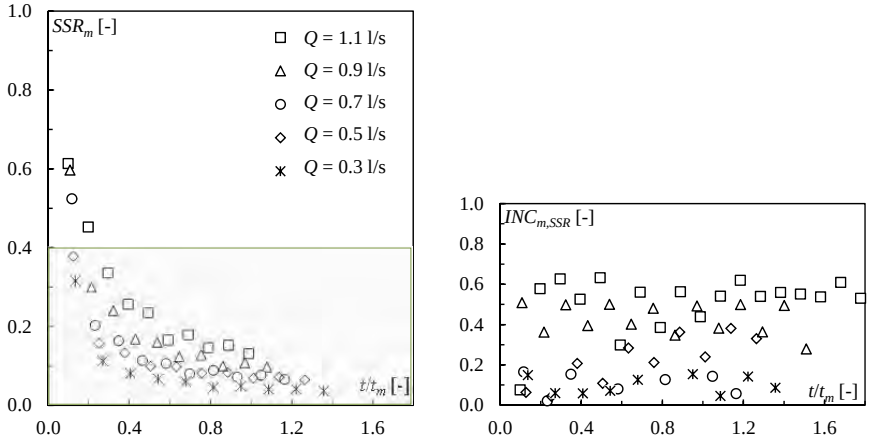

Figure 6.12 Mean suspended sediment ratio SSR_m (a) and mean relative increase $INC_{m,SSR}$ (b) as a function of dimensionless time t/t_m for five different discharges

Increased in- and outflow cycle magnitude leads to higher overall *SSR* and correlations with the discharge cycles. Thus, *SSR* is higher during inflow sequences and lower during outflow sequences.

The systematically increasing *SSR* during inflow sequences could have three origins.

- First, suspended sediment from the mixing tank enters the main basin. However, quantities from the mixing tank are not high enough to explain the difference of 10 to 20% between in- and outflow sequences.
- Second, resuspension of already settled particles could occur. This contribution to the increase of *SSR* could not be quantified in the experiments, but is expected to be very small due to very low flow velocities near the bottom.
- Third, the main reason for the higher *SSR* during inflow sequences, the kinetic energy input from the entering jet allows mixing the volume. Hence, particles in settling stage are again moved vertically as well as horizontally in the water body due to the induced flow patterns, and *SSR* increases.

Table 6.2 Discharge Q, corresponding mean residence time t_m and suspended sediment ratio $SSR_{m,final}$ for different cycle frequencies Kt_P

Q [l/s]	t_m [s]	Kt_P [-]	$SSR_{m,final}$ [%]
0.3	30’056	0.6	5.5
		0.8	5.6
		1.0	3.7
		1.2	3.8
0.5	18’034	1.0	6.5
0.7	12’881	0.6	8.7
		0.8	7.8
		1.0	6.7
		1.2	6.7
0.9	10’019	1.0	10.6
1.1	8’197	0.6	18.2
		0.8	17.9
		1.0	13.2
		1.2	11.0

Continuous in- and outflow sequences for the two highest discharges allow an increase of the mid-term suspended sediment ratio by 50 to 60%.

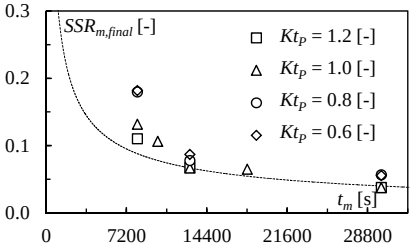

Figure 6.13 Mean suspended sediment ratio at the end of the experiment $SSR_{m,final}$ as a function of mean residence time t_m for different cycle frequencies Kt_P

6.5.2 Cycle frequency

Results of the parameter study on the cycle frequency are presented in Figure 6.14. Increased cycle frequencies Kt_P = 0.6 or 0.8 inhibit the evolution of steady flow conditions in the main basin. The evolution of *SSR* is highly fluctuating and does not correlate with the discharge cycles anymore.

In case of low discharges Q = 0.3 and 0.7 l/s, no clear tendency is observed for the different configurations. *SSR* is increased by 5 to 40% after the five in- and outflow cycles (Figure 6.14a, b). Short sequences never provide sufficient time to reach steady state conditions, influencing mixing efficiency.

At Q = 1.1 l/s, the discharge cycles are correlated with the temporal evolution of *SSR*, for all tested frequencies (Figure 6.14c). High cycle frequency leads to mean suspended sediment ratios SSR_m by 60 to 80% higher than without operation, for Kt_P = 1.0 and 1.2 to 50 and 60% (Table 6.2.).

Especially during the first settling period, cycle frequency is a key parameter affecting the efficiency of the entire operational sequence. If in this phase high cycle frequency is applied, the *SSR* can be considerably increased for the first cycles as well as the mid-term ones.

6.5.3 Relative sequence duration

The in- and outflow cycles observed in engineering applications are rarely regular in magnitude and frequency. Thus, in addition to the tested ranges of discharges and cycle duration, the relative sequence duration $t_{P,IN}/t_{P,OUT}$ was varied in two tests. For an inflow sequence of half of the outflow sequence, a net water withdrawal from the main basin results. The opposite scenario consists in a reduction in outflow to half of the inflow sequence duration.

Figure 6.15 shows that a relative sequence duration $t_{P,IN}/t_{P,OUT}$ = 2.0 results in considerably higher suspended sediment ratio. The shorter outflow sequences reduce the particle settling between two inflow sequences, increasing sediment suspension. The mean relative increase achieves 50% and at the end of five cycles $INC_{m,SSR}$ = 0.43.

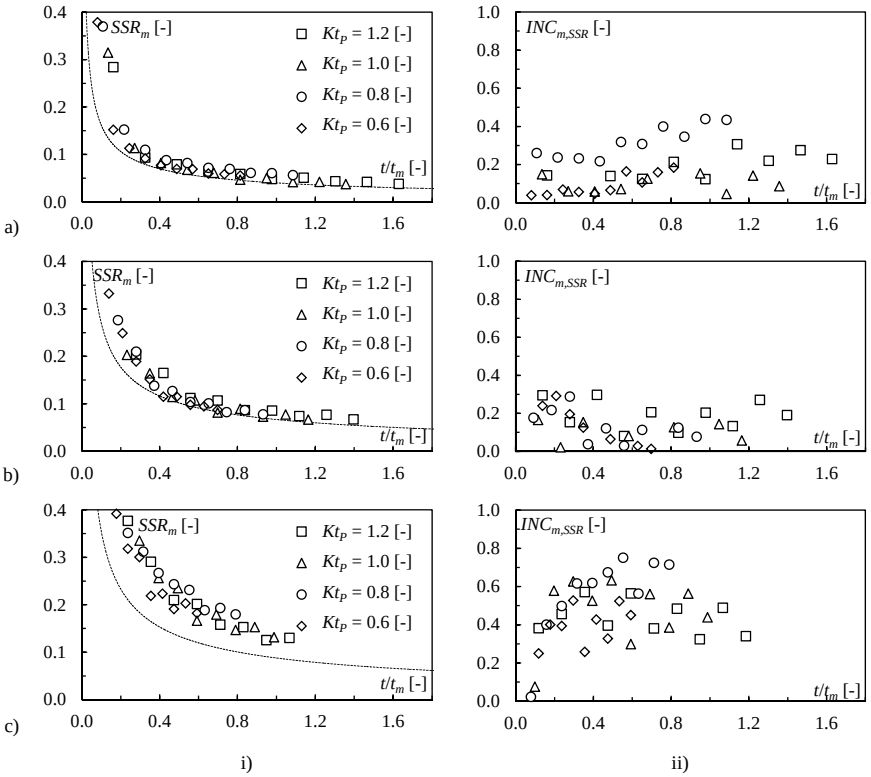

Figure 6.14 Mean suspended sediment ratio SSR_m (i) and mean relative increase $INC_{m,SSR}$ (ii) as a function of dimensionless time t/t_m for C_0 = 0.8 g/l, different cycle frequencies Kt_P and discharges Q = 0.3 (a), 0.7 (b) and 1.1 l/s (c). The dashed line represents the settling curve of suspended sediment in stagnant water

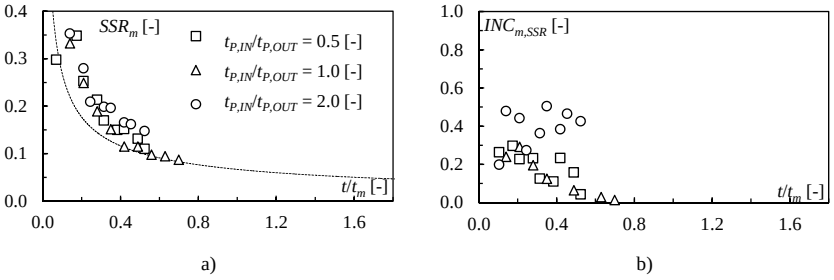

Figure 6.15 Mean suspended sediment ratio SSR_m (a) and mean relative increase $INC_{m,SSR}$ (b) as a function of dimensionless time t/t_m for C_0 = 0.8 g/l, Kt_P = 0.6, Q = 0.7 l/s and different relative sequence durations $t_{P,IN}/t_{P,OUT}$. The dashed line represents the settling curve of suspended sediment in stagnant water

6.5.4 Initial sediment concentration

The initial sediment concentration influences the suspended sediment ratio *SSR* by up to 40%. Compared to the reference state without operation, higher initial sediment concentration leads to increased *SSR*, as shown in Figure 6.16. While for C_0 = 0.3 and 0.8 g/l the mean relative error fluctuates around $INC_{m,SSR}$ = 0.10, $INC_{m,SSR}$ = 0.30 for C_0 = 1.5 g/l.

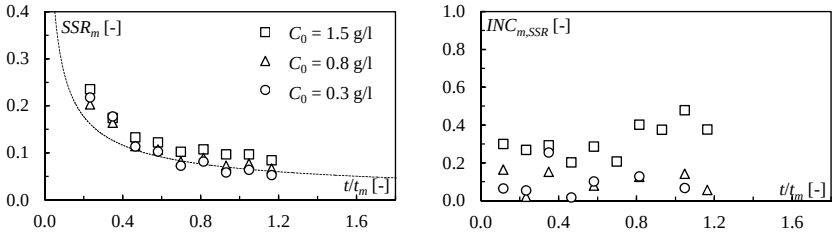

Figure 6.16 Mean suspended sediment ratio SSR_m (a) and mean relative increase $INC_{m,SSR}$ (b) as a function of dimensionless time t/t_m for Kt_P = 0.6, Q = 0.7 l/s and different initial sediment concentrations C_0. The dashed line represents the settling curve of suspended sediment in stagnant water

6.5.5 Intake position

Figure 6.17 gives the results for three prolongated tests for Q = 1.1 l/s, Kt_P = 1.0 and different intake positions z_i/B_{MB} over the reservoir bottom. On the one hand, in- and outflow sequences increase *SSR* not only over five cycles, but also over up to ten in- and outflow cycles. On the other hand, an intake located closer to the reservoir bottom or to the free surface generates flow conditions to keep fine sediment in suspension. *SSR* ratios are up to 80% higher than for the reference test and 20% higher compared to the initial intake position z_i/B_{MB} = 0.25.

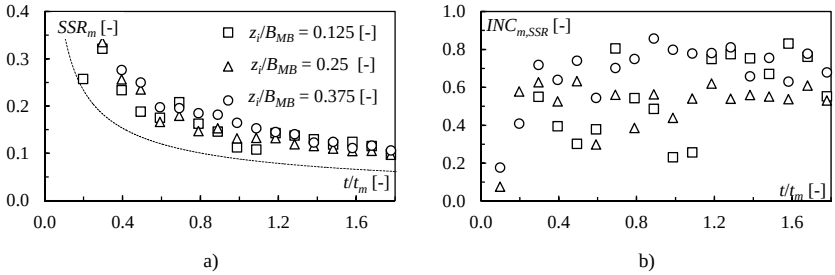

Figure 6.17 Mean suspended sediment ratio SSR_m (a) and mean relative increase $INC_{m,SSR}$ (b) as a function of dimensionless time t/t_m for C_0 = 0.8 g/l, Kt_P = 1.0, Q = 1.1 l/s and different intake positions z_i/B_{MB}. The dashed line represents the settling curve of suspended sediment in stagnant water

6.5.6 Sediment balance of the system

The sediment balance *SB* of the system was established on the influx (*ISR*) and evacuated sediment rate (*ESR*) for the main basin:

$$SB(t) = \frac{M_{S,IN}(t) - M_{S,OUT}(t)}{M_0} = ISR(t) - ESR(t) \qquad \text{(Eq. 6.8)}$$

SB defines the normalized sediment mass transferred from one reservoir to the other. Negative sediment balance indicates particle evacuation from the main basin.

Before, the *ISR* and *ESR* developed similarly in time. *SB* calculations confirm this behavior. Even if the transported mass during in- and outflow sequences is quite high, the sediment balance in the system is not significantly influenced by the in- and outflow cycles. The sediment balance is $-0.03 < SB < 0.04$ for all tested configurations (Figure 6.18). Thus, in-and outflow cycles move a lot of sediment back and forth but do not contribute to sediment redistribution between the two reservoirs.

Neither cycle magnitude nor cycle frequency affect the sediment balance in one or the other direction. Relative sequence duration does, sediment balance shifts to values between $SB = -0.03$ and 0.03 according to inflowing or outflowing water.

For nearly all test configurations, the sediment balance is positive at the end of the experiment. The main basin was slightly supplied with sediment from the mixing tank due to the tested cycle configuration with starting inflow sequence. A test with reversed in- and outflow cycles (Figure 6.7d) confirms this statement, presents a negative sediment balance in the same order of magnitude.

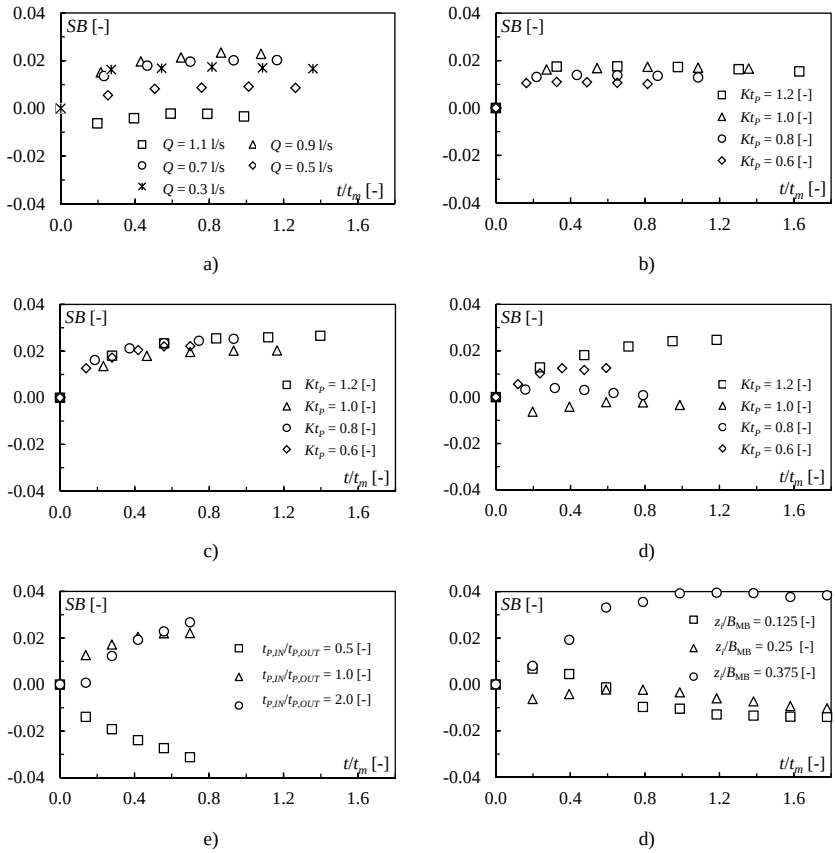

Figure 6.18 Sediment balance *SB* as a function of dimensionless time t/t_m for C_0 = 0.8 g/l, Kt_P =1.0 and different discharges Q (a), for different cycle frequencies Kt_P and discharges Q = 0.3 (b), 0.7 (c) and 1.1 l/s (d), for Q = 0.7 l/s and different relative sequence durations $t_{P,IN}/t_{P,OUT}$ (e) and for Q = 1.1 l/s and different intake positions z_i/B_{MB} (f)

6.6 Conclusions

The influence of in- and outflow sequences on the behavior of fine sediment were investigated in laboratory experiments. The test facility consists of two interconnected rectangular basins, between which water is moved back and forth. Suspended sediment was reproduced by walnut shell powder. Particle concentrations in the system were continuously measured by two turbidity probes. Ultrasonic Velocity Profilers (UVP) allowed 2D horizontal flow field measurements at several levels in the test volume.

A parametric study of frequency and magnitude of the in- and outflow cycles, the initial sediment concentration as well as the intake position was carried out to evaluate the suspended sediment ratio *SSR* and sediment exchange rates. An initial test in stagnant water

conditions described the settling behavior of the investigated sediment and served as reference scenario for evaluating the efficiency of the tested in- and outflow cycles.

The range of cycle magnitude was chosen according to discharges, velocities and residence times of real case, considering Froude similarity, situating the experimental scale at λ_L = 50 to 100 approximately. The cycle frequency was evaluated in a numerical model. The initial duration of the in- and outflow sequences corresponds to the time to develop steady state conditions in the test volume. The mean residence time t_m is defined as time normalizing parameter.

Experimental results show that settling down of fine particles can be considerably reduced by the in- and outflow sequences. However, the initial settling phase of particles is only marginally influenced by the tested in- and outflow cycles. Approximately 60% of settling takes place during t/t_m = 0.2, corresponding to the first or the first two cycles, according to discharge.

High cycle magnitude and frequency lead to maximum *SSR*. For low discharge, the evolution of *SSR* is not clearly correlated to the in- and outflow cycles. Compared to conditions without operation, *SSR* can be increased by 10 to 40%. For high discharge, the evolution of concentration correlates with discharge cycles and leads to suspended sediment ratios between 50 to 80% higher than in calm water conditions based on the duration of the experimental data.

Especially during the first settling period, cycle frequency is a key parameter for the efficiency of the operational sequence. If high cycle frequency is applied in the starting period, *SSR* can be considerably increased. Furthermore, longer experiments for high discharges keep sediment in suspension not only during the first cycles. Even after t/t_m = 1.6, *SSR* remained about 60% higher than without operation.

Increased *SSR* were obtained for intake positions closer to the bottom or to the free water surface. The resulting flow conditions with more vertical movement in the water body keep more particles in suspension.

Varying relative sequence duration increase *SSR*. When inflow sequences are intercepted by shorter outflow sequences, particle settling is reduced due to increased turbulence in the test volume.

The overall sediment balance *SB* remains equilibrated over the test period and is smaller than 4% for all tested configurations. Thus, the sediment balance in the system is not significantly influenced by the in- and outflow sequences even if the total moved mass during in- and outflow sequences is high. As suspended sediment concentration decreases rapidly at the beginning of the settling phase, the exploitation direction of the first sequence defines if the sediment balance of the main basin is positive.

Chapter 7

Conclusions

7.1 Synthesis

Sedimentation is of major concern for many storage reservoirs and endangers reliability, efficiency as well as structural safety of hydropower schemes. During flood events, high erosion in the watersheds leads to high sediment yield into the reservoirs. In Alpine catchments, turbidity currents are the most common source of reservoir sedimentation. From the river delta they follow the thalweg to the deepest part of the storage, often close to the dam and intake structures. In the so-called muddy lake fine sediment start settling down.

In pumped-storage schemes, the water body in the areas close to the intake/outlet structure is known to be influenced by hydropower exploitation. Thermal stratification, nutrient content and ecosystem issues can be altered. Sediment may sometimes be resuspended and entrained. However, the effect of the in- and outflow sequences on particle dynamics and settling process is hardly investigated yet.

Hence, the purpose of the present study is to use the turbulence induced by pumped-storage operation, to maintain fine sediment in suspension for evacuation through the headrace system or flushing facilities. The influence of in- and outflow sequences on flow patterns and suspended sediment behavior in reservoirs was investigated in prototype measurements and laboratory experiments, in combination with numerical modeling.

7.1.1 Prototype measurements of flow conditions in a pumped-storage reservoir

The lower reservoir of the Grimsel 2 pumped-storage scheme in the Swiss Alps was equipped with three Acoustic Doppler Current Profilers (ADCP) to continuously sample flow velocities in front of the circular shaped intake/outlet structure at the lake bottom over four and nine days periods. Frequency analysis of the recorded velocity signal indicates correlation between the sampled flow patterns and the pumped-storage activity. The predominant period is $1/f$ = 1 day, corresponding to the daily pumped-storage cycles of the plant. Seiche frequencies were not discovered in the velocity spectra.

One- and two-dimensional velocity profiles were established based on the collected in situ data. They show that pumping (withdrawal from the reservoir) only affects the water body close to the intake. At 30 m from the intake/outlet, flow velocities of about v = 6 cm/s were recorded and at 150 m velocity profiles were not anymore influenced by the withdrawal. Periods without pumped-storage activities showed rather random velocity fluctuations in the water body. During turbine mode (inflow into the reservoir), flow velocities up to v = 12 cm/s were recorded by the ADCP, even at 150 m from the outlet. This operation mode systematically generates flow patterns with important backflow between 5 and 20 m above the reservoir bottom and a main outflow sector in E-SE direction. The natural confinement generates a large scale circulation cell, rotating counterclockwise in the basin in front of the intake/outlet.

Numerical model simulations confirmed the in situ observations, reproducing the main characteristics of the flow patterns in front of the intake/outlet. The reservoir's response to hydropower operation could be studied. Steady flow fields were observed only after 150 minutes of continuous turbine operation. Scenarios comprising a temperature difference of ΔT_w = +/-5 °C between the inflowing and the resident water showed no significant change in flow patterns.

Turbulent kinetic energy (TKE) input due to turbine operations is some 25 times higher than the natural TKE input by wind-forcing. This impacts the thermal stratification of the water column and increases mixing frequency. From a reservoir sedimentation point of view, the high TEK input is favorable as it keeps fine sediment in suspension and consequently slows down particle settling.

Prototype flow velocity measurements in the intake/outlet area of a reservoir combined with numerical modeling allows

- detection of main flow directions and backflow zones in a reservoir,
- quantification of flow velocities in the surroundings of the intake/outlet, and
- evaluation of temporal response of the water body to in- and outflow sequences.

In any case, the topography of the reservoir bottom is a key parameter governing the development and the main directions of flow patterns and recirculation cells. Due to the autonomous power supply, the ADCP provide an adequate mid-term monitoring system.

7.1.2 Turbidity monitoring in a pumped-storage plant

Over a period of eight months, the suspended sediment concentration was continuously measured by a turbidity probe installed on the upstream part of the pressurized shaft of the Grimsel 2 pumped-storage plant in the Swiss Alps. The monitoring system was conceived to provide data storage, remote access as well as real-time data display.

Sampled data revealed several changes in mean suspended sediment concentration C_m during the measurement period. In November/December a monthly average around C_m = 80 mg/l was measured. From February to April, when the reservoirs were ice- and the watershed snow-covered, particle load was low with values from C_m = 55 to 60 mg/l. With the beginning of snowmelt in May and June suspended sediment concentration increased to C_m = 75 to 85 mg/l.

Over the eight months monitoring period, approximately 45'000 t of fine sediment were transported by pumped-storage operations between the two lakes. This is double the mass of sediment expected to deposit annually in the upper reservoir. However, the suspended sediment balance was equilibrated. Most of the suspended sediment entering the reservoirs was transported back when exploitation mode inversed. Thus, mixing processes keep the main part of the fine sediment in suspension in front of the intake/outlet structures but does not lead to redistribution between the reservoirs.

Pumped-storage sequences were directly correlated to the short-term evolution of sediment concentration, especially when reservoir levels were low. During pumping mode, high particle load was observed more frequently. Maximum concentration ratios between pumping and turbine mode were of $C_{m,Pump}/C_{m,Turb} = 1.16$, while the lowest was 0.93. However, moved sediment load is strongly correlated to the frequency and magnitude of pumped-storage sequences.

Monitoring of sediment concentration in the waterways of a pumped-storage plant allows

- detection of increased sediment load in the system, indicating high suspended sediment concentration in the intake/outlet area of the reservoirs, and
- monitoring of the long-term sedimentation issues through the continuous observation of sediment balance of the two reservoirs.

It would enable the plant operator to actively manage reservoir sedimentation, if the hydropower scheme provides the features for releasing high sediment loads.

7.1.3 Experimental study on in- and outflow sequences

The influence of in- and outflow sequences on the behavior of fine sediment was investigated in laboratory experiments. The test facility consisted of two interconnected rectangular basins, between which sediment-laden water was moved back and forth. Suspended sediment concentration in then system was derived from continuous turbidity measurements. Ultrasonic Velocity Profilers (UVP) measured horizontal 2D flow patterns at several levels in the basin, describing the jet development during inflow conditions. Basin width B_{MB} and mean residence time $t_m = V/Q$ were used for lengths and time normalization.

Previous to tests with sediment, the time to reach steady state conditions in the test volume was defined by numerical modeling (ANSYS-CFD). This so-called "time to peak" between $t_P/t_m = 0.099$ and 0.136 depends on discharge and defined the experimental duration for the initial in- and outflow cycle configuration. A test in calm water conditions described the settling behavior of the fine sediment and served as reference scenario for the in- and outflow cycles.

Five parameters were varied for the test series: the magnitude or discharge Q, the cycle frequency Kt_P, the relative cycle duration $t_{P,IN}/t_{P,OUT}$, the initial sediment concentration C_0 as well as the intake position z_i/B_{MB}. To evaluate their influence on sediment settling, the temporal evolution of the suspended sediment ratio SSR was compared to the reference test without in- and outflow cycles. The influx sediment rate ISR and evacuated sediment rate ESR allow calculation of the sediment balance SB of the system.

Experimental results lead to the following conclusions:

- The initial settling phase of particles is only marginally influenced by the tested in- and outflow cycles. Approximately 60% of settling takes place during a period of $t/t_m = 0.2$, corresponding to the first or the first two cycles of the experiment, depending on discharge.
- Rather low cycle magnitude with $t_m \geq 12'881$ s increases *SSR* by 10 to 40% compared to "no operation" scenarios. Evolution of *SSR* is not well correlated to the in- and outflow cycles. At high magnitude with $t_m \leq 8'197$ s, evolution of *SSR* correlates with discharge cycles and leads to suspended sediment ratios between 50 to 60% higher than in calm water conditions.
- Combined with high cycle magnitude, increasing cycle frequency leads to maximum *SSR* in the system, due to high kinetic energy input during inflow sequences and fast changes in exploitation direction. For $t_m = 8'197$ s, *SSR* can be increased by up to 80% higher than without in- and outflow cycles. For $t_m \geq 12'881$ s, no tendency could be observed, *SSR* remaining some 10 to 40% higher than in the reference test.
- Cycle frequency is a key parameter during the first settling period, affecting the efficiency of the entire sequence. If high frequency is applied, the mid-term *SSR* can be considerably increased.
- *SSR* can be kept at a high level over a longer experimental duration for high magnitude $t_m = 8'197$ s. Tests revealed that even after $t/t_m = 1.6$ *SSR* remains about 60% higher than without in- and outflow operation.
- High ratios of $t_{P,IN}/t_{P,OUT}$ lead to increased *SSR*, as inflow sequences are intercepted by shorter outflow sequences. Particle settling is reduced due to frequent and repetitive increase of turbulence in the test volume.
- For $t_m = 8'197$ s, an intake position closer to the bottom ($z_i/B_{MB} = 0.125$) or the free water surface ($z_i/B_{MB} = 0.375$) lead to an increase of *SSR* by 20% compared to $z_i/B_{MB} = 0.25$. Amplified vertical recirculation keeps more particles in suspension.

For all tested in- and outflow configurations, the sediment balance of the system remained equilibrated over the test period. It is thus not significantly influenced by the in- and outflow sequences, even if the suspended sediment mass exchange during in- and outflow sequences is considerably high. As suspended sediment concentration decreases rapidly in the starting settling phase, the initial exploitation defines the global sediment balance over the cycles.

7.1.4 Concluding remarks

Both prototype measurements and laboratory experiments show the influence of pumped-storage activities (in- and outflow sequences) on the flow patterns as well as the settling behavior of fine sediment in reservoirs.

Outflow (withdrawal) has less impact on flow patterns, as the velocity field is only locally influenced near the intake structure. During inflow sequences the jet is mixing the water body and can generate big recirculation cells. These phenomena are influenced by the intake/outlet position and geometry as well as by the shape of the storage volume. Cycle magnitude influences the kinetic energy in a reservoir. According to experimental results, high

discharges generate up to three times more energy than low discharges. Cycle frequency has less influence. An intake position close to the bottom or the free water surface leads to higher energy levels.

The evolution of the suspended sediment ratio *SSR* of fine sediment is correlated to the magnitude and frequency of the in- and outflow cycles for a certain discharge threshold. The prototype monitoring of sediment concentration reflected the pumped-storage sequences at low reservoir levels. Both approaches indicate that the global sediment balance of pumped-storage operations is equilibrated. As long as suspended sediment concentration is similar in both reservoirs, the sediment balance is thus essentially correlated to the pumped-storage operation.

7.1.5 Recommendations

Applied to a real-life problem, i.e. the arrival and deposition of a turbidity current in the area of a pumped-storage intake/outlet structure, it is expected that an important settling occurs during the first hours after the turbidity current event, which can not entirely be avoided by an adequate plant operation. However, according to experimental results, the quantity of fine sediment kept in suspension can be considerably increased when operating the plant at high discharge and with short pumped-storage sequences in this phase. Later on, pumped-storage operation at high cycle magnitude is the most promising measure to slow down sediment settling.

However, when one reservoir contains considerably higher sediment concentrations than the other, the pumped-storage activity could lead to a redistribution of sediment and thus result in a non-desired artificial sediment inflow to a reservoir. Such behavior has not been investigated experimentally in this study. Prototype monitoring did not reveal net sediment exchanges neither but it has been shown in former research that pumped-storage operation can contribute to sediment redistribution, especially during summer months, when natural sediment input is usually highest. A long-term monitoring of suspended sediment concentration by the means of a system applied in this research would allow a better understanding and an estimation of sediment exchange rates between pumped-storage reservoirs.

With respect to the design of intake and outlet structures, the optimum configuration should aim a maximum kinetic energy input to generate high turbulence in the zones near the intake/outlet structure, mainly during inflow sequences. In fact, the kinetic energy provides a quantifiable parameter with important influence on sedimentation by fine particles and can be determined based on numerical computations or in situ measurements of flow velocities.

In future, the increased demand of grid regulation and peak energy supply will probably lead to quite short and frequent pumped-storage cycles with the corresponding effects on the water body close to the intake/outlet structures. Considering the influence of the in- and outflow sequences on fine sediment behavior at an early stage of the planning and design of the intake/outlet structures of pumped-storage power plants will allow implementing adequate sediment management of their reservoirs.

7.2 Outlook

Prototype monitoring, experimental modeling and numerical simulations have been investigated in the present research. Each of them contributed to the general conclusions of the thesis. However, in each of the applied methods, potential to be exploited in future research remains.

7.2.1 Further prototype monitoring

The ADCP measuring devices can have certain limits in use due to the lack of sound scatterers in the water. Further ADCP recording in Alpine reservoirs could be carried out to review and optimize sampling frequencies and bin lengths for particular in situ conditions. Further research could be conducted on the application of ADCP for suspended sediment concentration sampling.

During the eight months of turbidity monitoring, no flood event was recorded. Technical reasons avoided sampling during summer, which would usually contribute with around 60% to the annual suspended sediment inflow in the reservoir. Longer series of continuous in situ turbidity measurements would allow a long-term sediment balance. In addition, the mixing effect of pumped-storage sequences during and after the arrival of turbidity currents could be quantified.

The two measuring systems could be applied simultaneously to investigate the correlation between flow patterns in front of the intake/outlet and suspended sediment concentrations in the waterways.

7.2.2 Further experimental and numerical research

Additional experimental work should focus on modified reservoir geometry with inclined side walls, similar to prototype conditions, as the influence of the basin shape has not been addressed yet. In- and outflow sequences would allow countless combinations of magnitude and frequency. The most interesting parameters to study are the relative cycle magnitude $Q_{,IN}/Q_{,OUT,}$ different initial sediment concentrations in the two basins $C_{0,MB}/C_{0,MT}$ as well as the intake position z_i/B_{MB}. Concerning the intake/outlet, the effect of the geometry and orientation of the structure should be investigated.

Further 3D numerical modeling could include calibration and simulation of two phase flow (water-sediment-mixture) to reproduce the experimental tests and compare results on sediment balance and suspended sediment ratio. Finally, numerical modeling of real reservoirs could be addressed, focusing on the suspended sediment behavior under pumped-storage operations.

Acknowledgements

This doctoral thesis was conducted at the Laboratory of Hydraulic Constructions (LCH) at Ecole Polytechnique Fédérale de Lausanne (EPFL).

I would like to thank my thesis director Prof. Anton Schleiss for motivating and supporting me with his scientific experience and his optimistic and flexible guidance. I am grateful for his confidence in my abilities. He offered me excellent working conditions to achieve my professional and personal objectives.

Then, I owe my recognitions to my thesis co-director Dr. Giovanni De Cesare who shared with me his remarkable knowledge about reservoir sedimentation and his fascination for science and research. I appreciated the many valuable advices and interesting discussions.

This research project was part of the *HydroNet* consortium funded by three organizations: the *Competence Center Energy and Mobility* (CCEM), *swisselectric research* and the *Swiss Federal Office of Energy* (SFOE – *hydropower research*). I acknowledge the support of Dr. Martin Kauert, Dr. Michael Moser and Dr. Klaus Jorde from the institutional partners.

I would like to thank the members of my jury, Prof. Flavio Anselmetti, Prof. Blake P. Tullis and Dr. Sven Hartmann, for accepting to review and evaluate this doctoral thesis and Prof. Jian Zhao for being the president of the jury.

Prototype measurements would not have been possible without the support of the Kraftwerke Oberhasli AG and its collaborators, especially Bruno Kehrli who navigated on Lake Grimsel during the ADCP positioning and Fritz Büchi who gave advices and made commitments in setting up and maintaining the monitoring system in the Grimsel 2 power plant. Special thanks are due to Theo Winkler for the operational data, to Prof. Ulrich Lemmin (ECOL-EPFL) for providing and programming the ADCP as well as to the many strong arms of LCH and Eawag helping during field work.

I thank Luca Bremen and Alexandre Pachoud for their conscious scientific work related to preliminary experiments and numerical modeling.

During five years, I was part of a creative, spontaneous, intelligent and sometimes crazy ensemble of engineers, researchers, secretaries, technicians and – above all – colleagues and friends. I thank all LCH members for the great team spirit and the countless (non-)scientific discussions. Special thanks to my dear friend Martin for friendship, laughs, critics and feedback on my thesis report, to my office mate Fadi for his great assistance in setting up the monitoring system and to Ana, Violaine, Ze Pedro and Javier for their help with Matlab and VBA codes. I appreciated the fruitful discussions with Jean-Louis Boillat as well as the excellent technical support by Cedric, Michel and others of the workshop team.

The men's volleyball squads of volleyball clubs Ecublens and Münchenbuchsee earn a big "merci". Throughout my whole stay at EPFL the two clubs offered me the possibility to play in their first team and thus satisfy my need for sports competition and daily work balance.

My deepest thanks and gratitude are addressed to my parents Brigitte and Ernst and my sister Sandra for their love, patience and motivation as well as for giving me the opportunity and the confidence to pursue my educational and professional way.

I am endlessly grateful to my beloved family. The critics, patience, comprehension, encouragements and love of my dear wife Katrin and the curiosity and smiles of our lovely daughter Ronja empowered me to perform at my best and to bring this PhD to a happy end.

References

Abramovich, G.N. 1963. The theory of turbulent jets. M.I.T. Press, Cambridge, Massachussetts.

Alam, S. 1999. The influence and management of sediment at hydro projects. *Hydropower & Dams* **6**(3): 54-57.

Anderson, M.A. 2010. Influence of pumped-storage hydroelectric plant operation on a shallow polymictic lake: Predictions from 3-D hydrodynamic modeling. *Lake and Reservoir Management* **26**(1): 1-13.

Anselmetti, F., R. Bühler, D. Finger, S. Girardclos, A. Lancini, C. Rellstab and M. Sturm 2007. Effects of Alpine hydropower dams on particle transport and lacustrine sedimentation. *Aquatic Sciences* **69**(2): 179-198.

Basson, G.R. 2009. Management of siltation in existing and new reservoirs. General Report Q89. 23rd Congress of the CIGB-ICOLD, Brasilia, Brazil.

Batuca, D.G. and J.M. Jordaan 2000. Silting and Desilting of Reservoirs. A.A. Balkema, Rotterdam.

Bechteler, W. 2008. Sediment Sources and Transport Processes. Insitut für Wasserwesen, Universität der Bundeswehr München, München, Germany.

Berezinskii, S.A., I.I. Ivanov and M.F. Sarkisova 1985. Intake of the Zagorsk and Kaisiadorys pumped-storage stations. *Power Technology and Engineering (formerly Hydrotechnical Construction)* **19**(4): 187-190.

Beyer Portner, N. and A.J. Schleiss 2000. Bodenerosion in alpinen Einzugsgebieten in der Schweiz. *Wasserwirtschaft* **90**(3): 88-92. (in German)

Blaser, S. and J. Bühler 2001. Werden durchlaufende Sedimentpartikel in hydraulischen Maschinen fragmentiert? *Wasser, Energie, Luft - eau, énergie, air* **93** (11): 305-311. (in German)

Blevins, R.D. 1984. Applied fluid dynamics handbook. Krieger Publishing Company, Malabar, Florida, US.

Boillat, J.L. and P. Delley 1992. Transformation de la prise d'eau de Malvaglia, étude sur modèle et réalisation. *Wasser, Energie, Luft - eau, énergie, air* **84**(7): 145-151. (in French)

Boillat, J.L. and H. Pougatsch 2000. State of the art of sediment management in Switzerland. International Workshop and Symposium on Reservoir Sedimentation Management, Tokyama, Japan.

Bonalumi, M., F.S. Anselmetti, R. Kaegi and A. Wüest 2011. Particle dynamics in high-Alpine proglacial reservoirs modified by pumped-storage operation. *Water Resources Research* **47**(9): W09523.

Bouffard, D. 2008. A new approach for studying small scale turbulence in the thermocline region of Lake of Geneva. Thesis 4110, Ecole Polytechnique Fédérale de Lausanne.

Bouvard, M. 1984. Barrages mobiles et ouvrages de dérivation: à partir des rivières transportant des matériaux solides. Editions Eyrolles, Paris, France. (in French)

Brown, P.P. and D.F. Lawler 2003. Sphere Drag and Settling Velocity Revisited. *Journal of Environmental Engineering* **129**(3): 222-231.

Bühler, J. and C. Siegenthaler 2003. Veränderungen im Oekosystem Brienzersee. Teilprojekt 3.2: Korngrössenverteilung, Zusammensetzung und Transport von Schwebstoffen im Grimselgebiet. Report, Amt für Gewässerschutz und Abfallwirtschaft des Kantons Bern (GSA), Bern, Switzerland. (in German, unpublished)

Bühler, J., C. Siegenthaler, R. Simitovic, A. Wüest and M. Zeh 2004. Trübeströme im Grimselsee. *Wasser, Energie, Luft - eau, énergie, air* **96**(5): 129-135. (in German)

Bühler, J., C. Siegenthaler and A. Wüest 2005. Turbidity currents in an alpine pumped-storage reservoir. *In:* Lee, J. H. W. & Lam, K. M., eds., Environmental hydraulics and sustainable water management, Hong Kong, China, 239-244.

Cardoso, S.S.S. and M. Zarrebini 2001a. Convection driven by particle settling surrounding a turbulent plume. *Chemical Engineering Science* **56**(11): 3365-3375.

Cardoso, S.S.S. and M. Zarrebini 2001b. Sedimentation of polydispersed particles from a turbulent plume. *Chemical Engineering Science* **56**(16): 4725-4736.

Chen, J. and K. Zhao 1992. Sediment management in Nanqin Reservoir. *International Journal of Sediment Research* **7**(3): 71-84.

Chhabra, S., T.N. Shipman and A.K. Prasad 2005. The entrainment behavior of a turbulent axisymmetric jet in a viscous host fluid. *Experiments in Fluids* **38**(1): 70-79.

Clark, R.M., F. Abdesaken, P.F. Boulos and R.E. Mau 1996. Mixing in Distribution System Storage Tanks: Its Effect on Water Quality. *Journal of Environmental Engineering* **122**(9): 814-821.

Cook, C.B., M.C. Richmond and J.A. Serkowski 2007. Observations of velocity conditions near a hydroelectric turbine draft tube exit using ADCP measurements. *Flow Measurement and Instrumentation* **18**(3–4): 148-155.

Cuthbertson, A.J.S. and P.A. Davies 2008. Deposition from Particle-Laden, Round, Turbulent, Horizontal, Buoyant Jets in Stationary and Coflowing Receiving Fluids. *Journal of Hydraulic Engineering* **134**(4): 390-402.

De Cesare, G. 1998. Alluvionnement des retenues par courants de turbidité. Thesis 1820, Communication N°7 du Laboratoire de Constructions Hydrauliques, A. Schleiss (ed.), Ecole Polytechnique Fédérale de Lausanne, Switzerland. (in French)

De Cesare, G., J.L. Boillat and A.J. Schleiss 2006. Circulation in Stratified Lakes due to Flood-Induced Turbidity Currents. *Journal of Environmental Engineering* **132**(11): 1508-1517.

De Cesare, G., A. Schleiss and F. Hermann 2001. Impact of Turbidity Currents on Reservoir Sedimentation. *Journal of Hydraulic Engineering* **127**(1): 6-16.

De Cesare, G. and A.J. Schleiss 1999. Turbidity current monitoring in a physical model flume using ultrasonic Doppler method. 2nd International Symposium on Ultrasonic Doppler Methods for Fluid Mechanics and Fluid Engineering, Villigen, Switzerland, 61-64.

Donald, M.B. and H. Singer 1959. Entrainment in turbulent fluid jets. *Chemical Engineering Research and Design* **37a**: 246-258.

Dorfmann, C. and H. Knoblauch 2008. ADCP measurements in a reservoir of a run-of-river Hydro Power Plant. *In:* Chara, Z. & Bares, V., eds., 6th International Symposium on Ultrasonic Doppler Method for Fluid Mechanics and Fluid Engineering, Prague, Tchech Republic, 45-48.

Elci, E., P.A. Work and E.J. Hayter 2007. Influence of Stratification and Shoreline Erosion on Reservoir Sedimentation Patterns. *Journal of Hydraulic Engineering* **133**(3): 255-266.

Ernst, G.G.J., R.S.J. Sparks, S.N. Carey and M.I. Bursik 1996. Sedimentation from turbulent jets and plumes. *Journal of Geophysical Research* **101**(B3): 5575-5589.

Fan, J. and G.L. Morris 1992. Reservoir sedimentation II: Reservoir desiltation and long-term storage capactiy. *Journal of Hydraulic Engineering* **118**(3): 370-384.

Finger, D., P. Bossard, M. Schmid, L. Jaun, B. Müller, D. Steiner, E. Schäffer, M. Zeh and A. Wüest 2007. Effects of alpine hydropower operations on primary production in a downstream lake. *Aquatic Sciences* **69**(2): 240-256.

Finger, D., M. Schmid and A. Wüest 2006. Effects of upstream hydropower operation on riverine particle transport and turbidity in downstream lakes. *Water Resources Research* **42**(8): W08429.

Fischer, H.B., J.B. List, R.C.Y. Koh and J. Imberger 1979. Mixing in inland and coastal waters. Academic Press, New York, US.

FLOTRON AG 2006. Grimselseeboden - Technischer Bericht: Bildflug, Geländemodell, Orthofoto. Report, Meiringen, Switzerland. (in German, unpublished)

Gartner, J.W. 2004. Estimating suspended solids concentrations from backscatter intensity measured by acoustic Doppler current profiler in San Francisco Bay, California. *Marine Geology* **211**(3–4): 169-187.

Girgidov, A.D., E.A. Loktionova and V.V. Prytkov 1990. Effect of the operation of a pumped-storage station on the thermal regime of a natural water body. *Power Technology and Engineering (formerly Hydrotechnical Construction)* **24**(7): 426-429.

Gordon, L., A. Lohrmann and T. Jonas 1999. Internal wave generation in lakes with very slow flow. IEEE Sixth Working Conference on Current Measurement, San Diego, CA, US, 212-215.

Goto, T. and S. Tsuchiyama 1998. Application of a Hydraulic and In-situ Measurement for the Construction of Reservoir Outlets. 3rd International Conference on Hydroscience and Engineering (ICHE), Cottbus/Berlin, Germany.

Graf, W.H. 1982. Storage losses in reservoirs. *International Water Power & Dams Constructions* **36**(4): 37-40.

Gray, J.R. and J.W. Gartner 2009. Technological advances in suspended-sediment surrogate monitoring. *Water Resources Research* **45**: W00D29.

Hachem, F. 2011. Monitoring of Steel Lined Pressure Shafts Considering Water-Hammer Wave Signals and Fluid-Structure Interaction. Thesis 5171, Communication N° 49 du Laboratoire de constructions hydrauliques, A. Schleiss (ed.). Ecole Polytechnique Fédérale de Lausanne, Switzerland.

Hartmann, S. 2007. Interreg IIIB - Ver und Entlandung von Stauräumen im Alpengebiet. *Wasserwirtschaft* (4): 31-35. (in German)

Hsiao, F.-B., Y.-C. Lim and J.-M. Huang 2010. On the near-field flow structure and mode behaviors for the right-angle and sharp-edged orifice plane jet. *Experimental Thermal and Fluid Science* **34**(8): 1282-1289.

ICOLD - International Committee of Large Dams 1989. Sedimentation control of reservoirs - Guidelines. **Bulletin 67**.

Imboden, D. 1980. The Impact of Pumped Storage Operation on the Vertical Temperature Structure in a Deep Lake: A Mathematical Model. *In:* Clugston, J. P., eds., Proceedings of the Clemson Workshop on Environmental Impacts of Pumped Storage Hydroelectric Operations, Clemson, South Carolina, US: Fish and Wildlife Service, Office of Biological Services, Report FWS/OBS-80/28, 125-146.

Jacobsen, T. 1999. Sustainable reservoir development: The challenge of reservoir sedimentation. Hydropower into the next century, Gmunden, Austria, 719-728.

Jaun, L., D. Finger, M. Zeh, M. Schurter and A. Wüest 2007. Effects of upstream hydropower operation and oligotrophication on the light regime of a turbid peri-alpine lake. *Aquatic Sciences* **69**(2): 212-226.

Jenzer Althaus, J. 2011. Sediment Evacuation from Reservoirs through Intakes by Jet Induced Flow. Thesis 4927, Communication N° 45 du Laboratoire de constructions hydrauliques, A. Schleiss (ed.). Ecole Polytechnique Fédérale de Lausanne, Switzerland.

Jirka, G. 2004. Integral Model for Turbulent Buoyant Jets in Unbounded Stratified Flows. Part I: Single Round Jet. *Environmental Fluid Mechanics* **4**(1): 1-56.

Kantoush, S.A., G. De Cesare, J.L. Boillat and A.J. Schleiss 2008. Flow field investigation in a rectangular shallow reservoir using UVP, LSPIV and numerical modelling. *Flow Measurement and Instrumentation* **19**(3–4): 139-144.

Kaskas, A.A. 1970. Schwarmgeschwindigkeiten in Mehrkornsuspensionen am Beispiel der Sedimentation. Thesis, TH Berlin, Germany. (in German)

Khosronejad, A. and C.D. Rennie 2010. Three-dimensional numerical modeling of unconfined and confined wall-jet flow with two different turbulence models. *Canadian Journal of Civil Engineering* **37**: 576-587.

Klebsattel, G. and M. Rost 2010. The Hornberg Reservoir of the Pump Storage Scheme Wehr, Schluchseewerk AG - Scheduled Maintenance after 35 Years in Operation. *Wasserwirtschaft* **100**(4): 128-130. (in German)

Knoblauch, H., S. Hartmann and G. De Cesare 2005. Sedimentmanagement an alpinen Speichern: Das EU-INTERREG IIIB Projekt ALPRESERV. *Österreichische Wasser- und Abfallwirtschaft* **57**(11): 185-190. (in German)

Kostaschuk, R., J. Best, P. Villard, J. Peakall and M. Franklin 2005. Measuring flow velocity and sediment transport with an acoustic Doppler current profiler. *Geomorphology* **68**(1–2): 25-37.

Laffitte, R. and G. De Cesare 2005. Quantified criteria for electricity generation systems. Hydro 2005, Villach, Austria, 1-12.

Lane-Serff, G.F. and T.J. Moran 2005. Sedimentation from Buoyant Jets. *Journal of Hydraulic Engineering* **131**(3): 166-174.

Laval, B., J. Imberger and A. Findikakis 2005. Dynamics of a large tropical lake: Lake Maracaibo. *Aquatic Sciences* **67**(3): 337-349.

LCH 2005. INTERREG IIIB - Projet ALPRESERV. Conférence sur la problématique de la sédimentation dans les réservoirs - Gestion durable des sédiments dans les réservoirs alpins. Communication N° 22 du Laboratoire de constructions hydrauliques, A. Schleiss (ed.). Lausanne, Switzerland. (in French & German)

Lemmin, U., C.H. Mortimer and E. Bauerle 2005. Internal seiche dynamics in Lake Geneva. *Limnology and Oceanography* **50**(1): 207-216.

Liang, H. and T. Maxworthy 2008. Experimental investigations of a swirling jet in both stationary and rotating surroundings. *Experiments in Fluids* **45**(2): 283-293.

Lyons, R.G. 2004. Understanding Digital Signal Processing (2nd Edition). Prentice Hall PTR.

Meilan, Q., K. Fujisak and K. Tanaka 2000. Sediment re-suspension by turbulent jet in an intake pond. *Journal of Hydraulic Research* **38**(5).

Meile, T., G. De Cesare, K. Blanckaert and A.J. Schleiss 2008. Improvement of Acoustic Doppler Velocimetry in steady and unsteady turbulent open-channel flows by means of seeding with hydrogen bubbles. *Flow Measurement and Instrumentation* **19**(3): 215-221.

MetFlow SA 2000. UVP monitor - User's guide. Lausanne, Switzerland.

Mikhailov, I.E., Y.V. Polikarpov and A.K. Fink 1992. Experimental investigations of water intake/outlet towers (shafts). *Power Technology and Engineering (formerly Hydrotechnical Construction)* **26**(3): 176-183.

Minella, J.P.G., G.H. Merten, J.M. Reichert and R.T. Clarke 2008. Estimating suspended sediment concentrations from turbidity measurements and the calibration problem. *Hydrological Processes* **22**(12): 1819-1830.

Morris, G.L. and J. Fan 1998. Reservoir sedimentation handbook: Design and management of dams, reservoirs, and watersheds for sustainable use. McGraw-Hill, New York, US.

Müller, P.J. and G. De Cesare 2009. Sedimentation problems in the reservoirs of the Kraftwerke Sarganserland - venting of turbidity currents as the essential part of the solution. 23rd Congress of the CIGB-ICOLD, Brasilia, Brazil.

Munnich, M., A. Wuest and D.M. Imboden 1992. Observations of the Second Vertical Mode of the Internal Seiche in an Alpine Lake. *Limnology and Oceanography* **37**(8): 1705-1719.

Oehy, C.D. 2003. Effects of obstacles and jets on reservoir sedimentation due to turbidity currents. Thesis 2684, Communication N°15 du Laboratoire de Constructions Hydrauliques, A. Schleiss (ed.), Ecole Polytechnique Fédérale de Lausanne, Switzerland.

Oehy, C.D., G. De Cesare and A.J. Schleiss 2010. Effect of inclined jet screen on turbidity current. *Journal of Hydraulic Research* **48**(1): 81-90.

Oehy, C.D. and A.J. Schleiss 2007. Control of turbidity currents in reservoirs by solid and permeable obstacles. *Journal of Hydraulic Engineering* **133**(6): 637-648.

Oliver, D.R. 1961. The sedimentation of suspensions of closely-sized spherical particles. *Chemical Engineering Science* **15**(3): 230-242.

Orwin, J.F. and C.C. Smart 2005. An inexpensive turbidimeter for monitoring suspended sediment. *Geomorphology* **68**(1): 3-15.

Oseen, C.W. 1972. Hydrodynamik. Akademische Verlagsgesellschaft, Leibzig, Germany. (in German)

Potter, D.U., M.P. Stevens and J.L. Meyer 1982. Changes in physical and chemical variables in a new reservoir due to pumped storage operations. *Journal of the American Water Resources Association* **18**(4): 627-633.

Rajaratnam, N. 1976. Turbulent jets. Elsevier, Amsterdam, The Netherlands.

Schleiss, A.J., G. De Cesare and J. Jenzer Althaus 2010. Verlandung der Stauseen gefährdet die nachhaltige Nutzung der Wasserkraft. *Wasser, Energie, Luft - eau, énergie, air* **102**(1): 31-40. (in German)

Schleiss, A.J. and C.D. Oehy 2002. Verlandung von Stauseen und Nachhaltigkeit. *Wasser, Energie, Luft - eau, énergie, air* **95**(7): 227-234. (in German)

Schneider, J., H. Badura, W. Troy and H. Knoblauch 2007. Determination of Parameters for Venting Turbidity Currents through a Reservoir. IAHR Congress, Venice, Italy.

Schott, F. and W. Johns 1987. Half-Year-Long Measurements With a Buoy-Mounted Acoustic Doppler Current Profiler in the Somali Current. *Journal of Geophysical Research* **92**(C5): 5169-5176.

Sequeiros, O.E., M.I. Cantero and M.H. Garcia 2009. Sediment management by jets and turbidity currents with application to a reservoir for flood and pollution control in Chicago, Illinois. *Journal of Hydraulic Research* **47**(3): 340-348.

Shammaa, Y. and D.Z. Zhu 2010. Experimental Study on Selective Withdrawal in a Two-Layer Reservoir Using a Temperature-Control Curtain. *Journal of Hydraulic Engineering* **136**(4): 234-246.

Shammaa, Y., D.Z. Zhu and N. Rajaratnam 2005. Flow Upstream of Orifices and Sluice Gates. *Journal of Hydraulic Engineering* **131**(2): 127-133.

Shammaa, Y., D.Z. Zhu and N. Rajaratnam 2009. Flow Field in a Rectangular Basin with a Line Inlet and a Circular Outlet. *Journal of Hydraulic Engineering* **135**(10): 857-864.

Sinniger, R., G. De Cesare and J.L. Boillat 1999. Propriétés des alluvions récentes dans les retenues alpines. *Wasser, Energie, Luft - eau, énergie, air* **92**(9): 255-258. (in French)

Stefan, H.G. and R. Gu 1992. Efficiency of Jet Mixing of Temperature-Stratified Water. *Journal of Environmental Engineering* **118**(3): 363-379.

Stevens, C. and G. Lawrence 1997. Estimation of wind-forced internal seiche amplitudes in lakes and reservoirs, with data from British Columbia, Canada. *Aquatic Sciences* **59**(2): 115-134.

Takeda, Y. 1995. Velocity profile measurement by ultrasonic doppler method. *Experimental Thermal and Fluid Science* **10**(4): 444-453.

Toniolo, H. and J. Schultz 2005. Experiments on sediment trap efficiency in reservoirs. *Lakes & Reservoirs: Research & Management* **10**(1): 13-24.

van Rijn, L.C. 1984. Sediment Transport, Part II: Suspended Load Transport. *Journal of Hydraulic Engineering* **110**(11): 1613-1641.

VAW - Versuchsanstalt für Wasserbau, Hydrologie und Glaziologie 1982. Auslaufbauwerk Grimselsee - Bericht über die hydraulischen Modellversuche. ETH Zürich, Switzerland. (in German, unpublished)

Vermeyen, T.B. 2002. Measuring Selective Withdrawal Characteristics Using an Argonaut Acoustic Doppler Velocimeter in Folsom Lake, California. *In:* Wahl, T. L., Pugh, C. A., Oberg, K. A. & Vermeyen, T. B., eds., Hydraulic Measurements and Experimental Methods, Estes Park, Colorado, US, 63.

Vermeyen, T.B. 2003. Acoustic Doppler velocity measurements collected near a municipal water intake, Lake Mead, Nevada-Arizona. *In:* Rizoli, J. A., eds., IEEE/OES Seventh Working Conference on Current Measurement Technology, San Diego, California, US, 16-20.

Wang, Z.-y. and C. Hu 2009. Strategies for managing reservoir sedimentation. *International Journal of Sediment Research* **24**(4): 369-384.

Wasewar, K.L. 2006. A design of jet mixed tank. *Chemical and Biochemical Engineering Quarterly* **20**(1): 31-45.

Wolanski, E., R. Gibbs, P. Ridd and A. Mehta 1992. Settling of ocean-dumped dredged material, Townsville, Australia. *Estuarine, Coastal and Shelf Science* **35**(5): 473-489.

Wüest, A., M. Zeh and J. Ackerman 2007. Lake Brienz Project: An interdisciplinary catchment-to-lake study. *Aquatic Sciences* **69**(2): 173-178.

Yu, W.-S., H.-Y. Lee and S.M. Hsu 2000. Experiments on Deposition Behavior of Fine Sediment in a Reservoir. *Journal of Hydraulic Engineering* **126**(12): 912-920.

Zanke, U. 1982. Grundlagen der Sedimentbewegung. Springer Verlag, Berlin, Germany. (in German)

Notation

Roman symbols

A	Area	[m^2]	2.2.1
$A_{i,eff}$	Effective in-/outflow section	[m^2]	3.2.2
a_s	Diameter of the particle	[m]	2.1.5
B	Width [m]	[m]	5.2.1
$b_{1/2}$	Jet half-width, defined as the transverse distance r for axial velocity $v(r)$ to fall to one half of the centerline value, v_{CL}	[m]	2.2.3
b_s	Diameter of the particle	[m]	2.1.5
C	Suspended sediment concentration	[mg/l]	4.2.1
C_1	Proportionality constant for the jet velocity	[-]	2.2.2
C_2	Proportionality constant relating $b_{1/2}$ and s	[-]	2.2.3
C_3	Constant	[-]	2.2.3
C_{calc}	Concentration estimated using the calibration equation	[g/l]	6.2.4
C_D	Drag coefficient	[-]	2.1.5
C_k^*	Efficiency factor, converting wind to turbulent kinetic energy	[-]	3.5.4
c	Volumetric sediment concentration	[-]	2.1.5
c_s	Shortest diameter of the particle	[m]	2.1.5
D	Diameter	[m]	2.2.1
d_m	Mean particle diameter	[µm]	5.2.4
d_s	Diameter of the particle	[m]	2.1.5
E_{kin}	Kinetic energy in the test volume	[$kg \cdot m^2/s^2$]	5.4.2
E_{turb}	Turbulent kinetic energy	[$kg \cdot m^2/s^2$]	5.4.2
ERR_C	Average error of concentration estimations	[g/l]	6.2.4
ESR	Evacuated sediment rate	[-]	6.4.3
F_D	Fluid drag force	[$kg \cdot m/s^2$]	2.1.5
Fr_j	Densimetric jet Froude number	[-]	2.2.1
f	Frequency	[Hz]	3.5.2
f_L	Frequency of longitudinal seiches	[Hz]	3.5.2
f_T	Frequency of transverse seiches	[Hz]	3.5.2
G	Gravity force	[$kg \cdot m/s^2$]	2.1.5
g	Gravitational acceleration	[m/s^2]	2.1.5
g'	Reduced gravitational acceleration	[m/s^2]	2.2.1
H	Height	[m]	3.2.2
INC_{SSR}	Normalized increase of suspended sediment ratio	[-]	6.4
ISR	Influx sediment rate	[-]	6.4.3
Kt_P	Frequency of in- and outflow cycles	[-]	5.2.4
L	Length	[m]	5.2.1
M	Sediment mass	[g], [kg], [t]	4.5.1
M_j	Jet momentum flux	[m^4/s^2]	2.2.1
M_{susp}	Suspended sediment mass	[g]	6.4
n	Number of sampling points or samples	[-]	5.5.3
P	Precipitation	[mm]	3.3.4

$P_{vE,N}$	Power of sampled velocity signal	$[mm/s]^2$	3.5.2
P_Q	Power of sampled discharge signal	$[m^3/s]^2$	3.5.2
p	Pressure	[m]	3.3.3
p_{rel}	Relative pressure	[bar]	5.4.1
Q	Discharge	$[m^3/s]$, [l/s]	2.2.1
Q_e	Volumetric flow rate of the bulk liquid entrained by the jet	$[m^3/s]$	2.2.4
Re_j	Jet Reynolds number	[-]	2.2.1
Re_s	Reynolds number of the settling process	[-]	2.1.5
r	Distance from the centerline in transverse direction	[m]	2.2.3
r_j	Jet nozzle radius	[m]	5.3.4
SB	Sediment balance	[-]	6.5.6
SF	Shape factor	[-]	2.1.5
SSR	Suspended sediment ratio	[-]	6.4
SSR_{Ref}	Suspended sediment ratio in stagnant water	[-]	6.4
s	Distance from the nozzle in the jet flow direction	[m]	2.2.2
T	Temperature	[°C]	3.2.1
t	Time	[s]	3.4.2
t_m	Mean residence time	[s]	5.2.1
t_P	Time to peak for in- or outflow sequence	[s]	5.1
TU	Turbidity	[FNU]	4.3.2
$\overline{u'v'}$	Turbulent shear stress per mass unit	$[m^2/s^2]$	2.2.1
U, v	Velocity	[m/s]	3.3.4
v_0	Approach pipe flow velocity	[m/s]	2.2.1
v_{CL}	Centerline jet velocity	[m/s]	2.2.2
V	Volume	$[m^3]$	4.2.1
w_s	Settling velocity	[m/s]	2.1.5
$w_{s,m}$	Settling velocity in fluid with suspended material	[m/s]	2.1.5
X	East coordinate in Swiss grid	[m]	A.1
x'	Longitudinal coordinate in the intake's local referential	[m]	3.5.1
x	Abscissa	[m]	3.5.1
Y	North coordinate in Swiss grid	[m]	A.1
y	Ordinate	[m]	5.2.1
y'	Transverse coordinate in the intake's local referential	[m]	3.5.1
Z	Vertical coordinate in Swiss grid	[m]	3.5.1
z_i	Position of the intake/outlet structure above the reservoir bottom	[m]	5.2.1

Indices

0	Initial	2.2.1
a	Air, Wind	3.3.4
CL	Centerline	2.2.2
E	East	3.5
final	End of the experiment	6.5.1
Gr	Grimsel	3.2.1
IN	Inflowing	3.5.4
i	Intake	3.2.2
j	Jet	2.2.1
L	Longitudinal	3.5.2
MB	Main basin	5.2.1
MT	Mixing tank	5.2.1
m	Mean	3.5.1
max	Maximum	4.4.3
mod	Model	5.2.4
N	North	3.5
n	Number of UVP sampling points	5.5.3
Oa	Oberaar	3.2.1
OUT	Outflowing	5.2.1
P	Peak	5.2.4
Pump	Pumping	3.2.2
prot	Prototype	5.2.4
S	Sediment or solid	2.1.5
T	Transversal	3.5.2
Turb	Turbine	3.2.2
turb	Turbulent	5.4.2
w	Water	2.1.5

Greek symbols

α_{jet}	Constant (= 0.055)	[-]	2.2.4
δ	Jet expansion angle	[°]	2.2.1
ΔH	Height variation	[m]	5.2.5
ΔT	Temperature difference	[°C]	3.4.2
ΔV	Volume difference	[m^3]	4.5.1
Δt	Time step	[s]	5.4.2
η_{Turb}	Turbulent kinetic energy input per unit of area and time	[kg/s^3]	3.5.4
η_a	Natural turbulent kinetic energy input per unit of area and time	[kg/s^3]	3.5.4
λ	Scale factor	[-]	5.2.4
λ_L	Geometric scale factor	[-]	5.2.4
$\lambda_{v,t,Q}$	Cinematic scale factor	[-]	5.2.4
v	Kinematic viscosity	[m^2/s]	2.1.5
ρ	Density	[kg/m^3]	2.1.5

Acronyms

ADCP	Acoustic Doppler Current Profiler	2.3.1
CCEM	Competence Center Energy and Mobility	1.1
CTD	Conductivity, temperature, depth sampling	4.2.2
EARSM	Explicit algebraic Reynolds stress model	5.4.2
Eawag	Swiss Federal Institute of Aquatic Science & Technology	4.3.2
EPFL	Ecole Polytechnique Fédérale de Lausanne	1.1
FFT	Fast Fourier Transform	3.5.2
ICOLD	International Committee on Large Dams	2.1
KWO	Kraftwerke Oberhasli AG	3.2
LCH	Laboratory of Hydraulic Constructions	1.1
MeteoSwiss	Swiss Federal Office of Meteorology and Climatology	3.3.4
SFOE	Swiss Federal Office of Energy	3.3.4
TKE	Turbulent kinetic energy	3.1
UVP	Ultrasonic Velocity Profiler	5.2.2
VAW	Laboratory of Hydraulics, Hydrology and Glaciology	3.2.2

Appendix A

Prototype monitoring – in situ measurement of flow fields in Lake Grimsel

This appendix provides complementary data acquired during the flow field measurements in Lake Grimsel described in Chapter 3. It presents the positions of the Grimsel 2 intake/outlet and the ADCP in the Swiss coordinate system, parameters other than velocity components sampled by the measuring devices, operational data from the power producer KWO as well as the results of signal processing.

ADCP positions

Table A.1 lists the coordinates of the Grimsel 2 intake/outlet and the theoretical positions of the nine ADCP (reality: accuracy of +/-5 m due to vessel movements during lowering). For profilers 1 and 2, altitude was derived from pressure measurement by the instrument (*). During the November campaigns, the profiler 3 battery underwent a short circuit and the device did not sample data (**).

Table A.1 Positions of Grimsel 2 intake structure and the Acoustic Doppler Current Profilers in Lake Grimsel

Coordinates in Swiss grid		*X* [m E]	*Y* [m N]	*Z* [m a.s.l.]
Intake/outlet structure (centerline)		667'460.2	158'055.4	1845.1
September 16th to 19th 2008	ADCP 1	667'506.1	158'075.2	1839.0*
	ADCP 2	667'597.9	158'114.9	1840.0*
	ADCP 3	667'689.7	158'154.5	1835.0
November 7th to 11th 2008	ADCP 1	667'457.6	158'085.3	1839.0*
	ADCP 2	667'463.0	158'025.6	1845.0*
	ADCP 3**	667'468.4	157'965.8	1863.0
November 12th to 20th 2008	ADCP 1	667'509.0	158'044.5	1838.0*
	ADCP 2	667'606.6	158'022.6	1835.0*
	ADCP 3**	667'704.2	158'000.7	1835.0

Operational data (KWO) and ADCP records

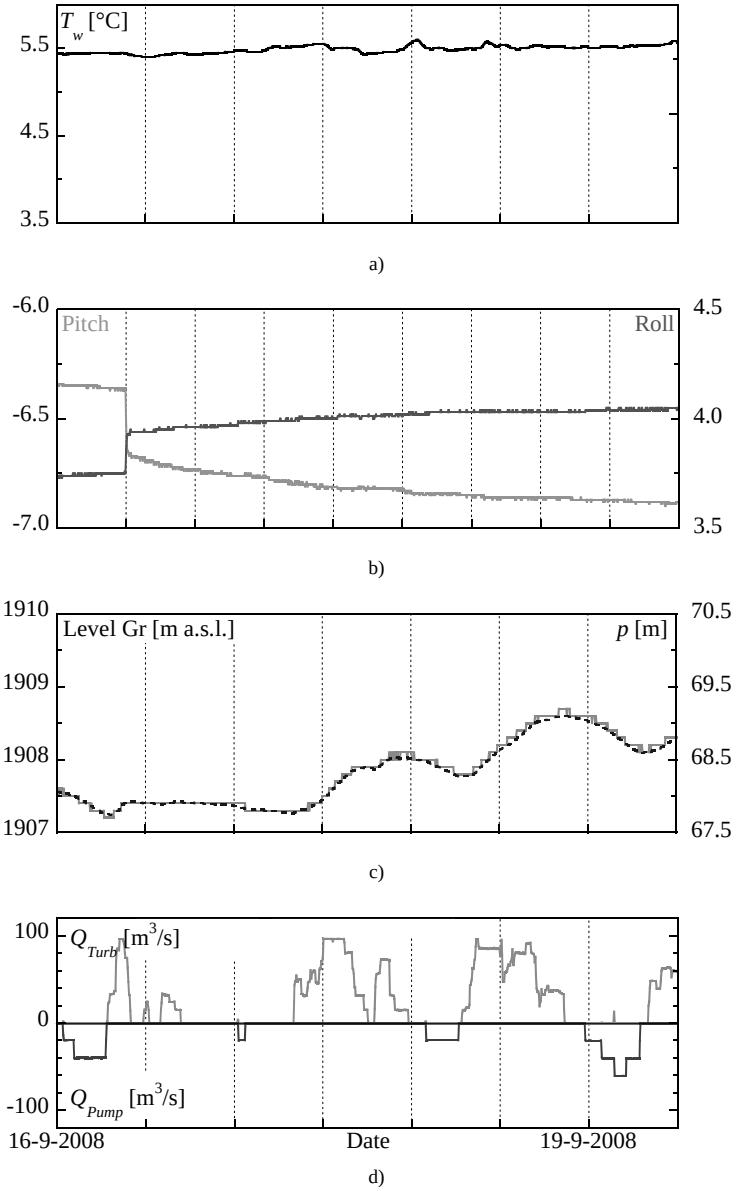

Figure A.1 In situ campaign September 16th to 19th 2008, data for profiler 1; ADCP records of water temperature T_w (a), pitch and roll (b) and pressure p (c, continuous line); Lake Grimsel level (c, dashed line) and operational discharge $Q_{Turb,Pump}$ (d) provided by KWO

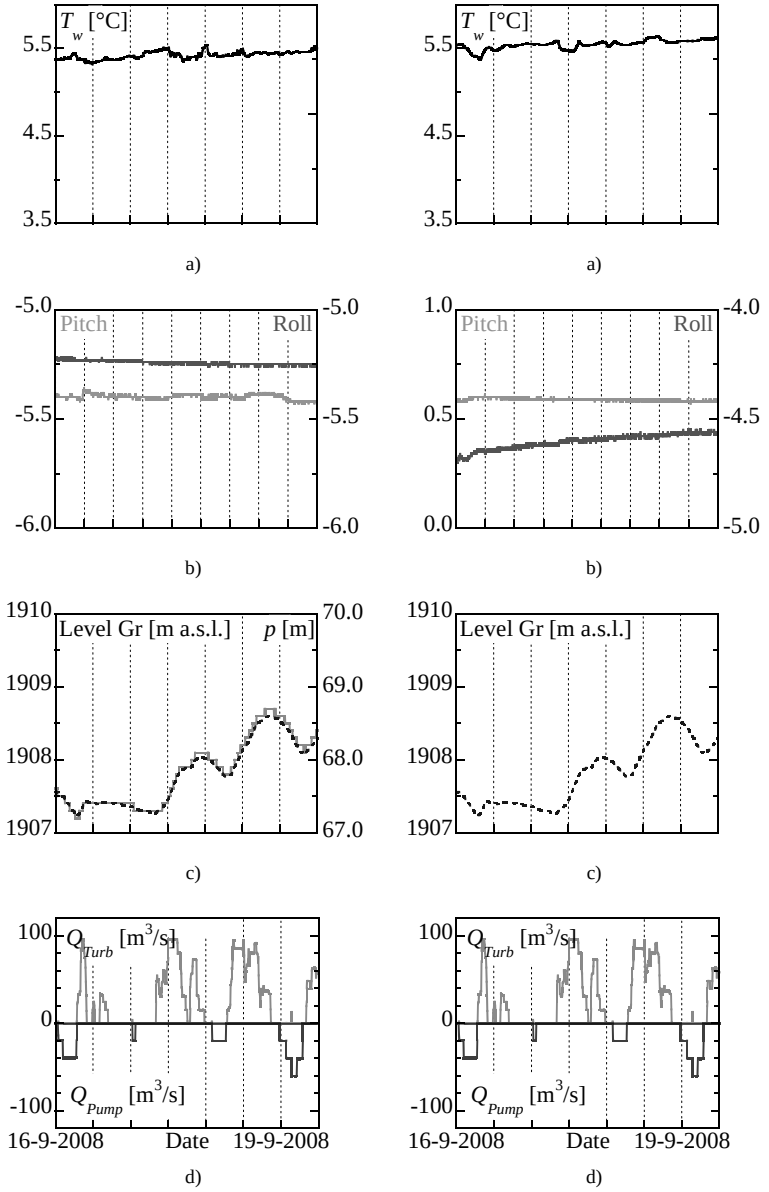

Figure A.2 In situ campaign September 16th to 19th 2008, data for profiler 2 (left) and profiler 3 (right); ADCP records of water temperature T_w (a), pitch and roll (b) and pressure p (c, continuous line); Lake Grimsel level (c, dashed line) and operational discharge $Q_{Turb,Pump}$ (d) provided by KWO

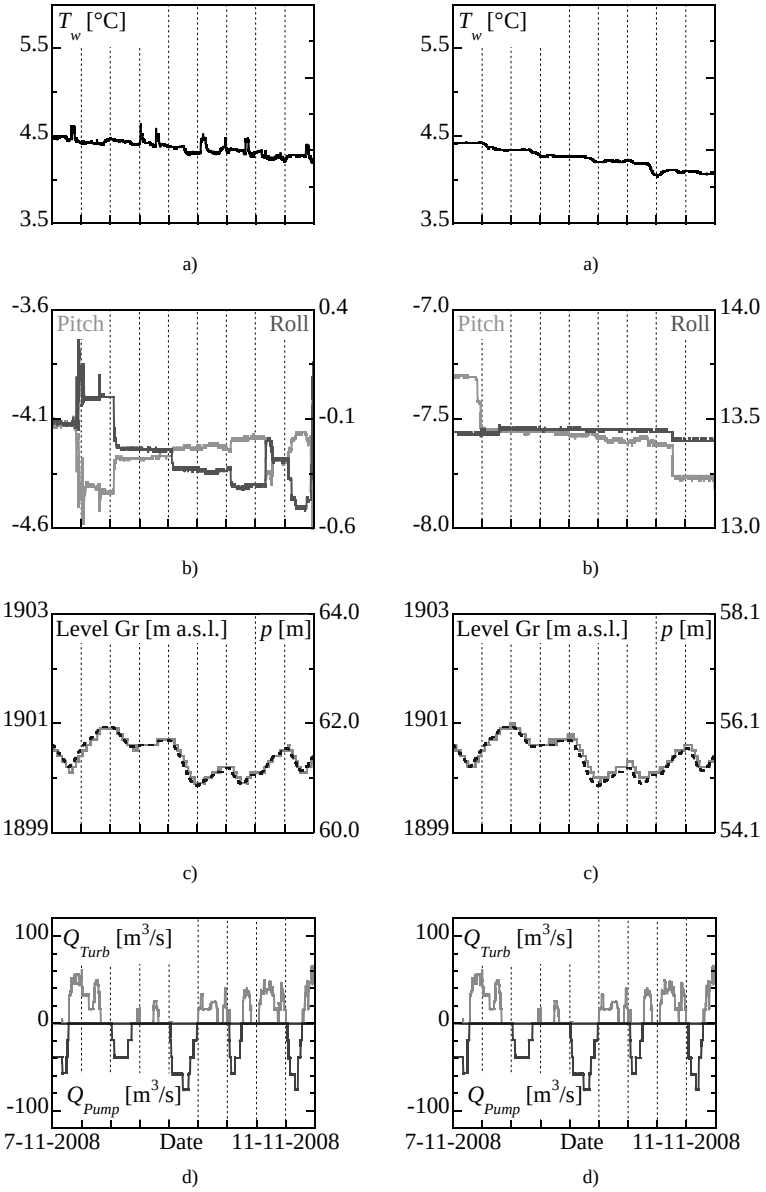

Figure A.3 In situ campaign November 7th to 11th 2008, data for profiler 1 (left) and profiler 2 (right); ADCP records of water temperature T_w (a), pitch and roll (b) and pressure p (c, continuous line); Lake Grimsel level (c, dashed line) and operational discharge $Q_{Turb,Pump}$ (d) provided by KWO

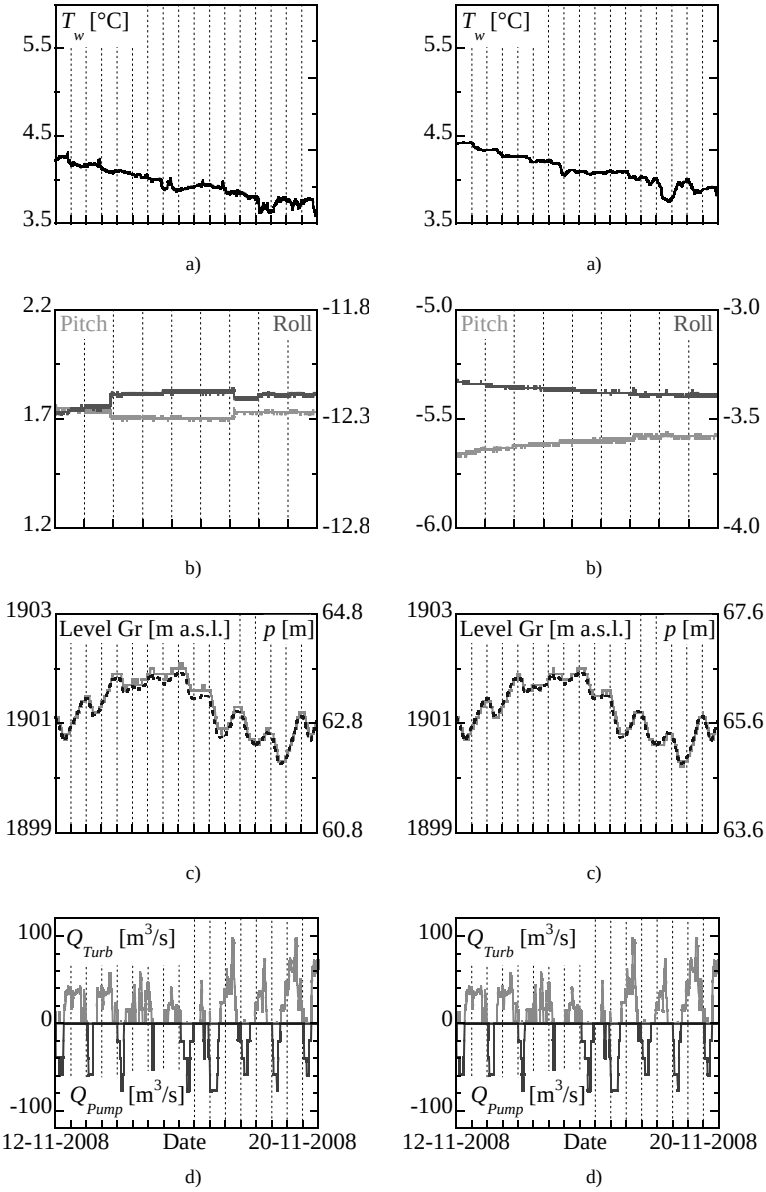

Figure A.4 In situ campaign November 12th to 20th 2008, data for profiler 1 (left) and profiler 2 (right); ADCP records of water temperature T_w (a), pitch and roll (b) and pressure p (c, continuous line); Lake Grimsel level (c, dashed line) and operational discharge $Q_{Turb,Pump}$ (d) provided by KWO

Spectral analysis of ADCP records

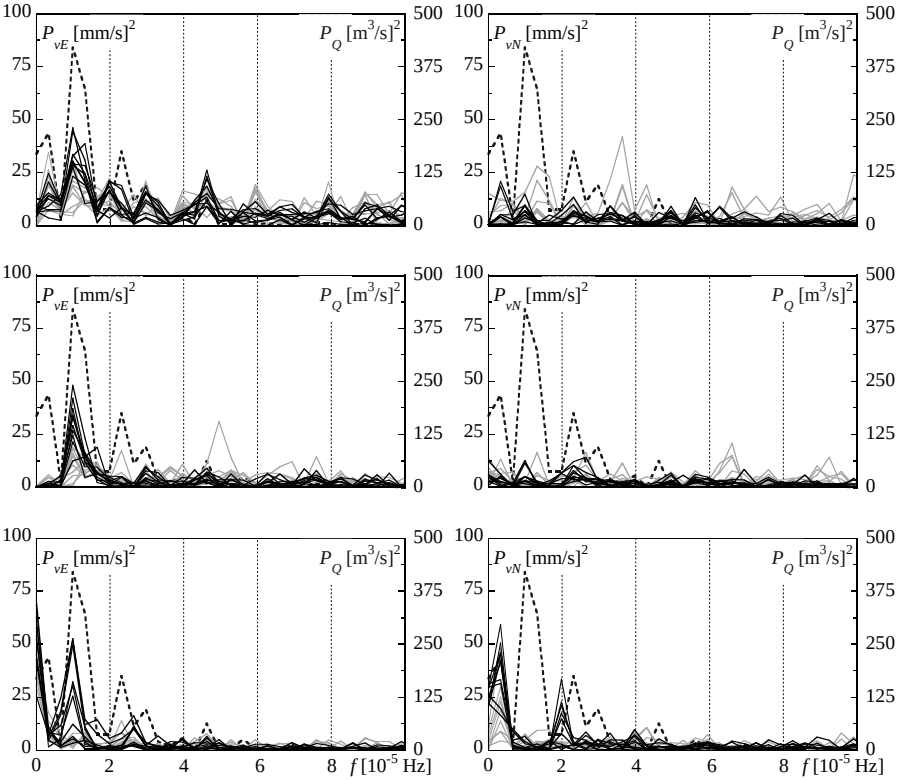

Figure A.5 In situ campaign September 16th to 19th 2008, discharge and velocity spectra for profiler 1 (top), profiler 2 (middle) and profiler 3 (bottom); E-velocity (a) and N-velocity components (b)

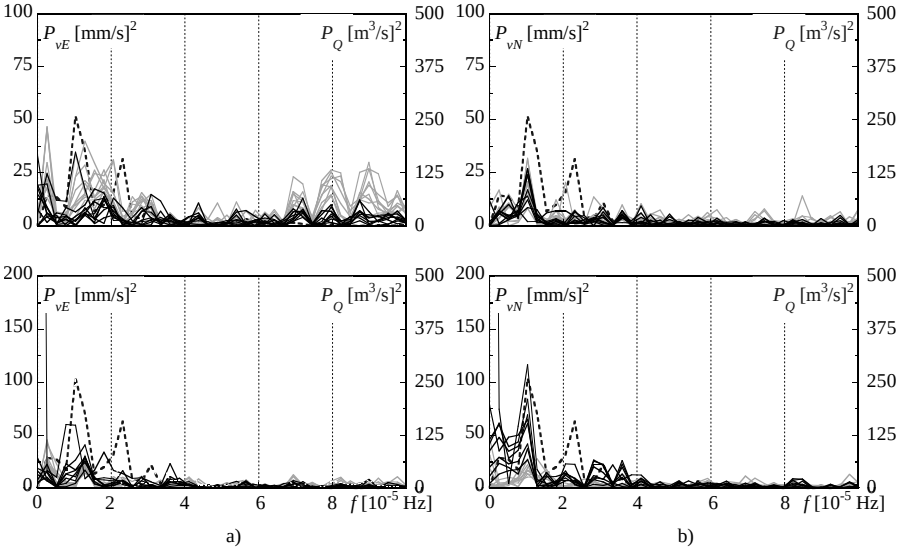

Figure A.6 In situ c campaign November 7th to 11th 2008, discharge and velocity spectra for profiler 1 (above) and profiler 2 (below); E-velocity (a) and N-velocity components (b)

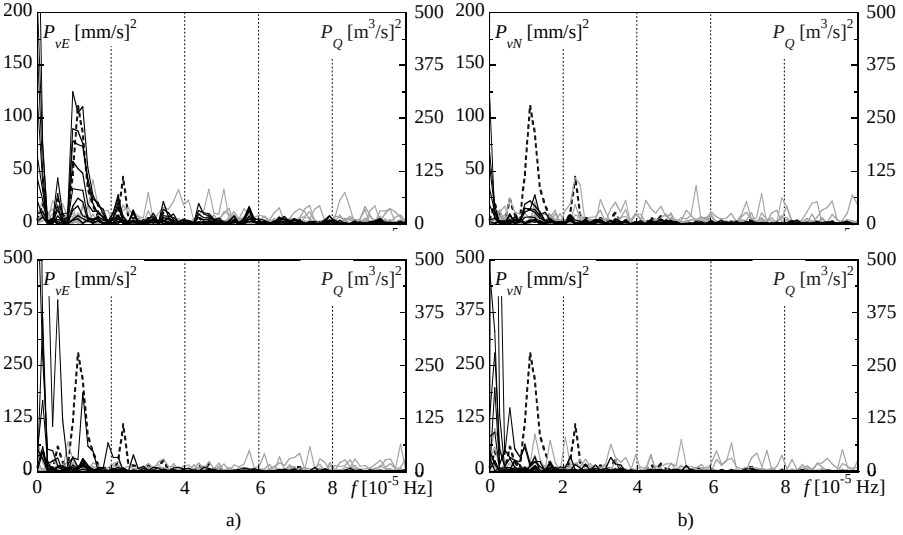

Figure A.7 In situ campaign November 12th to 20th 2008, discharge and velocity spectra for profiler 1 (above) and profiler 2 (below); E-velocity (a) and N-velocity components (b)

Appendix B

Prototype monitoring – turbidity measurements at the pressurized shaft of Grimsel 2

The following figures illustrate the evolution of suspended sediment concentration over the monitoring period from October 2010 to June 2011. They complete what has been presented in Chapter 4. The plots show the monthly concentration data, each time with corresponding operational discharge and reservoir levels.

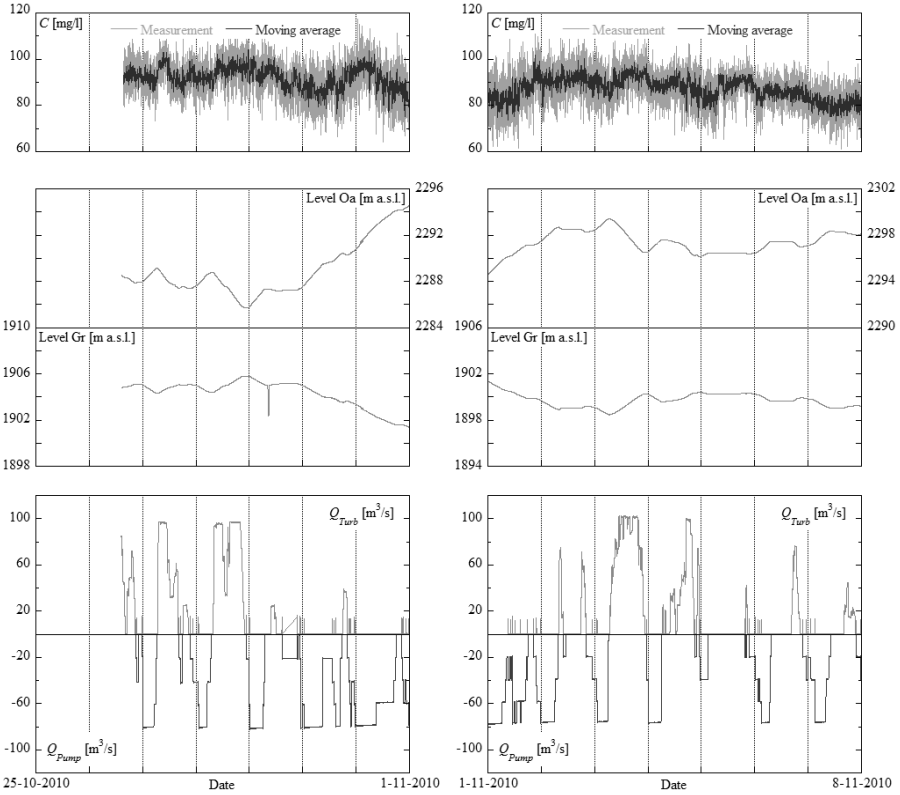

Figure B.1 Turbidity monitoring plots for the weeks from October 25th 2010 to November 8th 2010, suspended sediment concentration *C* (top), reservoir levels Lake Oberaar (Oa) and Grimsel (Gr, middle) and KWO discharge data $Q_{Turb,Pump}$ (bottom)

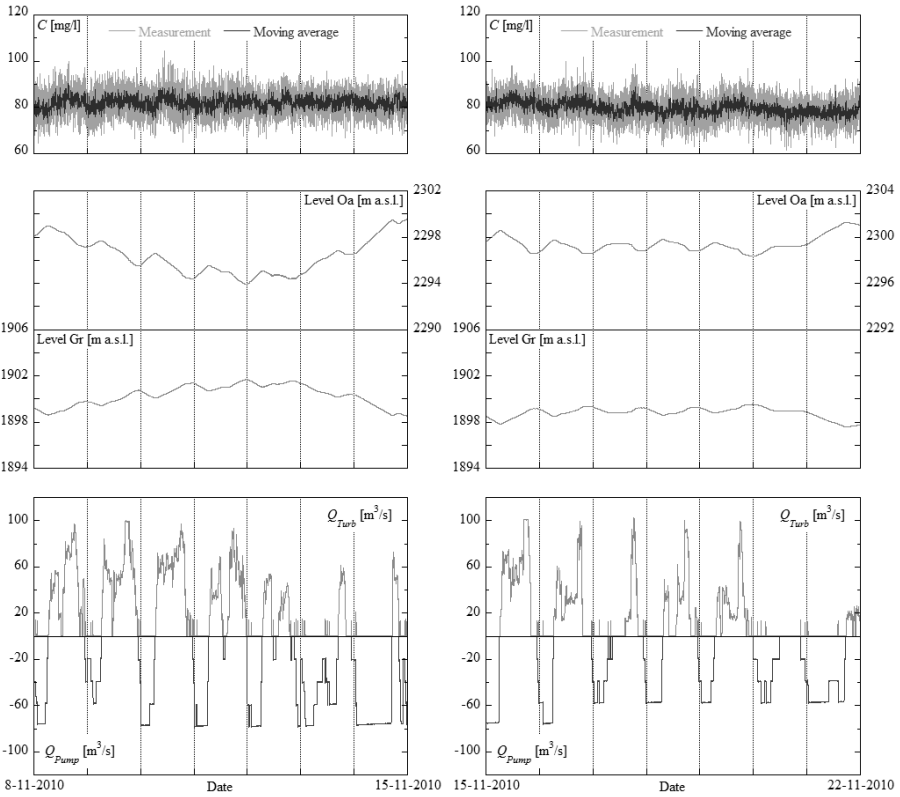

Figure B.2 Turbidity monitoring plots for the weeks from November 8th 2010 to November 22nd 2010, suspended sediment concentration *C* (top), reservoir levels Lake Oberaar (Oa) and Grimsel (Gr, middle) and KWO discharge data $Q_{Turb,Pump}$ (bottom)

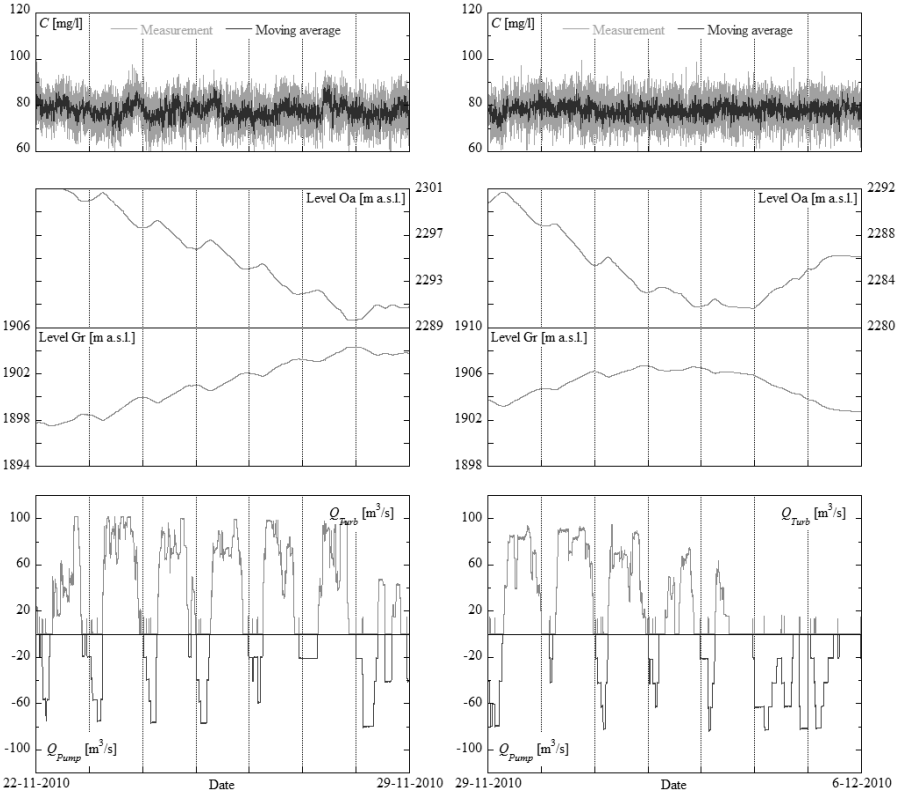

Figure B.3 Turbidity monitoring plots for the weeks from November 22nd 2010 to December 6th 2010, suspended sediment concentration *C* (top), reservoir levels Lake Oberaar (Oa) and Grimsel (Gr, middle) and KWO discharge data $Q_{Turb,Pump}$ (bottom)

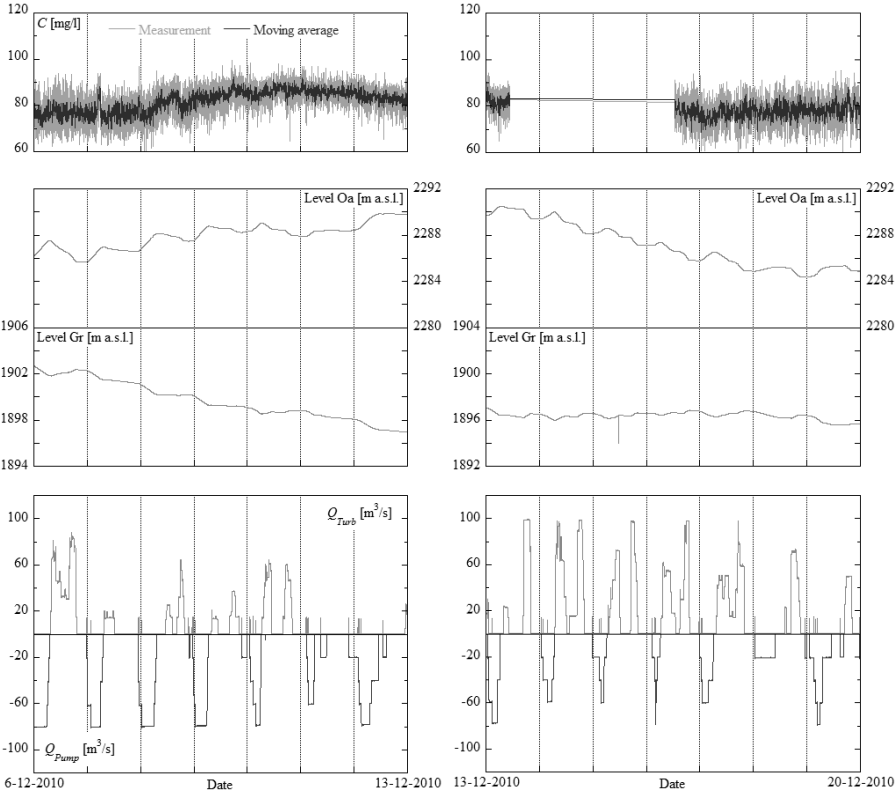

Figure B.4 Turbidity monitoring plots for the weeks from December 6th 2010 to December 20th 2010, suspended sediment concentration *C* (top), reservoir levels Lake Oberaar (Oa) and Grimsel (Gr, middle) and KWO discharge data $Q_{Turb,Pump}$ (bottom)

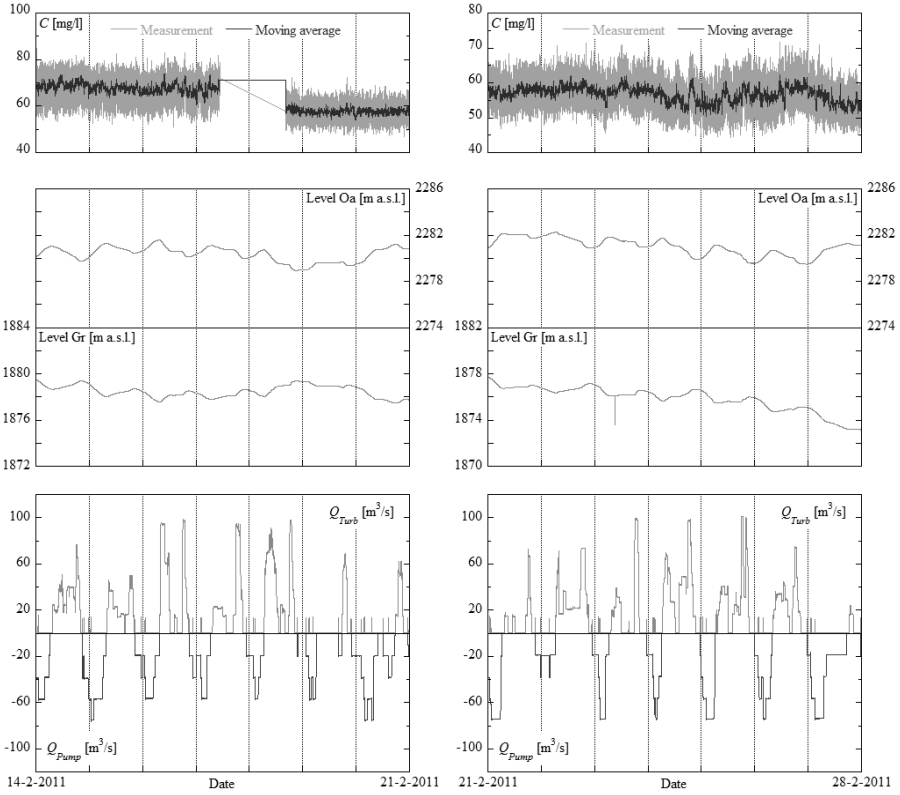

Figure B.5 Turbidity monitoring plots for the weeks from February 14th 2011 to February 28th 2011, suspended sediment concentration *C* (top), reservoir levels Lake Oberaar (Oa) and Grimsel (Gr, middle) and KWO discharge data $Q_{Turb,Pump}$ (bottom)

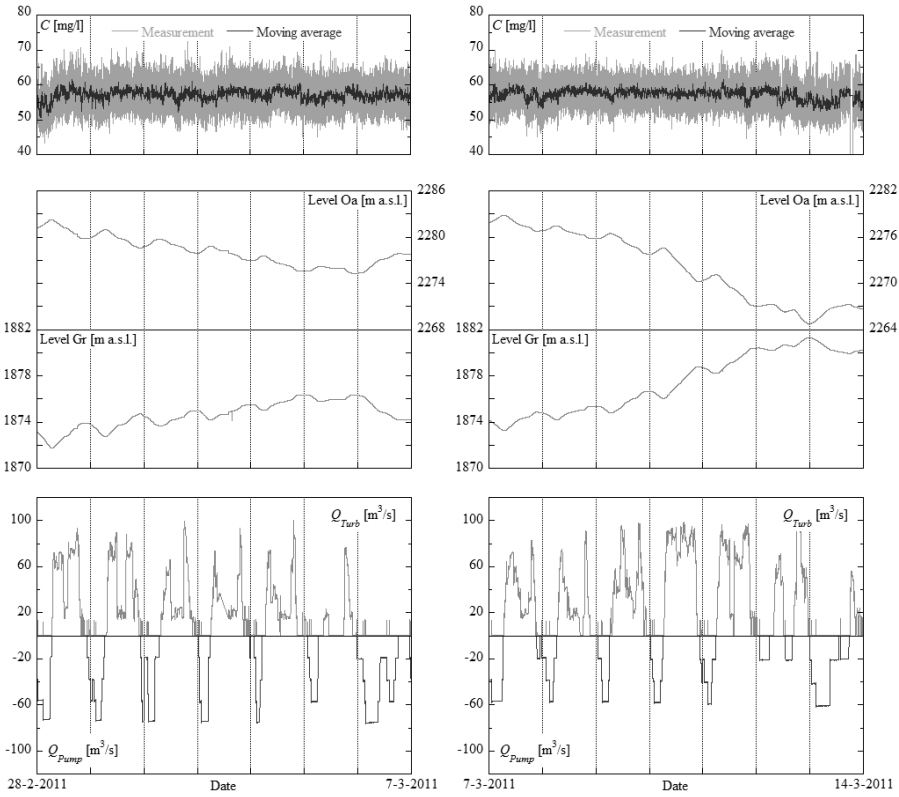

Figure B.6 Turbidity monitoring plots for the weeks from February 28th 2011 to March 14th 2011, suspended sediment concentration *C* (top), reservoir levels Lake Oberaar (Oa) and Grimsel (Gr, middle) and KWO discharge data $Q_{Turb,Pump}$ (bottom)

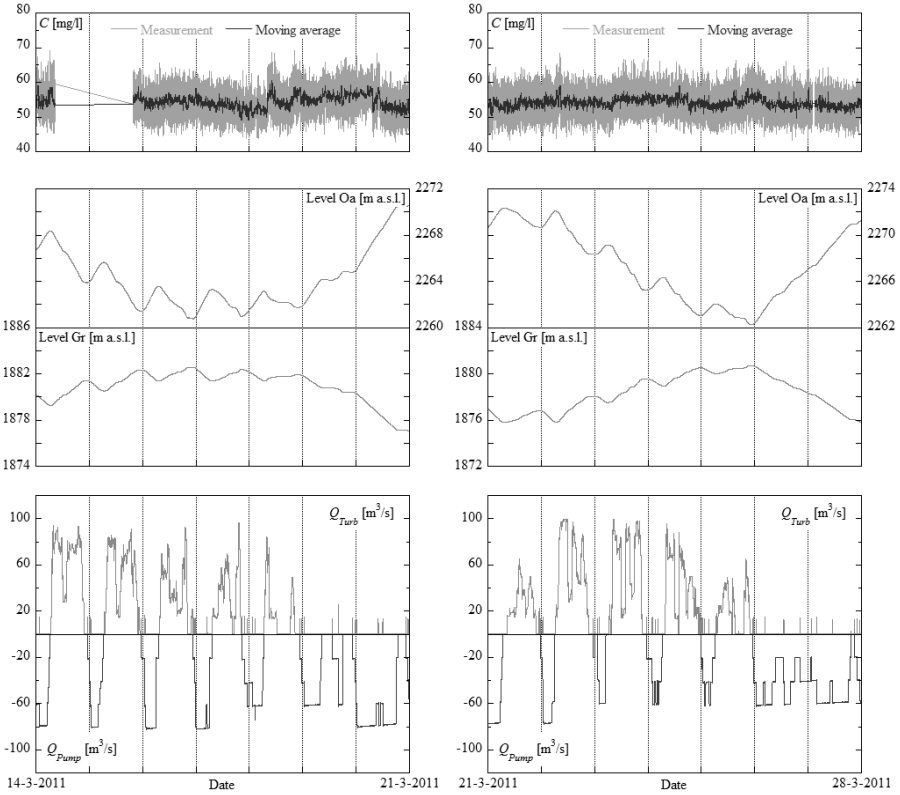

Figure B.7 Turbidity monitoring plots for the weeks from March 14th 2011 to March 28th 2011, suspended sediment concentration *C* (top), reservoir levels Lake Oberaar (Oa) and Grimsel (Gr, middle) and KWO discharge data $Q_{Turb,Pump}$ (bottom)

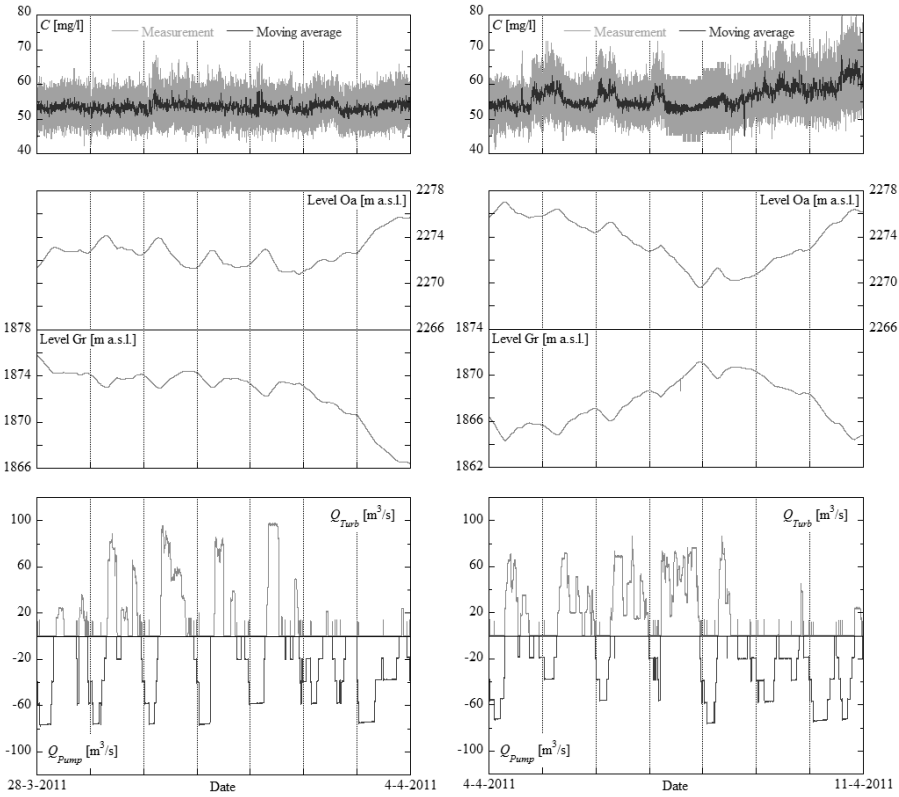

Figure B.8 Turbidity monitoring plots for the weeks from March 28th 2011 to April 11th 2011, suspended sediment concentration *C* (top), reservoir levels Lake Oberaar (Oa) and Grimsel (Gr, middle) and KWO discharge data $Q_{Turb,Pump}$ (bottom)

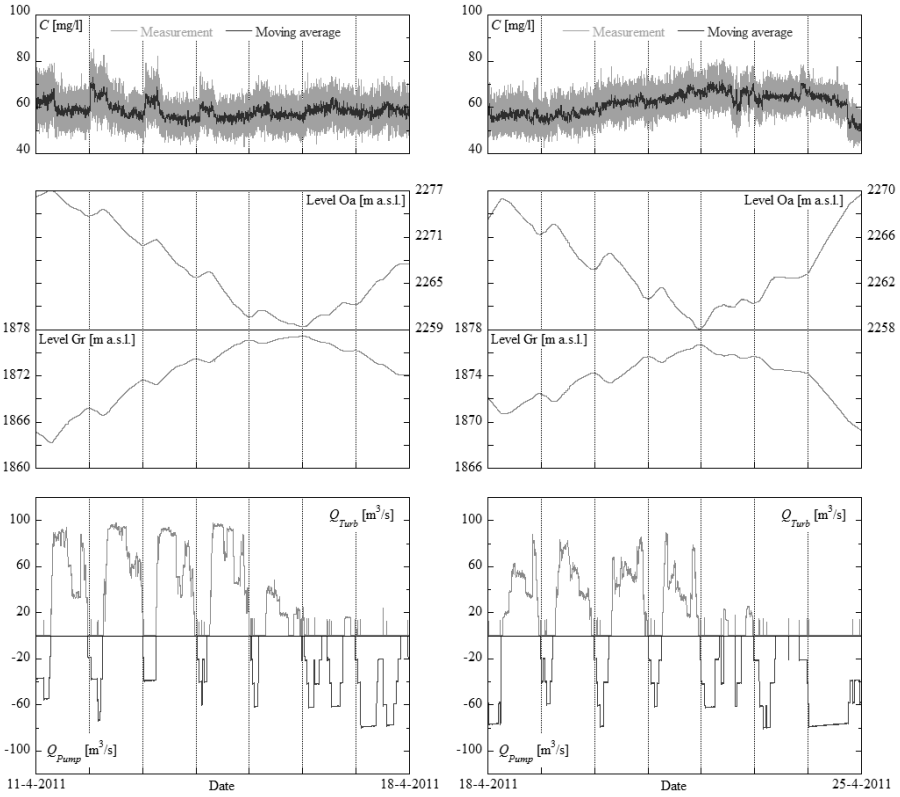

Figure B.9 Turbidity monitoring plots for the weeks from April 11th 2011 to April 25th 2011, suspended sediment concentration *C* (top), reservoir levels Lake Oberaar (Oa) and Grimsel (Gr, middle) and KWO discharge data $Q_{Turb,Pump}$ (bottom)

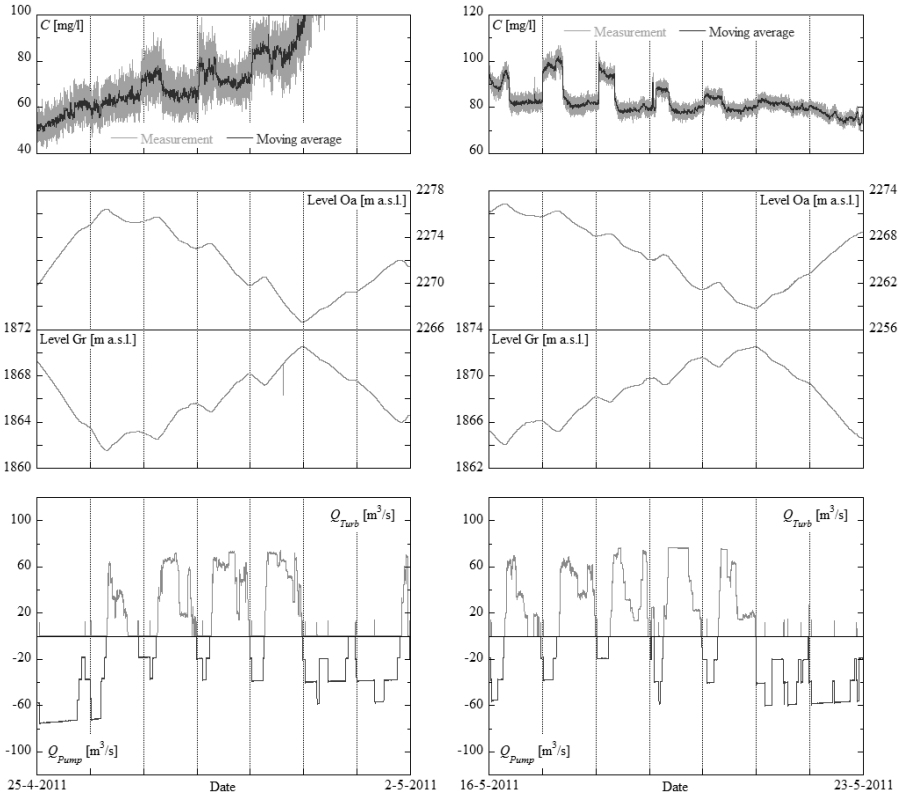

Figure B.10 Turbidity monitoring plots for the weeks from April 25th 2011 to May 2nd 2011 (left) and from May 16th 2011 to May 23rd 2011 (right), suspended sediment concentration C (top), reservoir levels Lake Oberaar (Oa) and Grimsel (Gr, middle) and KWO discharge data $Q_{Turb,Pump}$ (bottom)

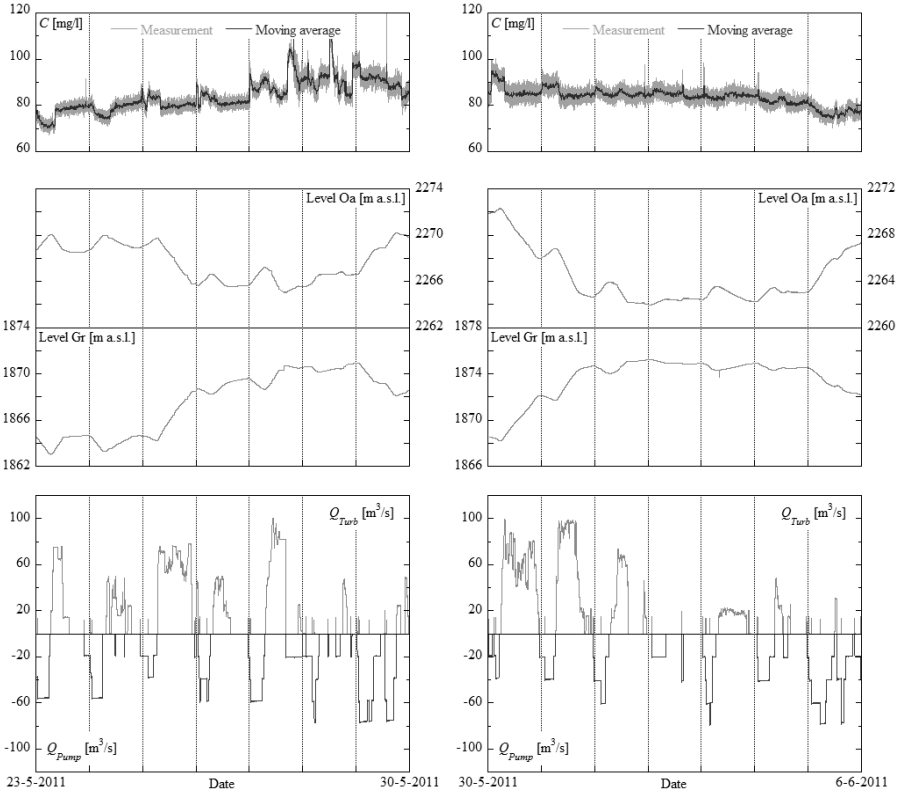

Figure B.11 Turbidity monitoring plots for the weeks from May 23rd 2011 to June 6th 2011, suspended sediment concentration *C* (top), reservoir levels Lake Oberaar (Oa) and Grimsel (Gr, middle) and KWO discharge data $Q_{Turb,Pump}$ (bottom)

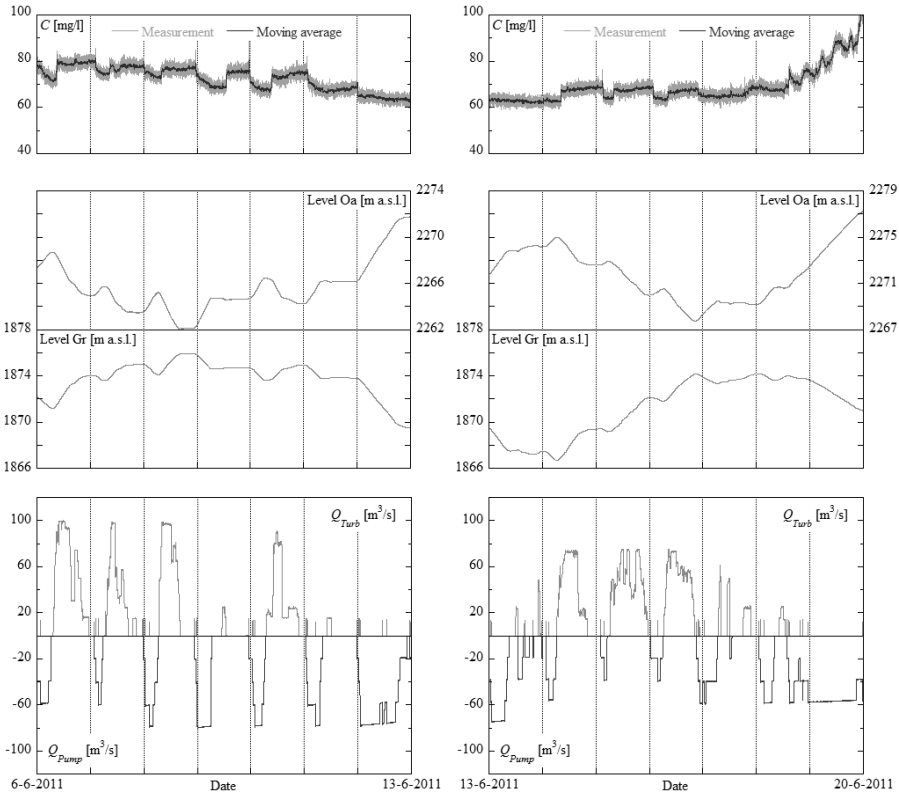

Figure B.12 Turbidity monitoring plots for the weeks from June 6th 2011 to June 20th 2011, suspended sediment concentration *C* (top), reservoir levels Lake Oberaar (Oa) and Grimsel (Gr, middle) and KWO discharge data $Q_{Turb,Pump}$ (bottom)

Appendix C

Laboratory experiments – test configurations and results

The following tables and figures complete the results given in Chapter 5 and Chapter 6. First, the test configurations are presented (Figure C.1, Table C.1). Then, the suspended sediment ratio *SSR* the relative increase INC_{SSR} and the discharge $Q_{IN,OUT}$ are given as a function of dimensionless time t/t_m.

Experimental test configurations

Table C.1 Test configurations for laboratory experiments (summary table)

Test run	Cycle magnitude (discharge)	Cycle frequency	Relative cycle duration	Initial sediment concentration	Intake position
	Q [l/s]	Kt_P [-]	$t_{p,IN}/t_{p,OUT}$ [-]	C_0 [g/l]	z_i/B_{MB} [-]
T00	-	-	-	0.3 0.8 1.5	-
T01	0.3	0.6	1.0	0.8	0.25
T02		0.8			
T03		1.0			
T04		1.2			
T05	0.5	1.0	1.0	0.8	0.25
T06	0.7	0.6	1.0	0.8	0.25
T07		0.8			
T08		1.0			
T08*		1.0			
T09		1.2			
T10	0.9	1.0	1.0	0.8	0.25
T11	1.1	0.6	1.0	0.8	0.25
T12		0.8			
T13		1.0			
T14		1.2			
T15	0.7	1.0	1.0	0.3	0.25
T16				1.5	
T17	0.7	1.0	1.0	0.73 vs. 0.8	0.25
T18				0.87 vs. 0.8	
T19	0.7	1.0	0.5	0.8	0.25
T20			2.0		
T21	1.1	1.0	1.0	0.8	0.125
T22					0.375

* inversed discharge cycles (starting sequence: outflow)

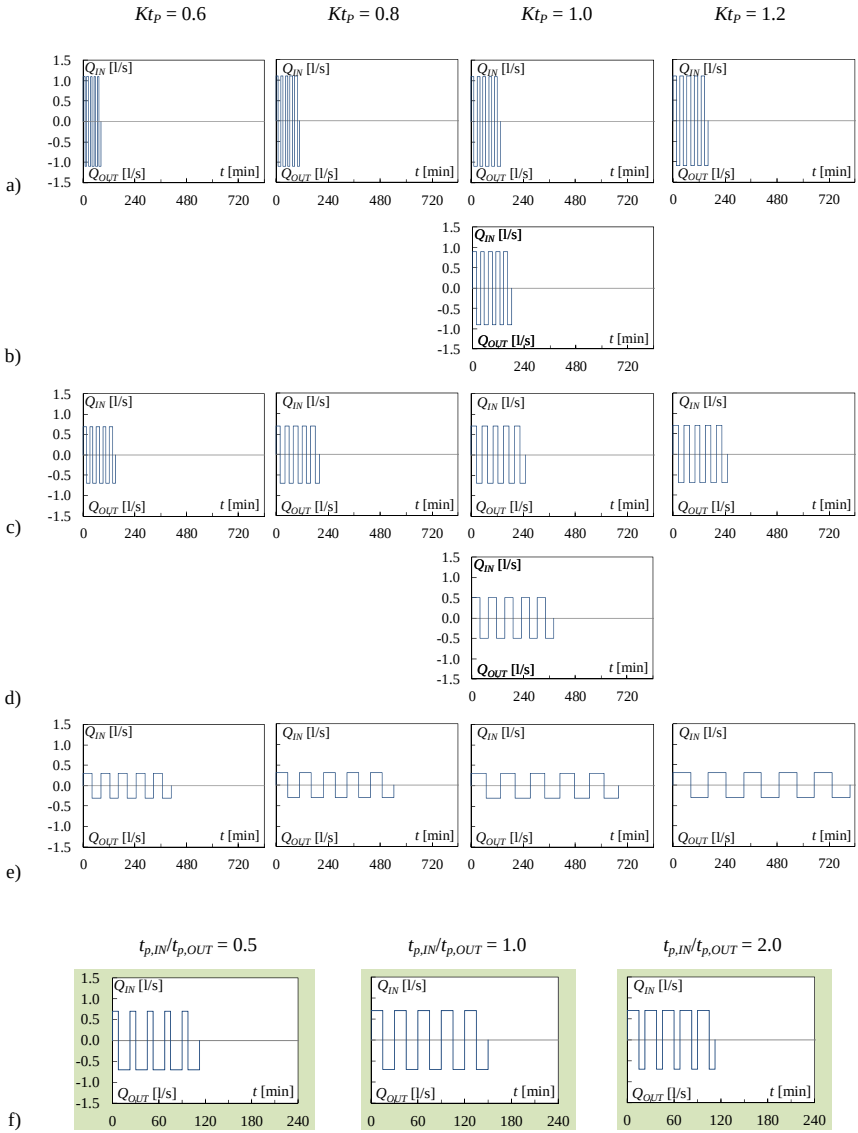

Figure C.1 Matrix of experimental test configurations, test sequences for discharges Q = 1.1 (a), 0.9 (b), 0.7 (c), 0.5 (d) and 0.3 l/s (e) as a function of time t and for different cycle frequencies Kt_P. Test configurations for discharge Q = 0.7, Kt_P = 0.6 and different relative cycle durations $t_{p,IN}/t_{p,OUT}$ (f)

Experimental results

Influence of cycle frequency Kt_P for discharge Q = 0.3 l/s

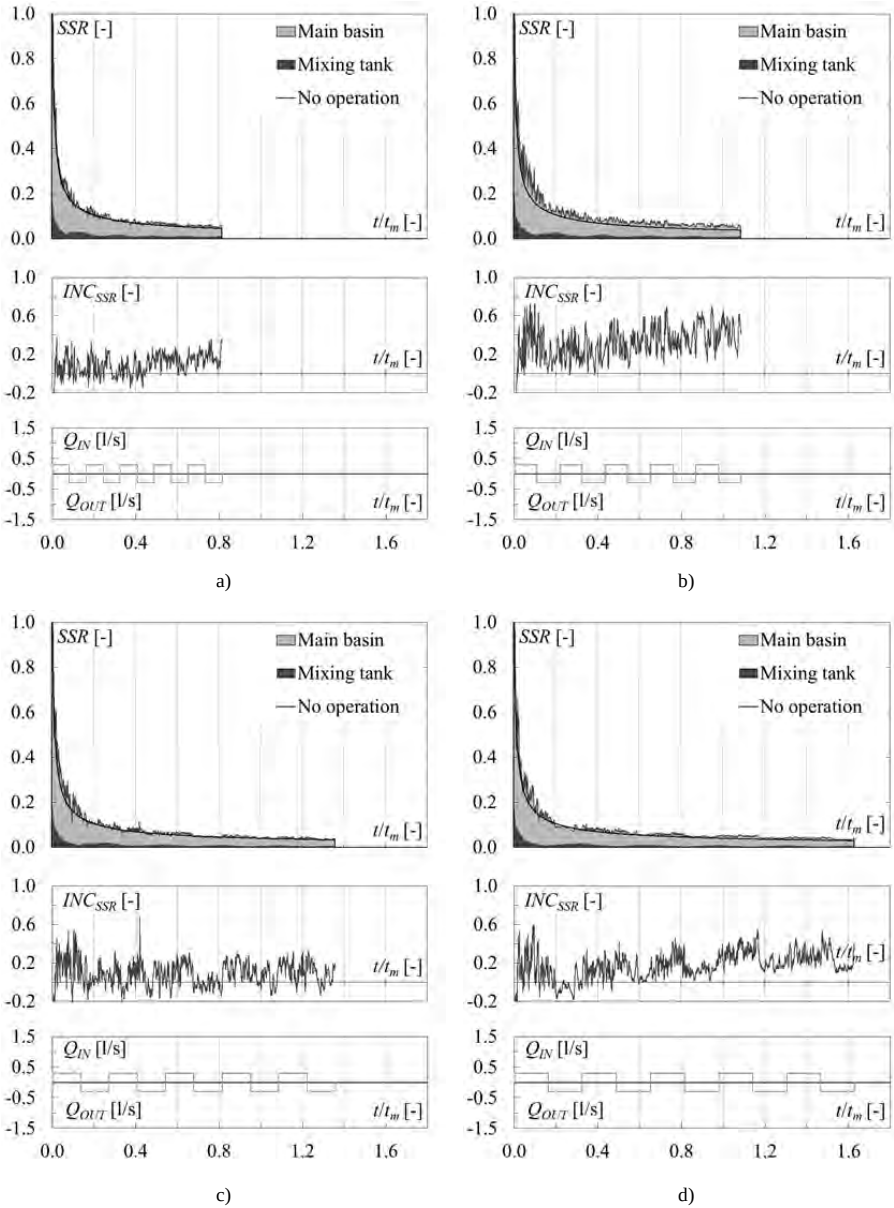

Figure C.2 Suspended sediment ratio *SSR*, dimensionless increase INC_{SSR} and discharge *Q* as a function of dimensionless time t/t_m for C_0 = 0.8 g/l, Q = 0.3 l/s and Kt_P = 0.6 (a), 0.8 (b), 1.0 (c) and 1.2 (d)

Influence of cycle frequency Kt_P for discharge Q = 0.7 l/s

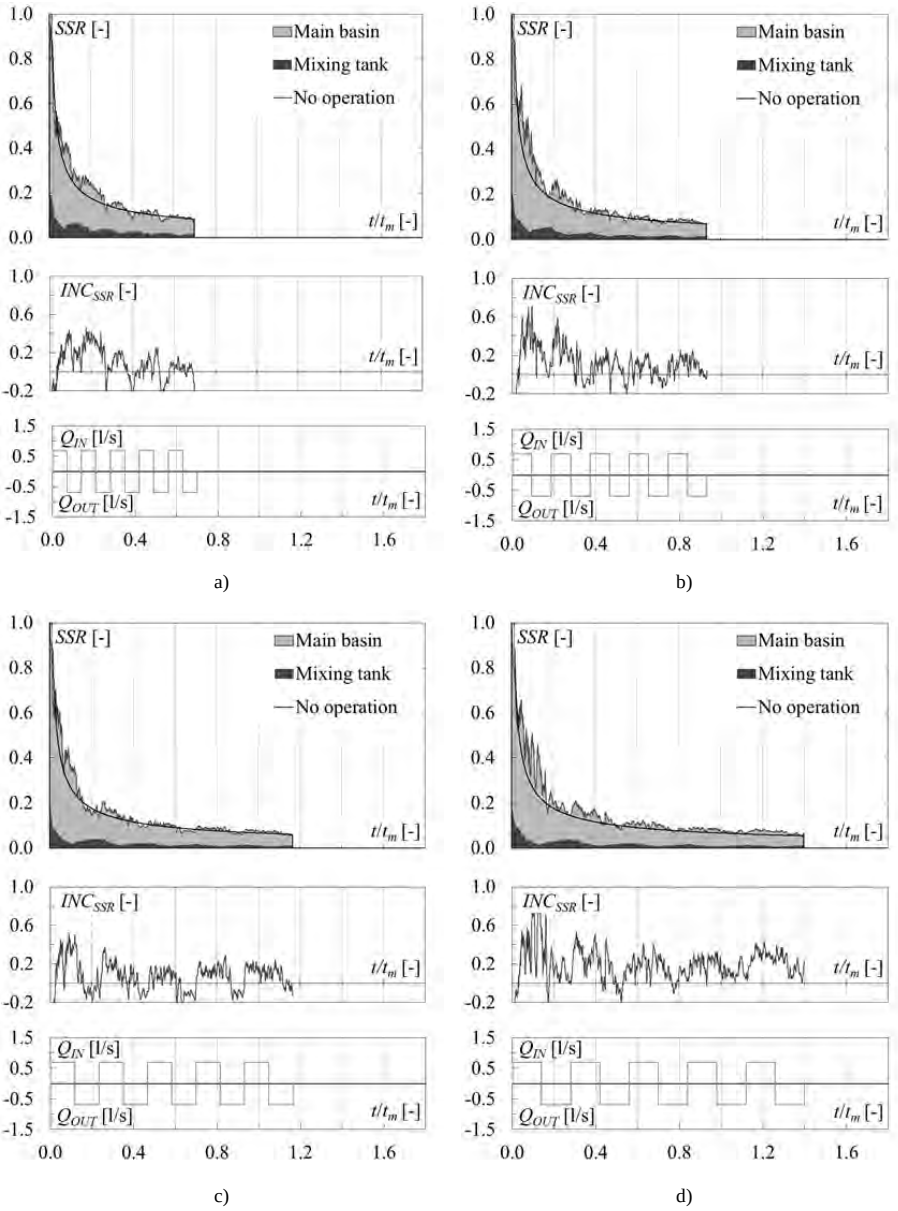

Figure C.3 Suspended sediment ratio *SSR*, dimensionless increase INC_{SSR} and discharge Q as a function of dimensionless time t/t_m for C_0 = 0.8 g/l, Q = 0.7 l/s and Kt_P = 0.6 (a), 0.8 (b), 1.0 (c) and 1.2 (d)

Influence of initial sediment concentration C_0 for discharge Q = 0.7 l/s and frequency Kt_P = 1.0

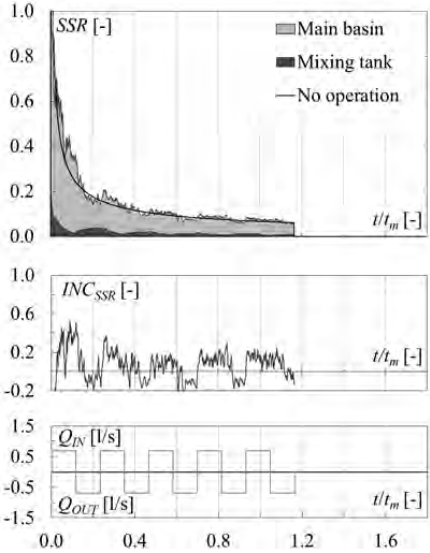

a)

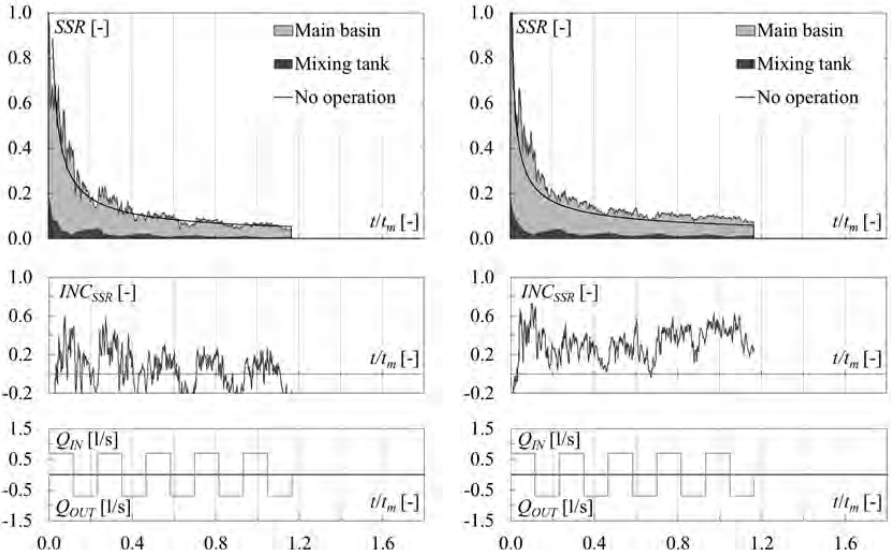

b) c)

Figure C.4 Suspended sediment ratio *SSR*, dimensionless increase INC_{SSR} and discharge Q as a function of dimensionless time t/t_m for Q = 0.7 l/s, Kt_P = 1.0 and initial sediment concentration C_0 = 0.8 (a), 0.3(b) and 1.5 g/l (c)

Influence of relative cycle duration $t_{p,IN}/t_{p,OUT}$ for discharge Q = 0.7 l/s and frequency Kt_P = 0.6

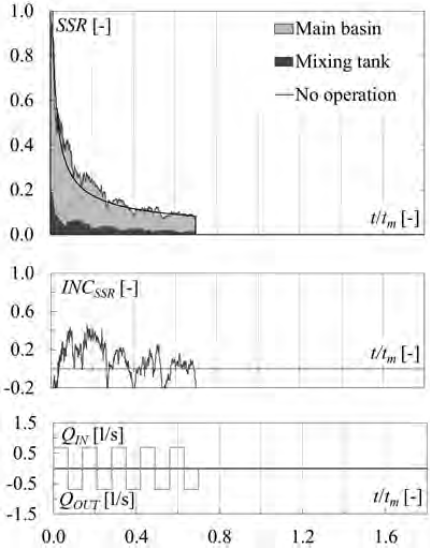

a)

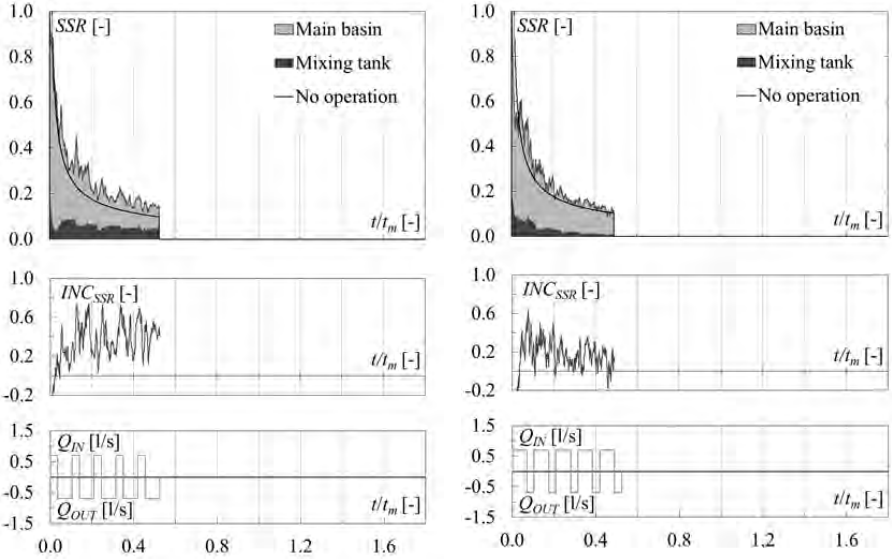

b) c)

Figure C.5 Suspended sediment ratio *SSR*, dimensionless increase INC_{SSR} and discharge Q as a function of dimensionless time t/t_m for C_0 = 0.8 g/l, Q = 0.7 l/s, Kt_P = 1.0 and relative cycle durations $t_{p,IN}/t_{p,OUT}$ = 1.0 (a), 0.5 (b) and 2.0 (c)

Influence of intake position z_i/B_{MB} for discharge Q = 1.1 l/s and frequency Kt_P = 1.0

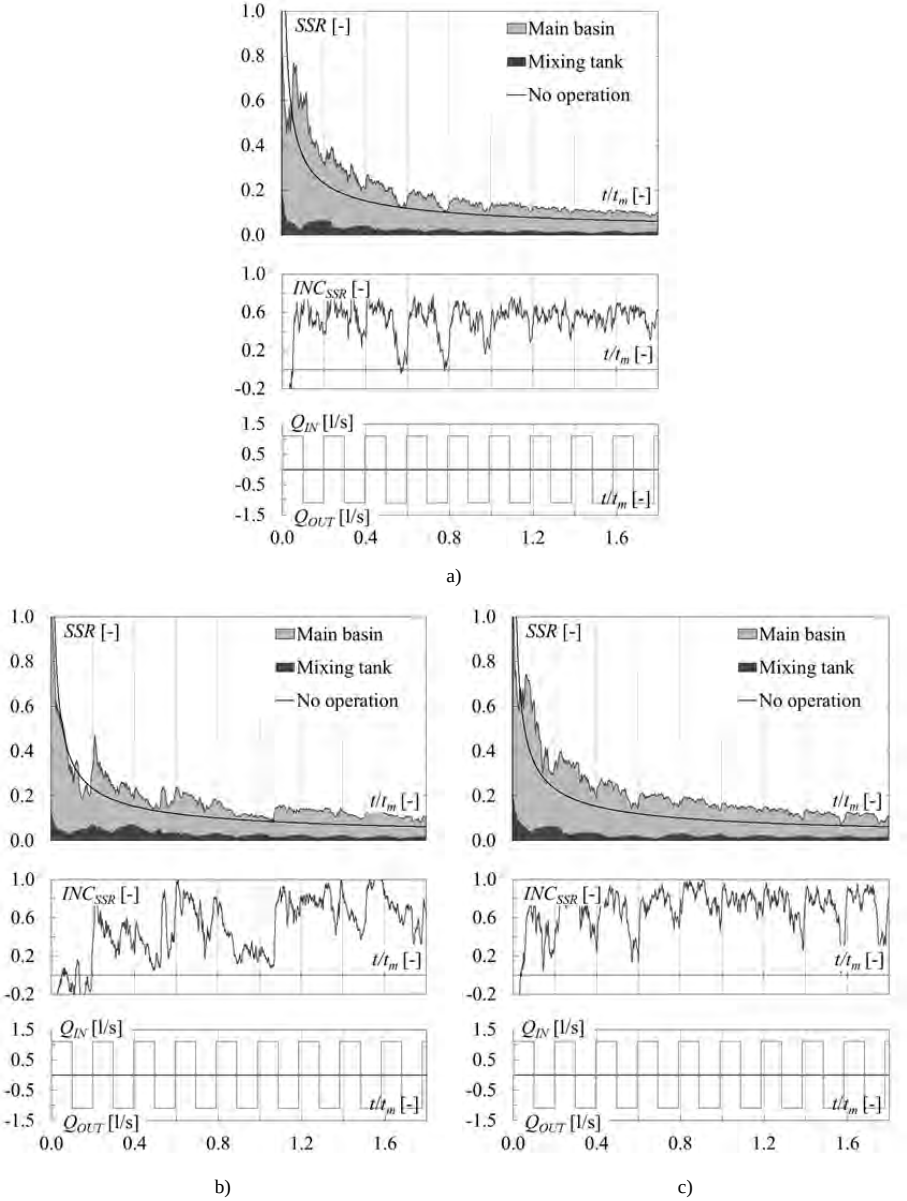

Figure C.6 Suspended sediment ratio *SSR*, dimensionless increase INC_{SSR} and discharge Q as a function of dimensionless time t/t_m for C_0 = 0.8 g/l, Q = 1.1 l/s, Kt_P = 1.0 and intake positions z_i/B_{MB} = 0.25 (a), 0.125 (b) and 0.375 (c)

Communications du Laboratoire de Constructions Hydrauliques ISSN 1661-1179
Ecole Polytechnique Fédérale de Lausanne
Editeur: Prof. Dr A. Schleiss

N° 40 2009 11. JUWI
Treffen junger Wissenschafterinnen und Wissenschafter an Wasserbauinstituten

N° 41 2010 Master of Advanced Studies (MAS) in Water Resources Management and Engineering, édition 2005-2007 - Collection des articles des travaux de diplôme

N° 42 2010 M. Studer
Analyse von Fliessgeschwindigkeiten und Wassertiefen auf verschiedenen Typen von Blockrampen

N° 43 2010 Master of Advanced Studies (MAS) in Hydraulic Engineering, édition 2007-2009 - Collection des articles des travaux de diplôme

N° 44 2010 J.-L. Boillat, M. Bieri, P. Sirvent, J. Dubois
TURBEAU – Turbinage des eaux potables

N° 45 2011 J. Jenzer Althaus
Sediment evacuation from reservoirs through intakes by jet induced flow

N° 46 2011 M. Leite Ribeiro
Influence of tributary widening on confluence morphodynamics

N° 47 2011 M. Federspiel
Response of an embedded block impacted by high-velocity jets

N° 48 2011 J. García Hernández
Flood management in a complex river basin with a real-time decision support system based on hydrological forecasts

N° 49 2011 F. Hachem
Monitoring of steel-lined pressure shafts considering water-hammer wave signals and fluid-structure interaction

N° 50 2011 J.-M. Ribi
Etude expérimentale de refuges à poissons aménagés dans les berges de rivières soumises aux éclusées hydroélectriques

N° 51 2012 W. Gostner
The Hydro-Morphological Index of Diversity:
a planning tool for river restoration projects

N° 52 2012 M. Bieri
Operation of complex hydropower schemes and its impact on the flow regime in the downstream river system under changing scenarios

N° 53 2012 M. Müller
Influence of in- and outflow sequences on flow patterns and suspended sediment behavior in reservoirs

ISSN 1661-1179

Prof. Dr A. Schleiss
Laboratoire de constructions hydrauliques - LCH
EPFL, Bât. GC, Station 18, CH-1015 Lausanne
http://lch.epfl.ch
e-mail: secretariat.lch@epfl.ch